Development of Artificial Intelligence Based Technique for Minimization of Errors and Response time in Head Tracking for Head Worn Systems

A THESIS

Submitted in the fulfilment of the requirement for the award of the Degree of

DOCTOR OF PHILOSOPHY

by

Aman Kataria
(Registration No.: 901304001)

Under the guidance of

Dr. Smarajit Ghosh
Professor, EIED, TIET

Dr. Vinod Karar
Chief Scientist & Professor
CSIR-CSIO, Chandigarh

THAPAR INSTITUTE
OF ENGINEERING & TECHNOLOGY
(Deemed to be University)

Department of Electrical and Instrumentation Engineering,
Thapar Institute of Engineering & Technology
(Deemed to be University)
Patiala - 147 004
Punjab, India

CERTIFICATE

I hereby certify that the work, which is being presented in the thesis entitled "***Development of Artificial Intelligence Based Technique for Minimization of Errors and Response Time in Head Tracking for Head Worn Systems***" to the Department of Electrical & Instrumentation Engineering, Thapar Institute of Engineering & Technology (Deemed to be University), Patiala in the partial fulfilment of the requirements for the award of the degree of "Doctor of Philosophy", is an authentic record of my own research work carried out under the guidance of Dr. Smarajit Ghosh and Dr. Vinod Karar and refers other research works, which are duly listed in the reference section.

The matter presented in this thesis has not been submitted in part or full for the award of any degree to any other university or institute.

(Aman Kataria)

Regd. No. 901304001

This is to certify that the above statement made by the candidate is correct and true to the best of my knowledge.

S. Ghosh
09-11-2020

(Dr. Smarajit Ghosh)
Professor
Department of Electrical and Instrumentation Engineering
Thapar Institute of Engineering & Technology (Deemed to be University)
Patiala, Punjab, India.

V. Karar

(Dr. Vinod Karar)
Chief Scientist & Professor
CSIR-CSIO, Chandigarh
India

ACKNOWLEDGMENTS

First, I thank the almighty God, who gave me the opportunity and strength to carry out this research work.

With great pleasure and privilege, I wish to express my heartfelt sense of gratitude to my supervisors, **Dr. Smarajit Ghosh,** and **Dr. Vinod Karar**, for their guidance, motivational support, and directions for completing this research work.

I am thankful to **Dr.Rafat Siddique (**Dean of Research and Sponsored Projects, TIET) for his support during this thesis work. Also, I am thankful to former Deans (Research and Sponsored Projects) **Dr. P. K. Bajpai** and **Dr. O. P. Pandey** for their support during this research work. I express my deepest gratitude to **Dr. Prakash Gopalan** (Director TIET, Patiala), and **Dr. R. S. Kaler** (Dean of Faculty Affairs and Head, Electrical and Instrumentation Engineering Department), for their encouragement and support. I am also thankful to **Dr. Gurbinder Singh** (Registrar TIET, Patiala) and staff for helping with the smooth proceeding of the administrative needs associated with the research work. I am also thankful to **Prof. S. Anantha Ramakrishna** (Director CSIO, Chandigarh) and **Prof. R.K. Sinha** (Ex-Director CSIO, Chandigarh) for allowing me to complete forward my research work in CSIO, Chandigarh. I am also thankful to **Dr. Divya Agrawal, Dr. Harry Garg, and Dr. S.S. Saini** for helping me to complete my research work.

I am thankful to all the faculty and staff members of the Department of Electrical and Instrumentation Engineering for their moral support and cordial behavior throughout the research period. I especially thank **Dr. Sunil Singla** (Associate Professor, Department of Electrical and Instrumentation Engineering), **Dr. Rajesh Kumar** (Professor, Department of Computer Science Engineering), **Dr. Prashant Singh Rana, and Dr. Ravinder Kumar** (Associate Professor, Department of Computer Science Engineering)

I am thankful to my Doctoral committee members **Dr. Maninder Singh** (Professor, Department of Computer Science Engineering), **Dr. Gagandeep Kaur**, (Associate Professor, Department of Electrical and Instrumentation Engineering), and **Dr. Jainy Sachdeva** (Associate Professor, Department of Electronics and Communication

Engineering), for their constructive comments and regularly ensuring the progress of research work.

I am totally indebted to my family for showering their blessings all the time and always stood beside me in my difficult times. I am thankful to my **Grandparents Mr. Tilak Raj Kataria & Late Smt. Krishna Kataria** for their unconditional love and blessings throughout my life. I am also thankful to my **Maternal Grandparents Late Sh. Parmanand Sekhri and Late Smt. Krishna Sekhri** for showering their blessings from heaven. Special thanks to my sister **Dr. Wishey Kataria**, My Brother in Law **Mr. Gulshan Bhatti** and my wife **Aditi Kataria** for her constant support during my research phase. I also thank my Parents in law **Sh. Karun Wasil and Smt. Babita Wasil** for their blessings and support. I also like to thank **Dr. Varun Wasil and Ritika Wasil** for their support and care during this journey**.** I offer the deepest gratitude to my mentors **Dr. Navdeep Goel** (Associate Professor, Punjabi University) for his unconditional support and blessings. I would like to especially thank my friend **Dr. Vishal Sharma** for standing beside me during my research. I would like to thank my friends and well-wishers **Tamoghana Bhattacharya, Sikander Hans, Ranjan Walia, Gaurav Bansal, Abhishek Handa, Jatinder Singh, Deepak Azad, Vineet Kumar, Sandeep Kumar Rawat, Anirudh Handa, S.P. Yadav, and Pradeep Singla** for their moral support throughout the various stages of this work. Words fall short to thank **Rametra uncle (US) and Dr. Nakul Prashar** without whom this journey wouldn't be possible**.** I also thank the entire staff of Hostel J for their constant support in my journey. Last but not least this thesis is dedicated to a very special gift to me from almighty God my son **Yasham Kataria** whose existence boosted my confidence for the completion of the thesis.

(Aman Kataria)

Dedicated to My Father Dr. Pawan K. Kataria and Mother Dr. Minoo Kataria

ABSTRACT

To overcome the problem of information access in-flight environment, displays such as Head Down Displays (HDD), Head-Up Display (HUD), Helmet Mounted Display (HMD), etc. are incorporated in the cockpits of fighter planes. The motive of the HUDs and the HMDs is to provide the vital information to the pilot of an aircraft so that the pilot need not look down in the cockpit or scan for gathering the flight, weapon, and aircraft information. With the development in head-up displays, the helmet-mounted displays were incorporated to provide the information to the pilot on its visor similar to the case of head-up displays. The information to be displayed on the HMD has to be synchronized with the view of the external environment in synchronism with the head movement of the pilot. For this, the head of the pilot has to be tracked continuously to achieve synchronization with the external environment. For head tracking, various techniques such as mechanical, acoustic, optical, electromagnetic, and inertial can be used. As electromagnetic and optical trackers are more robust, lightweight, accurate, and cost-effective trackers as compared to the other three trackers, therefore, in this work, electromagnetic and optical tracking methods are used for head tracking and validating and predicting the missing data and error estimation. The head tracking devices form a vital component of head-wearable displays. Head tracking devices are used in modern aircraft, especially in combat aircraft. A head tracker updates the position of the head movements of the pilot. As soon as the pilot turns his head, the head tracker passes the orientation data to the controlling computer, which updates the displayed information consequently. Thus, the pilot can get numerous amount of real-time data that is associated with head orientation. To find out the angular coordinates of the pilot's line of sight, the orientation of the pilot's head has to be evaluated. The angular orientation of the pilot's head is comprised of both translational and rotational.

The Head tracker provides accurate information to flight computers about the orientation of the pilot's head with a high degree of accuracy.

In this work, six degrees of freedom coordinates of the human head motion consisting of three translational coordinates X, Y, and Z, and three rotational coordinates Yaw, Pitch, and Roll are acquired using the electromagnetic and optical tracker. The 6-DoF coordinates of the head are acquired in the Cockpit Simulator under different environmental conditions such as different light intensities and distance between transmitter and receiver of the tracker. All the experiments are conducted in the cockpit simulation laboratory at CSIR – Central Scientific Instruments Organisation, (CSIR-CSIO), Chandigarh, India.

The acquired 6-DoF coordinates of the head are missed due to interferences leading to the 6-DoF missing data set due to the factors like interferences, head of the pilot exceeding the limit of Head Motion Box (HMB), etc. Also, the trackers become more prone to external interferences, ferromagnetism in the case of the electromagnetic tracker, and stray light in the optical tracker. The effect of interferences in the tracking of the head using electromagnetic and optical tracking is also studied in detail. The error in the electromagnetic tracker is calculated with interferences caused by different metals and alloys. Similarly, error in the optical tracker is calculated with interferences caused by different light intensities. Therefore, to avoid the recalibration of the position of the trackers in the cockpit, it is necessary to calibrate the head trackers with respect to the range of HMB. The missing instances of the head coordinates in the 6-DoF data caused by the different kind of interferences is predicted using Self Healing Neural Model, Back Propagation Neural Network, Autoregressive Linear Model and Adaptive Neuro-Fuzzy Inference System. These methods are well-established in predicting the data in such kind of conditions. It is found that the accuracy of prediction is achieved

highest using Self Healing Neural Model for both large and small data sets. Accuracy using the Adaptive Neuro-Fuzzy Inference System is higher in small data sets as compared to the large data set. A Self Healing Neural Model is applied to predict the data with 1%, 2%, 10%, 25%, and 35% missed 6-DoF coordinates of the head. The percentage of missing data has been taken in the range of 1% to 35% to simulate the errors due to wide range movement of the head of the pilot beyond the HMB range as well as due to the excessive interference of light in case of optical tracking and magnetic interferences in case of the magnetic tracking method. The results obtained using the Self Healing Neural Model are also compared with other soft computing and regression data predicting techniques. The latency of the electromagnetic and optical trackers may vary depending on the prediction load on the algorithm which again depends on the percentage data missed.

Thus, the SHNM algorithm has been developed for predicting the missing data and is then compared with other methods like BPNN, ALM, and ANFIS for accuracy in prediction of missed data due to various factors and latency has been estimated for each of these cases.

TABLE OF CONTENTS

LIST OF FIGURES

LIST OF TABLES

List of Symbols Used

HMDs	Head-Mounted Displays
HMB	Head Motion Box
UAVs	Unmanned Aerial Vehicles
DoF	Degrees of Freedom
CVCS	Cockpit Visual Coupled System
HT	Head Tracker
HUDs	Head-Up Displays
SR-CDKF	Square-Root Central Difference Kalman Filter
SPKFs	Sigma Points Kalman Filters
DRF	Dynamic Reference Frame
MRI	Magnetic Resonance Imaging
MEMS	Micro-Electro-Mechanical Systems
3D	Three-Dimensional
FOR	Field Of Regard
VRPN	Virtual Reality Peripheral Network
RGB-D	Red-Green-Blue Depth
FEGA-MTL	Flexible Graph Guided Multi-Task Learning
LK	Lucas-Kanade
RANSAC	Random Sample Consensus
SIFT	Scale-Invariant Feature Transform

POSIT	Pose From Orthography And Scaling with Iterations
KLT	Kanade-Lucas-Tomasi
KF	Key-Frames
2D	Two Dimensional
SURF	Speeded-Up Robust Features
BME	Biased Manifold Embedding
GRNN	Generalized Regression Neural Network
GWN	Gabor Wavelet Network
RBF	Radial Basis Function
SHNM	Self-Healing Neural Model
ARLM	Autoregressive Linear Model
BPNN	Back Propagation Neural Network
AC	Alternate Current
LLM	Logic-Learning Machine
VR	Virtual Reality
IR	Infrared
DC	Direct Current
HyHOPE	Hybrid Head Orientation and Position Estimation
GUI	Graphical User Interface
FoV	Field of View
LEDs	Light Emitting Diodes
CMOS	Complementary Metal Oxide Semiconductor

ANNs	Artificial Neural Networks
FIS	Fuzzy Inference Systems
ANFIS	Adaptive Neuro-Fuzzy Inference System
MFs	Membership Functions

1. INTRODUCTION

In today's era in the field of avionics, head tracking plays an important role, as one of the most contending tasks for current fighter aircraft is to facile the maximum information to the pilot. As aircraft gain their speed during the flight, it becomes more intricate for the pilot in the combat role as the environmental conditions become more antagonistic and the situation becomes more demanding for the pilot. Thus, it becomes a crucial subject to deliver maximum flight information to the pilot. Aircraft spatial orientation plays a vital role in aviation, especially when technology is indulged. The ability to detect the direction of the aircraft - whether it is heading towards the ground or approaching other aircraft or approaching other locations/directions, is particularly a challenging task. It becomes an arduous job for the pilot in unfavorable conditions like night or stormy weather. These problems can be overcome by using head-mounted displays (HMDs). For this, head tracking is important because different information can be displayed on HMDs.

1.1 HEAD TRACKING

Tracking, also known as Position or Orientation tracking, is employed in augmented reality where the orientation and position of real physical targets are demanded. The tracking of an object can be applied to any aircraft and even unmanned aerial vehicles (UAVs) [1, 2]. Tracking can also be employed to detect the vehicles using UAVs by embedding them with optical trackers [3]. Apart from tracking, any kind of obstacle detection and global navigational data can also be projected on the helmet-mounted display [4]. Cartesian coordinates X, Y, and Z are required to specify the point in three dimensions [5, 6]. A head tracker is a device that monitors the head movement. It relays the movement information to the control mechanism to move the camera in the same orientation

as the head does. The head tracking devices form an important constituent of head-wearable displays. Post-processing may include the display of filtered images on the visor of HMD through various techniques like linear canonical transform [7, 8]. These devices are used in modern aircraft especially combat aircraft. They project information similar to that of the see-through head-up display. It allows pilots to view critical flight and data projected onto the inside of their visor, so they do not have to look down at their cockpit instruments to lock on the sensor or weapons to target. This increases situational awareness and gives the pilot a critical advantage in aerial battles.

The concept of head-wearable displays was put forward by Albert Bacon Pratt in 1916 as reported by Marshall [9]. The sighting and the gun were integrated on a helmet and the mouth of the pilot controlled the fire command. That was the pioneer model of head-wearable displays and might be the first to distinguish it from a user perspective by being monocular (one-eye display), or binocular (i.e., stereoscopic images). Initially, the graphics-driven head-wearable display was pioneered by Sutherland in the late 1960s [5]. This could display a 2D image by the traditional coaxial optics, but the volume and weight were very large. Head-mounted displays had been employed in military applications as military helmets worn by the pilots [10, 11]. Head-wearable displays are worn on the head and they provide a large - size image before the user [12, 13]. It consists of a miniature display source, optical imaging system, optical beam combiner, tracking system, circuit, and mechanical system. It is small in size, light in weight, large in the FOV (field of view) and has high resolution and performance, which makes it practical for a variety of applications. Integrated with head-position, orientation, and eye-tracking sensors, it also proves to be a very powerful tool for training, such as immersive ground-based simulator training. Besides, it could also be used in industrial production, medical treatment, and entertainment [14, 15].

The head tracker provides accurate information to flight computers about the orientation of the pilot's head with a high degree of accuracy and low impact on weight, size, etc. of head-wearable display [16]. For accurate tracking of the head motion, the tracker must be capable to track the translational and orientation coordinates of the head motion, which are determined by **X, Y, and Z** positional coordinates and three angles known as **Roll, Yaw, and Pitch**. Thus, six degrees of freedom (6-DoF) is required to track the motion of the head accurately. Figure 1.1 depicts the head tracking enabled Helmet Mounted Display.

Figure 1.1: Helmet Mounted Display

1.2 HELMET MOUNTED DISPLAY

Head-mounted displays are physical information viewing devices that can provide information immaculately compared to other devices in aviation and medical telemetry applications [17]. They can be used as a hand-off information source. The output information (video) can be made responsive to the head as well as other parts of the body movements using a body area network [18]. This singular approach contributes to applications like virtual reality to create artificial surroundings, in medical assistance during surgical procedures. Also, recent development in video games is one of the main thrusts in the advancement of virtual environment technology [19]. As far as avionics is concerned, virtual reality is being used for aircraft simulation and training and

avionics display applications [20]. To veritably extract the benefits of the HMD in avionics, it is embedded in Cockpit Visual Coupled System (CVCS), which includes HMD itself along with a head tracker (HT) and a video source [21].

HMDs can help the pilot of a fighter plane to control the missile sensor following the pilot's line of sight, which allows the pilot to point the targets away from the frontward line of sight of the fighter plane [22]. Similarly, HMDs can be synchronized with forward-looking infrared sensors in helicopters, which helps to fly at night. HMD is to be designed to sense six degrees of freedom (6-DoF) in which there are two types of coordinates namely translational and rotational. Translational coordinates are the values of X, Y, and Z-axis, and rotational coordinates consist of elevation, azimuth, and tilt of the pilot's head relative to the airframe with sufficient precision even under high gravity and during rapid head movement [23, 24]. Figure 1.2 shows the inner view of HMD as seen by the pilot.

Figure 1.2: Typical symbology displayed on HMD

1.3 MOTIVATION FOR WRITING THIS THESIS

Head tracking is an important part of the Head Mounted Display. It makes sure that the head movements of a user/pilot are correctly identified. For this purpose, there exist various techniques to track the head such as electromagnetic tracking, optical tracking, inertial tracking, mechanical tracking, etc. The data acquired by the tracker must be accurate. Sometimes, due to technical errors such as stray lights, stray magnetic field, movement of the head beyond head motion box (HMB) in the cockpit, etc., the head tracker can fail to correctly acquire 6-DoF coordinates namely X (forward and backward translational coordinate of the pilot's head), Y (left and right translational coordinate of the pilot's head), Z (up and down translational coordinate of the pilot's head), Yaw (rotational coordinate of the pilot's head along Z-axis), Pitch (rotational coordinate of the pilot's head along Y-axis) and Roll (rotational coordinate of the pilot's head along X-axis). The Cockpit Simulator developed by CSIR - Central Scientific Instruments Organisation (CSIR-CSIO), Chandigarh, India is designed to get the practical experience of Head-Up Display during the flight, which is also indigenously designed by CSIR-CSIO, India. While conducting some experiments for head tracking using magnetic and optical trackers, it was found that there were some factors, that led to the inaccurate acquisition of coordinates of the head. In magnetic head tracking, the coordinates got missed due to factors such as stray magnetic field, movement of the head beyond HMB, etc. Using an optical tracker for the identification of head motion, some coordinates of head motion were not recorded due to stray light interference as well as the movement of the head beyond HMB. The factors mentioned above, leading to improper head tracking, can get magnified to a large extent during actual flight conditions. An attempt is made while experimenting in the cockpit simulator to deal with this problem. A Self Healing Neural Model along with other soft

computing techniques is used to predict the missing 6-DoF coordinates to assure proper tracking of head motion.

1.4 TAXONOMY OF HEAD TRACKERS

The taxonomy of the head tracking system is illustrated in Figure 1.3. The taxonomy discusses the different robust methods of head tracking. The taxonomy mainly describes the types of magnetic and optical tracking. Basic execution of head tracking is described in Figure 1.4

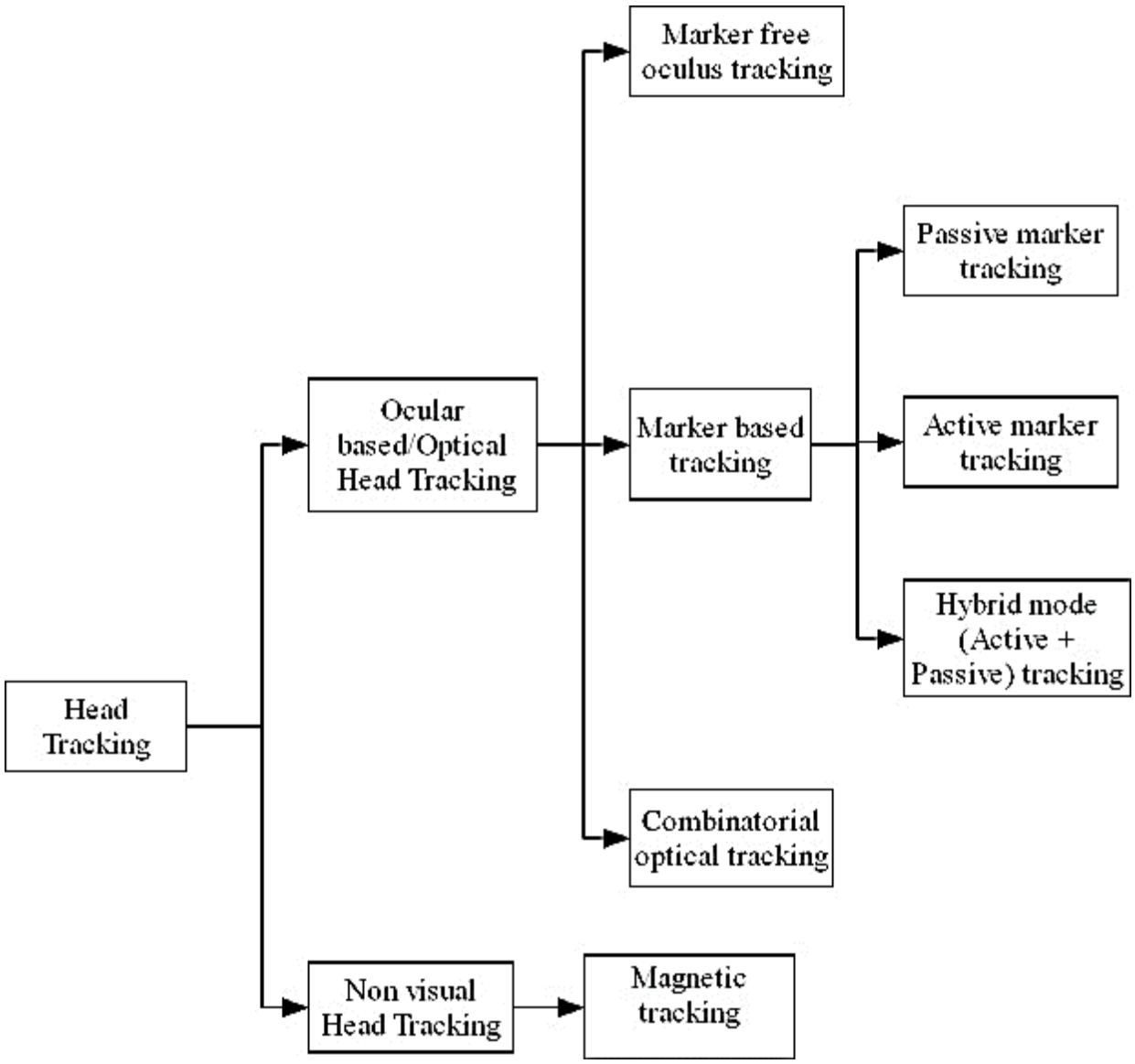

Figure 1.3: Taxonomy of Head Tracking

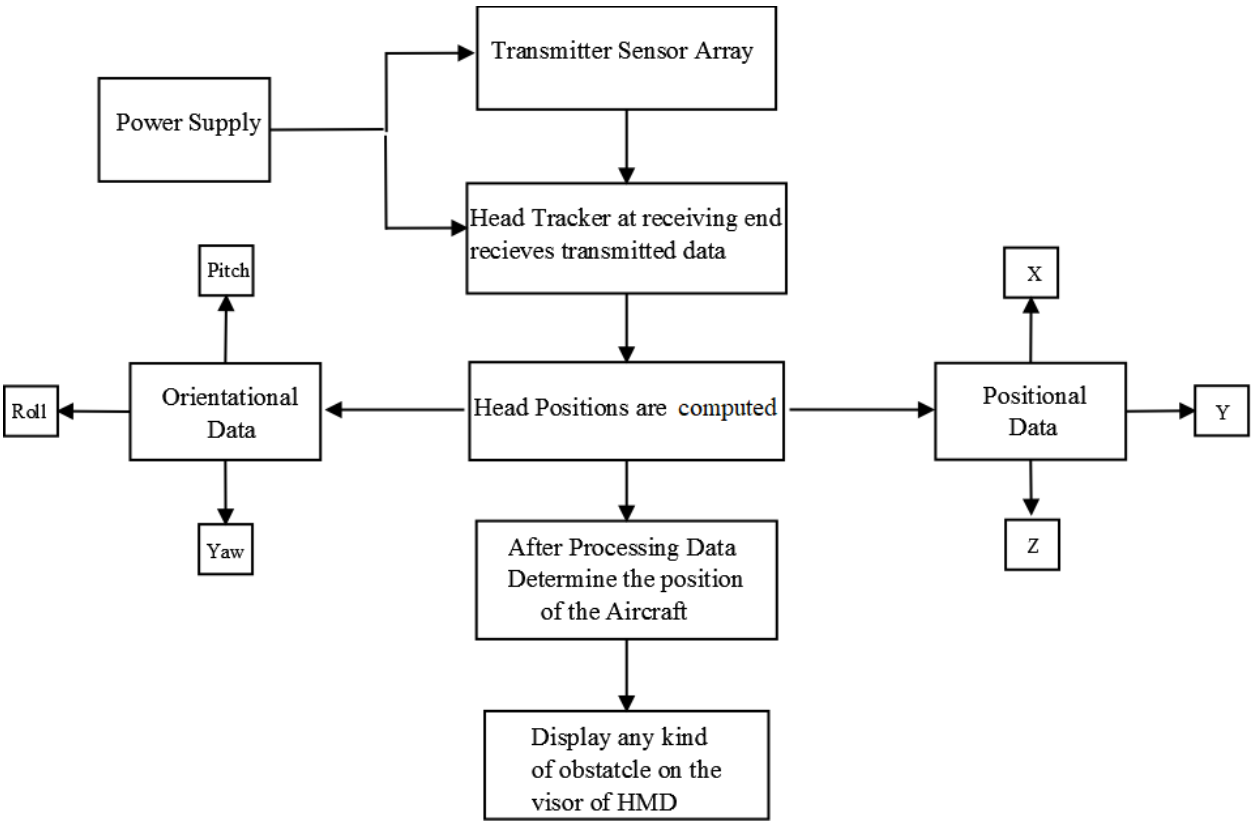

Figure 1.4: Basic execution of head tracking

1.5 OBJECTIVES

1. To analyze the effect of relative placements in terms of orientation and distance of transmitter and receiver sensors (mounted on cockpit and helmet in single and hybrid mode).
2. To characterize and form the basis of error patterns in terms of latency and positioning accuracy.
3. To characterize the errors in different combinations.
4. To develop fuzzy logic and artificial neural network based soft computing method for optimization of head tracking position estimation and latency reduction.

1.6 ORGANISATION OF THESIS

This thesis work is divided into five chapters. Chapter 1 describes the introduction of Head tracking and Head Mounted Display and the objectives of the thesis. Chapter 2 provides a literature survey of the work done in the field of tracking. Chapter 2 also discusses the research gaps in the field of head tracking. Chapter 3 describes the different methods of head tracking and also focuses on the five different techniques of head tracking. The survey of the two tracking techniques (electromagnetic and optical tracking) used in the acquisition of 6-DoF coordinates of the head is also presented in this Chapter. Overview of different soft computing and regression techniques is also mentioned in Chapter 3. Chapter 4 discusses the methods of different soft computing and regression techniques to predict the missing 6-DoF coordinates of the head. Chapter 5 discusses the experiments conducted to acquire the 6-DoF coordinates of the head using electromagnetic and

optical tracking. This chapter also discusses the results of the prediction of the missing 6-DoF coordinates of the head motion using electromagnetic and optical tracking. The effect of interferences in both electromagnetic and optical tracking is also discussed in this chapter. Finally, Chapter 6 includes the conclusion and future scope in the field of head tracking. In the end, the references, which have been used in the thesis, are presented.

1.7 CONCLUSION

Tracking, also known as position or orientation tracking, is employed in augmented reality where the orientation and position of real physical targets are demanded. This chapter provides an introduction to various head tracking techniques and the basics of head-mounted displays. Modern fighter aircraft employ glass cockpit and associated displays such as Head Down Displays, Head-Up Displays, Helmet Mounted Displays, etc. to aid the pilot in making split-second decisions. The HMD provided the functionality of see-through HUD display coupled with tracking of head movements, larger FOV, and provision of locking targets based on the head-tracked movements. There are various types of head tracking methods, which have their advantages and disadvantages based on their working principles and the target application. Hence, the taxonomy of different types of trackers is also discussed. The chapter also describes the basic working of a head tracker and the need for head tracking in aviation. There are several problems in head tracking especially when it is used in aircraft and simulators such as latency, accuracy in head tracking, interferences such as stray light or magnetic field, etc. Therefore, the motivation of the thesis is also provided in this section. The objectives of this thesis are also presented in this chapter. Finally, the organization of the thesis is also presented in this chapter.

2. LITERATURE SURVEY

Several research works had been conducted in the field of object tracking. Many attempts had been made to improve the accuracy of the tracking whether it is concerning the movement of hand, eyes, body, or head. Tracking has a wide area of applications, out of which clinical applications, augmented gaming industry, photographic applications, and aviation are the significant ones.

Head tracking was popular in aviation since the introduction of helmet-mounted displays (HMDs). HMDs are very sophisticated and advanced head wearable helmets worn by the pilots of the fighter jets. They were used to visualize the critical information and vital parameters of the fighter planes. Although head-up displays (HUDs) are also used to visualize the information of the plane and to provide the information to the pilots during aerial battles, it can be difficult to access the HUD for gathering the information. The same information could be provided to the pilot on the visor of the helmet. The visor of the HMD acts as a HUD to the pilot. However, the head of the pilot will be never stable. Therefore, the information visualizing on the visor of the HMD must be in synchronization with the coordinates of the head of the pilot and external environmental view. The information could be misleading or will be out of phase concerning the visor of HMD if coordinates of the head of the pilot and external environmental view are not in synchronization. With the exponential growth in the field of HUDs [25, 26] since the 1980s, the origin of the HMDs [27, 28] came into existence.

For the technological advances in HMDs, it was necessary to improve the tracking of coordinates of the head. Thus, many trackers were devised for head tracking. Various technologies like electromagnetic, optical, acoustic, inertial and mechanical head tracking, etc. were developed.

Each technology had its merits and demerits and was employed according to the merits of the working principle for the application. Acoustic tracking became prevalent for underwater object tracking [29]. Electromagnetic [30] and optical [31] tracking were preferred in aviation due to their high accuracy of head tracking. There were various problems with each tracking technology. Electromagnetic tracker has a problem of interference due to ferromagnetism. Occlusions and stray light interference affect the performance of an optical tracker. Mechanical trackers were very bulky, and their execution was complex. Acoustic trackers suffered from the external noise present in the environment. The accuracy also depended on the working environment of the head trackers. In this chapter, various problems have been discussed with respect to optical, electromagnetic, inertial and acoustic trackers. Various issues in the hybridization of tracking technologies have also been explored in this chapter.

Ribo ***et al.*** [32] devised a method of optical tracking, which emphasized accuracy, jitter, and prediction. They relied on photogrammetric calibration approaches determining lens distortion, and interior and exterior orientations. They also deduced the epipolar constraints to reduce the tracking region into a line. For prediction, they used linear prediction in combination with dynamic search frame size thus allowing in adaptation to different motions of the targets. For prediction, the linear method approach was easy to deploy and was straightforward to apply as a prediction scheme, which had shown to provide satisfactory performance in combination with the dynamic adaptation of the frame size. They used 25 retro-reflectors for tracking the scene at 30 Hz.

Rae and Ritter [33] used an artificial neural network to recognize head orientation. They employed three neural networks: one for color segmentation, second for localization of the face, and third for recognition of the head orientation without using infrared detectors or retro-reflectors. They also analyzed the accuracy achieved at different steps of the process.

Gee and Cipolla [34] had presented a geometrical model for estimating the gaze direction of the human face. They computed the ratios between facial features like eyes, mouth, and nose. They presented a real-time gaze tracking system, which extracted the mouth and eye points from the gray-scale images using simple methods. These points were then used to compute the facial normal. They did not mention the accuracy of their proposed system.

Ballard and Stockman [35] described two different methods for detecting facial feature points. One method relied on the eye and nose twinkle, the other one used a deformable template. After detection of the feature points, they were used for facial normal computation. In their proposed system, the uncertainty in the extraction of features resulted in an error of 15% in the Pitch angle and 22.5% in the Yaw angle. Their system was used as an application of a human-machine interface to control a mouse pointer on a computer screen.

Asteriadis ***et al***. [36] used convolutional neural networks for face tracking and head pose estimation, and image processing was also used. They did not report the accuracy of the acquisition of the 6-DoF data. The prime focus was only Yaw and Pitch angles. Moreover, it was assumed that the number of pixels with saturation values of a pre-defined sample area of each person was close to the number of face pixels in the subsequent frame, which could lead to the inaccuracy of the system if the assumed hypothesis was wrong.

Bauer ***et al.*** [37] proposed a model for predicting target registration error accuracy by using different kinds of error propagation rules. They designed a set of experiments to estimate the real parameters of the model for any given tracking system. They described the results of their work in which they discussed the effects of different sources of errors. Along with this, they also presented a set of tools that could be used to describe the accuracy.

He ***et al.*** [38] developed a hybrid tracking system using an optical tracker and inertial tracker. They improved the accuracy of the tracking system during occlusion, where the inertial tracker tracks the head during the failure of an optical tracker. In their proposed system, the optical tracker acquired 3-DoF positional coordinates and the rest of the 3-DoF orientation movements were acquired using an inertial tracker. Their experimental results showed the root mean square errors (RMSE) of orientation and position were 0.04° and 0.134 mm.

Sen and Kazanzides [39] presented an approach using Particle filter and extended Kalman filter (Bayesian filters) to compute the accurate dynamic performance of an electromagnetic tracking system. They proposed a system in which the electromagnetic tracker could acquire 6-DoF data of a fast-moving target (head). As described by Nafis ***et al.*** [40], the electromagnetic were more prone to dynamic inaccuracies subjected to high-velocity moving targets. The focus was just to analyze the dynamic accuracies of different electromagnetic trackers.

Himberg ***et al.*** [41] proposed a system to predict head orientation coordinates using multiple delta quaternions extended Kalman filter. Their proposed system tracked angular head velocity and angular head acceleration. Their purpose was to predict the orientation movement of the head to avoid the delay caused by several factors like ferromagnetism. Their study could not report the problem arising due to missing of acquired data.

Roetenberg ***et al.*** [42] designed a Kalman filter to estimate the orientations of the human body segment (head) by combining signals of gyroscope magnetometer and accelerometer from miniature sensors. They acquired the 6-DoF data using a magnetic tracker under the influence of iron plate causing ferromagnetism using their proposed filter. They compared the acquired data with that of an optical tracker, which was free from ferromagnetic interference. They obtained drift-free data, but they did not mention the solution to the missing data.

Harada ***et al.*** [43] proposed a system embedded with accelerometers and magnetometers to estimate gravity and the geomagnetic field. That method was developed to eliminate the effect of motion. They also attempted to reduce the effect of magnetic disturbances. They used Sigma Points Kalman Filters (SPKFs) to determine the appropriate filter for the proposed system. For accuracy and stability, they used the Square-Root Central Difference Kalman Filter (SR-CDKF). However, the effect and solution of missing data were not accounted for in their experiment.

Khadem ***et al.*** [44] compared five optical trackers to compute the jitter, which helped to judge the precision of optical trackers. According to their study, to make tracking effective, the placement of a dynamic reference frame (DRF) needed to be optimal with respect to the tracking camera. Measurement of jitter could help in understanding the dependency of system inaccuracies on the position of DRF with respect to the camera. They used **FlashPoint™ (Image Guided Technologies, Inc., Boulder, Colorado) and Polaris™ (Northern Digital Inc., Ontario, Canada)** optical tracking systems. Both the tracking systems were tested in five different cameras and DRF configurations. Their study lacked discussion about the missing data due to occlusion or stray light interference.

Al-Rahayfeh and Faezipour [45] discussed various applications of eye tracking and head tracking. They presented a survey of different techniques of head tracking like computer vision-based head movement detection, acoustic signal-based methods and accelerometer, and gyro sensor-based techniques. They also mentioned the hybrid techniques. Their study was mainly focused on applications of head tracking, detection accuracy, and angle accuracy. Their study did not mention the response time and delay time due to missing data.

He ***et al.*** [46] discussed the problems arising in an optical tracker by occlusion. They fused the inertial sensor with an optical tracker to overcome this problem. Using this technique, they

were able to reduce cumulative errors in measurement of position. Experiments were performed using an inertial tracker to avoid incomplete tracking of the head using optical. There was no concern about the inaccuracies generated due to missing data.

Hu ***et al.*** [47] used the magnetic tracker for tracking the human part. They devised a linear model challenging the classical non-linear mathematical approach. Their study was inclined to prove the reliability of the linear algorithm over the nonlinear model. According to them, the linear model was faster in tracking, the computation was reliable, and complexity was low. Their experiments were based on a real localization system in which their algorithm resulted in a solution by the matrix and algebra computations.

Ooi ***et al.*** [48] proposed a method for real-time correction for arbitrary head motion using active markers. The application of head tracking in their study was inclined towards the biomedical area. The tracking technology used in their experiment was electromagnetic. They discussed the correction of head posture 6-DoF coordinates acquired with the unwanted abrupt motion of the head. According to their study, it led to clearer images of brain MRI (Magnetic Resonance Imaging). Due to ferromagnetism, the problem of loss of the tracked data or data missed due to other factors were not discussed in their study.

Krevelen and Poelman [49] presented the survey of various tracking technologies like optical, retinal, video, and projective. They categorized their study on the different parameters of a tracker as brightness, contrast, resolution, field of view, power, occlusion, and application for outdoor or indoor use. They also discussed the design and applications of magnetic, optical, mechanical, and inertial trackers. The study on the limitations of the trackers was mainly focused on portability, auto-calibration, depth perception, overloading, over-reliance, and social

acceptance. The problems in acquiring the 6-DoF data from the tracker were not discussed in their study.

Suau ***et al.*** [50] focused on a real-time algorithm for head and hand tracking. Their approach was based on resolving the ambiguities and overlaps in the data acquired. They estimated the position with depth-based template matching. In head tracing, their prime focus as a limitation was occlusions and human head size. The tracking technique involved was optical. The better results could be achieved by using the hybrid technique like the fusion of optical and magnetic trackers.

LaValle ***et al.*** [51] introduced a low-cost MEMS (Micro-Electro-Mechanical Systems) sensor deployment for head tracking. They fused the gyroscope with the magnetic tracker. They also discussed an attempt to eliminate the errors using gravity and magnetic fields. They also presented a predictive tracking method to reduce the latency, which improved the user experience. Their focus was to correct the angular coordinates of the head (tilt and Yaw correction). The latency occurring due to missing data were not reported in their study.

Ragan ***et al.*** [52] presented a study on head tracking referring to small-scale spatial judgments. They studied the effects on the performance of a given task, which involved precise spatial inspections of complex three-dimensional (3D) structures. The participants were asked to differentiate between the structural gaps and the intersections present between the components of 3D models designed which were the replica of real underground cave systems. The participants were able to judge small-scale spatial judgments. As reported by them, they made a few errors due to the addition of head-tracked rendering. They controlled the field of regard (FOR) and stereoscopy to increase the accuracy of the system.

Kobayashi ***et al.*** [53] proposed a method to track through the human head. They used multiple cameras for tracking. They proposed a technique using cascaded classifiers based on

AdaBoost and Haar-like features for the evaluation of the hypothesis. In their experiment, the most suitable classifier was adaptively selected by considering each hypothesis and position of the camera. The authors did not acquire the 6-DoF data as they only tracked the likelihood of the human head (only 3-DoF data) leading to inaccuracy at the coordinate level.

Choi and Kim [54] presented a real-time 3D head tracking handling rotation and translation. They incorporated three approaches into the particle filter. They employed the 3D ellipsoidal head model to manage large head rotation across the X-axis. They also used an online appearance model, which could adapt both short-term and long-term appearance changes in the appearance model image effectively. Finally, they took the adaptive state transition model to track fast-moving 3D heads used for estimating the most probable state using the motion history model. The authors noticed that the tracking accuracy of the 3D ellipsoidal was 15% more than the 3D cylindrical head model.

Rougier ***et al.*** [55] proposed a system for 3D head tracking for fall detection. They used a single calibrated camera for tracking head movement by extracting the 3D head trajectory of a person in a room. In their experiment, the head was represented as a 3D ellipsoid, which was tracked with a hierarchical particle filter based on color histograms and shape information.

Parvizi and Wu [56] presented a method of head motion detection, which was based on contour analysis on depth images. In their method, the authors used a sequence of depth-valued images as system inputs using a 3D time of flight depth sensor. They used depth thresholding techniques to segment the background and foreground layers of the image. The regions, which were moving, were further processed in each frame and contour analysis was performed to determine the objective head coordinates in the image. After passing this information to the tracker, the target was tracked in the scene.

Yoon ***et al.*** [57] presented an algorithm for human head detection for a distance exceeding 2.5 meters between a camera and head. The assumptions for the human head and other body parts were made that their shape was like an omega (Ω). To separate the background from these omega shapes, three features of gray, color, and edge were used and combined. After capturing the gray, color, and edge features, the head and body regions were split using the proposed algorithm. Finally, the ellipse fitting and head region verification algorithm was applied to track the coordinates of the head.

Pavlik and Vance [58] used a Wii remote game controller inbuilt infrared camera as an optical tracker. They tried to make a low-cost infrared tracker and accelerometer from the Wii remote for tracking the position of the head. They embedded the Wii remote infrared camera with Virtual Reality Peripheral Network (VRPN) to make a standard head tracker. They tested the infrared optical tracker on Windows and Linux platform and they found that their tracker could render up to 100*Hz* of tracking input. They did not discuss the occurrence of noise.

Lopez ***et al.*** [59] defined different interaction methods of the users with a mobile phone operating system using a mobile phone inbuilt front camera. The inbuilt front camera in the mobile phone was employed in their experiment as an optical tracker to track the head movements of the user. That could help to develop new interaction gestures of a user's head to control some of the applications of mobile single-handedly without using a mobile screen or keypad. The total latency in their experiment in 640 × 480 resolution was 119 ms, which was quite disturbing, and in 320 × 240 resolution, it was 91ms. There was no discussion of the effect of stray light interference in their experiment.

Papadakis ***et al.*** [60] proposed a system to minimize the head tracking latency in immersive simulations by controlling and measuring the head tracking coordinates. They employed

InsertiaCube3 inertial head tracker to minimize the latency of tracking. Their experiment of head tracking was limited to 3-DoF. The refresh rate of 60Hz was achieved with the latency of 2 ms for the case of the inertial tracker. No external sources of noise were discussed in their work.

Zhang ***et al.*** [61] proposed the fusion of the Kernel and Bayesian framework for object tracking. In their algorithm, the object to be tracked was characterized employing a spatial-constraint mixture of the Gaussian-based appearance model along with a multichannel chamfer matching based shape model. According to them, the two models discussed were a compliment to each other and had the discriminative combinations to distinguish the object from the background. They embedded the kernel method-mean shift algorithm into the Bayesian framework to obtain a heuristic prediction in the hypothesis generation process, which reduced the computational load suffered by conventional Bayesian trackers.

Ariz ***et al.*** [62] provided a public database of videos for pose estimation and head tracking. They tried to establish a new framework for algorithm validation. They recorded the position data with a magnetic sensor and transmitter, which was aligned and synchronized with a simple commercial webcam. With the webcam, the authors provided ground-truth data for 3D rotation and translation of the head. According to the authors, this 3D ground-truth data could be used for the evaluation of head tracking. To prove the authenticity of the ground-truth data, they evaluated three heads tracking methods with three head models and combined them to provide nine different head pose estimation sets of results. They also compared the performance of the dataset with state-of-the-art algorithms.

Wang ***et al.*** [63] presented a keypoint-based solution for 3D head tracking. The authors selected reference key points that were robust to various distortions in the face for improving keypoint matching quality. That procedure was done by combining simulation and normalization

techniques within a learning scheme. They used keypoint matching as a standard tool to solve complex problems in vision applications. In their experiment, they tended to learn key points that were explicitly invariant to the 3D pose tracking of the head in the video. They also tried to remove motion jitter in their experiment.

Chutorian and Trivedi [64] presented a head posture estimation system to provide assistance during vehicle driving to avoid automotive collisions. They presented a procedure for static head-pose estimation and an algorithm for visual 3-D tracking. They employed localized gradient orientation histograms as input to support vector regressors for initial pose estimation. They compared the mean error of their algorithm with the normal crossover method and principal component analysis (PCA) projection with support vector regression method both in day and night driving. They used a Vicon optical motion capture system to gather precise ground truth head pose data for evaluation.

Mollet and Chellali [65] presented a method in which they used the **ARvision 3D** virtual reality helmet worn by the user to control a group of robots with teleoperation through head tracking. The authors aimed to enable a group of teleoperators to control groups of robots to achieve complex tasks like inspection of an area or to explore unknown parts of an unknown environment. In their experiment, a magnetic tracker along with an accelerometer was used for head tracking. They also designed a Collaborative Virtual Environment composed of different objects and entities using Microsoft Robotics Studio.

Silva ***et al.*** [66] presented a low resource and real-time head tracking system for interactive applications such as detection of the user/player attention state using a predefined attention model in an attention aware game framework. The authors tested their systems on four different games:

a racing game, an adventure game, a Tetris game, and an educational game to improve attention and awareness especially for autistic children.

Sko and Gardner [67] integrated head tracking in gaming applications using a standard webcam and face-tracking software. According to their experiment, the user's head could perform various controls in the game using his/her head. The user could control the game by zooming (leaning into the screen) and peering (tilting and leaning). Some other head movements they discussed were: spinning (caused a rapid camera rotation up to 180°, by flickering action of the user's head), threshold zooming technique (which was activated when the head came within preset proximity of the screen), and iron slighting technique (which was used to aiming down the barrel of the weapon in combat gaming).

Cazzato ***et al.*** [68] investigated methods of a noninvasive and unconstrained method for gaze and head pose estimation extracted by the RGB-D device. According to the authors, their proposed method did not require any initial calibration; also, it could operate in the unconstrained environment. The authors compared their results with already existing invasive and supervised pattern recognition modules. The maximum error reported in their work was 6.9°.

Cascia ***et al.*** [69] proposed a stable, fast, and improved technique for 3D head tracking in varying illumination conditions. The authors modeled the head as a texture-mapped cylinder. The head tracking was mathematically formulated as a problem of image registration in the modeled cylinder texture map image. The problem of varying illumination and the head motion was solved by modeling the residual error of registration as a linear combination of orthogonal illumination templates and texture warping templates. The authors used an electromagnetic head tracker to obtain ground truth data.

Nabati and Behrad [70] presented an approach to track 3-DoF coordinates of the head from monocular camera images to control the movements of the mouse pointer on the screen along with clicking the events. The motive of the authors was to provide a non-contact device to control the mouse pointer on a computer system for severely disabled people. Initially, they extracted the face area Adaboost algorithm and Haar-like features. They then detected the locations of point features and tracked them over video frames by the LK algorithm. The 2D transformation model between consecutive frames was estimated by matching features using the RANSAC algorithm. Then, using four-point correspondences, the 3D rotation matrix, and the translation vector between the web camera and the 3D head position was estimated. In the final step, they applied 3D rotation and translational matrix to estimate the movements of the mouse pointer on the PC screen.

Yan ***et al.*** [71, 72] proposed a flexible graph guided multi-task learning (FEGA-MTL) method to classify the coordinates of the head of the person moving freely in an open environment under the large field of view surveillance cameras. They partitioned the monitored scene into a dense uniform spatial grid and after that FEGA-MTL clustered the partitions of the grid simultaneously into the regions with similar facial appearance along with learning region-specific head pose classifiers. FEGA-MTL developed the optimal scene partitioning and pose classifiers associated with it using head pose classes and grid partitions based on the camera geometry. The region-specific classifier was invoked for head pose estimation after determination of the target's position using a person tracker.

Zhao ***et al.*** [73] presented a method, which focused mainly on the tracking of the head with large motion, especially for the movement along the Z-axis. The authors used a scale-invariant feature transform (SIFT) based registration algorithm to handle this problem. Features of the SIFT algorithm were detected and tracked between two images. After that, the 3D points corresponding

to the detected and tracked features were obtained from a stereo camera. Using the detected 3D points, a registration algorithm in a Random sample consensus (RANSAC) framework was used to detect the outliers and head pose was estimated.

Prasad and Aravind [74] discussed a method for a robust head posture tracking system that was capable to track the 3D pose of a user's head in video sequences that was captured using a single camera. According to them, the proposed system was able to estimate 3D pose parameters accurately without the knowledge of parameters of the camera. The face of the user was modeled using a parametrized facemask in three dimensions. Scale-invariant feature transform (SIFT) was used to match the consecutive image frames. They also proposed an interpolation technique that was used to capture the 3D movement of the feature points to compute 2D-3D correspondences between the face and the 3D model. Finally, the pose of the head was established using Pose from Orthography and Scaling with Iterations (POSIT) algorithm (for head pose estimation) in a Random sample consensus (RANSAC) framework, which fitted the 3D deformable face model upon the given face image.

Ruddaraju ***et al.*** [75] used multiple camera systems to track the coordinates of the head in an indoor environment. They tried to obtain the coordinates of the head using triangulating multiple facial features, which were obtained in real-time from eye trackers. The authors used three calibrated IBM Blue eyes infrared lighting cameras. The user could move the head from -30° to +30° to track the coordinates of the head.

Yang and Zhang [76] discussed a robust model-based stereo head tracking algorithm, which operated in real-time on a PC. They used an individualized head model of three dimensions, which was coupled with the epipolar constraint from the stereo image pair. The face model used by them was a triangular mesh consisting of up to 300 triangles in which each vertex in the mesh had crucial

information, i.e. chin, eye, etc. The authors built a personalized face model for each user using rapid face modeling, which was originally developed by Liu ***et al.*** [77].

Cai ***et al.*** [78] discussed an approach to track the movements of the head in three dimensions in real-time using multiple cameras with unknown camera placements. They used the generic face model to overcome the problems arisen due to a lack of knowledge of the placement of cameras. They proposed a drift-free, fast, and feature point tracking using the reference frames of high confidence over spatial and temporal domains. The authors used the Bayesian framework and Kanade-Lucas-Tomasi (KLT) tracker to track the movements of the head.

Malassiotis and Strintzis [79] tracked the coordinates of the head using a 3D sensor that generated a dense image of the scene. They claimed that their algorithm was robust and independent of the illumination. They used 3D head-shoulder geometry to track the 6-DoF coordinates of the head motion. The authors also used a Bayesian framework for continuous 3D head pose estimation.

Schodl ***et al.*** [80] used a three-dimensional textured model of the human head to track the coordinates of the head and face. The authors achieved tracking by projecting an image of the face onto a polygonal head model and finding the six translation and rotation parameters to register the rendered images of the textured model with the video images. The parameters were obtained by mapping the derivative of the error with the respect to the intensity gradients present in the image. The error was minimized by using a robust estimator and performing gradient descent.

Madrigal ***et al.*** [81] presented a method that incorporated 2D and 3D cues for the head pose estimation. They also proposed a concept of Key-Frames (KF), which was a set of frames where the orientation and position of the head were computed automatically in an off-line mode. Each Key-Frame consisted of 2D information that was encoded by Speeded-Up Robust Features

(SURF) descriptors and 3D information from a depth image. The RGB-D sensor acquired both 2D as well as 3D information. The new frame was compared against all the Key-Frames and the most relevant was selected. The 3D transformation between the selected Key-Frame and the current frame was estimated using depth image and the iterative closest point algorithm in an online framework. The authors claimed that the proposed system was able to handle partial occlusions.

Balasubramanian ***et al.*** [82] proposed a method to estimate the angle of head posture from the face images to capture the geometrical relationship between the data points in the high dimensional image feature space. The authors proposed a supervised approach to a manifold-based non-linear algorithm to track the head position. The proposed Biased Manifold Embedding (BME) framework was based on the concept of using the information of pose angle of the face images to compute a biased neighborhood of each point in the feature space prior to the determination of the low dimensional embedding. The authors used the Generalized Regression Neural Network (GRNN) to learn non-linear mapping. Finally, linear multivariate regression was applied to the low dimensional space to compute the pose angle.

Krueger and Sommer [83] introduced Gabor Wavelet Network (GWN), which was the model-based approach for object representation. The authors combined the merits of the continuous wavelet transform with the Radial basis function (RBF) networks in their proposed Gabor Wavelet Network. The authors used GWN in the estimation of the head posture as an application. The feature information was encoded in the coefficients of the wavelet. Then in the final step, the authors used a neural network similar to the logic-learning machine (LLM) to compute the coordinates of the head posture from the wavelet coefficients.

Gourier ***et al.*** [84] proposed a method to track the head posture over a wide range of angles from a low-resolution image. In their work, the faces were detected using chrominance-based

features. The input for linear auto-associative memory was grey-level normalized face imagettes. For each pose, one memory was computed using the Widrow-Hoff learning rule.

2.1 GAPS OF RESEARCH

Due to an electrical fault or due to the movement of the head beyond Head Motion Box (HMB) or any other external interference, the Cartesian and polar data of the head movements may not be recorded or missed, which may also cause decreased response time of the head tracker. Existing literature reports that research has been carried to increase the accuracy and response time of the head trackers, but the scenario of the missed data is not considered due to factors such as deviated position, orientation beyond HMB boundaries, and external interferences. Some other identified research gaps are as follows:

- The placement of trackers is not considered in studies.
- The effect of distance and light intensity on the acquisition of the data from an optical tracker has not been reported with reference to latency, missing data, and tracking accuracy.
- The effect of missing 6-DoF coordinates of the head in both optical and magnetic tracker has not been mentioned explicitly.
- An efficient algorithm is not reported yet, which recover the missing 6-DoF coordinates of the head for both optical and magnetic tracker arising due to the above-mentioned situations.

Table 2.1 provides a summary of various types of head trackers used over the years.

Table 2.1: Summary of various types of head trackers used for head tracking

$\downarrow -Low, \uparrow -High, \otimes -Not\ available\ \oslash -Not\ applicable\ for\ Electromagnetic\ and\ Inertial\ Tracker$

Author	Type of Data Acquired	Tracker type	Parameters improved/ Application	Limitations	Cost	Field of View (FOV)	Solution to missing data
Ribo ***et al.*** [32]	6-DoF tracking	Optical	Presented an optical tracking using photogrammetric calibration approaches determining lens distortion, interior, and exterior orientation.	The effect of stray light interference was not studied.	↑	⊗	No
Rae and Ritter [33]	6-DoF tracking	Optical	Used three neural networks for color segmentation, localization of the face, and head tracking without using retroreflectors.	No external interference was studied.	↓	⊗	No
Gee and Cipolla [34]	3-DoF tracking	Optical	Presented a geometrical model for estimating the gaze direction of the human face.	No external interference was studied.	↓	⊗	No
Ballard and Stockman [35]	6-DoF tracking	Optical	Described two different methods for detecting facial feature points. One method relied on the eye and nose twinkle, the other one uses a deformable template	No external interference was studied.	↓	⊗	No

Asteriadis ***et al.*** [36]	3-DoF tracking (only angular coordinates)	Optical	Used convolutional neural networks for face tracking and head pose estimation specifically Yaw and Pitch angles.	No external interference was studied.	↓	⊗	No
Bauer ***et al.*** [37]	6-DoF tracking	Optical	Proposed a model for predicting target registration error accuracy by using different kinds of error propagation rules.	No external interference was studied.	↓	⊗	No
Sen and Kazanzides [39]	6-DoF tracking	Electromagnetic	Presented an approach using Particle filter and extended Kalman filter (Bayesian filters) to calculate the accurate dynamic performance of an electromagnetic tracking system.	No external interference like ferromagnetism was studied.	↑	⦸	No
Himberg ***et al.*** [41]	6-DoF tracking	Electromagnetic	Presented a system to predict head orientation coordinates using multiple delta quaternion extended Kalman filter.	No external interference like ferromagnetism was studied.	↑	⦸	No

Roetenberg ***et al.*** [42]	6-DoF tracking	Optical and Electromagnetic	Designed a Kalman filter to estimate the orientations of the head by combining signals of gyroscope magnetometer and accelerometer sensors.	No external interference like ferromagnetism for electromagnetic tracking and stray light interference for optical tracking was studied.	↑	⦸	No
Harada ***et al.*** [43]	6-DoF tracking	Electromagnetic	Proposed a system embedded with accelerometers and magnetometers to estimate gravity and the geomagnetic field	External interference like ferromagnetism was studied along with the solution, but only for the orientation angles.	↓	⦸	No
Khadem ***et al.*** [44]	6-DoF tracking	Optical	Compared five optical trackers to calculate the jitter, which helped to judge the precision of the optical trackers.	No external interference was studied.	↓	⊗	No

Al-Rahayfeh and Faezipour [45]	6-DoF tracking	Optical and Inertial	Presented a survey of different techniques of head tracking.	No external interference was studied.	↓	⊗	No
He ***et al.*** [46]	6-DoF tracking	Optical and Inertial	Developed a hybrid tracking system using an optical tracker and inertial tracker.	The problem of occlusion was solved using an Inertial tracker, but no remedy for interference in the inertial tracker was reported.	↑	⊗	No
Hu ***et al.*** [47]	6-DoF tracking	Electromagnetic	Used a magnetic tracker for tracking the human part and devised a linear model challenging the classical non-linear mathematical approach.	Elimination of noise was tried only through simulation for magnetic tracking.	↓	⦸	No
Ooi ***et al.*** [48]	6-DoF tracking	Electromagnetic	Proposed an electromagnetic tracking-based method for real-time correction for arbitrary head motion using active markers.	No external interference like ferromagnetism was studied.	↑	⦸	No

Krevelen and Poelman [49]	6-DoF tracking	Optical	Presented the survey of various tracking technologies like optical, retinal, video, and projective.	No external interference was studied.	↓	⊗	No
Suau ***et al.*** [50]	6-DoF tracking	Optical	Focused on the real-time algorithm for head and hand tracking along with an estimation of the position with depth-based template matching.	No external interference was studied.	↓	⊗	No
LaValle ***et al.*** [51]	6-DoF tracking	Electromagnetic and Inertial	Introduced a low-cost MEMS sensor deployment for head tracking.	The focus was mainly on angular coordinates.	↓	⦸	No
Ragan ***et al.*** [52]	6-DoF tracking	Optical	Discussed spatial judgment in 3D structures.	No external interference was studied.	↓	⊗	No
Choi and Kim [54]	6-DoF tracking	Optical	The 3D ellipsoidal model was better as compared to the cylindrical model	No external interference was studied.	↓	⊗	No
Rougier ***et al.*** [55]	6-DoF tracking	Optical	Presented 3D head detection for fall detection.	The effect of stray light interference was not studied.	↓	⊗	No

Parvizi and Wu [56]	6-DoF tracking	Optical	Tracking accuracy was increased using a 3D time-of-flight depth sensor.	No external interference was studied.	↓	⊗	No
Yoon ***et al.*** [57]	6-DoF tracking	Optical	Accuracy of tracking was increased for a distance exceeding 2.5 m.	The effect of stray light interference was not studied.	↓	⊗	No
Pavlik and Vance [58]	6-DoF tracking	Optical	Tracking refresh rate of 100*Hz* was achieved.	The effect of stray light interference was not studied.	↓	43°	No
Lopez ***et al.*** [59]	3-DoF Tracking	Optical	Head tracking to control mobile applications.	No discussion about the effect of stray light.	↑	45° (without fisheye lens)	No
Papadakis ***et al.*** [60]	3-DoF Tracking	Inertial	Tracking latency of 90ms $\pm$ 10% was achieved.	No discussion about the effect of stray noise in the case of the inertial tracker.	↑	⦸	No
Zhang ***et al.*** [61]	3-DoF Tracking	Optical	Fused kernel and Bayesian framework to reduce the computational load in head tracking.	The effect of stray light interference was not studied.	↓	⊗	No

Ariz ***et al.*** [62]	6-DoF tracking	Optical and Magnetic	Provided a dataset for head tracking evaluation.	No study related to external interference in optical and magnetic tracking was discussed.	↓	⊗	No
Wang ***et al.*** [63]	6-DoF tracking	Optical	Provided keypoint-based solution for fast and accurate 3D head tracking.	No study related to external interference in optical tracking was discussed.	↓	⊗	No
Chutorian and Trivedi [64]	6-DoF tracking	Optical	Presented a method of head tracking of the driver in the vehicle to avoid an automotive collision.	The effect of stray light interference was not studied.	↑	⊗	No
Silva ***et al.*** [66]	3-DoF tracking	Optical	Presented a low resource and real-time head tracking system for interactive applications.	No kind of interference was studied.	↓	⊗	No

Sko and Gardner [67]	6-DoF tracking	Optical	Used head tracking as an application in gaming.	No kind of interference was studied.	↓	≈ 120°	No
Cazzato ***et al.*** [68]	6-DoF tracking	Optical	Presented a noninvasive and unconstrained head and gaze tracking.	No external interferences were studied.	↓	57°	No
Cascia ***et al.*** [69]	6-DoF tracking	Optical	Proposed a stable technique for 3D head tracking in the varying illumination conditions.	No kind of interference was studied.	↑	⊗	No
Nabati and Behrad [70]	3-DoF tracking	Optical	Proposed a method to track the head coordinates to control the mouse pointer on the PC screen.	No external interferences were studied.	↓	⊗	No
Yan ***et al.*** [71] [72]	3-DoF tracking	Optical	Proposed a method to estimate the head pose of a person under free environment using surveillance cameras	No external interferences were studied.	↓	⊗	No
Prasad and Aravind [74]	3-DoF tracking (only angular coordinates)	Optical	Presented a system to track the coordinates of the user's head from video sequences captured with a camera.	No study related to external interference in optical tracking was studied.	↓	⊗	No

Ruddaraju ***et al.*** [75]	3-DoF tracking	Optical	Presented an indoor head tracking system using multiple cameras.	The problem of occlusion was mentioned but no remedy was presented.	↑	≈ 60°	No
Yang and Zhang [76]	6-DoF tracking	Optical	Presented a model-based stereo head tracking method in which the face model was converted into triangular meshes containing information of the facial features.	No study related to external interference in optical tracking was studied.	↓	⊗	No
Cai ***et al.*** [78]	3-DoF tracking	Optical	Discussed an approach to track the head movements using multiple cameras with unknown placements of the cameras.	No external interferences were studied.	↑	⊗	No
Malassiotis and Strintzis [79]	6-DoF tracking	Optical	Used 3D head-shoulder geometry to track the 6-DoF coordinates of the head motion under the Bayesian framework.	No study related to external interference in optical tracking was studied.	↓	⊗	No
Schodl ***et al.*** [80]	6-DoF tracking	Optical	Achieved tracking by projecting an image of the face onto a polygonal head model.	No external interferences were studied.	↓	⊗	No

Madrigal ***et al.*** [81]	6-DoF tracking	Optical	Proposed a concept of Key-Frames, which was a set of frames where the orientation and position of the head were calculated automatically in an off-line mode.	Their proposed system was able to handle partial occlusions only.	↑	⊗	No
Balasubramanian ***et al.*** [82]	3-DoF tracking (only angular coordinates)	Optical	Proposed a method to estimate the angle of head posture from the face images using the Biased Manifold Embedding framework.	No study related to external interference in optical tracking was studied.	↓	≈ 180°	No
Krueger and Sommer [83]	3-DoF tracking	Optical (Model-based)	Used Gabor Wavelet Network as an application for head pose estimation.	No external interferences were studied.	↓	⊗	No
Gourier ***et al.*** [84]	3-DoF tracking (only angular coordinates)	Optical	Proposed a method to track the head posture over a wide range of angles from a low-resolution image using the Widrow-Hoff learning rule.	No external interferences were studied.	↓	⊗	No

2.2 CONCLUSION

This chapter discusses a literature survey of the work done in the field of head tracking. It discusses in detail the work done in head tracking using optical, electromagnetic, inertial, and other techniques. This chapter discusses the problems encountered during the acquisition of data for head tracking. It also discusses the origin of the head-up display, which ultimately leads to the requirement of the head-mounted displays and hence the head tracker. This leads the facility of a head-up display in the helmet-mounted display. Electromagnetic and optical trackers are more convenient as compared to inertial, mechanical, and acoustic trackers. Electromagnetic and optical trackers used in head-mounted displays are more robust, lightweight, accurate, and cost-effective trackers as compared to the other three trackers. Therefore, in this chapter, the literature survey of electromagnetic and optical tracking along is discussed. Some related work of the inertial tracker is also mentioned in this chapter. This chapter also discusses the research gaps in the field of head tracking such as the effect of missing 6-DoF coordinates of the head in both optical and magnetic trackers, which had not been mentioned explicitly in the reported research in this area. Also, efficient algorithms are not reported yet for recovering missing 6-DoF coordinates of the head for both optical and magnetic tracker arising due to situations such as external interferences, movement of head tacker beyond the range of head motion box for which generally such head trackers are designed for aviation applications.

3. HEAD TRACKING METHODS AND RELATED SOFT COMPUTING METHODS

3.1 HEAD TRACKING METHODS

Various kinds of head tracking techniques are used for tacking head motion. This chapter deals with the discussion of five basic head tracking techniques: Electromagnetic head tracking, Optical head tracking, Acoustic head tracking, Inertial head tracking, and Mechanical head tracking.

3.1.1 ELECTROMAGNETIC HEAD TRACKING

Electromagnetic head tracking employs magnetic sensors to update the position and orientation of head movements. They are mounted onto the helmet to determine the position of the head using the strength of the magnetic field. The magnetic field is produced by a set of coils in the cockpit. According to change in a magnetic field, sensor output gets varied followed by necessary computation and processing to determine the position and orientation of head movements [85]. A narrow-band magnetic field transmitter in a cockpit is a common technology for tracking the pilot's Line of sight (LOS) [86]. A common LOS tracker is based on transmitting a narrow band magnetic field within the cockpit area and analyzing the signal received at the helmet to compute the pilot's head orientation in the real-time domain [87]. Magnetic tracking is accomplished by creating a magnetic field that can be sensed by a set of sensors. An assembly of many orthogonal coils, known as a transmitter, generates a low-frequency field. Another sensor is located on the receiver. The receiver senses the changes in the magnetic field caused by movement. These changes are recorded and processed by an algorithm that determines the position and orientation

of the receiver with the transmitter. This position and orientation data are then sent to the computer to update the virtual environment display. Magnetic tracking systems can measure 6-dimensional positions. Accuracy is impaired seriously in magnetic tracking by distortions of the magnetic fields caused by many types of metal items, which are omnipresent within the cockpit area or at real sites [88].

Unfortunately, there is one major disadvantage of magnetic trackers in the form of electromagnetic field itself, which gets distorted by many kinds of metal. Usually, it is impossible to banish all metal from the sphere of influence of the transmitter emitting the electromagnetic field, especially when using a long-range transmitter. Monitors contain coils, walls, ceiling, and floors of the building contain metal trellises and struts, chairs and tables have metal frames, etc. While tracking systems using direct current seems to be somewhat less susceptible to distortion by metal than alternating current systems, all ferromagnetic metal still influence the field generated by the transmitter. Distortion of the magnetic field directly results in mismatches between the tracking sensor's true position (and orientation) and the position (orientation) as reported by the tracking system.

Advantages of magnetic head tracking system:

- Low cost
- No drift
- No lighting conditions and background or line of sight constraints
- Both wireless and wired models, real-time operations

Disadvantages of magnetic head tracking system:

- High latencies due to filtering
- Electromagnetic interference from radio

- Accuracy diminishes with distance
- Ferromagnetic/metal conductive surface causes field distortion [88].

Applications of magnetic head tracking system:

- Biomechanics
- Virtual reality
- Biomedical 3D imaging
- Sport analysis
- Behavior studies
- Simulations and avionics [89].

3.1.2 OPTICAL HEAD TRACKING

It involves the usage of a variety of detectors, from ordinary video cameras to LEDs to detect either ambient light or light emitted under the control of the position tracker. Infrared light is often used to prevent interference with other activities. The optical head tracking system is compacter and lighter than magnetic, immune from cockpit geometry variation, and magnetic field effects. The optical tracker operates using the remote measurement of the head position by the camera. An optical tracking system consists of three subsystems: Optical image system, mechanical tracking platform, and tracking the computer.

1. *Optical tracking imaging:* It converts the detected light variations into measured coordinates through conversion to digital image or measurement of the detected light intensity. Depending upon the design, it can be a digital camera or an Infrared LED source.

2. *Mechanical tracking:* It holds the optical imaging system and manipulates the optical imaging system in such a way it always points to the target being tracked.

3. *Tracking computer:* It captures images from an optical imaging system followed by the analysis of the image to extract the target position. It, thus, controls the mechanical tracking platform to follow the target. The tracking computer has to be able to capture the image at a relatively high frame rate. This posts a requirement on the bandwidth of the image capturing hardware. The other challenge in implementation is that the image processing software has to be able to extract the target image from its background and compute its position.

Advantages of optical head tracking system:

- It provides a high-resolution image of the target being tracked.
- High availability
- Working over a large area
- Fast
- High accuracy
- No magnetic interference problem

Disadvantages of optical head tracking system:

- The high cost of an optical tracking system has made this a limited area of research although, with inexpensive CMOS, it may become more relevant in the near future.
- Visible wavelengths are less optimal.

Applications of optical head tracking system:

- Used to track the various objects including airplanes, launch vehicles, and satellites.

- It had also been used to find space crafts and space debris although it has a disadvantage over radar as it requires objects to be reflecting or emitting sufficient light [90].

3.1.3 ACOUSTIC HEAD TRACKING

This technique uses three microphones and three emitters to compute the distance between a source and receiver via triangulation. The ultrasonic frequency (above 20 kHz) is used so that the emitter will not be heard. Hence, the acoustic tracker uses a triangulation technique that is usually based on sound propagation time. The ultrasonic frequency range is generally used so as not to be audible to people.

Assuming that the speed of sound is known, the delay between sound emission by a speaker, and detection by a microphone yields the distance between speaker and microphone. This assumption can be compromised by changes in the speed of sound due to temperature changes or other atmospheric changes. Distance values from three known fixed receivers (microphones) to a moving speaker allows the emitter (speaker) position to be triangulated. The emitter is usually the moving component since a single emission from one speaker can easily be received by multiple microphones without confusion. Line of sight must always be maintained between the emitters and receivers since it is assumed that sound can follow a straight trajectory between emitter and receiver. Acoustic trackers require line of sight between emitters and receivers, are easily influenced by temperature gradients and air currents, and are subjected to interference from echoes and other acoustic sources, especially in the noisy environment of military aviation. The update rate is limited, primarily by the speed of sound, to about 30 samples/sec. Currently available acoustic tracking devices are not as accurate or dependable as the state of the art magnetic or optical tracking devices, and militarized versions are not currently available. Acoustic devices do

not suffer from metal and electromagnetic interference as do magnetic systems, or from sunlight interference as do optical trackers; but the problems listed above are at least as severe.

Future development of acoustic technologies may solve or reduce the practical problems, but at present both magnetic and optical technologies are significantly more mature and are more likely to find practical use in airborne environments [91].

Advantages of Acoustic head tracking system:

- Inexpensive
- Wide area
- Encumbrance

Disadvantages of Acoustic head tracking system:

- Inaccurate
- Interference
- Requires line-of-sight

3.1.4 INERTIAL HEAD TRACKING

Inertial head tracking utilizes accelerometers and gyroscopes. An inertial tracker involves a set of three orthogonal accelerometers and gyro sensors fixed to the head of the pilot. The orientation of the head is computed by integrating the outputs of the gyro sensors. The outputs of the gyro sensors are proportional to the angular velocity about each axis. The positional coordinates of the head are computed by double integrating the outputs of the accelerometers by using their predetermined orientations.

The inertial sensor is available, which can measure angular velocity and specific force (the vector sum of gravity and acceleration forces) for an inertial stable reference frame.

Methods for the position and orientation tracking with such instruments have been developed for inertial navigation and the same principles can be applied to tracking a person's headgear. If an initial orientation is known, angular velocity can be integrated to continually estimate the orientation angle. Once orientation with respect to gravity is known, gravity can be subtracted from specific force data to yield acceleration with respect to the gravitational field. If an initial position and velocity are known, acceleration can then be integrated to continually estimate the current position and orientation. Inertial sensors measure motion with respect to an inertial stable reference frame; so to measure head motion with respect to an aircraft cockpit, information from an inertial package that is fixed to the airframe must be subtracted from measurements made by the head-mounted package [85, 92].

Inertial sensors provide high bandwidth angular velocity and acceleration information and can provide position and orientation information with very high resolution, but the requirement for frequent drift correction constrains inertial head tracking to use in conjunction with other head tracking techniques. There is currently a commercially available system that uses a combination of acoustic and inertial sensors to measure headgear position and orientation. An early version of that device was described by Foxlin and Durlach [92]. The head-mounted inertial package measures approximately 3.5 cm × 3 cm × 3 cm. The device was not, however, intended for use on an aircraft and the current system makes no provision for subtracting vehicle motion. Inertial sensors, particularly angular rate sensors, have been used quite successfully to add high frequency (lead) information to systems employing other head tracking techniques. For example, Emma and Tachi described an optimal estimation technique for combining inertial angular rate information with magnetic head tracker data [93].

Advantages of inertial head tracking system:

- Inexpensive
- Wide area
- Orientation very accurate
- Minimal interference
- Encumbrance

Disadvantages of inertial head tracking system:

- Position poor
- Need to re-center
- Inaccurate over time
- More drift

3.1.5 MECHANICAL HEAD TRACKING

The change in position is measured by physically connecting the remote object to a point of reference with joint linkages. Mechanical head tracker sometimes referred to as goniometers, work by mechanically coupling headgear to the environment (e.g. airframe) through a set of linkages connected by flexible joints. The position of each joint is measured by a transducer, and the set of joint positions is used to calculate headgear position and orientation in 6 degrees of freedom. Transducers are typically optical encoders, potentiometers, strain gauges, or some combination of these. There is a very small number of commercially available mechanical devices, that are specifically designed to track headgear position and orientation. Many goniometers have been built for use in research and simulation laboratories. The mechanical tracker can have relatively low cost, and are capable of good accuracy, high update rate, a reasonable range for a seated user, and very good dependability; but the mechanical linkage takes up valuable cockpit space, are subject

to mechanical damage, affect inertial forces, and pose a difficult ejection safety problem. Despite excellent performance parameters, future in-flight use of mechanical head trackers is likely to be restricted to the helicopter, transport, or ground-based, applications, and then only when low cost is important. Mechanical trackers will probably continue to be extremely useful as low-cost research and development tools [94].

Advantages of a mechanical head tracking system:

- Accurate
- Fast
- Low lag
- Minimal environmental interference
- No calibration requirement

Disadvantages of a mechanical head tracking system:

- Low range
- Cost
- One tracked point (body/others are hard to track)

In this thesis, head tracking is done using two trackers: Optical and Electromagnetic tracker.

Tracking is to detect the exact position of the HMDs or any other parts of bodies and any object. Tracking can be positional or orientation in terms of coordinates and when both are combined, the system is recognized as six degrees of freedom (6-DoF) system. Directions of head tracking in a 6-DoF system are X, Y, and Z is known as positional coordinates, and Roll, Yaw, and Pitch are known as orientation coordinates.

Magnetic tracking (or electromagnetic tracking) is a technology-based on the principle of electromagnetism used for tracking the head or another part of the body. It is a low-cost

technology, which can render simple and levelheaded accuracy without any hindrance or occult output. It can refract both orientation and positional coordinates by implication of small sensors affixed on any part of the body, object, or helmet of the pilot to perceive a particular set of generated magnetic fields.

The electromagnetic tracking technology is a simple application of orthogonal magnetic fields (either AC or DC). A mutually perpendicular field-generating coil generates the field consecutively that induces some currents to the receiving end of the head tracker. The alterations in induced current are directly proportional to the distance of each particular magnetic coil from the field transmitter setup. The transmitter assembly is customized with three orthogonal sets of coils, which generates a magnetic field when a current is applied. Current is applied to these coils in such a sequence that develops three orthogonal fields during each cycle. Therefore, nine induced currents are generated inside the magnetic sensor coils, which are used to compute the positional, and orientation coordinates of the pilot's head. The workspace of electromagnetic tracking is limited and cannot be more than 5.5 meters.

The optical tracking method includes a prominent and diverging collection of technologies. Currently, vast research is going in this particular area as compared to other tracking technologies. Various factors in optical tracking vary widely like cost and performance. Normally the common attribute is the dependency on the sensing of some particular type of light. The concerned light may or may not be obvious to the human eye. The light source can be the coherent laser, may be produced by the tracking system itself or can be passive. On the detector, side simple video cameras or lateral effect diodes may be indulged. Interference from other light sources is the primary problem in the optical tracking systems

In this chapter, work related to the first two objectives namely: "To analyze the effect of relative placements in terms of orientation and distance of transmitter and receiver sensors

(mounted on cockpit and helmet in single and hybrid mode)" and "To characterize and form the basis of error patterns in terms of latency and positioning accuracy" have been reported and discussed in detail. Artificial Neural Networks [95] can be applied to predict the missing data. In this chapter, the data acquisition process of head tracking from both optical and electromagnetic trackers under different combinations of simulated field operating conditions and their effect on the acquired data is discussed. Prediction of missing data is done using the Self Healing Neural Model (SHNM) [96]. The experimental work reported in this chapter includes a six-degrees-of-freedom (6-DoF) optical tracker **(TrackIR™ 5)** to record the coordinates of the pilot's head motion in real-time on the simulator bed. During the process of acquisition of the coordinates of the head movement by the optical tracker, the data may be missed due to stray light interference or any other kind of occlusion or movement of the head beyond HMB limits. Self Healing Neural Model is a robust model as this model incorporates the concept of dummy neurons to supersede the failed entities sanctioning the system to cerebrate as no failure has occurred. Therefore, to predict the missing data, Self Healing Neural Model (SHNM) was applied to the five different sets with a different number of instances of missing data. The five sets were divided in accordance with the different percentages of missing instances i.e., 1%, 2%, 10%, 25%, and 35%. More than 88% of accuracy was achieved in the prediction of five different sets of missing data. Results are also compared with the Back Propagation Neural Network (BPNN) and Autoregressive Linear Model (ARLM).

3.2 ELECTROMAGNETIC HEAD TRACKING

3.2.1 INTRODUCTION

Electromagnetic tracking is a low-cost technology, which can render simple and level-headed accuracy without any hindrance or occult output. Magnetic tracking can refract both orientation and positional coordinates by implication of small sensors affixed to the helmet of the pilot to perceive a particular set of generating magnetic fields [86, 87]. This 6 DOF electromagnetic technology is a simple application of orthogonal magnetic fields (either AC or DC).

3.2.2 ELECTROMAGNETIC TRANSMITTER

A mutually perpendicular field generating coil generates the field inducing some currents to the receiving end of the head tracker [89]. The alterations in induced current are directly proportional to the distance of each particular magnetic coil from the field transmitter setup. The transmitter assembly is customized with three orthogonal sets of coils, which generates a magnetic field when a current is applied. Current is applied to these coils in such a sequence that develops three orthogonal fields during each cycle. Therefore, nine induced currents are generated inside the magnetic sensor coils, which are used to compute the position and orientation coordinates of the pilot's head. Each of the three emitted magnetic fields develops one induced current in each of three magnetic sensor coils thereby resulting in nine current elements of a rotation matrix affiliated with each sensor. The typical electromagnetic transmitter is shown in Figure 3.1.

Figure 3.1: Electromagnetic Transmitter

3.2.3 ELECTROMAGNETIC RECEIVER

On the receiving end, air-core coils are preferably used over Hall elements as they are inexpensive, linear in nature, and are easy to fabricate [97]. There are other detection methods but the use of air coils is more advantageous due to its small size. The sampling frequency is preferably in the range of 30 Hz to 120 Hz. Despite being rugged and free from errors induced due to stray light in the cockpit of the aircraft, magnetic tracking has a few shortcomings. The typical electromagnetic receiver is shown in Figure 3.2.

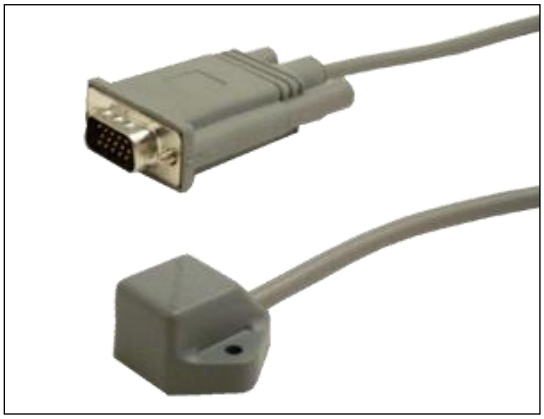

Figure 3.2: Electromagnetic Receiver

3.2.4 FACTORS AFFECTING THE TRACKING OF THE HEAD USING AN ELECTROMAGNETIC TRACKER

A magnetic tracking system gives critically distorted and dislodged positional coordinate information if the sensor is near to any ferromagnetic material. Therefore, preferably the operational area of the aircraft must be designed with non-ferromagnetic material as magnetic tracking systems are enormously sensitive to the ferromagnetic material. The operative range of the magnetic tracking system somehow depends on the nature of the current (AC or DC) used. The magnetic tracking system can be operated using AC or DC current. A magnetic tracking system operated with the direct current has less range but is less prone to field distortion occurred due to eddy currents induced in the ferromagnetic elements when the field is varying. In DC, the field is allowed to generate for a very short span of time in which measurement is to be carried out. This way the effect of eddy currents can be reduced up to some extent. To increase the range of magnetic tracking system alternating current is used. A magnetic field can be amplified when the transmitting coil is operated along with a capacitor and the carrier frequency is clipped to the resonance of the LC circuit. When the magnetic field is high, the problem of inducing eddy currents becomes quite obvious due to ferromagnetic materials near the AC field. As far as the existing technologies are concerned, **Ascension, Inc**. employs direct current (DC) and **Polhemus, Inc.** utilizes alternating current (AC) to generate the field. The flaws of magnetic tracking systems are also dependent on the physical aspects of magnetic fields. The power of a magnetic field is abated in terms of power inversely with the square of the increasing distance between the transmitter and receiver. This can typically happen when the head tracker is moved beyond the permissible limit of HMB for which the magnetic head tracker is designed. This leads the magnetic tracking system to operate in a limited amount of range [98]. But as far as its application in avionics is concerned, the range is not an issue. Apart from these flaws, magnetic sensors also tend to receive noise from

other stray magnetic fields that are generated by other electrical devices in the cockpit, which may include a head-up display, head-down display, monitors, or any other electrical winding. The connecting wires of the magnetic head tracker may also produce a significant unwanted magnetic field, which may degrade the computation of positional, and orientation coordinates.

3.2.5 ERRORS IN ELECTROMAGNETIC HEAD TRACKING

With the recent developments, many techniques have been involved in efforts to palliate the errors related to magnetic tracking systems. The position errors can occur due to the improper acquisition of coordinates of the head due to the presence of any metallic substance leading to ferromagnetism or due to the movement of the head beyond HMB limits for which the magnetic head tracker has been designed. Several attempts have been made to reduce the position errors to improve the tracking accuracy of the electromagnetic head tracker. Position errors were reduced by 79% by Livingston and State in a two-meter sphere surrounding area. They constructed a table, which included 720 valid entries out of 12801 samples. Only positional coordinates were included in the table. Therefore, orientation errors were corrected up to the least extent. However, the table which included both orientation and positional coordinates consisted of 332826 samples in the same surrounding area [98]. Several attempts were made to increase the accuracy by deviating the sampling frequency of the magnetic tracking system, which was relative to the frequencies that occurred due to noise sources in the natural environment. Errors were reduced by sampling at almost twice the carrier frequency of the present electrical power by Nixon *et al* [99]. However, they failed to reduce errors when multiple noise sources were present at different frequencies. The performance of the magnetic tracker depends on various factors. Manufacturers claim latency of the magnetic tracker of the order of 5 ms, but the observed latency is 25-30 ms, and latency is further increased by using the multiple numbers of sensors. As the number of sensors increases,

the update rate of the magnetic tracker may decrease due to multiplexing. Orientation accuracies are claimed from 0.35 to 2.5 inches. In both cases, the values may change to a great degree depending upon the distance between the receiver and transmitter and also the external noise sources present [100]. Position tracking is somehow a challenging task in magnetic tracking [101]. As proved by Skopowski, magnetic trackers lacked the accuracy to use them as true 6 DOF trackers [102, 103]. These limitations can be avoided by using other tracking technologies or using hybrid-tracking technology. The errors in tracking are discussed in detail in Chapter 5.

3.2.6 AVAILABILITY OF ELECTROMAGNETIC TRACKERS

There are different types of electromagnetic trackers available with different manufacturers for electromagnetic tracking. Each tracker has different specifications in terms of the degree of freedoms (DoF), different workspace, frame rate, number of receiving sensors, latency, acquisition speed, power supply, and weight of the tracker. From the trackers mentioned in Table 3.1, Polhemus Patriot electromagnetic tracker is chosen in this work due to its maximum DoF, number of sensors, low power supply, and minimum cost. The Survey of commonly available electromagnetic trackers other than the Polhemus Patriot electromagnetic tracker with their technical specifications is discussed in Table 3.1.

Table 3.1: Survey and Technical Specifications of Electromagnetic Trackers

V_R	M_L	DOF	NOS	U_R	S_A (RMS)		L_Y	R_N	O/P			Interface	OS	
					P_{Coor}	O_{Coor}			PCC	EA	QO		Win	Linux
VR-Space	WinTracker III	6	3	30 outputs/Sec (with 3receivers)	0.06”	0.3°	7ms	0.01cm, 0.01°	✓	✓	✓	USB	✓	✓
Polhemus	PATRIOT	6	1-2	60 Hz per sensor	0.1”	0.75°	18.5ms	0.0038cm , 0.01°	✓	✓	✓	USB and RS-232	✓	×
Polhemus	PATRIOT Wireless	6	1-4	50 Hz per sensor	0.3”	1°	20ms	0.005cm, 0.005°	✓	✓	✓	USB and RS-232	✓	×
Polhemus	G^4	6	1-3	120 Hz per sensor	0.5”	1°	≈ 10ms	---	✓	✓	✓	RF link	✓	×
Polhemus	FASTRAK	6	1-4	120 Hz per sensor	0.03”	0.15°	4ms	0.000508 cm, 0.025°	✓	✓	✓	USB and RS-232	✓	×
Polhemus	LIBERTY	6	1-16	240 Hz per sensor	0.03”	0.15°	3.5ms	0.000381 cm, 0.0012°	✓	✓	✓	USB and RS-232	✓	×
Polhemus	LIBERTY LATUS	6	1-16	94 Hz per sensor	0.1”	0.5°	5 ms	0.00508c m, 0.005°	✓	✓	✓	USB and RS-232	✓	×
Ascension Technology Corp	driveBAY	6	1-4	420 Hz per sensor	0.055”	0.5°	---	0.1397cm , 0.005°	✓	✓	✓	USB	✓	×
Ascension Technology Corp	trakSTAR	6	1-4	420 Hz per sensor	0.055”	0.5°	---	0.050 cm, 0.1°	✓	✓	✓	USB and RS-232	✓	×

V_R = Vendor, M_L = Model, DOF = Degree of Freedom, NOS = Number of sensors, U_R =Update Rate, S_A(RMS) = Static Accuracy, P_{Coor} = Positional coordinates, O_{Coor} = Orientation coordinates, L_Y = Latency, R_N = Resolution, O/P = Output, PCC = Positional Cartesian coordinates, EA = Euler angles, QO = Quaternion orientation, USB = Universal Serial Bus, OS = Operating System, Win = Window

3.2.7 RELATED WORK OF ELECTROMAGNETIC HEAD TRACKING

In avionics, helmet-mounted display (HMD) is an important system to deliver feedback regarding the aircraft flight control system as well as the external environmental factors. The HMD allows the pilot to acquire more situational awareness and can also help the weapon system of the plane in setting the target in accordance with the direction of the head of the pilot. To get the proper view in the visor of HMD, it is necessary that tracking of the head of the pilot should be nearly accurate. Head tracking is a pivotal part of HMD [5, 104] used in aviation and virtual reality (VR) used in flight simulators.

Tracking is the process of synchronizing the coordinates of the environmental scene (both with and without moving objects) in real-time. Various techniques are utilized for pose estimation of the head such as electromagnetic tracking, inertial tracking [105], and optical tracking [106]. The 6-DoF data acquired in all the techniques are a combination of positional coordinates **(X-axis, Y-axis, and Z-axis)** and angular or orientation coordinates **(Yaw angle, Pitch angle, and Roll angle)** Electromagnetic tracking employs the use of electromagnetic field [107, 108] generated by the transmitting coil and the electromagnetic disturbance produced due to change in slight head position is detected by the sensing coils placed on the helmet/head of the pilot.

Various methods of head tracking are present, but very little emphasis is laid to eradicate the problems arising due to missing data [109, 110]. Hagedorn *et al.* [111] described a method for calibration of the tracking technique through the electromagnetic method. Both positional and orientation errors were induced using different interpolation methods.

In these related works of head tracking, no method related to the recovery of missing or corrupted 6-DoF data is discussed. In this thesis, due to no problem of occlusion and high update

rate, a magnetic tracker **(Polhemus Patriot^{TM})** is used to acquire the data of head movement. A set of transmitting and sensing coils is used in the magnetic tracker [112]. The transmitter end is stationary and the sensing coil is fixed on the of the pilot's head. The detail of the setup is discussed in Figure 3.3, Figure 3.4, and Figure 3.5. The number of sensing coils can be 1-3. However, due to the presence of ferromagnetism and metal conduction arising due to movable seats, instruments panel, overhead panel, and side consoles in the cockpit, a substantial amount of interference is created. This hinders the acquisition of 6-DoF data of the pilot's head through the magnetic tracker, which may lead to the missing values of the 6-DoF data [113]. The prediction of missing data using the Self Healing Neural Model (SHNM) will be discussed [96]. The results of SHNM are also compared with the results obtained by BPNN [114, 115].

Head tracking has various applications apart from avionics. HMD equipped with a head tracker can be used in the teleoperation of the search and rescue robot, where the camera embedded onboard in the robot follow the head movements of the operator to control the motion of the robot thus rendering an immersive sensation to the operator [116]. An interface is proposed where the HMD is used in tele-surveillance using an Unmanned Air Vehicle (UAV). Head tracking is used to pilot the blimp by controlling it through the head's movement. A vibrotactile belt is also used to experience the effect of wind increasing the feeling of telepresence [117].

The head tracking is also used to control the movements of an AIBO's robot camera. The orientation of an AIBO's camera can be controlled through the head pose of the operator. This application also leads to the generation of panoramic images from overlapping snapshots captured by AIBO's robot camera [118].

Head tracking is also used to design the driver assistance system to understand the driver's focus of attention during driving. This can help in avoiding the automotive collision caused due

to driver distraction and negligence during driving. To avoid collision hybrid head orientation and position estimation (HyHOPE) system is designed using a single video camera and a 3D tracking algorithm to track the 3D motion of the driver's head [119]. For simulation purposes, a simulator bed with multiple GUI monitors can be designed in which a methodology can allow a user to operate all the monitors by combining mouse input and head tracking. The user can select a particular monitor by moving the head, allowing the user to carry out seamless simulations [120]. For all these applications, the coordinates of the head must be acquired correctly. Every tracking technology has some limitations. The operation of an optical tracker is dependent on the line of sight, which means if an occlusion occurs the acquisition of coordinates of the head may get missed. Similarly, due to drift errors, an inertial tracker may suffer from improper data acquisition, which may lead to the missing data. In the case of electromagnetic tracking, ferromagnetism causes inaccurate head tracking.

3.3 OPTICAL HEAD TRACKING

3.3.1 INTRODUCTION

As discussed above, optical tracking is a 3D localization technology utilizing two or more optical sensors. The optical tracking method includes the prominent and diverging collection of technologies. Currently, vast research is going in this particular area as compared to other tracking technologies. Various factors in optical tracking vary widely like cost and performance [102]. In an optical tracking technique, the head of the pilot is equipped with retro-reflective markers, which reflect the incoming infrared light back to the camera [121]. The camera detects the infrared reflections, which are further processed by the optical system internally. The internal system of the optical tracker calculates the 2D marker position in image coordinates. Normally the common attribute is the dependency on the sensing of some particular type of light. The

concerned light may or may not be obvious to the human eye. The light source can be the coherent laser or may be produced by the tracking system itself or can be passive. On the detector side, simple video cameras or lateral effect diodes may be indulged. Interference from other light sources is the primary problem in optical tracking systems. Other limitations in the optical tracking system depend upon the type of light source used. The optical tracking system essentially comprises optical transmitters and optical receivers.

3.3.2 OPTICAL TRANSMITTER

An optical transmitter consists of an infrared camera or a light source, which acts as a source to generate the infrared (IR) light. In this work, **the TrackIR^{TM} 5** optical tracker has been used to track the coordinates of the head.

Figure 3.3: Optical Transmitter

The optical transmitter shown in Figure 3.3 generates an infrared light, which is detected by the optical receiver as shown in Figure 3.4.

3.3.3 OPTICAL RECEIVER

The optical receiver, as shown in Figure 3.4, is embedded with three retroreflectors, which receives the incoming infrared light from the optical transmitter and reflects the same through

retroreflectors to the transmitter. This method helps to track the actual coordinates of the object to be tracked. The field of view (FOV) of the tracker is approximately 52°.

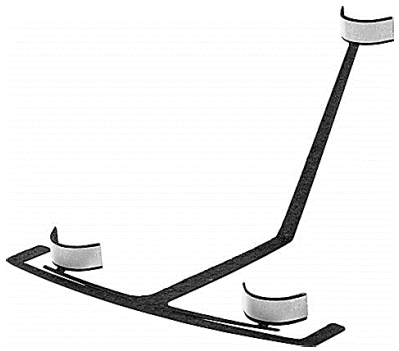

Figure 3.4: Optical Receiver with Retroreflectors

3.3.4 TRACKING SCHEMES OF OPTICAL TRACKING

An optical tracking system is a pattern recognition technology, which has different schemes as discussed in this section.

3.3.4.1 Outside-In

In this tracking technology, as shown in Figure 3.5, the sensors are fixed and stationary while emitter, which themselves are infrared LEDs, and are allowed to move. The sensors sense the light in the working volume. Mostly, the optical trackers used are outside-in. Using 2D sensors, a minimum of two outside-in sensors can be employed to triangulate the position of the target. For 1D optical sensors, a minimum of three sensors is required to detect the target. For tracking orientation coordinates using outside-in trackers, it must detect the positions of the three-point target. This scheme is used in the experimental work mentioned in this thesis to track the coordinates of the head. In the experiments conducted in optical tracking, the Outside-In tracking scheme is used with one optical tracker as a transmitter as shown in Figure 3.3 and a tracker clip embedded with three retroreflectors in it as a receiver as shown in Figure 3.4.

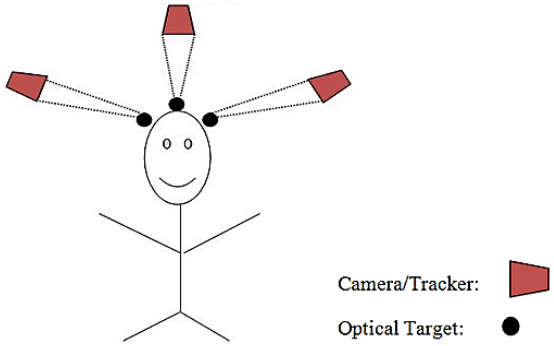

Figure 3.5: Outside-In tracking scheme

3.3.4.2 Inside-Out

In this technology, the sensors are mounted on the pilot's head and the optical targets are fixed to the cockpit as shown in Figure 3.6.

In the Inside-out technique, even a small rotation in the head will lead to the movement of LEDs on the ceiling in the image range of cameras. However, this technology is not suitable for use in the cockpit because the large array of infrared LEDs is required as its targets and reflections of cockpit screens can cause errors in the fields of view.

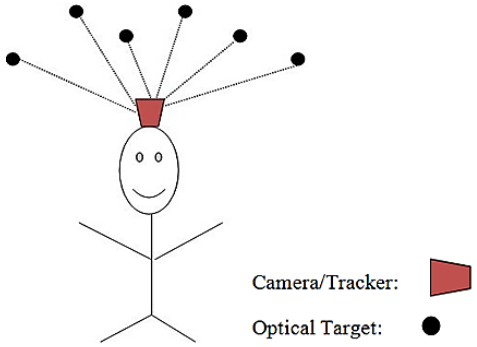

Figure 3.6: Inside-Out tracking scheme

In both technologies, orientation and positional coordinates are determined. There is a small advantage in accuracy in outside-in technology: Small movement in sensor actuates relatively ample shifts in the apparent position of the emitters. The Hi-ball tracker is an inside-out optical tracking technology designed for head tracking. It implements a large number of infrared LEDs as

emitters mounted on the ceiling. The Hi-ball tracker comprises six lenses and six photodiodes, which are organized in such a way that each diode can detect LEDs through the lenses. By sequentially turning the LEDs on and off, it is determined which LEDs are in view of each of the photodiodes, that ultimately detect the position and orientation of the head. Accuracy in the position is high up to 0.5 mm and orientation is obtained within 0.05 degrees. The update rate as claimed by the manufacturer is more than 2000 Hz with a latency of 12 ms [122]. Dependencies on the specially prepared ceiling and incapability to track in all orientations are the primary drawbacks of inside-out optical head tracking technology [123, 124]. To implement the outside-in optical head tracking system in an aircraft cockpit, Honeywell LED array helmet tracker was designed [125, 126]. It implements an array of four LEDs mounted on the helmet, which are tracked by an infrared camera. From the four LEDs, the head positional coordinates and orientation can be calculated [127-129].

3.3.4.3 Inside-Outside-In

This technique uses both outside-in and inside-out schemes as shown in Figure 3.7. It provides orientation and position tracking with high accuracy, even with low-resolution optical trackers. Using this technique, the field of view is high and high performance can be obtained in all 6 degrees of freedom. The benefit of this mixed strategy is the less head-mounted weight, which includes a single optical tracker and lens. Both trackers and sensors can be fused into the small CMOS module [130, 131].

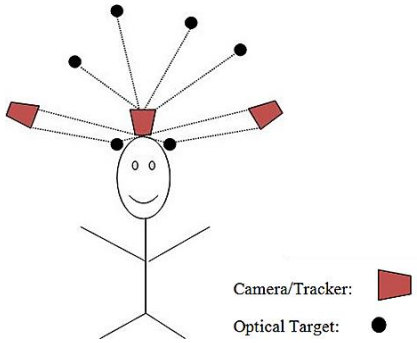

Figure 3.7: Inside-Outside-In tracking scheme

3.4 AVAILABILITY OF OPTICAL TRACKERS

There are different types of optical trackers available with different manufacturers for optical tracking. Each tracker has different specifications in terms of the degree of freedoms (DoF), different workspace, frame rate, FOV, latency, acquisition speed, power supply, and weight of the tracker. The TrackIR^{TM} 5 is chosen in this work due to its appropriate working distance according to the area of cockpit simulator, maximum DoF, appropriate FOV, low power supply, and low cost. The survey of commonly available optical trackers other than TrackIR^{TM} 5 with their technical specifications is discussed in Table 3.2.

Table 3.2: Survey and Technical Specifications of Optical Trackers

V_R	M_L	DOF	F_R	W_D(Mts.)	FOV		A_C (mm)	A_{Speed}	L_y (ms)	Power supply	Power	W_t(gm)
					H	V						
Atracsys	easyTrack 500	NA	NA	3	---	---	0.02	4 LED/ms	10	240V/110V	5V,4W	1600
OptiTrack	Prime 41	NA	180FPS	30.5	51°	51°	---	0.01 ms	5.5	GbE, PoE+	15W	1450
Advanced real time tracking	ARTTRACK 2	6	60FPS	4.5	88°	58°	---	---	---	12V	15W	960
Advanced real time tracking	ARTTRACK 3	6	60FPS	7	88°	58°	---	---	---	48V	35W	1500
Advanced real time tracking	ARTTRACK 5	6	150 FPS	7.5	98°	77°	---	---	---	GbE, RJ45, PoE+	25.5W	950
Advanced real time tracking	TRACKPACK	6	60 FPS	3	95°	72°	---	---	---	12V	6W	410
Advanced real time tracking	TRACKPACK/ IS	6	60 FPS	2.5	72°	58°	---	---	---	12V	6W	840
NDI	Optotrak Certus	6	150 FPS	7	---	---	0.1mm	---	52	100-240V	---	18000
Origin Instruments	DynaSight	3	65 FPS	5	75°	75°	2mm	---	9-28	15V	---	---

V_R= Vendor, M_L= Model, DOF= Degree of Freedom, F_R= Frame Rate, W_D= Working Distance in meters, FOV= Field of View, H= Horizontal, V= Vertical, A_C= Accuracy in millimeter, A_{Speed}= Acquisition Speed, L_Y= Latency in milli secs, W_t= Weight in grams

3.5 GENERAL METHODS OF SOFT COMPUTING

Soft Computing is an emerging method of computing, which combines the ability of the human mind to reason, train, and learn in an environment of uncertainty and imprecision in a single framework. It is the fusion of different methodologies, which are designed to model and enable to find solutions to real-world problems, which are very difficult to model in mathematics. Soft computing can evolve its programs and have characteristics of approximation. Neural Networks, Support Vector Machines (SVM), Machine Learning, Back Propagation Neural Networks, and Adaptive Neuro-Fuzzy Inference System (ANFIS) are the basic methods of soft computing.

1. **Neural Networks:** A neural network is a collective network of neurons, famously known as an artificial neural network, composed of artificial neurons or nodes. In a better sense, a neural network can be a biological neural network, comprised of real biological neurons, or an artificial neural network, for solving artificial intelligence (AI) problems [132]. Weights are modeled by the connections of the biological neuron. The excitatory connection is represented by the positive weight and inhibitory connections are represented by the negative value of weight. Modifications of all the inputs in a neural network are modified by weight and are summed up, which is known as a linear combination. In the final step, the amplitude of the output is controlled by an activation function. These artificial networks may be used for predictive modeling, adaptive control, and applications where they can be trained via a dataset. Self-learning resulting from experience can occur within networks, which can derive conclusions from a complex and seemingly unrelated set of information [133].

2. **Support Vector Machine:** Support Vector Machine (SVM) is a machine-learning algorithm that can be supervised and can be used for both classification or regression challenges.

However, it is mostly used in classification problems [134]. In this algorithm, each data item is plotted as a point in m-dimensional space (where m is the number of features you have) with the value of each feature being the value of a particular coordinate [135]. Then, the classification is performed by finding the hyperplane that differentiates the two classes very well as shown in Figure 3.8

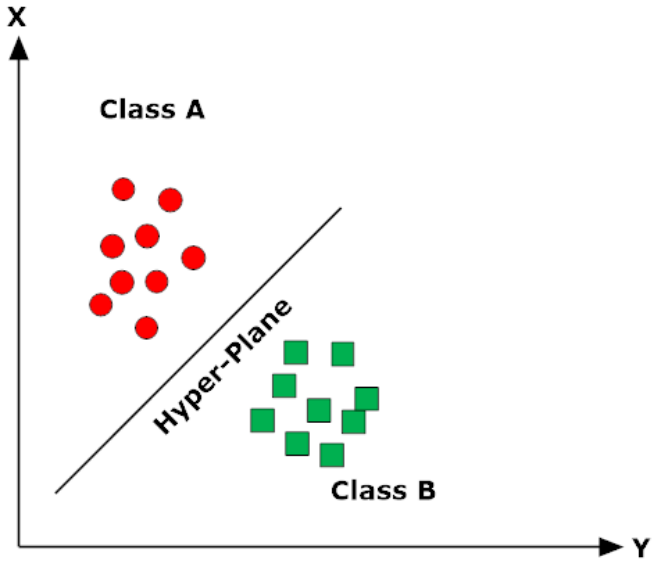

Figure 3.8 Classification in Support Vector Machine

3. Machine Learning: Machine learning is a set of algorithms that parse data and learn from the data to make informed decisions and it follows the function that is learned from the data [136]. However, in the case of prediction at some point machine-learning algorithm will give an inaccurate outcome. Some manual adjustments would be needed to get the desired result. The decisions made by machine learning are based on what it had learned only [137].

4. Back Propagation Neural Network: Backpropagation is a method used in artificial neural networks to calculate a gradient that is needed in the calculation of the weights to be used in the network for the prediction [138]. It is a generalized delta rule to multilayered feedforward

networks, which was made possible by employing the chain rule to iteratively compute the gradients for each layer. Backpropagation is a special case of a more general technique called automatic differentiation [139].

5. Adaptive Neuro-Fuzzy Inference System: An adaptive neuro-fuzzy inference system (ANFIS) is a Takagi–Sugeno fuzzy inference system based artificial neural network. ANFIS was developed in the early 1990s. It is a blend of neural networks and fuzzy logic principles and has the potential to capture the benefits of both in a single framework [140]. Its inference system corresponds to a set of fuzzy IF-THEN rules that have the learning capability to approximate nonlinear functions. Therefore, ANFIS can be termed as a universal estimator [141].

3.6 REGRESSION TECHNIQUE FOR PREDICTION

In statistical modeling, regression analysis is a set of statistical processes for estimating the relationships among variables. It includes many techniques for modeling and analyzing several variables. The popular regression technique used to predict data is Autoregressive Linear Model.

Autoregressive Linear Model: An autoregressive (AR) model is used to describe certain time-varying processes in prediction and is a representation of a type of random process [142]. The autoregressive model specifies that the output variable depends linearly on its previous values, thus the model is in the form of a stochastic difference equation. In machine learning, an autoregressive model learns from a series of timed steps and takes measurements from previous actions as inputs for a regression model to predict the value of the next time step [143].

3.7 CONCLUSION

In this chapter, different kinds of tracking techniques are presented. The trackers discussed are mechanical, acoustic, optical, electromagnetic, and inertial head trackers. Electromagnetic and optical trackers are more robust, lightweight, accurate, and cost-effective trackers as compared to the other three trackers. Factors affecting the tracking of the head using an electromagnetic tracker and optical tracker are also discussed. The survey and technical specifications of both electromagnetic trackers and optical trackers are also discussed in this chapter. Various tracking schemes of the optical tracker are presented in this chapter. The outside-in scheme is used in the experimental work to track the 6-DoF head coordinates. In the experiments conducted in optical tracking, the Outside-In tracking scheme is used with one optical tracker as a transmitter and a tracker clip embedded with three retroreflectors in it as a receiver. Finally, general methods of soft computing for the prediction of data are also discussed. Neural Networks, Support Vector Machines (SVM), Machine Learning, Back Propagation Neural Networks, and Adaptive Neuro-Fuzzy Inference System (ANFIS) are the basic methods of soft computing. The SHNM and BPNN methods have been chosen for prediction of missed head tracking data due to advantages in these algorithms such as handling large data sets, prediction accuracy,s and are well-established methods. The ARLM is also considered because of its simplicity to handle large data sets. The ANFIS is also considered for data prediction owing to its advantage of handling small data sets with good accuracy.

4. SOFT COMPUTING METHODS FOR PREDICTION OF MISSING DATA

This chapter covers the discussion about the objective "Development of fuzzy logic and artificial neural network-based soft computing method for optimization of head tracking position estimation and latency reduction".

There are several problems in head tracking regarding inaccuracy and interferences. Head Motion Box (HMB) which is the permissible range of head motion of the pilot using the head-mounted display in the cockpit during flight or training. In electromagnetic tracking, the major source of interference is ferromagnetism and motion of head exceeding the limit of HMB in the cockpit. Similarly, in an optical tracker, the tracking is hindered by stray light interference, improper placement of the transmitter in the cockpit while the range of HMB can also affect the orientation as well as translational coordinates of the head motion. Therefore, for proper tracking of the head motion, the missing 6-DoF head coordinates are predicted using neural techniques. In this work, Self Healing Neural Model is used to predict the data as SHNM utilizes the recuperation process in a separate routine than the authentic reading module. The prediction results obtained using SHNM are compared with Back Propagation Neural Network and Auto-Regressive Linear Model. The missing 6-DoF head coordinates are also predicted using ANFIS which is discussed in the next chapter.

There are possible techniques, which can be used to predict the missing instances of the head as shown in Figure 4.1.

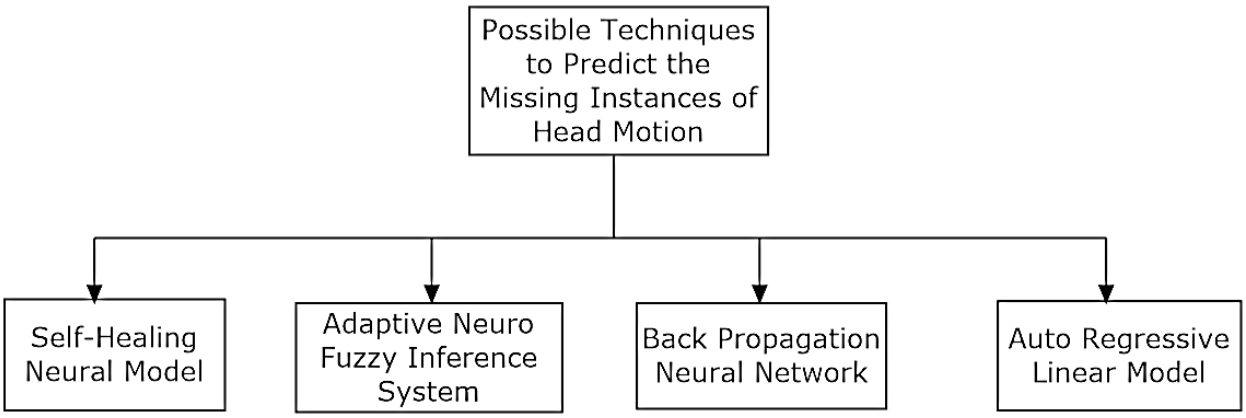

Figure 4.1: Different techniques to predict the missing instances of head

4.1 SELF HEALING NEURAL MODEL

Classification of the problem: The proposed work is modeled around the data, classified into a series of components, which include X, Y, and Z coordinates and Yaw, Pitch, and Roll. The data is directly available from the sensors, which is a certain stance of failures or gap may produce missing or erroneous values that have to be replaced for better predictability.

Prediction with SHNM: The time of prediction is accounted based on a threshold percentage up to which no effect is considered on the overall performance of the system. For example after x % of missing values, the system does not provide correct observations, thus, as soon as the system reaches this threshold, the SHNM is invoked to recover the missing values. The time moment of prediction is based on the instance when a given percentage of missing data is encountered for any of the parameters. For threshold taken the minimum number of missing instances (1%) has been taken into account. The missing data is to be predicted from the past data, which includes the interpolation method. The extrapolation method is not used, so there will be no temporal complexity. The method used is not in real-time as the core functionality of the Self Healing Neural Model involves the fortification for continuous operations of the system that has certain failures

associated with the run time or in the observed data. This model incorporates the concept of dummy neurons to supersede the failed entities sanctioning the system to consider as no failure has occurred. Due to this concept, the recovery of missing data is done with higher accuracy than the conventional methods of data prediction like Back Propagation Neural Network and Auto-Regressive Linear Model. The results obtained in SHNM are also better than ANFIS as it produces less accurate results in the prediction of missing 6-DoF head coordinates in the large data set. However, this model has a feature of generating the values, which otherwise would have been engendered by the genuinely operating entity in the defined system. A similar concept is adopted and applied to identify the missing values in the case of head tracking. This model is invoked as soon as some missing data is accounted for in available data or the input system. Once the model reads the missing contents and its configurations are defined, a certain number of dummy neurons are induced which operates towards the generation of missing data. The thresholds can be set to circumscribe the range of values. Moreover, this model can be modified to apply to authentic-instances as well as offline content. However, in the case of authentic-time, the overheads can be an issue, which needs to be tackled. At present, this issue is resolved by a non-localized parallel run of the algorithm, which utilizes the recuperation process in a separate routine than the authentic reading module. The six-dimensional data with missing instances are given as input in an autoregressive approach. LM model is used in the standard SHNM for training.

The proposed model is used to predict the missing number of instances. The model, when it is subjected to missing instances, identifies the data loss, regulates its feedback and learning rate, and then finally converges to heal the overall data set for prediction [96]. The healing function, which is governed by the constraints, controls the healing process. This will be explained in this chapter. The operational view of the Self Healing Neural Model is described in Figure 4.2. The model

comprises the ‘k’ number of the total number of instances of 6-DoF data initially configured to provide the correct sequence of coordinates of motion of the head. Further, the system is affected by missing data due to some random interference denoted by E. The decision to remodel the network or to use it with missed data for the remaining (k-E) 6-DoF data is taken by the healing model. Also, the healing range of the whole SHNM network is considered by the model, and if it is applicable the network gets healed by recovering the whole network by the formation of dummy-neurons. This method of decision, modification, and recovery is known as Decide and Recover system.

The main motive of the SHNM is to balance the neural network without affecting its feedback and learning rate. E is the total number of instances and $k - E$ is the number of missing instances.

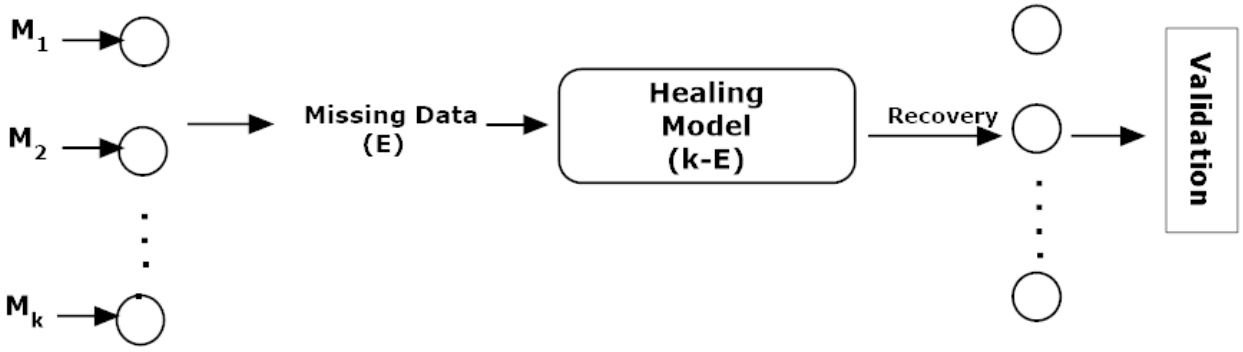

Figure 4.2: Operational view of Self Healing Neural Model for the prediction of missing coordinates

The internal working of the healing phase of the Self Healing Neural Model is shown in Figure 4.3.

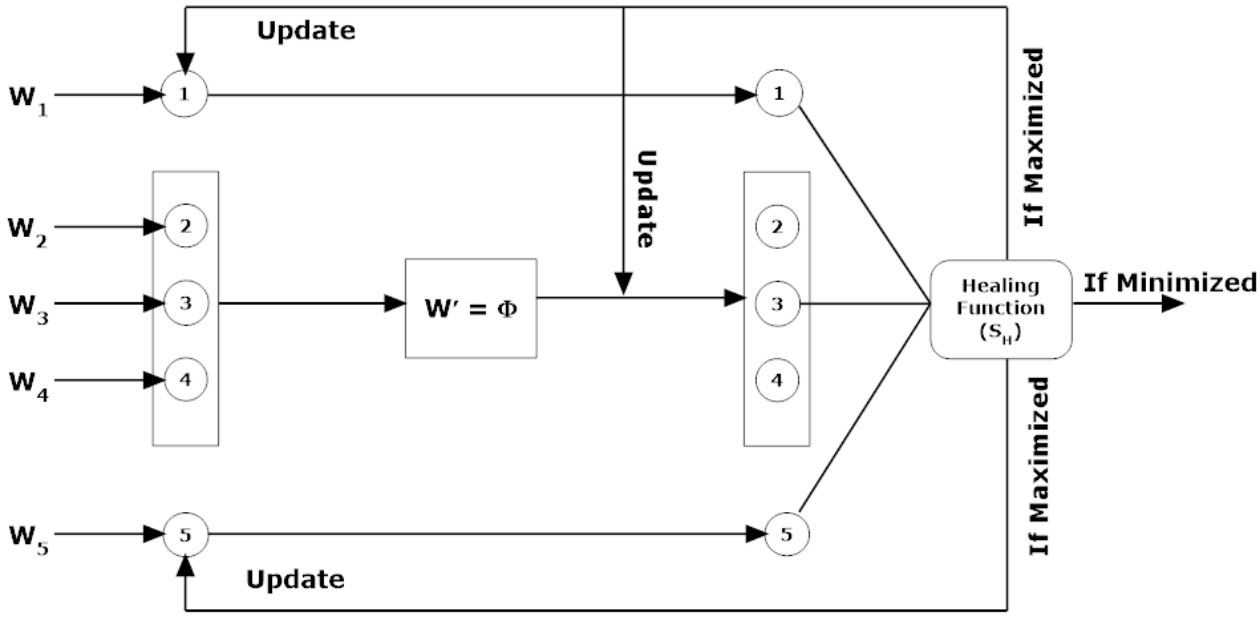

Figure 4.3: Operation of the healing phase in Self Healing Neural Model

4.1.1 BACKGROUND OF SELF HEALING NEURAL MODEL (SHNM)

This method provided a stabilized state with high accuracy and lesser errors during recovery in case of network failures among the UAVs [96]. This methodology provides the possibility to validate the recovery of missing values in an optical and electromagnetic head tracking system. It provides the facility of using "Dummy Neurons" for the missing values whereas the other neural models [144] do not explicitly deal with the recovery of missing values. A cost of healing function S_H is used which is given by Equation (4.1).

$$S_H = \left(\sum_{i=1}^{S_T} e^{\sqrt{\frac{1}{k}\sum_{j=1}^{k}(W_j - W_a)^2}} + \sqrt{\frac{1}{S_T}\sum_{j=1}^{S_T}(E_j)^2} \right) \qquad (4.1)$$

where $'k'$ is the total number of instances in the data set, $'S_T'$ is the number of available data sets with the same number of instances, $'W_j\,'$ is denoted as the weight of the neural network, $'W_a\,'$ is

the average weight, $'E_j'$ is the number of missing instances in the given data sets, $'i'$, and $'j'$ are the number of iterations in the experiment for the corresponding variables. The first part of the equation considers the weight-based derivation of the available values, whereas the second part of the equation accounts for the missing value in the dataset (metric) used to calculate the healing function. This function is repeated for every variable and recovery is performed separately for different parameters. The missing data is denoted by dummy neurons, which was further predicted by the healing function Equation (4.1). Time constraint is eliminated from the equation applied in the proposed system Equation (4.1) unlike used in SHNM. Figure 4.4 shows the basic flowchart in which the working of the Self Healing Neural Model is discussed.

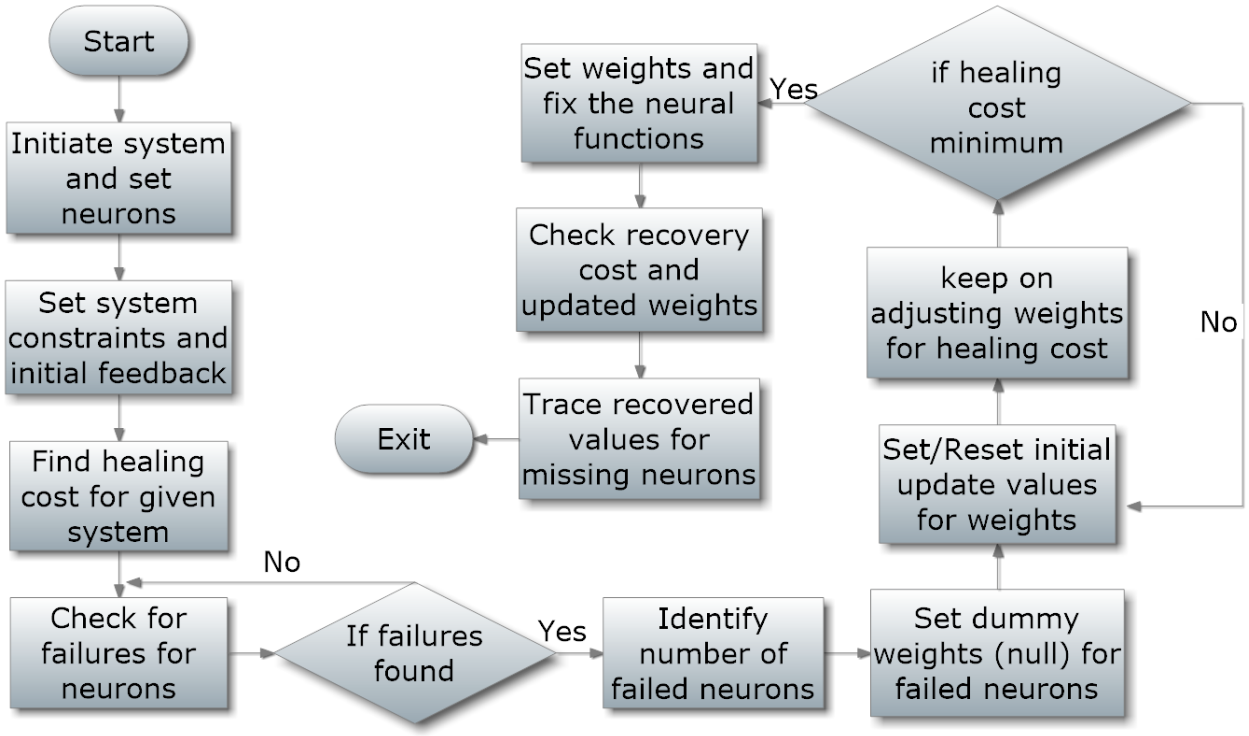

Figure 4.4: Flowchart of the working of Self Healing Neural Model

4.2 ADAPTIVE NEURO-FUZZY INFERENCE SYSTEM

Adaptive Neuro-Fuzzy Inference System (ANFIS) is a technique having many applications including prediction. In 1993, Jang introduced the adaptive neuro-fuzzy inference system (ANFIS) [145]. According to the author, the working and functionality of the ANFIS are similar to that of Takagi-Sugeno type inference model. ANFIS has become a very popular, effective, and efficient modeling technique. It combines the pre-established artificial neural networks (ANNs) learning laws and fuzzy logic theory in the common framework of adaptive networks. The most popular application of fuzzy logic theory is Fuzzy inference systems (FIS). The membership functions are adjusted manually by trial and error method in fuzzy inference systems [146]. The ANNs, which can learn, performing like a black box, means that the model designers cannot discover how the model achieved its output. However, the FIS model performs like a white box, regarding the achievement of the output. In ANFIS, the application of the ANN technique for the development of the parameters of the fuzzy model allows the user to learn from a given set of training data similar to ANN. Simultaneously, the final solution mapped out into the fuzzy model can be represented and illustrated as a collection of IF-THEN rules.

The architecture of ANFIS is shown in Figure 4.5. Five layers are used in the construction of the model. Each layer consists of different nodes described by the node function. Fixed nodes, which are denoted by circles, represent the sets of parameters that are fixed in the model. Conversely, adaptive nodes that are denoted by the squares represent the sets of parameters and these are adjustable in these nodes.

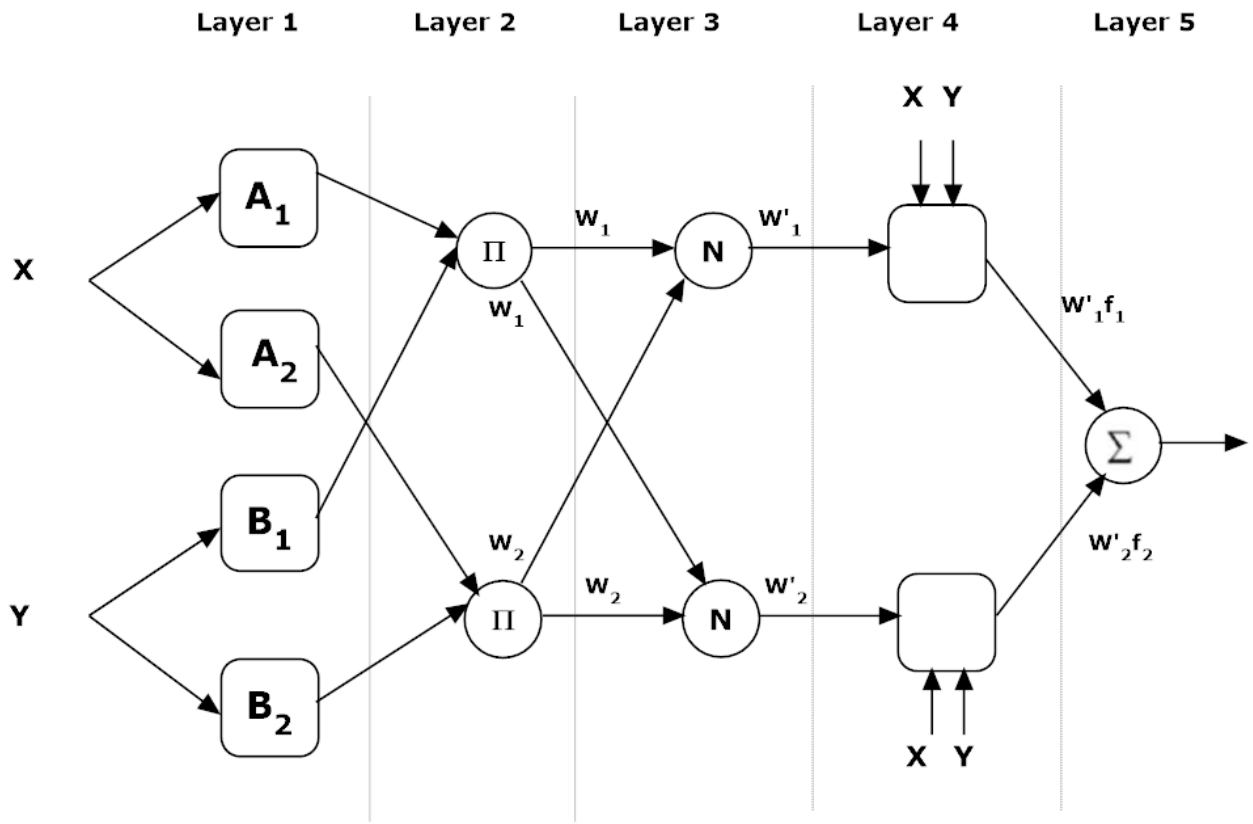

Figure 4.5: Basic structure of ANFIS

The structure of ANFIS includes five layers that can be explained as follows, where O_i^j represents the output of the i[th] node and the j[th] layer.

Layer 1: In this layer, each node represents a node function represented by Equations (4.2) and (4.3)

$$O_i^1 = \mu_{A_i}(x) \; for \; i = 1, 2 \qquad (4.2)$$

$$O_i^1 = \mu_{B_{i-2}}(y) \; for \; i = 3, 4 \qquad (4.3)$$

where x and y are the input to the node i, A_i and B_i are the linguistic labels associated with the membership functions μ_A and μ_B respectively. The Gaussian membership function by the

$$\mu_{A_i}(x) = e^{-\left((x-b_i)^2 / 2a_i^2\right)} \qquad (4.4)$$

$$\mu_{B_i}(y) = e^{-\left((y-b_i)^2 / 2a_i^2\right)} \qquad (4.5)$$

Layer 2: Each node in this layer is a fixed node, which is marked by a circle and labeled by Π. The node function is to be multiplied by input signals to serve as an output signal as given by Equation (4.6)

$$O_i^2 = w_i = \mu_{A_i}(x) \,.\, \mu_{B_i}(y), \qquad for\ i = 1, 2 \qquad (4.6)$$

where O_i^2 is the output of layer 2. The firing strength of the rule is represented by the output signal w_i.

Layer 3: Each node in this layer is a fixed node, which is marked by a circle and labeled by $'N'$. The node function $'N'$ is to normalize the firing strength by the computation of the ratio of the i^{th} node firing strength to the firing strength of the sum of all rules as represented by Equation (4.7)

$$O_i^3 = w_i' = \frac{w_i}{w_1 + w_2} \qquad for\ i = 1, 2 \qquad (4.7)$$

Where O_i^3 is the output of Layer 3. Normalized firing strength is denoted by the quantity $'w'$'

Layer 4: Each node in this layer is adjustable, which is marked by a square. The node function is given by Equation (4.8)

$$O_i^4 = w_i' . f_i \qquad for\ i = 1, 2 \qquad (4.8)$$

where f_1 and f_2 are fuzzy if-then rules given by:

- Rule 1: IF x is A_1 and y is B_1, THEN $f_1 = p_1x + q_1y + r_1$
- Rule 2: IF x is A_2 and y is B_2, THEN $f_2 = p_2x + q_2y + r_2$

Where p_i, q_i and r_i are a consequent set of parameters.

Layer 5: Each node in this layer is fixed which is marked by the circle and labeled by Σ, along with the node function to compute the overall output given by Equation (4.9)

$$O_i^5 = \sum_i w_i' . f_i = \frac{\sum_i w_i f_i}{\sum_i w_i} = f_{out} = Overall\ Output \qquad (4.9)$$

The working scheme of ANFIS is different from neural and regression techniques. Its working is based on fuzzification and defuzzification of the data. In this thesis, the ANFIS is used to predict missing 6-DoF head coordinates.

In this section, the prediction of missing head coordinates in the small dataset (400 instances of the head coordinates) is described. The data set is divided randomly as 70% for the training and 30% for the testing. Table 4.1 shows the specifications of the ANFIS model used for the prediction of the missed head coordinates.

Table 4.1: Specifications of the Adaptive Neuro-Fuzzy Inference System Model

Parameter	Description/Value
Structure of FIS	Sugeno
Initial FIS for training	genfis1 (grid clustering)
Type of Input Membership function	Gaussian
Type of Output Membership function	Linear
Number of inputs	5
Number of outputs	1
Number of input membership functions	3,3,3,3,3
Optimization method	Hybrid
Training epoch number	100

According to Table 4.1, the structure of the ANFIS is Sugeno type. The choice of the type of input and output membership functions and the number of the input membership function is determined through trial and error. The prediction of missed head coordinates is discussed in this section using a small data set (400 instances). The figures consisting of a comparison of the prediction of missed head coordinates using ANFIS, Back Propagation Neural Network, and Self-healing Neural Model are shown in Appendix C of this thesis.

Figure 4.6 shows the Fuzzy logic designer for prediction using ANFIS. The type of input membership functions shown in Figure 4.6 is Gaussian.

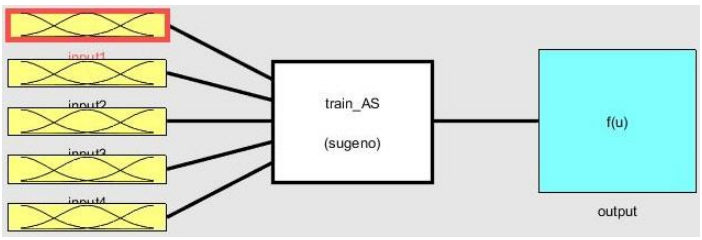

Figure 4.6: Fuzzy logic designer for ANFIS with the small data set

Figure 4.7 shows the plot of 6-DoF head motion coordinates data used in ANFIS for training.

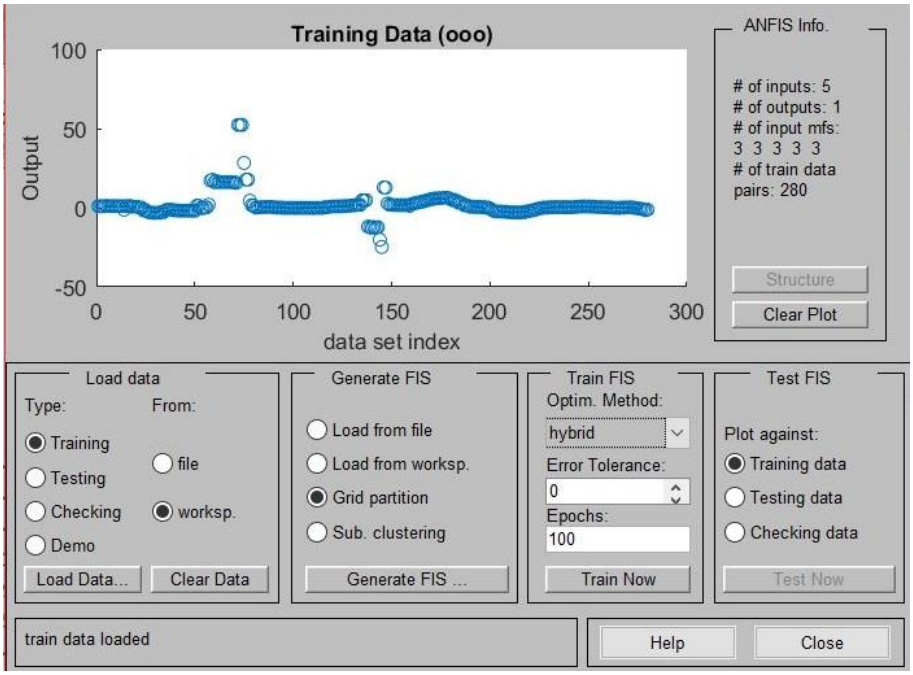

Figure 4.7: Training data used in ANFIS

Figure 4.8 shows the plot of 6-DoF head motion coordinates data used in ANFIS for testing.

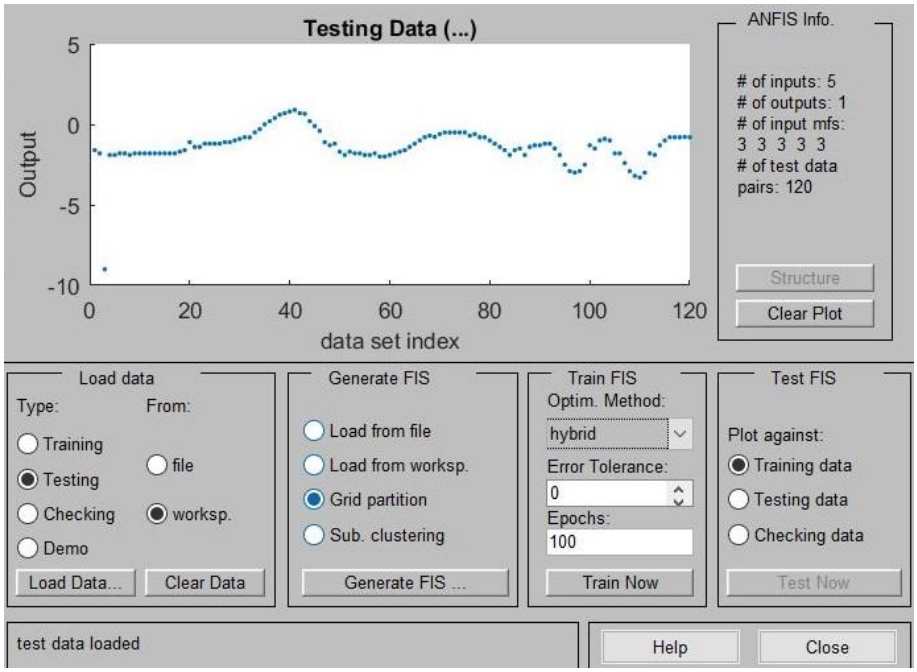

Figure 4.8: Testing data used in ANFIS

Figure 4.9 shows the testing of the FIS with the training data set used in ANFIS for the prediction of missing 6-DoF head motion coordinates.

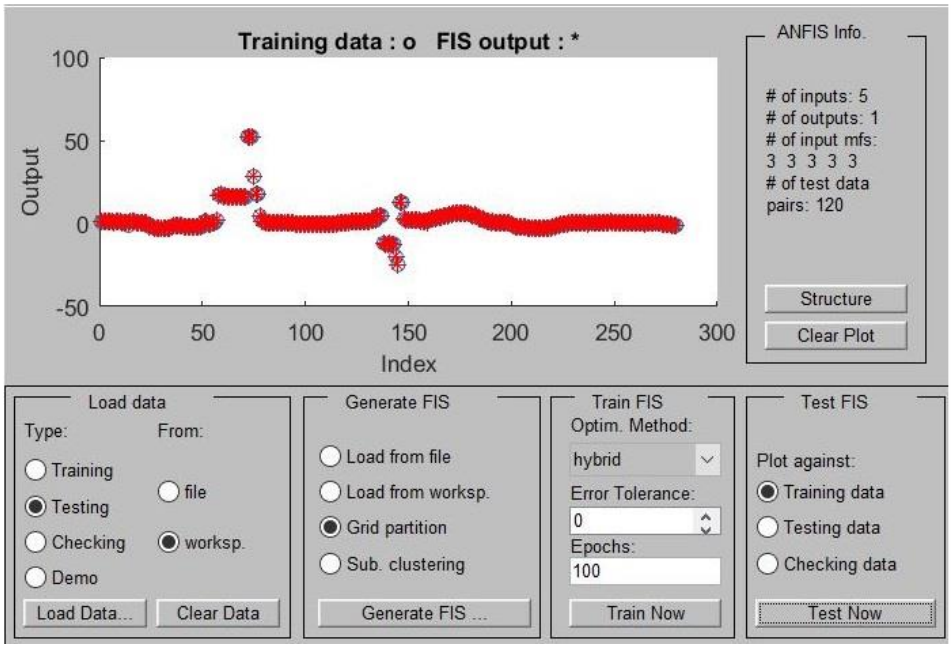

Figure 4.9: Plot of training data against FIS output

Figure 4.10 shows the testing of the FIS with the testing data set used in ANFIS for the prediction of missing 6-DoF head motion coordinates.

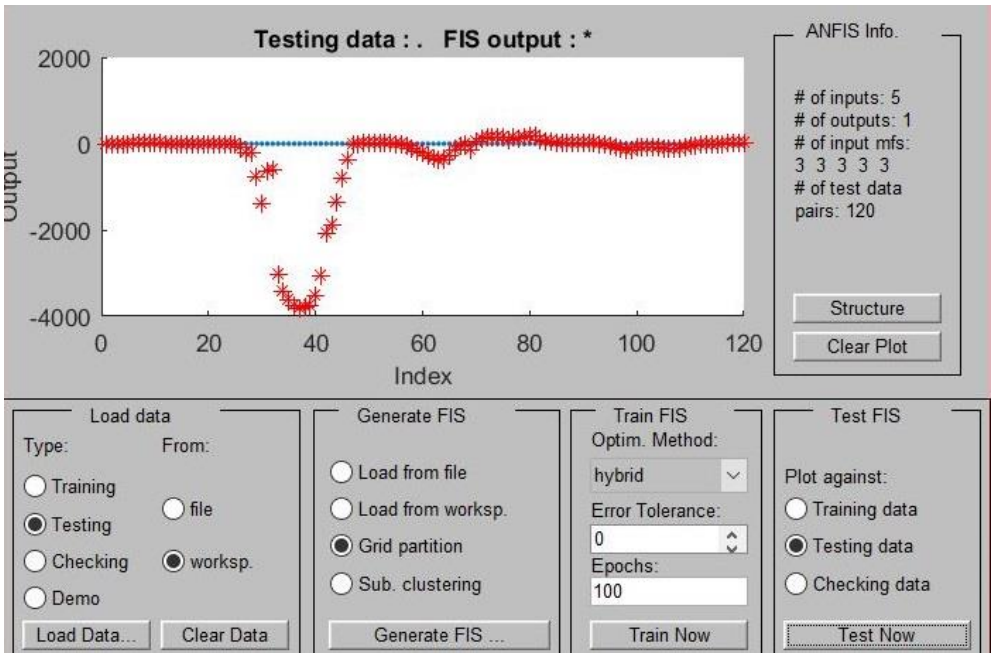

Figure 4.10: Plot of testing data against FIS output

Figure 4.11 describes the ANFIS model used for the prediction of the missing head motion coordinates

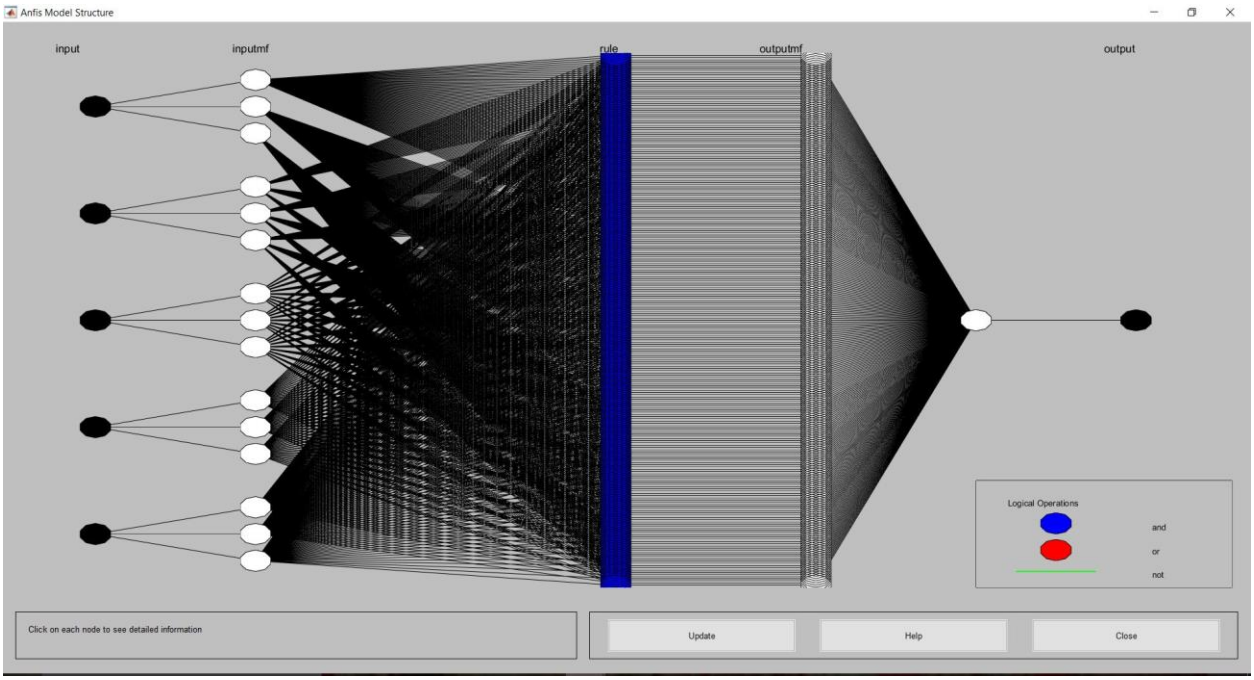

Figure 4.11: Structure of the ANFIS model

The five inputs, in this case, are (Y, Z, Yaw, Pitch, and Roll). The output with missing data, in this case, is taken as the dataset of X coordinate.

4.3 BACKPROPAGATION NEURAL NETWORK

Backpropagation neural network (BPNN) is a method used in artificial neural networks to compute the gradient, which is required in the calculation of the weights to be used in the given network. It is commonly used to train neural networks with more than one hidden layer. It is a particular case of a generic technique known as automatic differentiation. The weights of neurons are adjusted in the gradient descent optimization algorithm by the computation of the gradient of the loss function using BPNN. This technique is also known as the backpropagation of errors as the error is computed at the output and is distributed back through the network layers. BPNN is a supervised learning method and is also a generalization of the delta rule to the multilayered feedforward networks. The existing BPNN model was used to train the actual 6-DoF data acquired by the trackers. In this technique, the weights were adjusted according to the mapping capability of a trained network. The experimental data is divided into Training (70%) and Test data (30%). The division of the data is random. The test data was not used during the training of the network by 70% of the training data. The test data (30%) was only used for evaluation of the prediction capability of missing instance data set using BPNN. In this section, an example of predicting missed 6-DoF coordinate using Back Propagation neural network is discussed.

Figure 4.12 shows the structure of the Back Propagation neural network used for the prediction of the missed head coordinates.

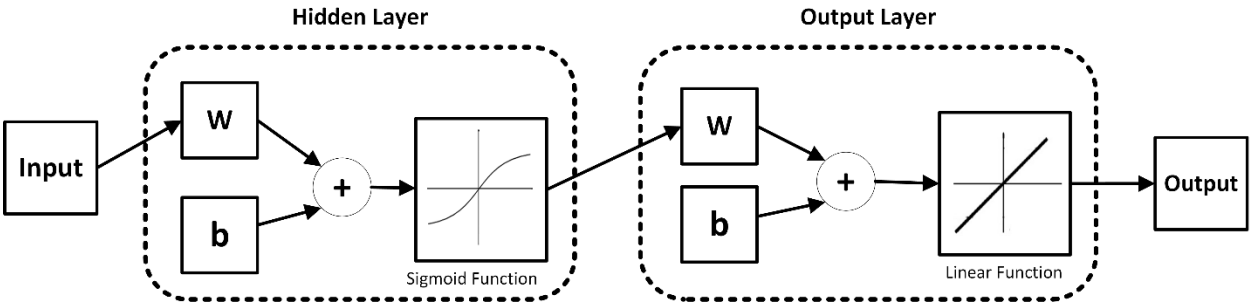

Figure 4.12: Basic structure of BPNN used for prediction of missing data

The feed-forward backpropagation network used for the prediction of the missing coordinates consists of one hidden layer with a sigmoid transfer function and one output layer with a linear transfer function was used. The training algorithm used in the predictor was Levenberg-Marquardt. Figure 4.13 shows the neural structure of the Back Propagation Neural Network used for the prediction of missed head motion coordinates.

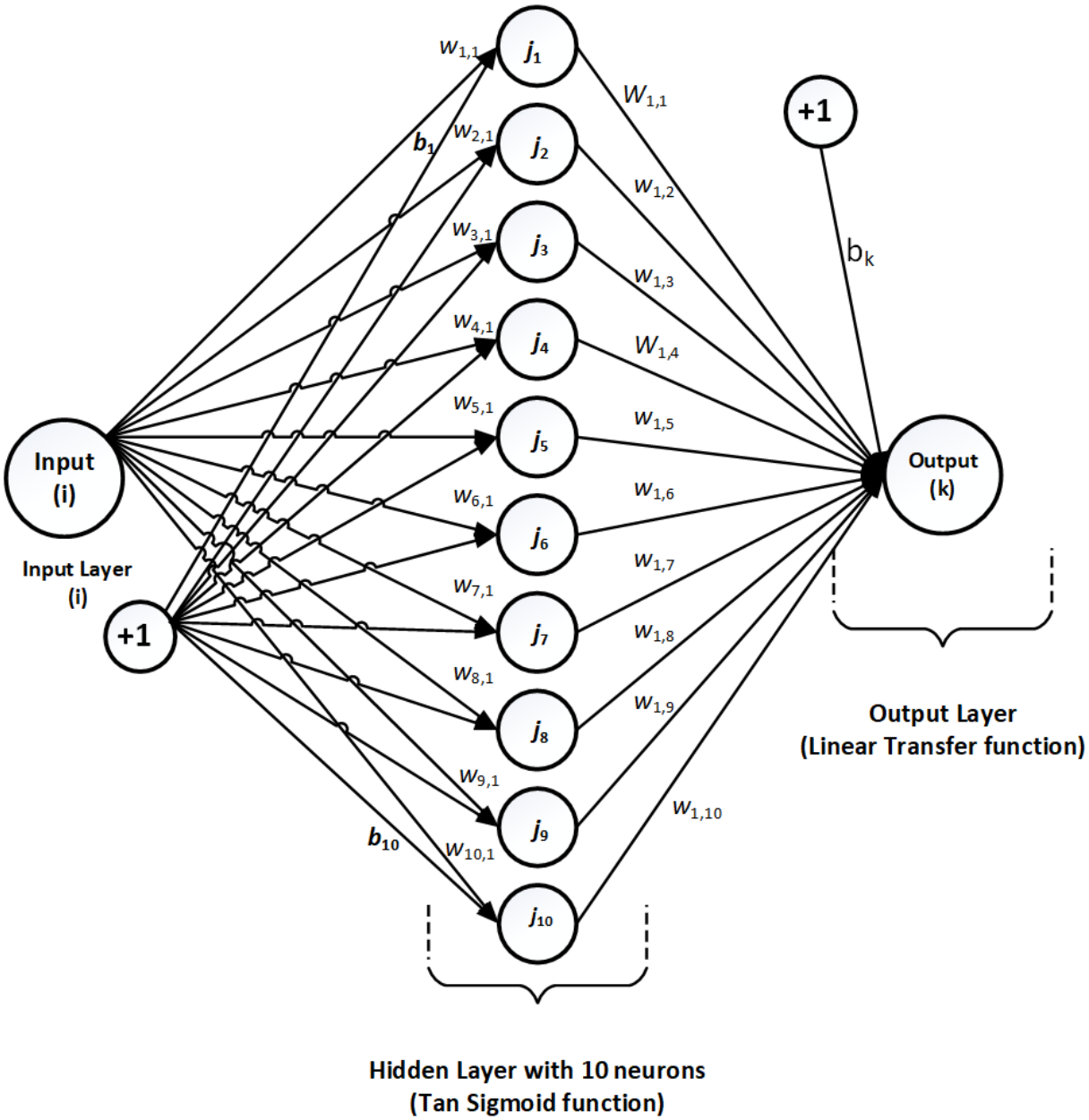

Figure 4.13: Neural structure of Back Propagation Neural Model

The basic equations in backpropagation are given by Equation (4.10) and (4.11),

$$O_j = W_{ji}^T . O_i + b_j \qquad (4.10)$$

$$O_k = W_{kj}^T . O_j + b_k \qquad (4.11)$$

Where W^T is the transpose of weight matrix

Here $j = 1{:}10$, $i = 1$ and $k = 1$

In Equation (4.10) w_{ji} is the weight between the input layer and the hidden layer, i is the input, O_i is the output of the input layer, O_j is the output of the hidden layer and b_j is the bias from the input layer to the hidden layer. In Equation (4.11) w_{kj} is the weight between the hidden layer and the output layer and b_k is the bias from the hidden layer to the output layer. The hidden layer is fed with the *tan sigmoid* activation function. The output O_k from the hidden layer is fed to the Linear transfer function given by $f\ (x_i) = x_i$

tan sigmoid activation function is given by the Equation (4.10a)

$$tansig = \frac{2}{1+e^{-2n}} - 1 \qquad (4.10a)$$

Table 4.2 represents the data set having the original and missing data set. The missed coordinate '0' is to be predicted using BPNN.

Table 4.2: Sample data set of original data and missing data used for the prediction of BPNN

Original data set	7.1	7.4	7.5	7.5	7.8	8.2	8.4	8.8	9.2	9.8
Missing data set	7.1	7.4	7.5	7.5	**0**	8.2	8.4	8.8	9.2	9.8

Table 4.3 represents the weights and bias used in BPNN from input to the hidden layer for the prediction of missed coordinate.

Table 4.3: Sample values of weights and bias used for the prediction of missing coordinates

j	1	2	3	4	5	6	7	8	9	10
W_{ji}	-13.946	-13.979	14.0068	-13.907	14.003	13.957	14.097	13.8175	13.7792	14.309
b_j	14.022	10.9233	-7.7897	4.9003	-1.4263	1.6022	4.4117	7.7252	11.213	13.691
W_{kj}	-0.1600	-0.1070	0.10784	0.01028	0.2837	0.1022	0.1321	0.10306	0.05660	-0.4409
b_k	0.5225	---	---	---	---	---	---	---	---	---

Using the values of weights and bias mentioned in Table 4.3 and substituting them in Equation (4.10) and (4.11), the missing coordinate can be predicted. The missing value predicted by the BPNN is 5.8.

The training parameters of the Back Propagation Neural Network for the prediction of the missing head motion coordinates are mentioned in Table 4.4

Table 4.4: Training parameters used in BPNN for prediction of missed head coordinates

Parameter	Value
Number of hidden layers	1
Number of neurons in the hidden layer	10
Number of neurons in the output layer	1
Transfer function for the hidden layer	Log Sigmoid
Transfer function for the output layer	Linear
Training function	LM
Maximum number of epochs	100
Backpropagation learning rate	Adaptive

The prediction results of missing 6-DoF coordinates using the electromagnetic tracker and optical tracker are covered in Chapter 5. The accuracy of the BPNN is also compared with the ANFIS and SHNM and covered extensively in Chapter 5.

4.4 AUTOREGRESSIVE LINEAR MODEL

The six-dimensional data used in the thesis is highly nonlinear in nature. Thus, the results of the Self Healing Neural Model are compared with the backpropagation network. The autoregressive linear model is a less complex method as compared to the backpropagation network.

An autoregressive linear model of order $'j'$ is given by the Equation (4.12)

$$X_t=\delta + \sum_i^j b_i X_{t-i} + \varepsilon_t \quad (4.12)$$

In Equation (4.12) $'X_t'$ is the parameter to be observed for prediction, X_{t-i} is the previous value, $b_i, \ldots . b_j$ are the parameters of the model and $'j'$ is the non-negative integer and $'\varepsilon_t'$ is white noise.

The Autoregressive linear model establishes a realization at time $'t'$ that is a linear combination of the $'j'$ previous realization and some noise term.

For j = 0 and X_t=ε_t, there is no autoregression term.

For the prediction of the 6-DoF coordinates, the X_t represents the present value of the coordinate and X_{t-i} represents the past value (delay) of the coordinate. In this case, the value of $'j'$ is two for the ARLM order 2 and three for the ARLM order 3. Hence, the order of the Autoregressive model is 1 and 2 in this case. It is evident that the prediction accuracy increases as the order of the model increases but with the increase in the order, the computational overheads increase due to which there is large a lag in the output. To avoid the computational overheads, the first and the second-order of the Autoregressive model is used. The predicted 6-DoF coordinates are compared with the much less complex method of prediction known as Auto Regressive Linear Model.

Modeling of ARLM in the prediction of missing coordinates in head tracking.

The equation of the Autoregressive model if order 3 used for the prediction of the missing data is given by Equation (4.13)

$$X_t=\delta + b_1X_{t-1} + b_2X_{t-2} + b_3X_{t-3} + \varepsilon_t \quad (4.13)$$

In Equation (4.13) $'X_t'$ is the value of the coordinate of the head to be predicted, $'\delta'$ is the constant (intercept), $b_1, b_2, \& \, b_3$ are the parameters of the model, $X_{t-1}, X_{t-2}, \; \& \; X_{t-3}$ are the previous values of the coordinates and ε_t is the noise, which is taken as **zero** in this case. For applying ARLM to predict missing data or value, a simple data set with missing 6-DoF head motion coordinate is shown in Table 4.5.

Table 4.5: Dataset with missing head motion coordinates

-1.7	-1.6	-0.3	0	4.8	8.7	12.1	17.3	0	24.8

In Table 4.5, the missing coordinate is denoted by '0'. The actual value of the missed coordinate is **'20.8'**. The parameters of ARLM are generated using 70% of the original dataset as training data set and using the remaining 30% dataset as a testing dataset. The data splitting for the training and testing is done randomly. Using ARLM of order three the parameters obtained are:

Table 4.6: Parameters of ARLM of order three

δ	-0.13251
b_1	1.432609
b_2	-0.22094
b_3	-0.24763

Assuming ε_t=0, substituting the values from Table 4.6 in the equation (4.13), the predicted value obtained is **'14.04'.**

In this work, the prediction of the missing 6-DoF coordinates, which are generated due to external interferences and due to exceeding the stipulated positional and orientation limit of head motion box in the cockpit, is done using Self Healing Neural Model (SHNM). The results

of SHNM are compared with conventional Back Propagation Neural Network (BPNN) and less complex Auto-Regressive Linear Model (ARLM). The comparison of prediction of the missing 6-DoF coordinates using SHNM is done with BPNN and ARLM separately in tabular form as well as graphically. The results of prediction in the data sets consisting of different range of missing head coordinates are discussed in chapter 5.

4.5 CONCLUSION

In this chapter, various problems arising in optical and electromagnetic head tracking are discussed. The problems in head tracking leading to the missing of 6-DoF head coordinates are predicted using different soft computing techniques. In this work, the prediction of the missing 6-DoF head coordinates using the Self Healing Neural Model is explained. Prediction of missing 6-DoF head coordinates using Back Propagation Neural Network and Auto-Regressive Linear Model is also explained in detail with examples in this chapter. ANFIS is also used to predict the missing 6-DoF head coordinates which are also discussed in this chapter. Autoregressive Linear Model is the regression technique to predict the data. Autoregressive, being the less complex method, was used to predict the missing 6-DoF coordinates. Its prediction accuracy increased with an increase in the order of the prediction. The order of ARLM is the number of immediately preceding values in the series that are used to predict the value at the present time. As the order of the ARLM increases, the undesirable overhead charges of the whole tracking system including prediction increases.

5. EXPERIMENTATION AND PREDICTION RESULTS OF OPTICAL AND ELECTROMAGNETIC TRACKERS

5.1 EXPERIMENTAL SETUP FOR ACQUISITION OF 6-DOF COORDINATES OF HEAD USING ELECTROMAGNETIC TRACKER

To overcome the problems arising in different tracking technologies, hybrid-tracking technology can be used in which multiple tracking technologies can be coupled. The accuracy of the head tracking will increase but this approach can increase the cost of tracking. In this work, a magnetic tracker is used to track the head movements of the pilot. The tracking accuracy of the magnetic tracker can get degraded as the coordinates of the head to be acquired may get missed due to the presence of ferromagnetism or due to the movement of the head tracker beyond HMB limits. To eradicate this problem, the missing data is recovered using SHNM. Apart from the application of head tracking in aviation, it can also be used in flight simulation as training in a flight simulator can be more productive and efficient than airborne training. For that, the cost of the magnetic tracker can be compromised by using the low magnetic field range trackers. In addition, the low field magnetic tracker will get affected highly by low ferromagnetism present in the environment, which can lead to missing data and will reduce the tracking accuracy of the magnetic tracker [147]. The missing data occurring due to even low ferromagnetism or due to the movement of head tracker beyond HMB limits can be recovered by using SHNM. This can help to build nearly a robust low-cost flight simulator to make the pilot aware of the process of head tracking even in situations that would be impractical for airborne training. This model can also be used to recover missing data from other tracking

technologies like optical, inertial tracking, etc. The accuracy obtained by SHNM is also compared with BPNN as it is relatively simple to implement and the mathematical formula present in the algorithm of the BPNN can be commonly applied to any network. The main steps of using the electromagnetic head tracking can be summed up below.

- Acquisition of 6-DoF coordinates of the head motion using **Polhemus Patriot^{TM}** electromagnetic tracker on the simulator bed.
- Application of SHNM on the data set containing missing instances of 6-DoF head coordinates that could occur due to ferromagnetism, any other kind of magnetic interferences, or due to exceeding the stipulated positional and orientation limit of head motion box in cockpit.
- Computation of accuracy of the recovered 6-DoF head coordinates by SHNM through supervised learning and comparing the obtained accuracy with BPNN and ARLM.

To give a better training outcome, it is believed that 6-DoF based head tracking based simulation could give pilot more reliability to flight control operations and the response of aircraft to the control inputs and various external forces. In magnetic head tracking, there can be various kinds of magnetic interferences, which can lead to the inaccurate computation of coordinates of the head of the pilot to be trained. The data acquired by the magnetic tracker can be missed mainly due to ferromagnetism present in the cockpit due to various electrical and metallic appliances or due to the movement of the head beyond the designated head motion box dimensions within which motion of the pilot's head is restricted or within which tracker gives continuous uninterrupted data. The missing of 6-DoF head coordinates occurred due to these reasons that can be recovered up to a considerable extent using Self Healing Neural Model. In this chapter, a system is proposed to predict the missing 6-DoF head coordinates to ensure the correct and

accurate tracking of the head of the pilot. This can also help to construct a low-cost flight simulator for flight training purposes. The Polhemus Patriot Electromagnetic Tracker is shown in Figure 5.1 and the experimental setup for tracking the head using an electromagnetic tracker is shown in Figure 5.2. The experimental process to predict missing 6-DoF head coordinates using an electromagnetic tracker is shown in Figure 5.3.

Figure 5.1: Polhemus Patriot Electromagnetic Tracker

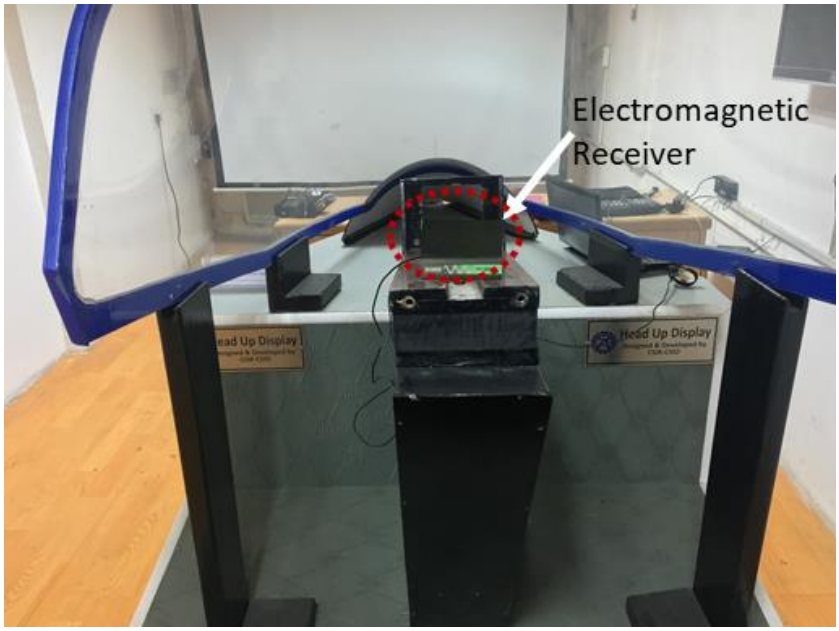

Figure 5.2: Experimental setup for the acquisition of 6-DoF head motion coordinates using Polhemus Patriot Electromagnetic Tracker (transmitter not visible in the figure)

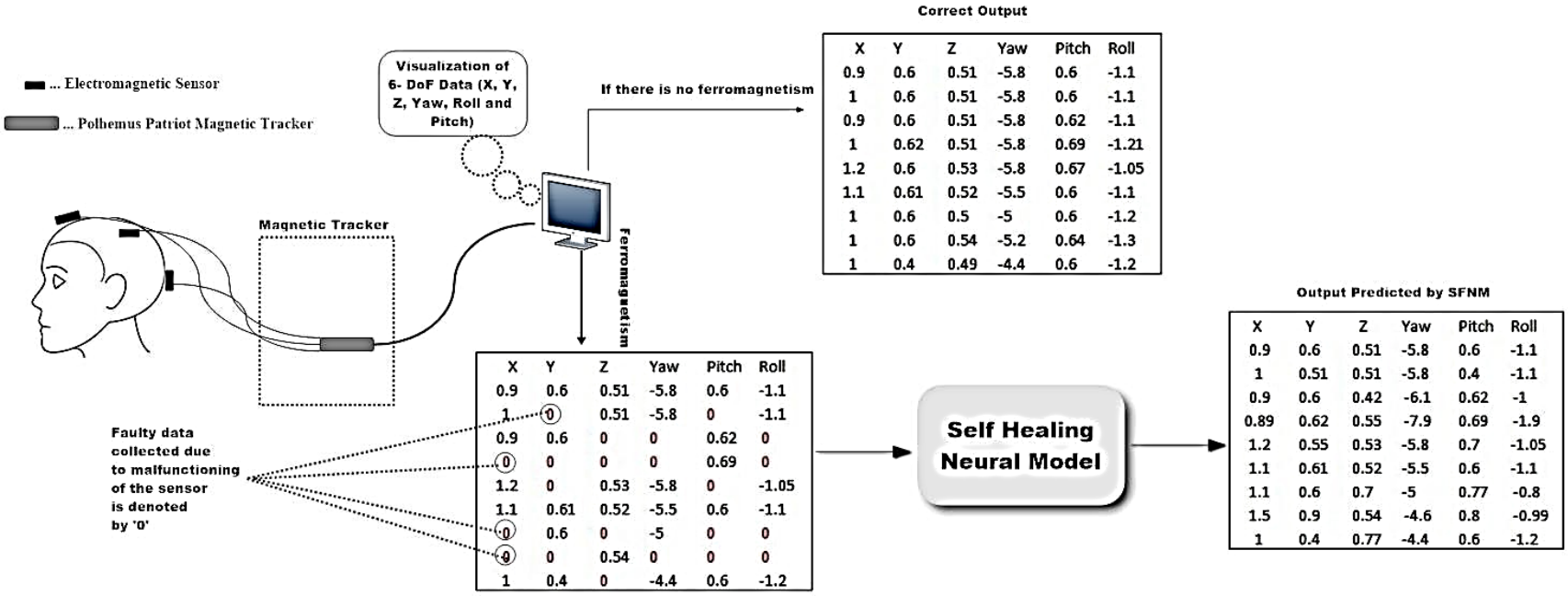

X	Y	Z	Yaw	Pitch	Roll
0.9	0.6	0.51	-5.8	0.6	-1.1
1	0.6	0.51	-5.8	0.6	-1.1
0.9	0.6	0.51	-5.8	0.62	-1.1
1	0.62	0.51	-5.8	0.69	-1.21
1.2	0.6	0.53	-5.8	0.67	-1.05
1.1	0.61	0.52	-5.5	0.6	-1.1
1	0.6	0.5	-5	0.6	-1.2
1	0.6	0.54	-5.2	0.64	-1.3
1	0.4	0.49	-4.4	0.6	-1.2

X	Y	Z	Yaw	Pitch	Roll
0.9	0.6	0.51	-5.8	0.6	-1.1
1	0	0.51	-5.8	0	-1.1
0.9	0.6	0	0	0.62	0
0	0	0	0	0.69	0
1.2	0	0.53	-5.8	0	-1.05
1.1	0.61	0.52	-5.5	0.6	-1.1
0	0.6	0	-5	0	0
0	0	0.54	0	0	0
1	0.4	0	-4.4	0.6	-1.2

X	Y	Z	Yaw	Pitch	Roll
0.9	0.6	0.51	-5.8	0.6	-1.1
1	0.51	0.51	-5.8	0.4	-1.1
0.9	0.6	0.42	-6.1	0.62	-1
0.89	0.62	0.55	-7.9	0.69	-1.9
1.2	0.55	0.53	-5.8	0.7	-1.05
1.1	0.61	0.52	-5.5	0.6	-1.1
1.1	0.6	0.7	-5	0.77	-0.8
1.5	0.9	0.54	-4.6	0.8	-0.99
1	0.4	0.77	-4.4	0.6	-1.2

Figure 5.3: Experimental description of electromagnetic head tracking and SHNM process for prediction of missing 6-DoF head motion coordinates

The system set up for this work comprises **Cockpit Simulator and Polhemus Patriot™** magnetic tracker. The interface of the magnetic tracker is USB 2.0 or RS-232. The physical dimensions of the tracker are 6.75″ (17.1 cm) L x 6.25″ (15.9 cm) W x 1.75″ (4.4 cm) H. The system is easy to set up and simple to use, but it is capable of performing all the complex calculations that provide both position and orientation data of the head of the pilot on the simulator bed. Dell Inspiron 15 5000 series is used for data acquisition operating under Microsoft Windows 10. Polhemus Patriot™ magnetic tracker acts as a source to generate the magnetic field. Change in the magnetic field is detected by the sensors, which can be varied in number from 1-3 and are embedded in the head of the pilot to get the position and orientation coordinates of the head. The 6-DoF data is collected as the head posture of the pilot and is varied in different directions and angles. The data acquired in this work has a total of 5200 instances. Each instance represents the particular position and orientation of the pilot's head. The sample data of the 6-DoF head coordinates used in this work is shown in Table 5.1. Units of translational coordinates are in centimeters and rotational coordinates are in degrees.

Table 5.1: Sample data set of Electromagnetic Tracker

X	Y	Z	Yaw	Pitch	Roll
0.9	0.6	0.51	-5.8	0.6	-1.1
1	0.6	0.51	-5.8	0.6	-1.1
0.9	0.6	0.51	-5.8	0.62	-1.1
1	0.62	0.51	-5.8	0.69	-1.21
1.2	0.6	0.53	-5.8	0.67	-1.05
1.1	0.61	0.52	-5.5	0.6	-1.1
1	0.6	0.5	-5	0.6	-1.2
1	0.6	0.54	-5.2	0.64	-1.3
1	0.4	0.49	-4.4	0.6	-1.2
1	0.4	0.49	-4.4	0.62	-1.2

The available data of 5200 instances including missing data acted as an input for the SHNM. The available data set was then checked for the number of missing instances. After the exploration of the missing data, the missing instances present in the available data were recovered using SHNM. The missing data sets can be constructed by inducing the deliberate magnetic field disturbance **(as discussed in Table 6.3 of section 6.3 in detail)**, moving beyond HMB or magnetic sensor range, or by turning off the sensor for a particular instant of time. The recovery process of missing data is ensured by each iteration carried by SHNM to recover each instance of missing data. After recovery, the data is analyzed for correctness and validation using supervised learning. Accuracy of the recovered data against actual data is computed in the final step. The threshold for the proposed system to compute the accuracy can be assumed based on the average of self-healing cost over the available data set. As it is observed through simulations that the threshold range of the 6-DoF head coordinates value from 0.5 to 1 yield the best results, hence 0.75 threshold value is used to compute the accuracy. Due to interference in the magnetic field caused by ferromagnetism or due to the movement of the head beyond the HMB range, the data acquisition may miss some coordinates of the pilot's head position for a short duration. Due to this, the performance of HMD may degrade due to failure in estimating the exact coordinates of the head movements. Therefore, the data, which was not recorded at the instant when the tracker malfunctioned due to field interference or field detection missed beyond HMB range movement of the head, can be recovered using SHNM. The process of recovery of missing data is presented in Figure 5.4.

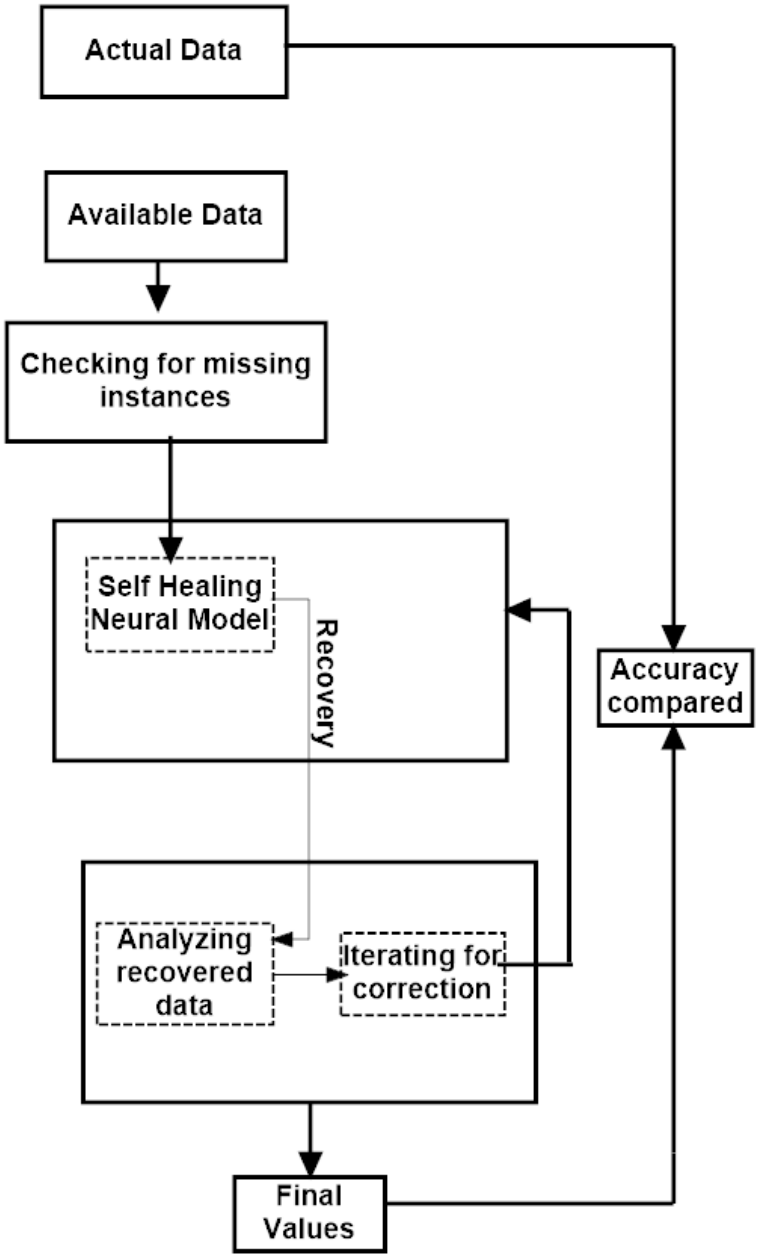

Figure 5.4: Process of data recovery in the proposed approach

5.2 RESULTS AND DISCUSSIONS ON PREDICTION OF MISSING 6-DOF HEAD MOTION COORDINATES IN ELECTROMAGNETIC HEAD TRACKING

5.2.1 PREDICTION OF MISSING 6-DOF HEAD MOTION COORDINATES USING SELF HEALING NEURAL MODEL

The errors caused by various factors listed above are considered and a prediction of position using an electromagnetic tracker is made. The Self Healing Neural Model is used to predict the missing 6-DoF head motion coordinates as discussed above.

In this section, the performance analysis of the proposed approach is discussed. The analysis is defined over both benchmark-training algorithms and individual results of the proposed approach. The prediction of missing 6-DoF head motion coordinates is done using five different data sets. Each data set has a different percentage of missing 6-DoF head coordinates. In this work, the data sets with 1%, 2%, 10%, 25%, and 35% missing 6-DoF head coordinates of the whole data set are predicted using SHNM. The 6-DoF head coordinates can be missed due to ferromagnetism and by exceeding the range of motion of the head in the cockpit from the stipulated amount of range of head motion box. The horizontal limit of the head motion box is 120 millimeters and the vertical limit is 70 millimeters in the cockpit. Due to this reason, the minimum missing percentage (1% and 2%) of 6-DoF data is taken into account for the prediction.

The criteria used for the computation of the accuracy is Mean absolute percentage error (MAPE). The percentage of the accuracy of the prediction is computed by Equation (5.1)

$$MAPE = 1 - \left(\frac{100}{n} \sum_{i=1}^{n} \left| \frac{x_i - \hat{x}_i}{x_i} \right| \right) \qquad (5.1)$$

where x_i is the actual value of the coordinate, $\hat{x}_i$ is the predicted value of the coordinate and n is the number of non-missing coordinates.

The predicted results of SHNM are compared with BPNN and ARLM. The data set with missing 6-DoF head coordinates can be constructed by inducing the deliberate magnetic field disturbance, moving head beyond HMB range, or turning off the sensor for a particular instant of time. The graphical representations of prediction of 1% and 2% missed 6-DoF head coordinates are not shown to avoid the repetition of graphs. Also, the missing data of 1% and 2% in the large data set is not observable graphically. In this chapter, the graphs for the prediction of missing head position coordinates are represented. The graphs for the prediction of 35% missing head position coordinates are represented in this chapter. The prediction of 10% and 25% missing head position coordinates in the electromagnetic head tracker is shown in Appendix A.

Figure 5.5 to Figure 5.7 shows the prediction of 35% missing head coordinates of X, Y, and Z respectively. The X, Y, and Z are the translational head coordinates. In these graphs, the blue line signifies the actual coordinates (used for training), the red line shows the missing coordinates (testing) and the green line shows the predicted data set of missed head coordinates using the Self Healing Neural Model. The x-axis is the translational value of head coordinates (in millimeter) and the y-axis shows the number of head coordinates in all three graphs.

In Figure 5.5 to Figure 5.16, the Y-axis represents the 6-DoF head motion data with missing coordinates of the position of the pilot's head and X-axis represents the corresponding physical value of 6-DoF coordinates.

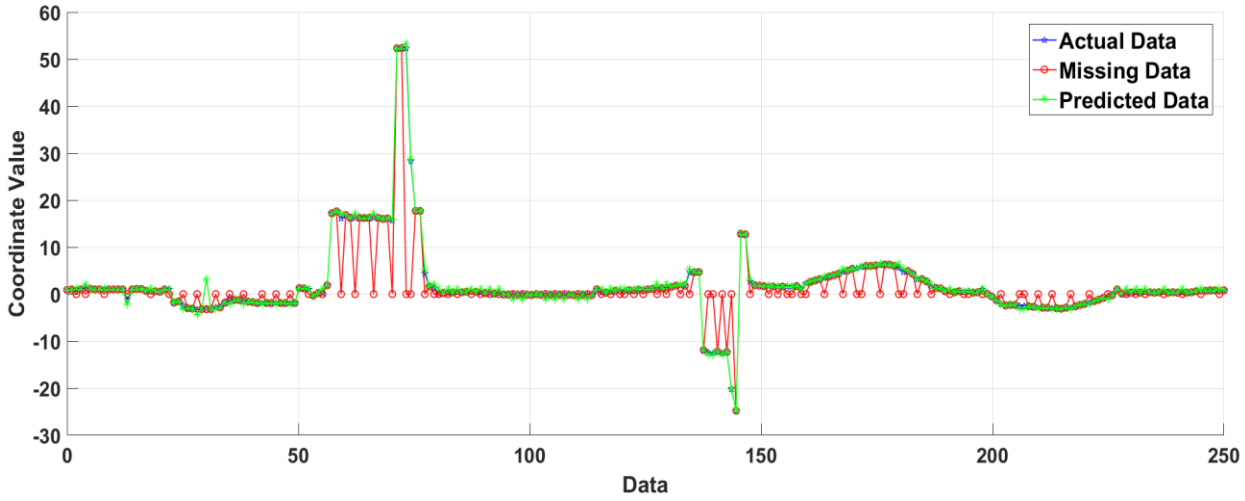

Figure 5.5: Prediction of X coordinates using SHNM for the data set with 35% missing 6-DoF head coordinates

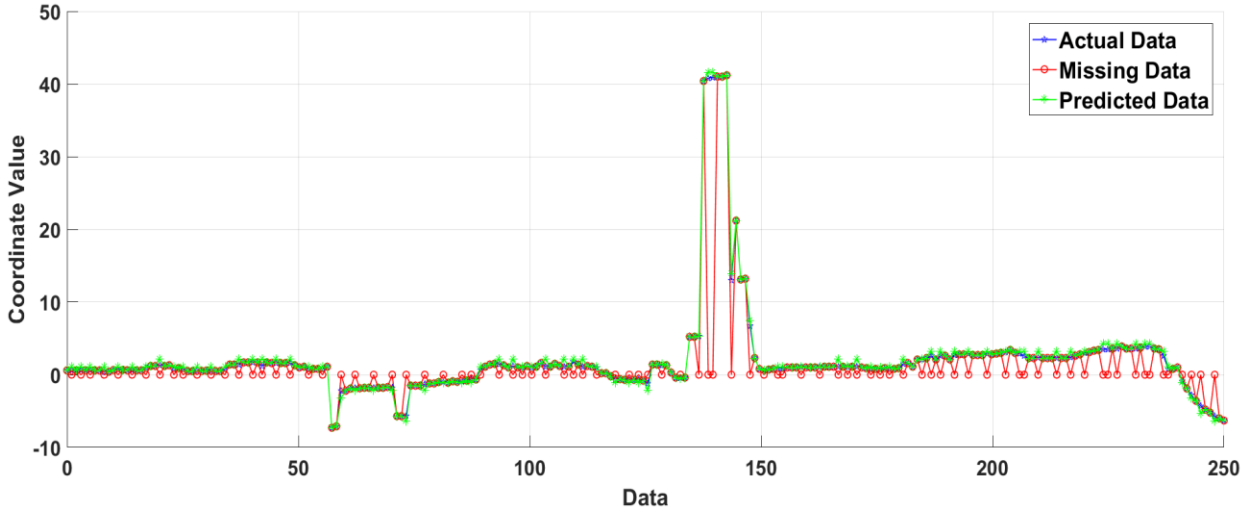

Figure 5.6: Prediction of Y coordinates using SHNM for the data set with 35% missing 6-DoF head coordinates

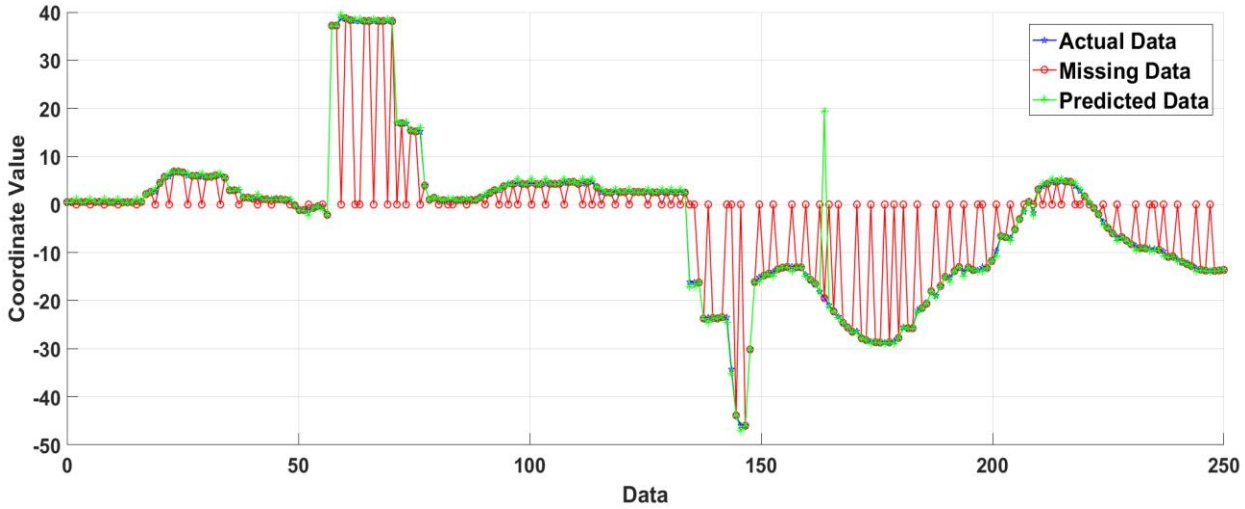

Figure 5.7: Prediction of Z coordinates using SHNM for the data set with 35% missing 6-DoF head coordinates

Figure 5.8 to Figure 5.10 shows the prediction of 35% missing head coordinates of Yaw, Pitch, and Roll respectively. The Yaw, Pitch, and Roll are the rotational head coordinates. In these graphs, the blue line signifies the actual coordinates (used for training), the red line shows the missing coordinates (testing) and the green line shows the predicted data set of missed head motion coordinates using the Self Healing Neural Model. The x-axis is the translational value of head coordinates (in degrees) and the y-axis shows the number of head coordinates in all three graphs.

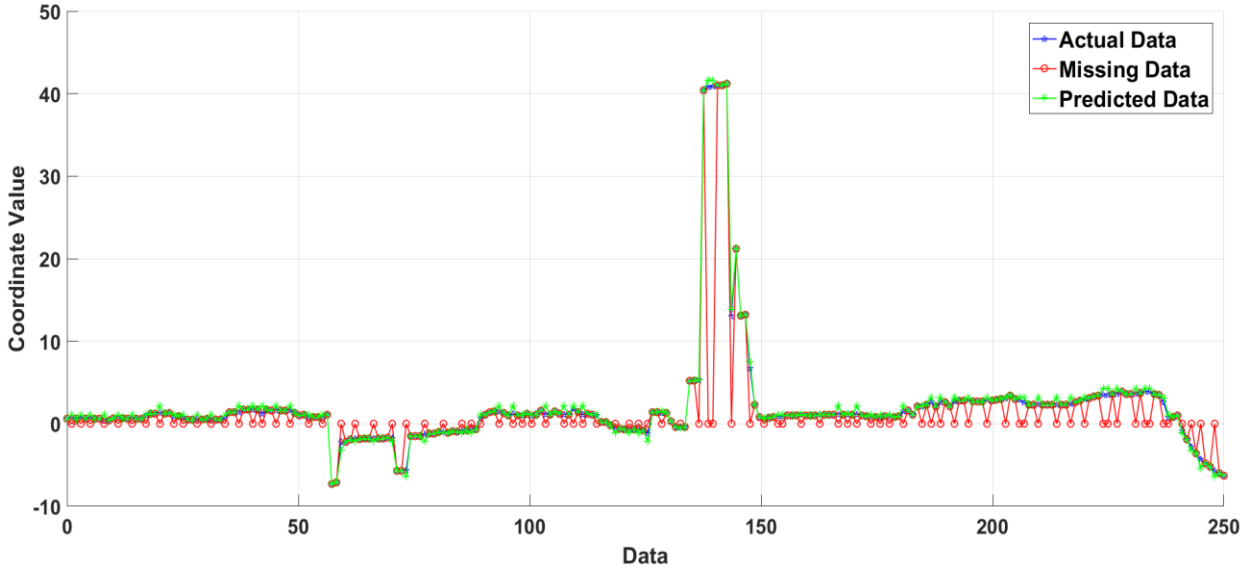

Figure 5.8: Prediction of Yaw angular coordinates through SHNM for the data set with 35% missing 6-DoF head coordinates

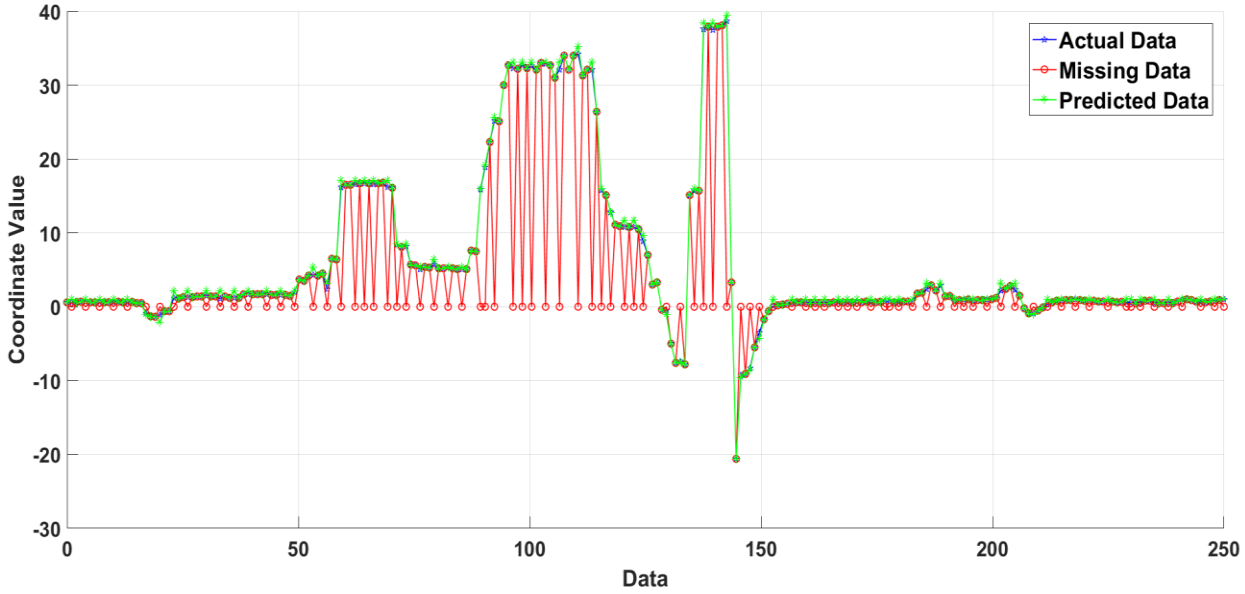

Figure 5.9: Prediction of Pitch angular coordinates through SHNM for the data set with 35% missing 6-DoF head coordinates

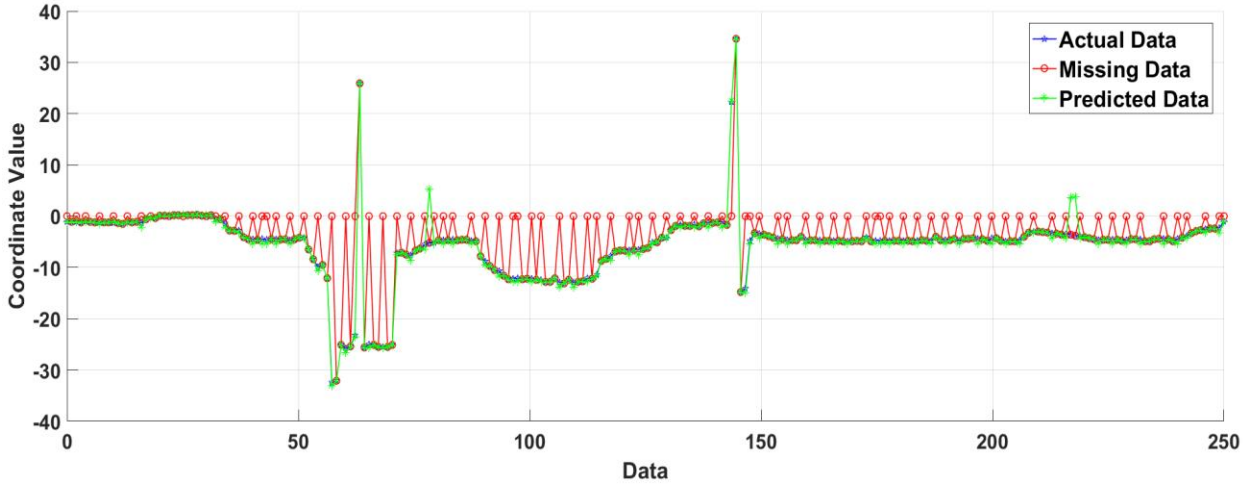

Figure 5.10: Prediction of Roll angular coordinates through SHNM for the data set with 35% missing 6-DoF head coordinates

5.2.2 COMPARISON OF ACCURACY OF SHNM AND BACK PROPAGATION NEURAL NETWORK IN PREDICTION OF MISSING 6-DOF HEAD MOTION COORDINATES

The comparison of the prediction with 35% missing 6-DoF head motion instances dataset of 6-DoF head coordinates with SHNM and BPNN are shown in Figure 5.11, Figure 5.12, Figure 5.13, Figure 5.14, Figure 5.15, and Figure 5.16.

There is some deviation in red and green curves in the graphs, which means that the accuracy of SHNM is better than BPNN, as the green curve is near to the blue curve, which is the expected output. At some places, the deviation is less because, in some instances, the recovered value predicted using BPNN is near to the value predicted by SHNM.

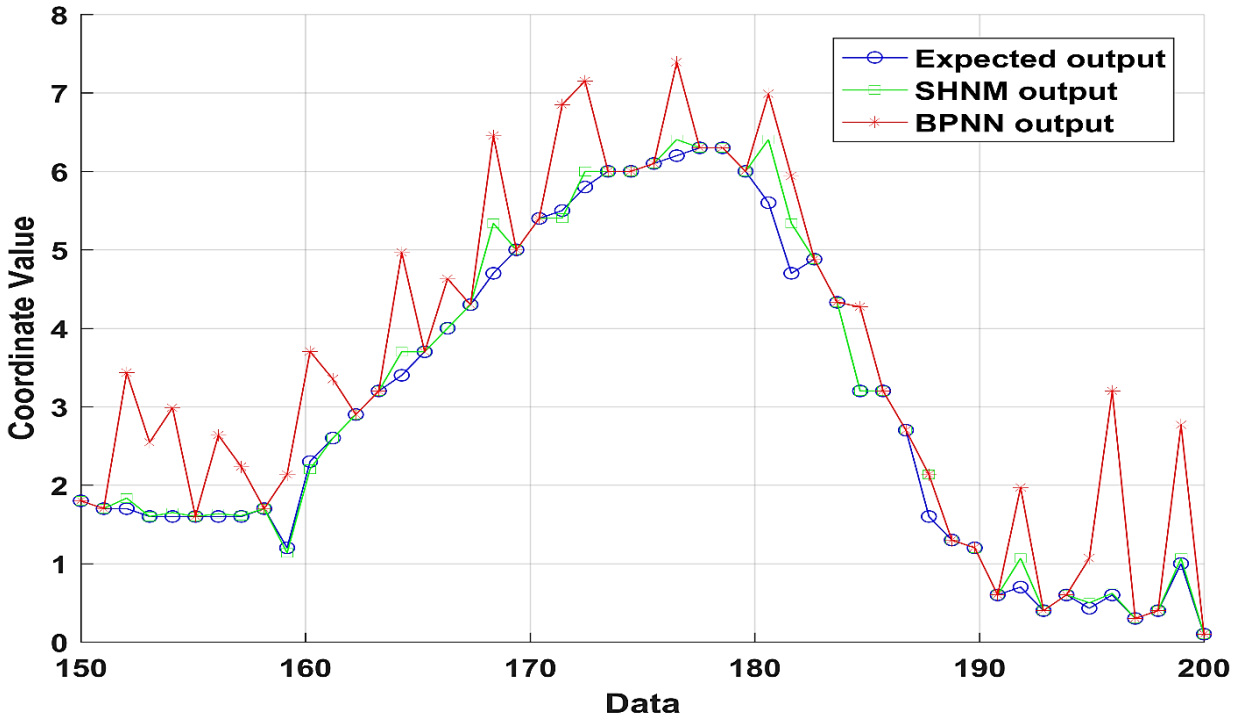

Figure 5.11: Comparison of prediction of X coordinates with SHNM and BPNN

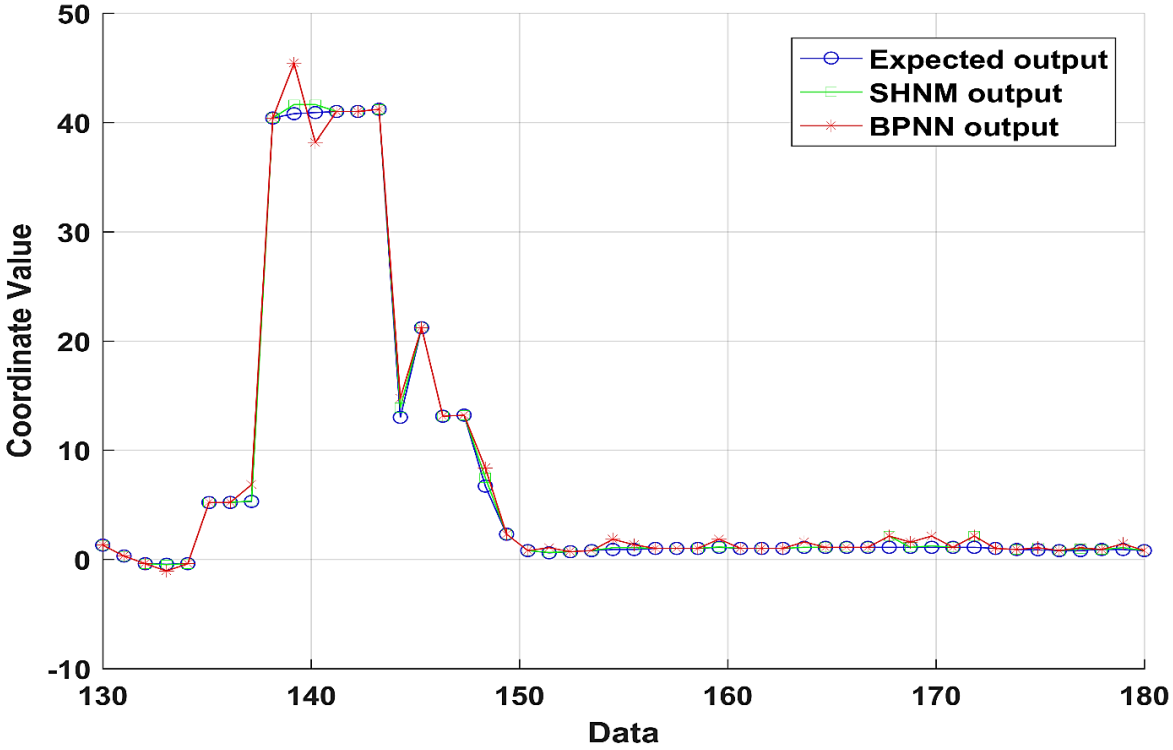

Figure 5.12: Comparison of prediction of Y coordinates with SHNM and BPNN

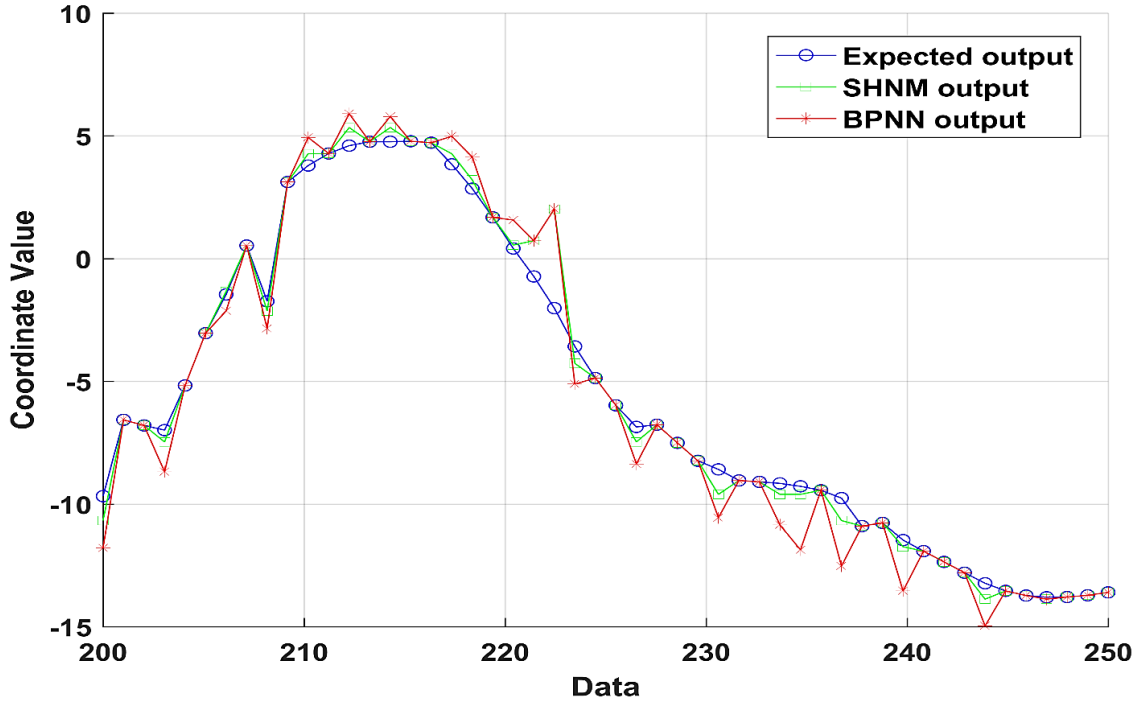

Figure 5.13: Comparison of prediction of Z coordinates with SHNM and BPNN

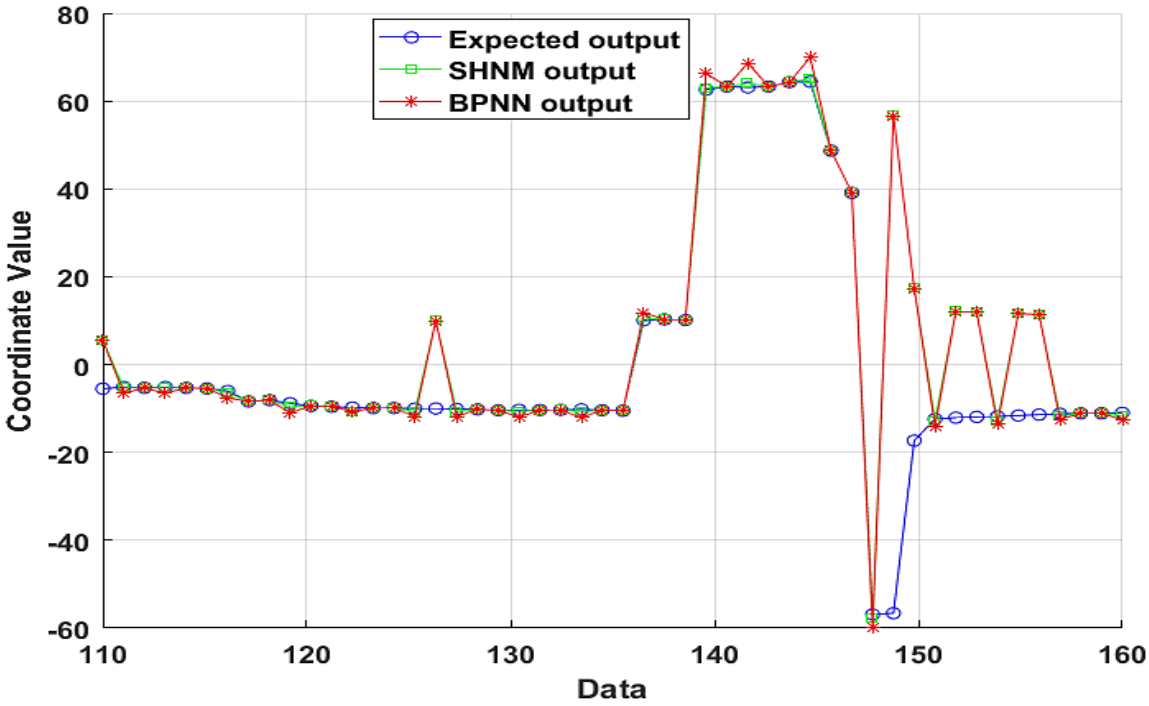

Figure 5.14: Comparison of prediction of Yaw angular coordinates with SHNM and BPNN

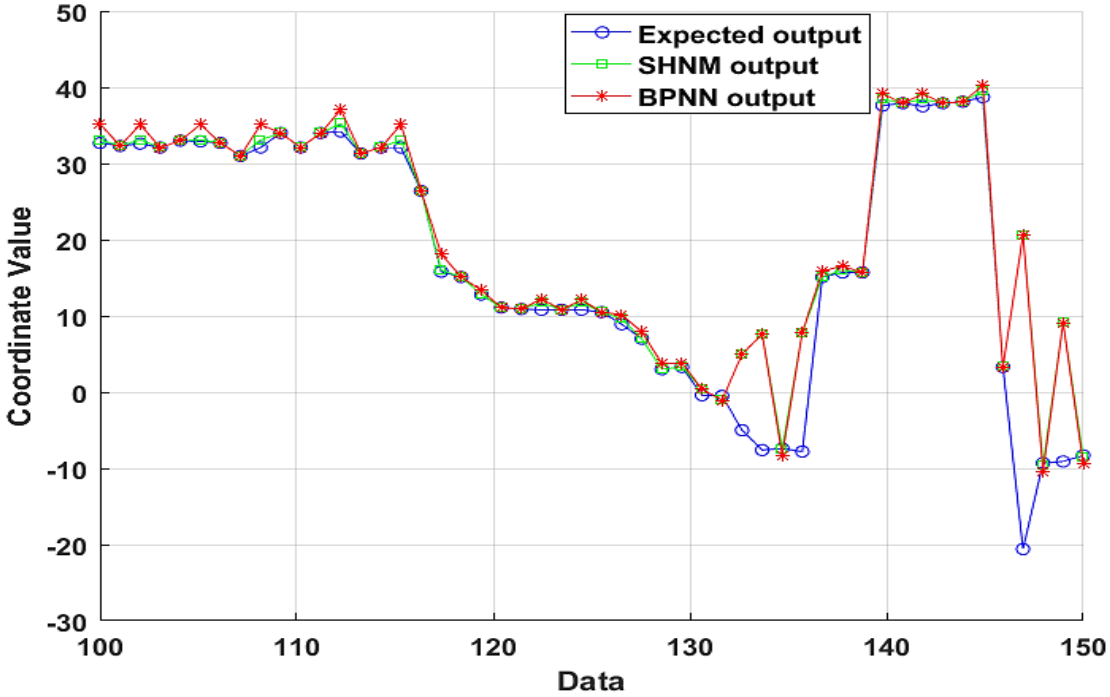

Figure 5.15: Comparison of prediction of Pitch angular coordinates with SHNM and BPNN

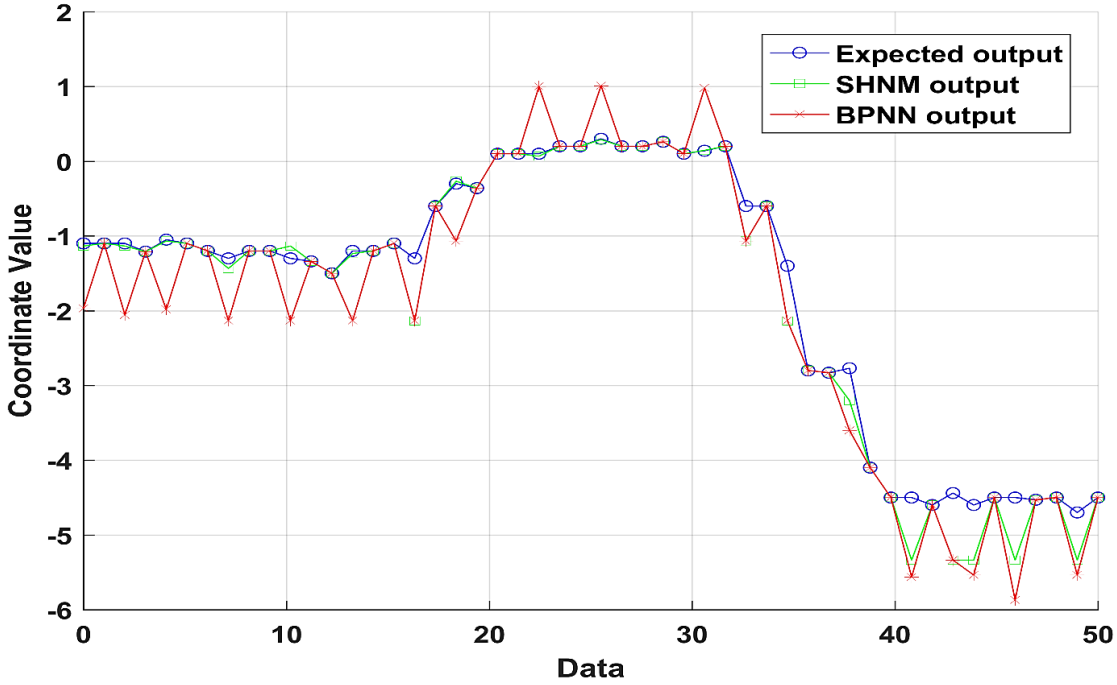

Figure 5.16: Comparison of prediction of Roll angular coordinates with SHNM and BPNN

5.2.3 COMPARISON OF SELF HEALING NEURAL MODEL AND AUTOREGRESSIVE LINEAR MODEL (ORDER TWO AND THREE) IN THE PREDICTION OF MISSING HEAD MOTION COORDINATES IN ELECTROMAGNETIC TRACKING

In this section, the predicted 6-DoF coordinates are compared with the Autoregressive Linear Model. The accuracy of the prediction depends on the order of the Autoregressive model used for the prediction. In this case, the ARLM of order 1 predicted the missing 6-DoF head coordinates with less accuracy as compared to the ARLM of order 2 and order 3. ARLM of order more than 3 is not used in this work to avoid the overhead complexity of the prediction system. Figure 5.17 represents the comparison of prediction accuracy of coordinate X using ARLM of order 3 and the Self Healing Neural Model. The threshold of the missing 6-DoF head coordinates is kept 1% in this experiment. The graphical representations of prediction of ALRM of order 3 of a dataset consisting of 10% missing 6-DoF head coordinates are shown in Figure 5.17 to Figure 5.28. The enlarged view of each coordinate is also represented in this section for better observation of the prediction. The percentage of prediction accuracy of missing 6-DoF head coordinates is computed against the ground truth 6-DoF data acquired in the absence of any kind of interference. Table 5.2 describes the comparison of the predicted results of the ARLM (order 3), SHNM, and BPNN with 1%, 2%, 10%, 25%, and 35% of missing head motion coordinates in a data set using the electromagnetic tracker.

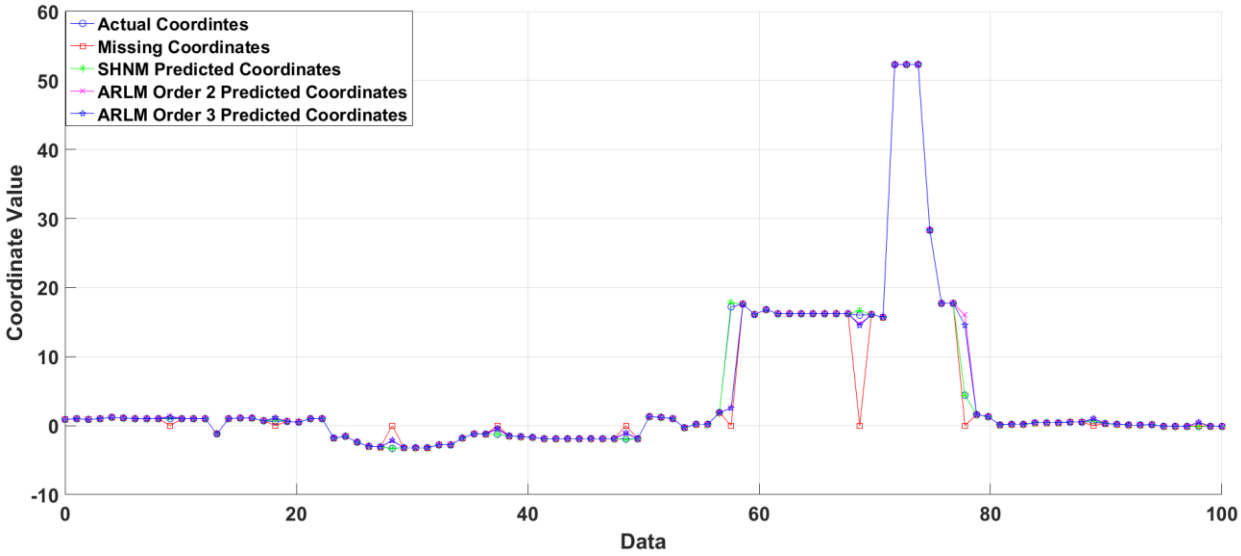

Figure 5.17: Comparison of prediction of X coordinates with SHNM and ARLM

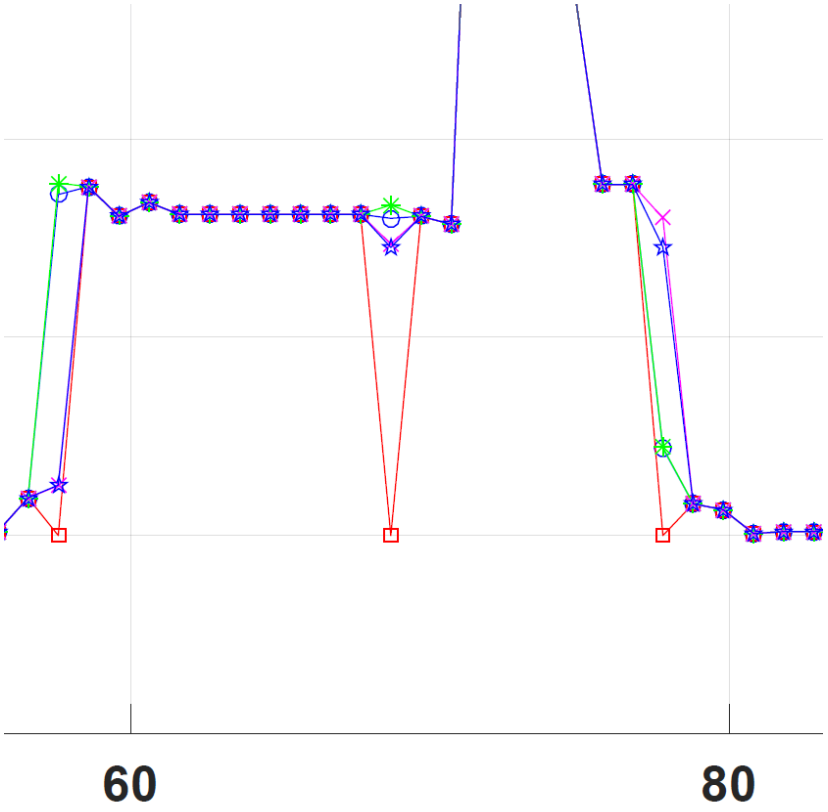

Figure 5.18: Enlarged view of the prediction of X coordinates with SHNM and ARLM

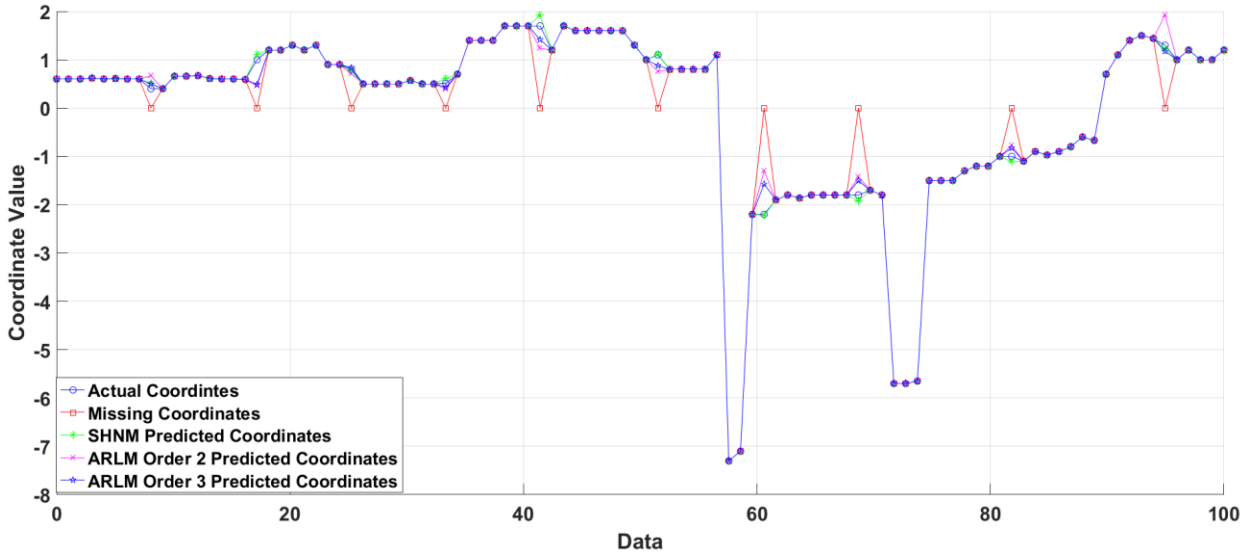

Figure 5.19: Comparison of prediction of Y coordinates with SHNM and ARLM

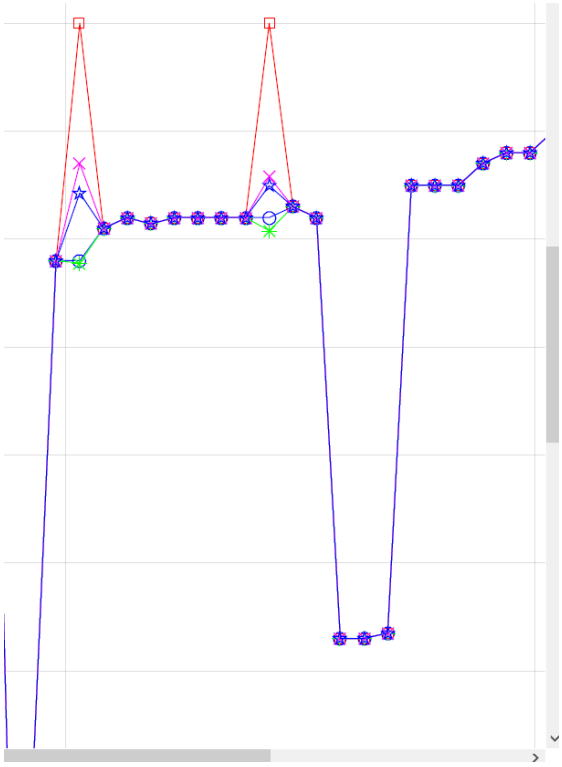

Figure 5.20: Enlarged view of the prediction of Y coordinates with SHNM and ARLM

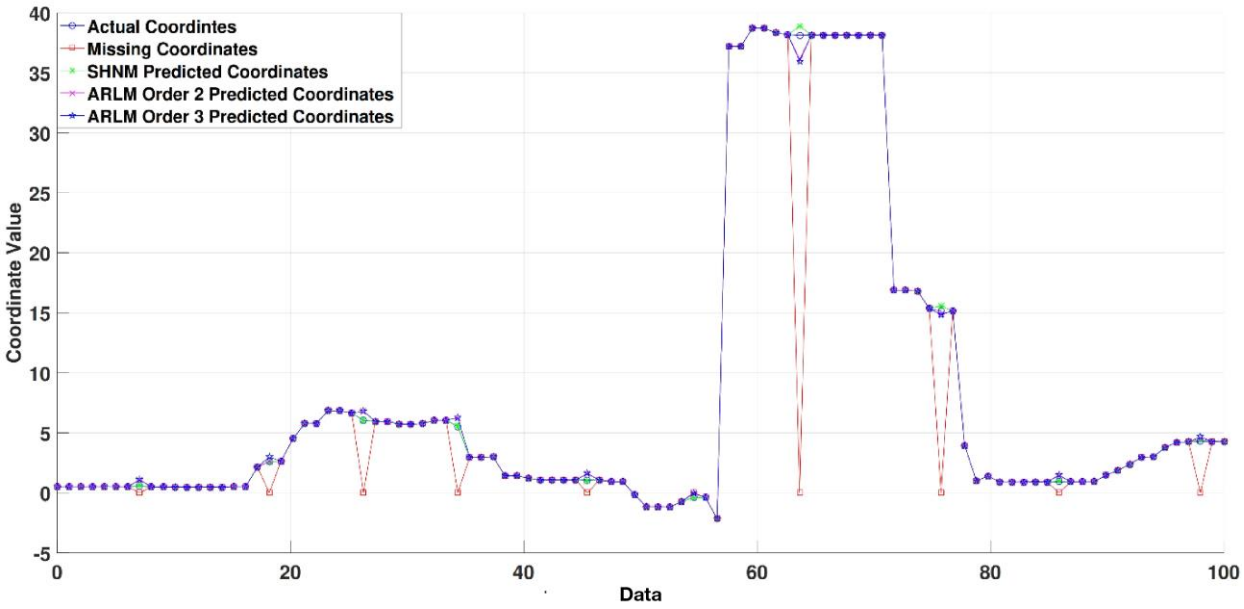

Figure 5.21: Comparison of prediction of Z coordinates with SHNM and ARLM

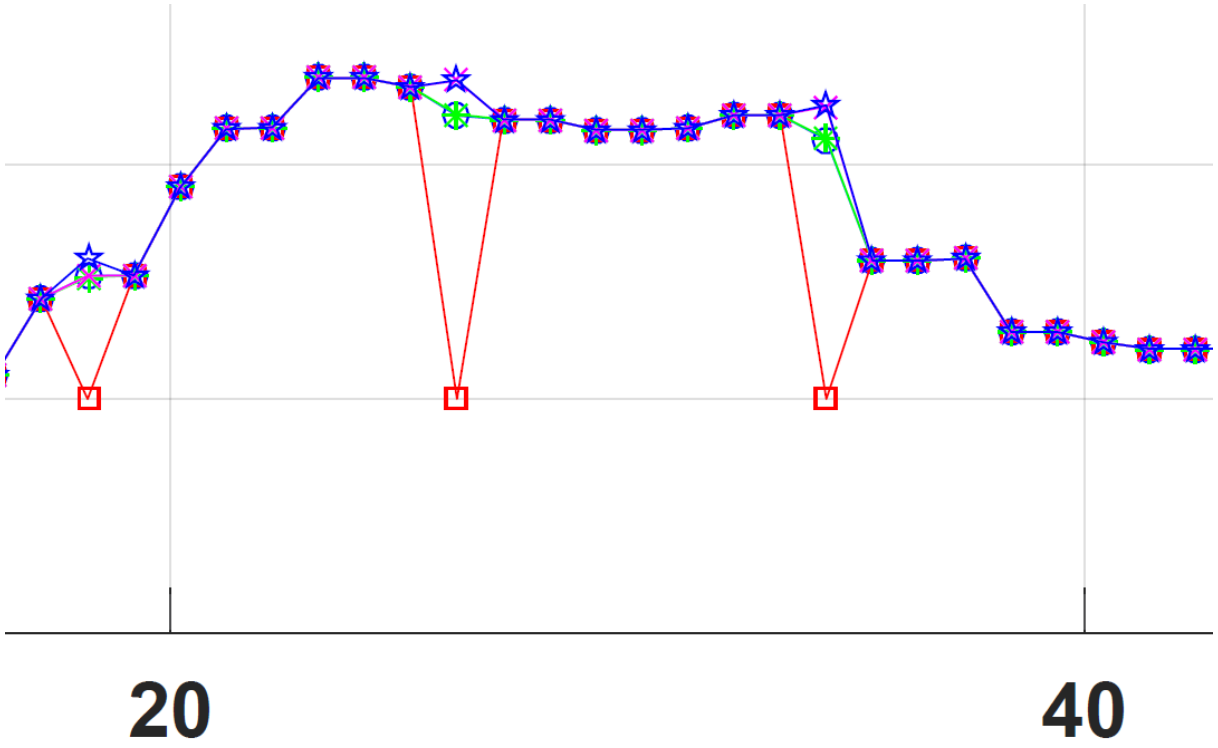

Figure 5.22: Enlarged view of the prediction of Z coordinates with SHNM and ARLM

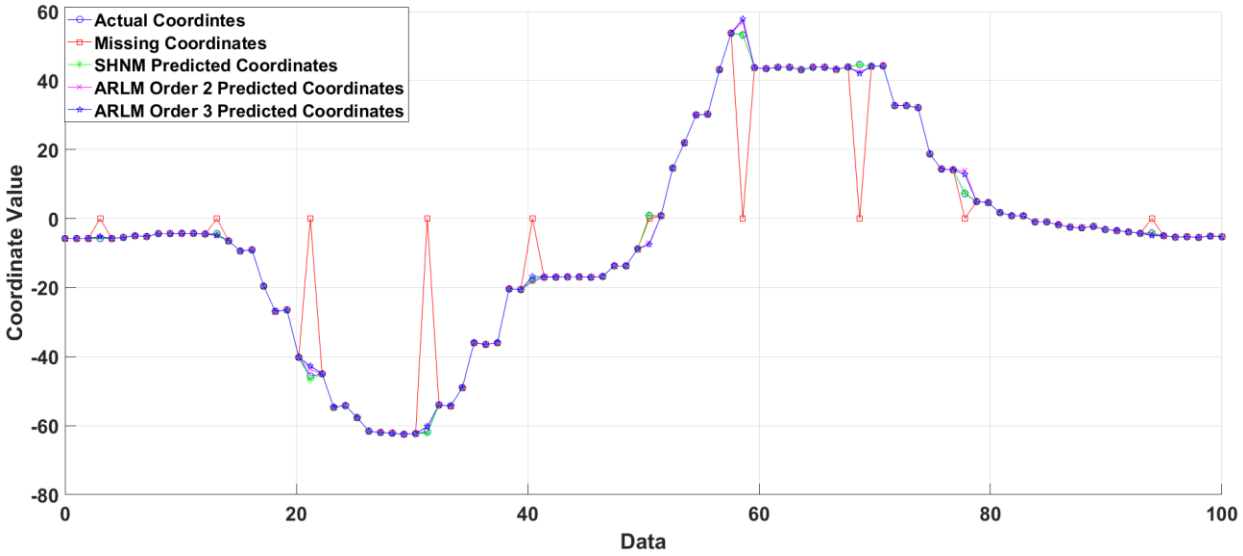

Figure 5.23: Comparison of prediction of Yaw coordinates with SHNM and ARLM

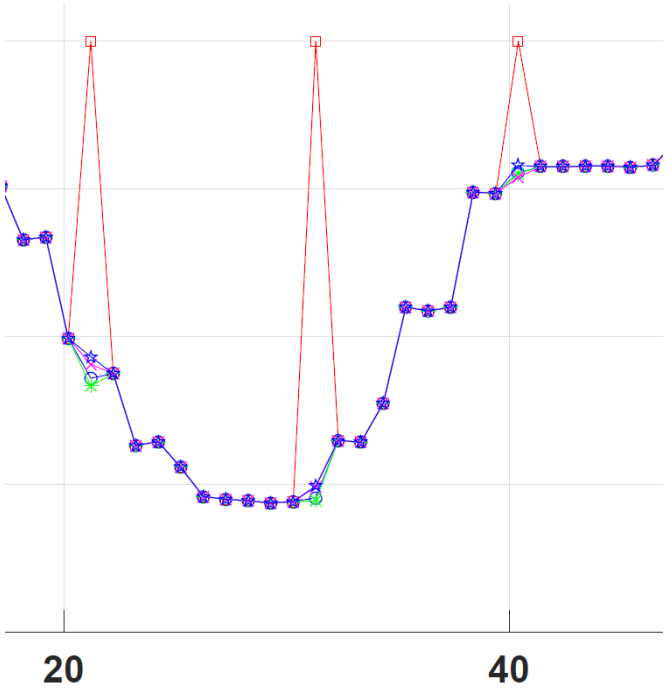

Figure 5.24: Enlarged view of the prediction of Yaw coordinates with SHNM and ARLM

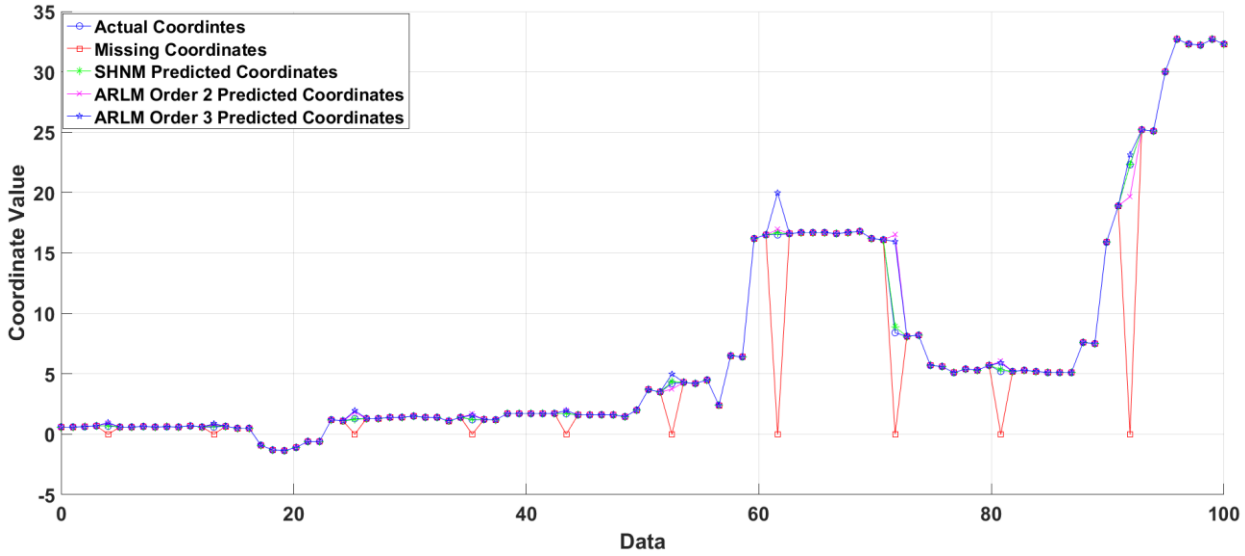

Figure 5.25: Comparison of prediction of Pitch coordinate with SHNM and ARLM

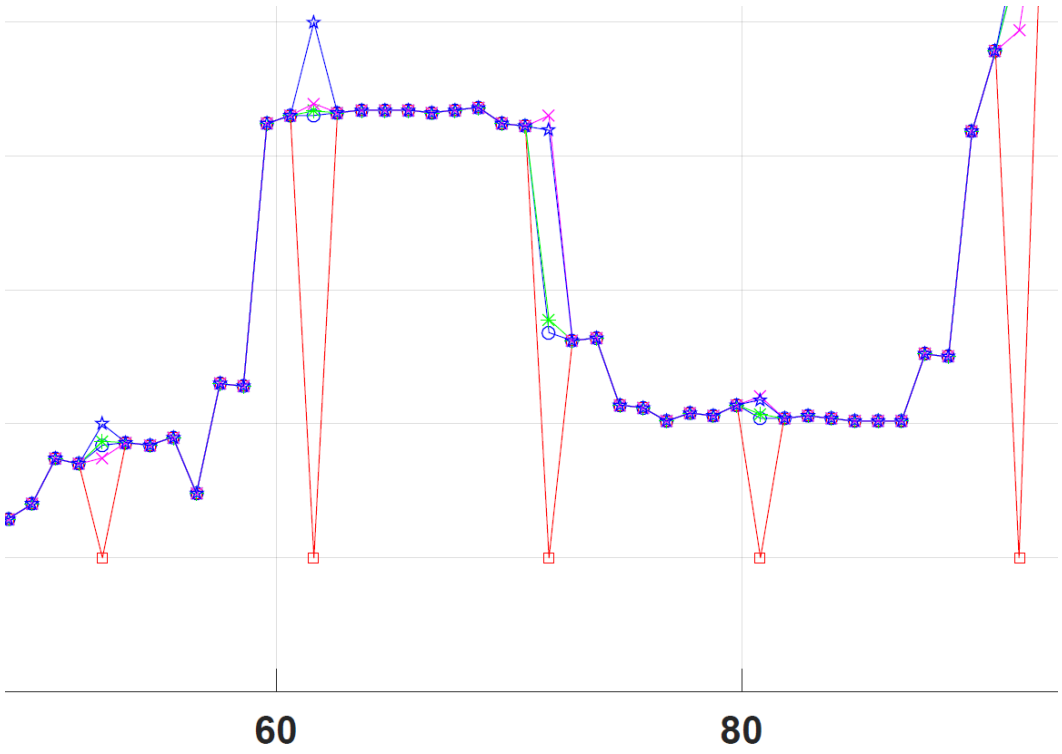

Figure 5.26: Enlarged view of the prediction of Pitch coordinate with SHNM and ARLM

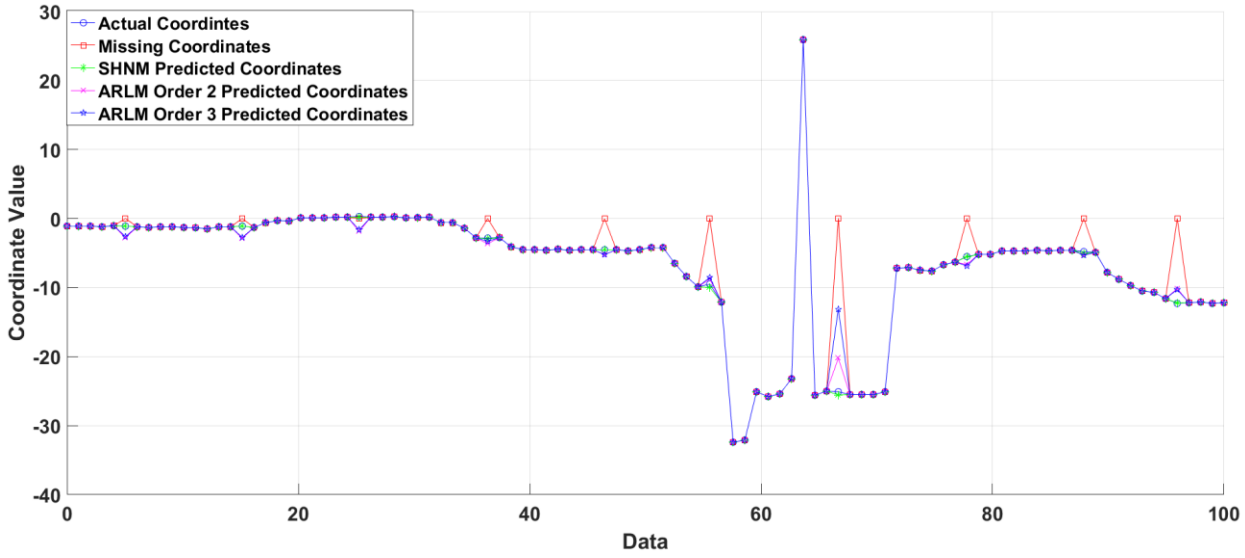

Figure 5.27: Comparison of prediction of Roll coordinate with SHNM and ARLM

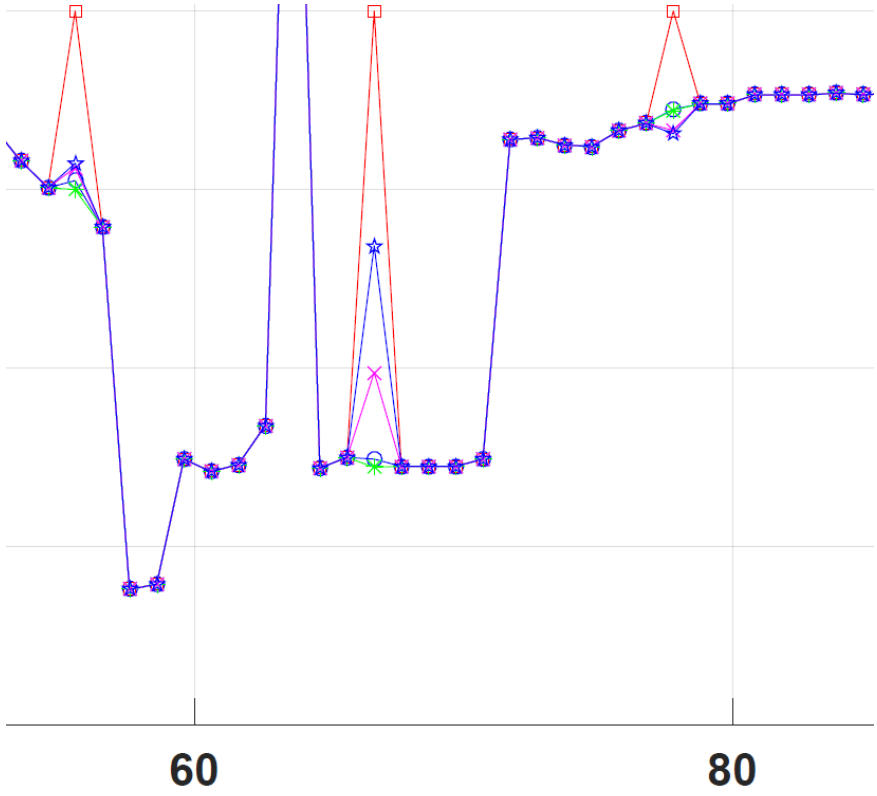

Figure 5.28: Enlarged view of the prediction of Roll coordinate with SHNM and ARLM

Table 5.2 represents the accuracy comparison of SHNM with BPNN and ARLM with different percentages of missing data using the electromagnetic tracker.

Table 5.2: The accuracy of comparison of the techniques used in the prediction of the 6-DoF missing head coordinates with different sets of missing data using the electromagnetic tracker.

Parameters	**Accuracy of data against the missing percentage**														
Missing Percentage Of 6-DoF→ Head Coordinates	1%			2%			10%			25%			35%		
Model used→	**SHNM**	BPNN	ARLM	**SHNM**	BPNN	ARLM	**SHNM**	BPNN	ARLM	**SHNM**	BPNN	ARLM	**SHNM**	BPNN	ARLM
X	**91.3%**	84.4%	86.7%	**90.4%**	84.1%	86.6%	**89.6%**	82.1%	84.5%	**88.4%**	83.2%	81.3%	**84.3%**	79.8%	75.1%
Y	**95.6%**	88.8%	89.7%	**95%**	90.1%	91.7%	**95.1%**	88.6%	90.2%	**91.7%**	84.2%	83.6%	**89.5%**	80.7%	74.4%
Z	**95.3%**	88%	89.2%	**94.8%**	88.3%	90.9%	**93.2%**	86.3%	87.9%	**89.1%**	83.3%	80.8%	**87.6%**	80.4%	76.1%
Yaw	**93.4%**	86.7%	87.9%	**91.9%**	89.9%	91.8%	**92.2%**	84.4%	86%	**89.9%**	81.9%	79.1%	**89.3%**	81.6%	77.3%
Pitch	**95.3%**	89.9%	90.3%	**94.5%**	90%	92.2%	**94.7%**	85.4%	88.8%	**91%**	84.3%	83.5%	**89.6%**	82.1%	78.9%
Roll	**89.9 %**	83.4%	85%	**87.9%**	82.1%	84.8%	**89%**	80.2%	84.1%	**86.7%**	79.8%	78.2%	**84%**	78.6%	71.2%

5.2.4 SUMMARY OF RESULTS OF ACCURACY IN ELECTROMAGNETIC TRACKER

This section discusses the summary of prediction accuracy achieved using different prediction techniques for the electromagnetic tracker. The prediction of missing 6-DoF head motion coordinates was done using Self Healing Neural Model (SHNM), Back Propagation Neural Network (BPNN), Adaptive Neuro-Fuzzy Inference System (ANFIS), and Autoregressive Linear Model (ARLM). The results of SHNM, BPNN, and ARLM are compared in Table 5.2. The comparison of SHNM, BPNN, and ANFIS is discussed in section 5.8. It was found that the performance of SHNM was superior to BNNN and ARLM. In the 35%, missing 6-DoF head motion coordinates data set the SHNM yielded the highest accuracy varying from 84% to 89.6% (all 6-DoF coordinates), whereas the variation in BPNN and ARLM was 78.6% to 82.1% and 71.2% to 78.9% respectively.

5.3 FACTORS AFFECTING THE TRACKING OF THE HEAD WHILE USING AN OPTICAL TRACKER

There are different factors affecting the tracking accuracy of the optical head tracker. Among these, factors namely distance between transmitter and receiver, orientation between transmitter and receiver, stray light intensity, and latency have been studied in this work. Each factor is discussed in brief below.

5.3.1 DISTANCE BETWEEN THE OPTICAL TRANSMITTER AND RECEIVER

Distance between transmitter and receiver plays an important role in object tracking while using the optical tracker. The tracking area of an optical tracker is limited and hence it is necessary that the distance between the transmitter and receiver be decided based on repeatable tracking performance. In this work, the maximum distance between transmitter

and receiver according to the workspace of the cockpit simulator has been taken as one meter. The head tracking is performed for four different distance ranges in this work, which is discussed in detail in the experiment section.

5.3.2 Different Placement and Orientation Schemes for Optical Tracker Experimentation

The FOV of an optical tracker plays an important role to judge its tracking limit. Limited FOV is due to the limit of head motion box limitation to the pilot while in an aircraft cockpit. It is the magnitude of the evident world that is seen at any moment. A human being has FOV of approximately 180° but the FOV of the head trackers is generally less. FOV is an important aspect of evaluating the performance of optical head tracking. It plays a vital role as FOV depends on the placement and orientation scheme of optical trackers. A larger FOV results in a greater sense of attention and better situational cognizance [148, 149].

FOV increases with an increase in the number of trackers but then it is also limited by the HMB space available to an aircraft pilot. The tracking and the placement schemes are shown in Figure 5.29(a) and Figure 5.29 (b) have opted for experimentation with the optical tracker. The placement of Figure 5.29(a) has been used in the present work is opted. The placement scheme as shown in Figure 5.29(c) can also be employed for 3D tracking of the object.

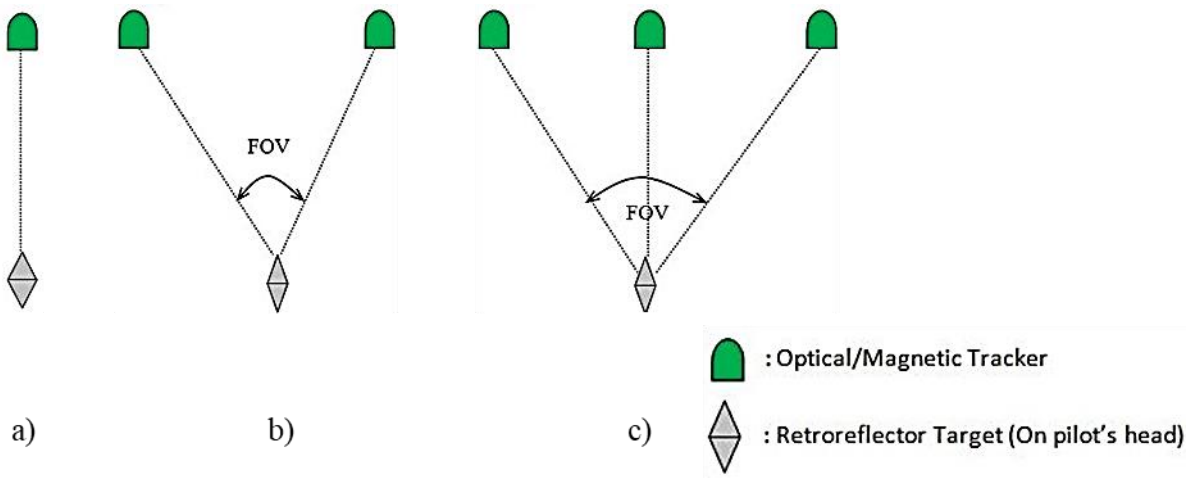

Figure 5.29: Different placement schemes of an optical tracker

5.3.3 STRAY LIGHT INTENSITY

The tracking accuracy of an optical tracker depends on the lighting conditions (basically stray light). To study the effect of light intensity on the tracking accuracy of an optical tracker, the 6-DoF data of the head coordinated is acquired under different light intensity ambiance. The data acquired under the different light intensities is discussed in the section.

5.4 EARLIER WORK DONE IN OPTICAL HEAD TRACKING

In earlier reported research, various kinds of tracking problems had been discussed. Bajana ***et al.***[150] presented a system in which they combined optical tracking and augmented reality to computing global data in local large areas. For this, they used two different tracking technologies: infrared marker-based on **OptiTrack™ and Vuforia software platform**. Muñoz-Salinas ***et al.***[151] used multiple cameras to track the position of the head. Their work used probability estimates produced by the multiclass support vector machines to calculate the probability distribution of the head postures. The distributions produced by the multiple cameras were fused to produce a more accurate and robust

estimate. It was found that their proposed system was highly sensitive to the occlusion. Deldjoo ***et al.***[152] integrated an optical tracking system in Ericsson 3D audio system for more immersion. They used the camera of Nintendo Wiimote in a successful attempt of developing a head tracker for a synchronized auditory and visual cue. Czupryński and Strupczewski [153] discussed statistical approaches for head tracking along with their mathematical models. They also discussed long-term stabilities of different head tracking techniques. They mentioned the hybrid approaches used in head tracking to reduce errors and latency. In these related works of head tracking, no method related to the recovery of missing or corrupted 6-DOF data were discussed. Hence, SHNM is employed considering its numerous advantages in such an application to eliminate this problem and to recover the missing data with high accuracy.

5.5 EXPERIMENTAL SETUP FOR ACQUISITION OF 6-DOF COORDINATES OF HEAD USING OPTICAL TRACKER

Head tracking can be done using different tracking techniques such as optical tracking, magnetic tracking, inertial tracking, etc. In this chapter, a six-degrees-of-freedom (6-DoF) optical tracker (TrackIR^{TM} 5) is used to record the coordinates of the pilot's head motion in real-time on the simulator bed. During the process of acquisition of the coordinates of head movement by the optical tracker, the data may be missed due to stray light interference or any other kind of occlusion. To predict the missing data, Self Healing Neural Model (SHNM) is applied.

Optical trackers have comparatively higher accuracy and their feature of being wireless allows the user to work in a large volume of space. The data acquired by the head trackers generally consists of 6-DoF coordinates. Due to various reasons like sensor malfunctioning

or stray light interference or movement of head tracker beyond HMB range, the 6-DoF data acquired by the optical tracker may be corrupted or missed causing reduced tracking accuracy. The work is based on missing data incidents.

5.5.1 ACQUISITION OF DATA USING OPTICAL TRACKER UNDER DIFFERENT PLACEMENT SCHEMES AND ORIENTATION

The experiment was conducted under different light intensities and different distances between transmitter and receiver. Experiments were conducted on the cockpit simulator at CSIR-CSIO, Chandigarh, India.

i) Cockpit Simulator

The experiment was carried out on the cockpit simulator developed by the CSIR - Central Scientific Instruments Organization, Chandigarh, India. As shown in Figure 5.30 an optical tracker was positioned on the cockpit simulator and the experiment was carried out under different lighting conditions.

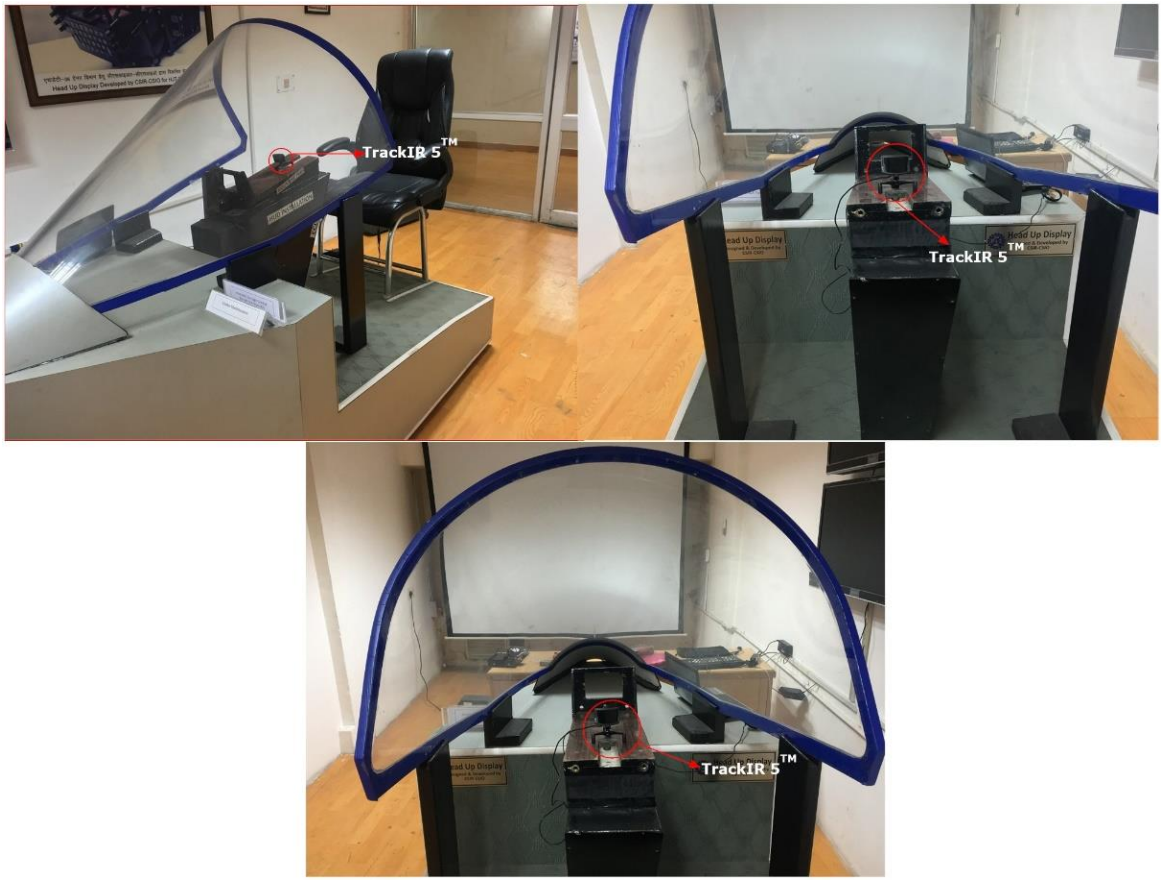

Figure 5.30: Cockpit Simulator with Optical Tracker TrackIR 5™ (encircled in red) at CSIR-CSIO, Chandigarh, India

ii) Optical Tracker

As shown in Figure 5.30, the TrackIR™ **5** is used to track the head movements of the pilot in the cockpit simulator used for simulation.

iii) Lux Meter

The light intensity was measured by using Lux meter (TES 1332) as shown in Figure 5.31.

Figure 5.31: Readings of Lux meter under different light intensities

iv) Data Acquisition

Dell Inspiron 5999 series was used to collect 6-DoF data of head movements. Data set were modeled after performing experiments under different environmental conditions such as variation in light intensity and variation in distance between the transmitter and the receiver. Light intensity and distance variation between the transmitter and the receiver helped in the study of the effect of distance between the optical transmitter and optical

receiver as well as the effect of different light intensities on the optical head tracking. It also helped in the prediction of the desirable conditions in which the optical tracker gave satisfactory output. Light intensity was measured as the rate at which energy of light is delivered per unit surface per unit time per unit area. Light intensity was measured in Lux (lx). The experiments were conducted for simulated ambient light intensity varying from 4 lux to 166 lux. In the experimentation analysis, the distance between the pilot's head transmitter and the receiver was kept in four distance ranges: 25 cm, 50 cm, 75 cm, and 100 cm. The 6-DoF data of the head movements were then collected by varying the head in different directions and orientations. Experimental setups are provided in Figure 5.32, Figure 5.33, Figure 5.34, and Figure 5.35.

Figure 5.32: Experiment conducted at light intensity value of 3 lux at different distances: 25 cm, 50 cm, 75 cm & 100 cm marked 1-4 respectively

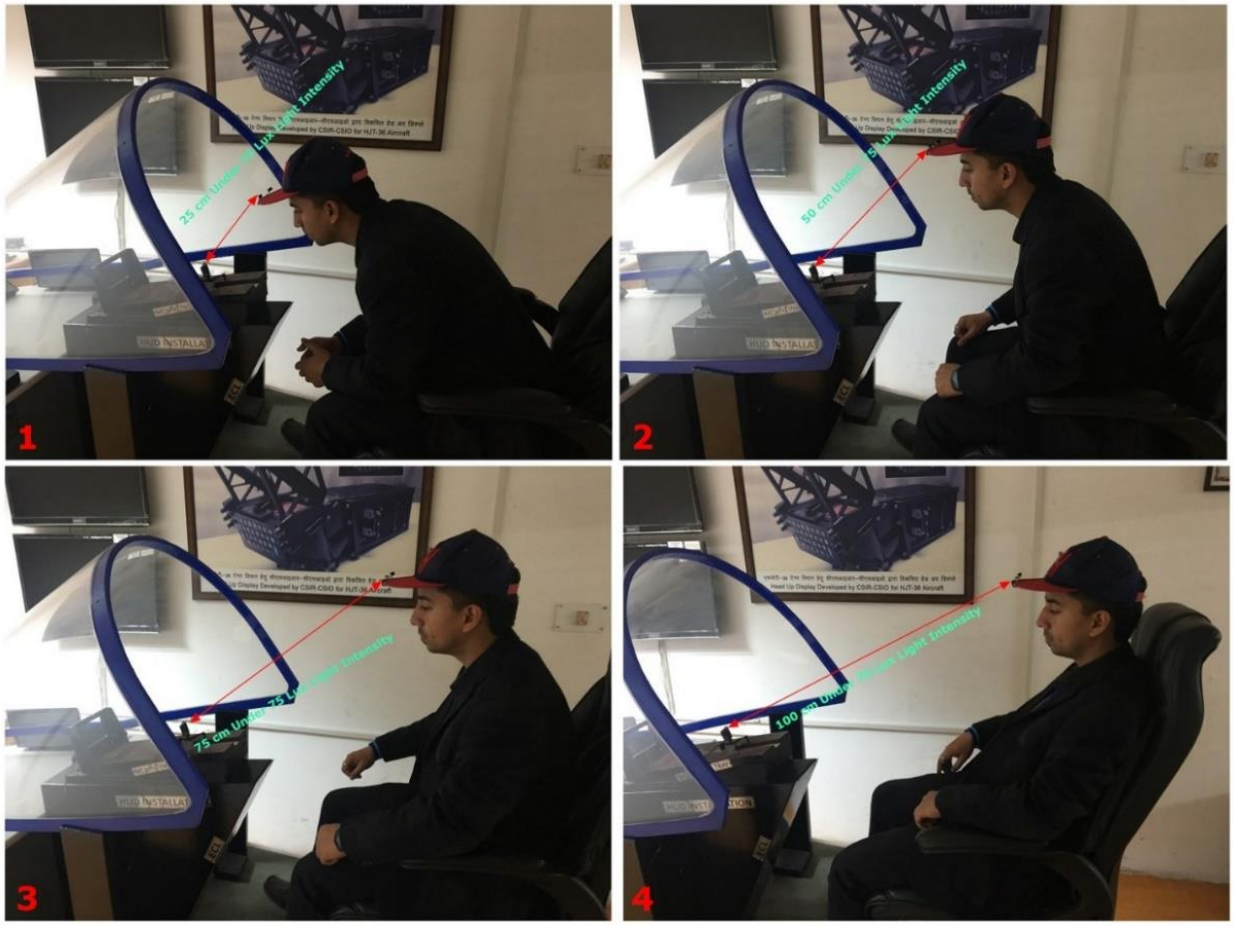

Figure 5.33: Experiment conducted at light intensity value of 75 lux light intensity at different distances: 25 cm, 50 cm, 75 cm & 100 cm marked 1-4 respectively

Figure 5.34: Experiment conducted at light intensity value of 111 lux light intensity at different distances: 25 cm, 50 cm, 75 cm & 100 cm marked 1-4 respectively

Figure 5.35: Experiment conducted at light intensity value of 165 lux light intensity at different distances: 25 cm, 50 cm, 75 cm & 100 cm marked 1-4 respectively

5.5.2 POST-PROCESSING OF ACQUISITION OF DATA

The data was acquired using **TrackIR™ 5 optical tracker** operating with FOV of 51.7° at a 120fps sampling rate with a response time of 10 ms. The interface of the optical tracker was USB 2.0. The physical dimensions of the tracker were 1.5" (3.81 cm) L x 2" (5.1 cm) W x 0.57" (1.45 cm) H. The TrackIR™ 5 optical tracker acted as a source to generate the Infrared (IR) light. The incoming IR light was reflected by three retro-reflective markers, which were assembled on the TrackClip. This was placed on the helmet/head of the pilot. The reflected IR light was detected by the infrared camera present in TrackIR™ 5, which

then tracked the positional and orientation coordinates of the head of the pilot. The description of 6-DoF data acquired using an optical tracker is given in Table 5.3.

Table 5.3: Description of the movements of the Head

DoF	Information
X	The forward and backward translational coordinate of the pilot's head
Y	Left and right translational coordinate of the pilot's head
Z	Up and down translational coordinate of the pilot's head
Yaw	The rotational coordinate of the pilot's head along the Z-axis
Pitch	The rotational coordinate of the pilot's head along the Y-axis
Roll	The rotational coordinate of the pilot's head along the X-axis

The number of instances acquired is 4400. The system is easy to set up and simple to use. It is capable of performing all the complex calculations that provided both position and orientation data of the head of the subject on the simulator bed. Each instance represents a particular position and orientation of the pilot's head. The sample data set is shown in Table 5.4. Units of translational coordinates are in centimeters and rotational coordinates are in degrees.

Table 5.4: Sample data set of the optical tracker

X	Y	Z	Yaw	Pitch	Roll
6.4	6.5	3.15	-14.4	23.5	-2.9
6.3	5.7	3.48	-14.3	16.6	-2.6
6.4	5.8	3.47	-14.6	17	-2.6
6.2	3.8	5.08	-14.7	5.9	-0.3
6	3	5.39	-14.5	5.2	-0.1
5.8	2.6	5.68	-13.9	4.8	-0.1
5.9	2.7	5.86	-13.4	4.9	-0.2
5.7	2.9	6.04	-13.1	5.3	-0.4
5.5	3	6.19	-13.3	5.4	-0.5
5.4	2.4	6.47	-13	3.9	-0.4

The sixteen different datasets were acquired through different experimental setups. Table 5.5 represents different experimental setups to acquire the coordinates of the head.

Table 5.5: Different Experimental setup for the acquisition of data using Optical Tracker

Experimental Setup	Light Intensity	Distance between Optical Transmitter and Receiver	Dataset opted for analysis
1.	3 Lux	25 cm	Out of the four experimental setups and among 16 data sets, the data acquired from the fourth experimental setup with 100 cm distance between Transmitter and Receiver was chosen for the analysis. As the light intensity and distance factor were maximum among all, therefore it was the best data set to be chosen for the analysis and prediction using SHNM.
		50 cm	
		75 cm	
		100 cm	
2.	75 Lux	25 cm	
		50 cm	
		75 cm	
		100 cm	
3.	111 Lux	25 cm	
		50 cm	
		75 cm	
		100 cm	
4.	165 Lux	25 cm	
		50 cm	
		75 cm	
		100 cm	

5.5.3 PREDICTION OF MISSING HEAD MOTION 6-DOF COORDINATES IN OPTICAL TRACKER USING SELF HEALING NEURAL MODEL

Referring to Table 5.5, different placements of the optical tracker with reference to the distance between the transmitter and the receiver are discussed. The tendency of 6-DoF head motion coordinates to get missed or corrupted is minimum when the distance between transmitter and receiver is minimum (25 cm in this case). A maximum number of 6-DoF head motion coordinates got missed when the distance is maximum (100 cm). Therefore, the data set used in this experiment for the prediction of missed 6-DoF head motion coordinates has a maximum distance of 100 cm between the transmitter and the receiver. The available data of 4400 instances including missing data acted as an input for the SHNM. The available data set was then checked for the number of missing instances present. "0s" denoted the missing instances and each "0" corresponded as a dummy neuron and its value was recovered by healing function S_H (From equation 4.1). The occlusion or interference due to the stray light or movement beyond the HMD range in the optical tracker could lead to some missing instances during data acquisition of the pilot's head coordinates for a short duration. To eliminate this problem, the coordinates of the head, which could not be recorded at the instant when the optical tracker malfunctioned due to occlusion or stray light interference or due to out of range of HMB, were recovered using SHNM. For the experimental purpose, the data set with missing 6-DoF coordinates was constructed by including the deliberate occlusion or inclusion of the stray light in front of the optical tracker for a particular instant of time. The recovery process of missing data was assured by each iteration carried out by SHNM to recover each instance of missing data. After

recovery, the recovered data was analyzed for correctness and validation using supervised learning.

In the final step, the accuracy of the recovered data against the actual data was computed using ground truth data as shown in the workflow in Figure 5.37. The threshold for the proposed system to compute the accuracy was assumed based on the average of self-healing cost over the available data set [96]. The simulations through SHNM was done in MATLAB R2016a.

The criteria used for the calculation of the accuracy is Mean absolute percentage error (MAPE). The percentage of the accuracy of the prediction is calculated as mentioned in Equation (5.1).

Figure 5.36 shows the real-time experimental setup of an optical tracking system with a software interface.

Figure 5.36: Experimental setup of the optical tracking system with the software interface

The proposed system along with the workflow is represented in Figure 5.37.

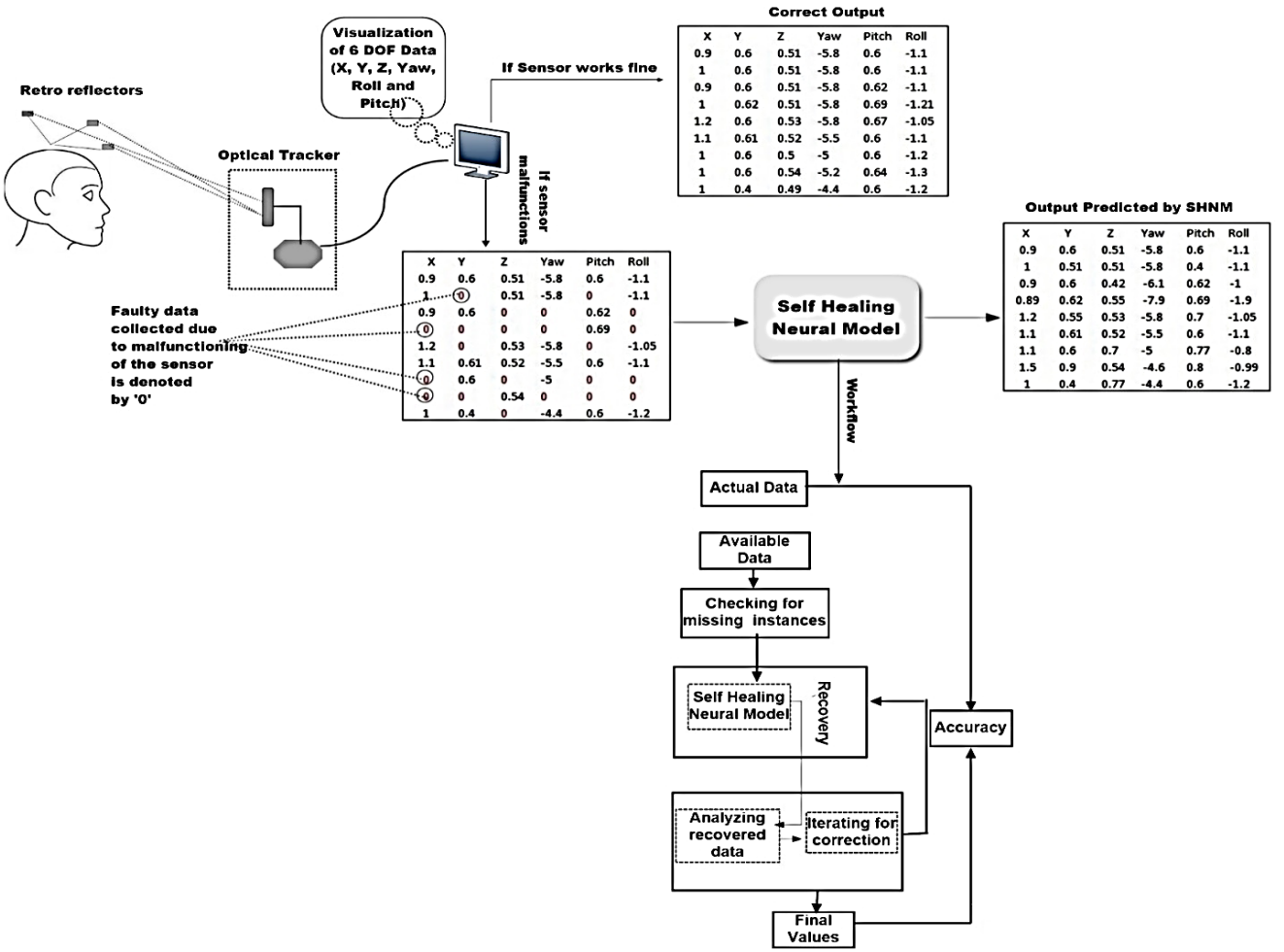

Figure 5.37: Experimental description of optical head tracking along with the workflow of the SHNM process for missing data prediction

5.6 RESULTS AND DISCUSSIONS ON ERRORS ESTIMATION IN OPTICAL HEAD TRACKING

5.6.1 PREDICTION OF MISSING 6-DOF HEAD MOTION COORDINATES USING SELF HEALING NEURAL MODEL

In this section, the performance analysis of the proposed approach is discussed. To simulate the conditions of missing data in MATLAB R2016a, five sets of different missing percentage (1%, 2%, 10%, 25%, and 35%) are generated from the original data set. The results obtained using SHNM were better than the other neural networks [154, 155] like the BPNN model and Auto-Regressive Linear Model (ARLM). The 6-DoF head coordinates can be missed due to stray light interference and by exceeding the range of motion of the head in the cockpit from the stipulated amount of range of head motion box. The horizontal limit of the head motion box is 120 mm and the vertical limit is 70mm in the cockpit. Due to this reason, the minimum missing percentage (1% and 2%) of 6-DoF data is taken into account for the prediction. The graphical representations of prediction of 1% and 2% missed 6-DoF head coordinates are not shown to avoid the repetition of graphs. In addition, the prediction of 1% and 2% missing 6-DoF head coordinates in large data set is not clearly observable graphically.

The graphs for the prediction of missing head position coordinates are represented. The graphs for the prediction of 35% missing head position coordinates are represented in this chapter. The prediction of 10% and 25% missing head position coordinates in the Optical head tracker is shown in **Appendix B.**

Figure 5.38 to Figure 5.40 shows the prediction of 35% missing head coordinates of X, Y, and Z respectively. The X, Y, and Z are the translational head coordinates. In these graphs, the blue line signifies the actual coordinates (used for training), the red line shows the missing coordinates (testing) and the green line shows the predicted data set of missed head coordinates using the Self-healing Neural Model. The x-axis is the translational value of head coordinates (in millimeter) and the y-axis shows the number of head coordinates in all three graphs.

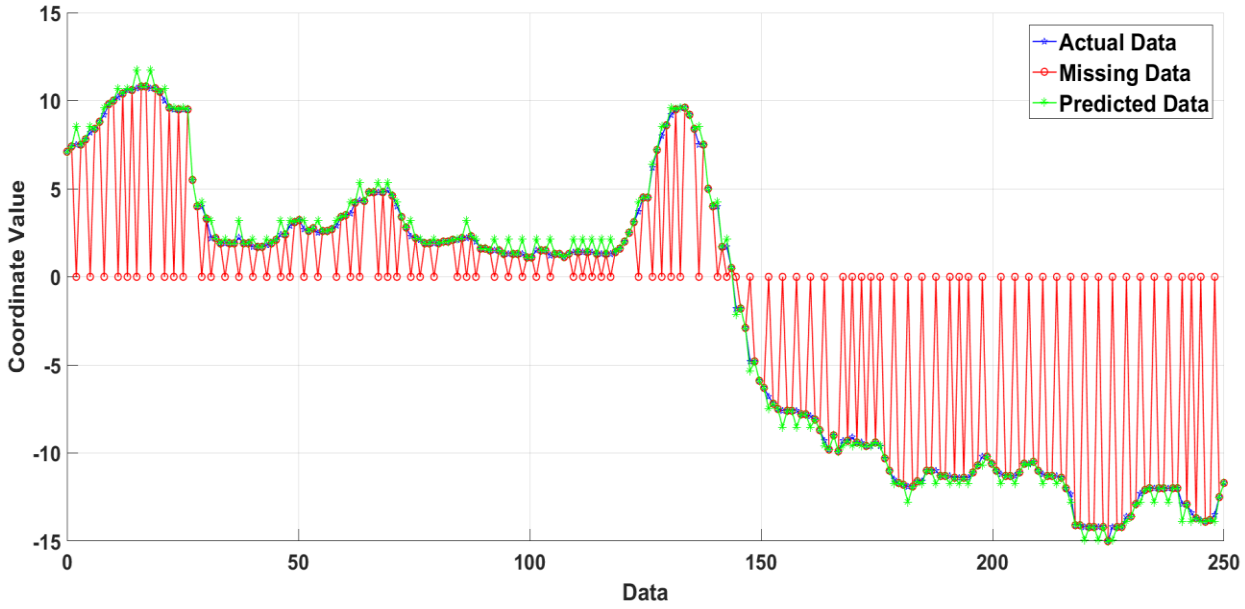

Figure 5.38: Prediction of X coordinates through SHNM for the data set with 35% missing 6-DoF head coordinates

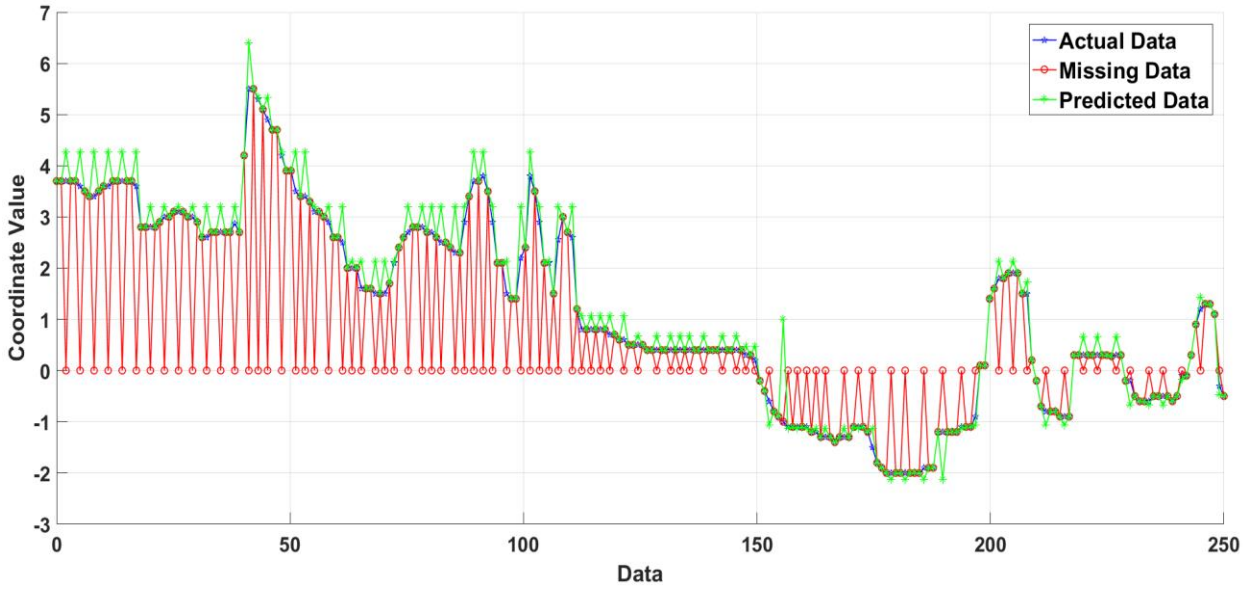

Figure 5.39: Prediction of Y coordinates through SHNM for the data set with 35% missing 6-DoF head coordinates

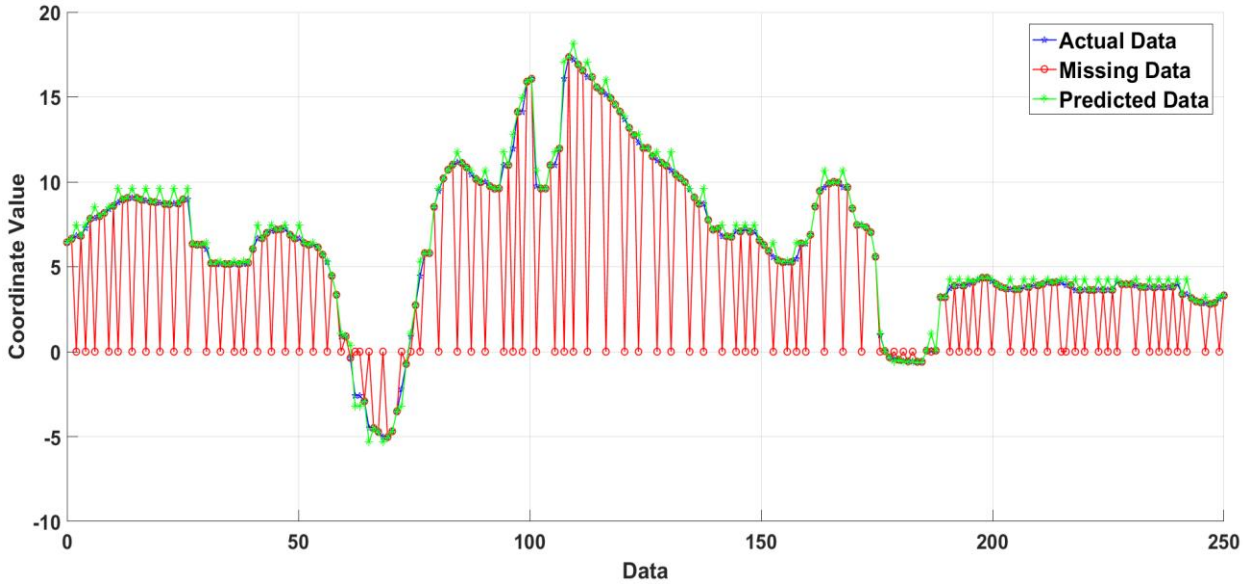

Figure 5.40: Prediction of Z coordinates through SHNM for the data set with 35% missing 6-DoF head coordinates

Figure 5.41 to Figure 5.43 shows the prediction of 35% missing head coordinates of Yaw, Pitch, and Roll respectively. The Yaw, Pitch, and Roll are the rotational head coordinates. In these graphs, the blue line signifies the actual coordinates (used for training), the red line shows the missing coordinates (testing) and the green line shows the predicted data set of missed head coordinates using the Self-healing Neural Model. The x-axis is the translational value of head coordinates (in degrees) and the y-axis shows the number of head coordinates in all three graphs.

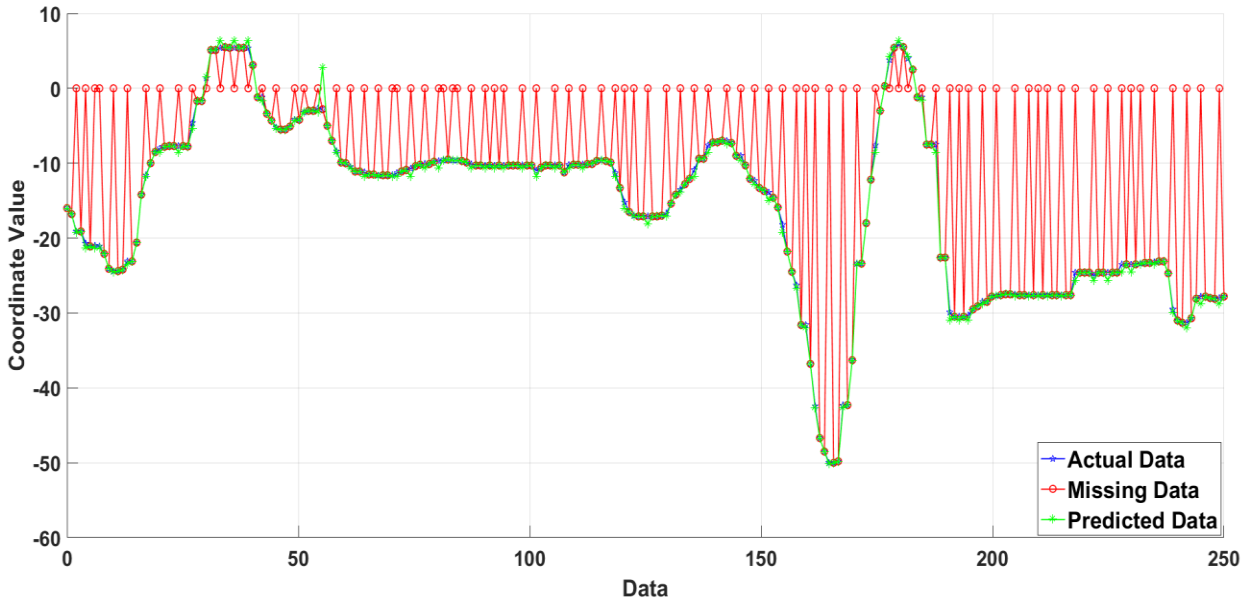

Figure 5.41: Prediction of Yaw angular coordinates through SHNM for the data set with 35% missing 6-DoF head coordinates

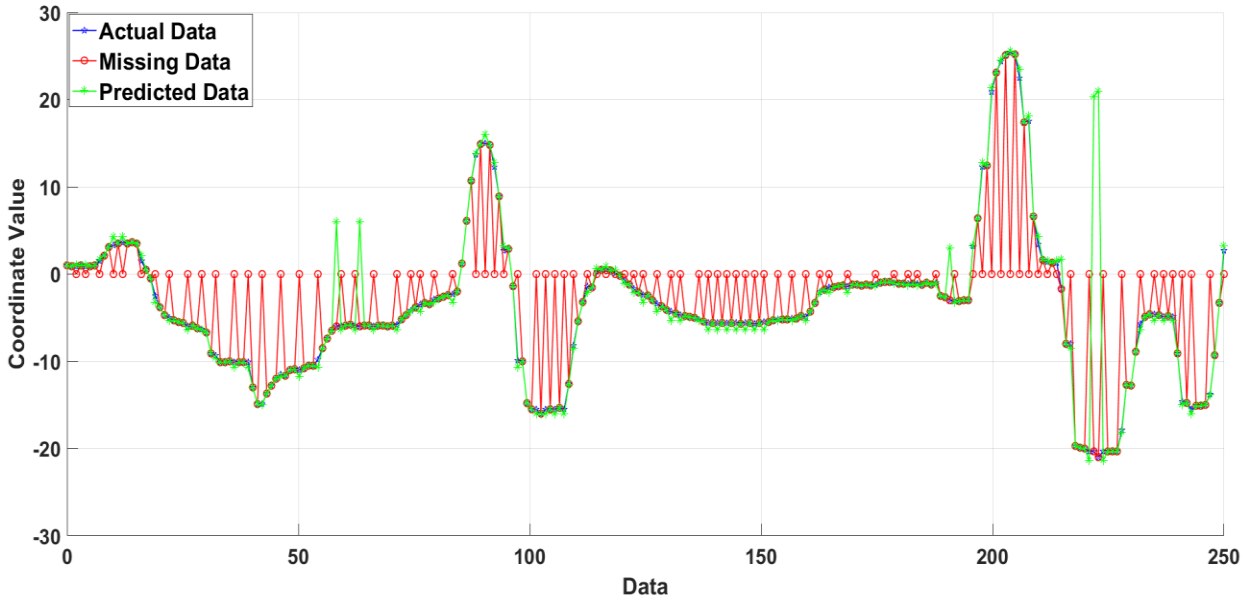

Figure 5.42: Prediction of Pitch angular coordinates through SHNM for the data set with 35% missing 6-DoF head coordinates

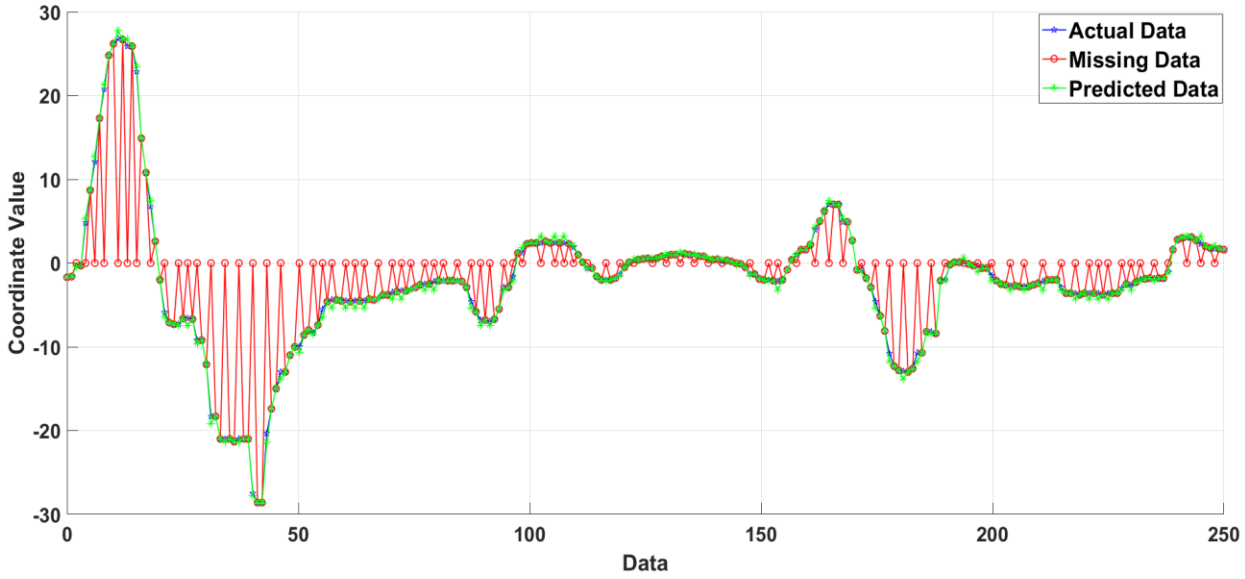

Figure 5.43: Prediction of Roll angular coordinates through SHNM for the data set with 35% missing 6-DoF head coordinates

5.6.2 COMPARISON OF ACCURACY OF SHNM AND BPNN IN PREDICTION OF MISSING 6-DOF HEAD MOTION COORDINATES

The comparison of the prediction with 35% missing instances dataset of 6-DoF data with SHNM and BPNN is provided in from Figure 5.44 to Figure 5.49. In Figure 5.44 to Figure 5.49 the Y-axis represents the 6-DoF coordinates of the head motion including the missing instances to be recovered and X-axis represents the corresponding value of 6-DoF coordinates. The expected output which is the true data set with non-missing values of coordinates is represented by a blue line and circled marker. The 6-DoF data set with missing coordinates is predicted by the SHNM is represented by green color with a square marker. Finally, the BPNN prediction results are represented with a red line using the star marker. There is some deviation in red and green curves in the graphs, which means that the accuracy of SHNM is better than BPNN, as the green curve is near to the blue curve, which is the expected output. At some places, the deviation is less because, in some instances, the recovered value predicted using BPNN is near to the value predicted by SHNM.

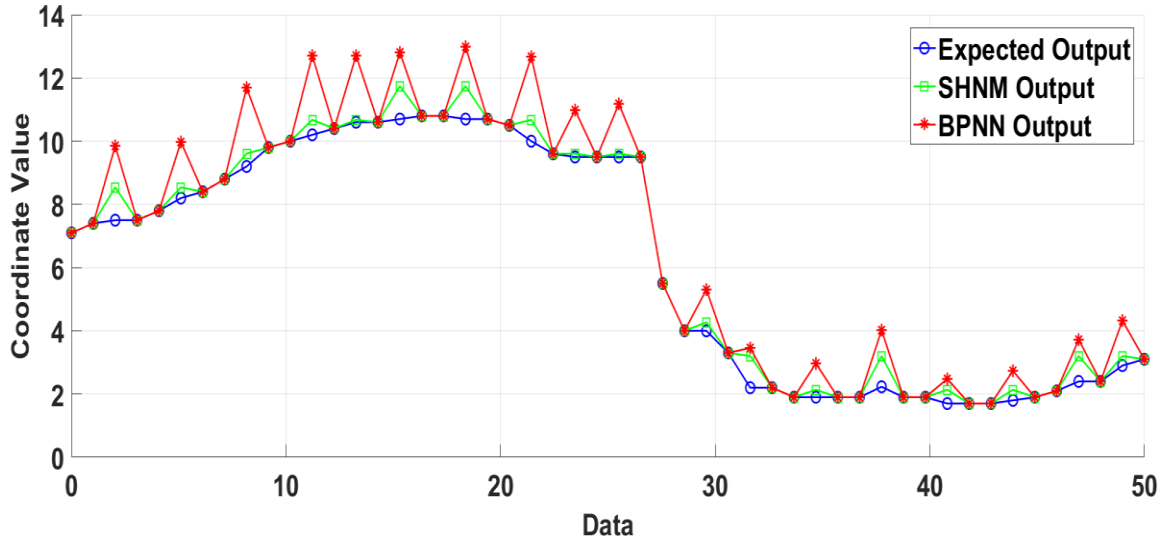

Figure 5.44: Comparison of prediction of X coordinates with SHNM and BPNN

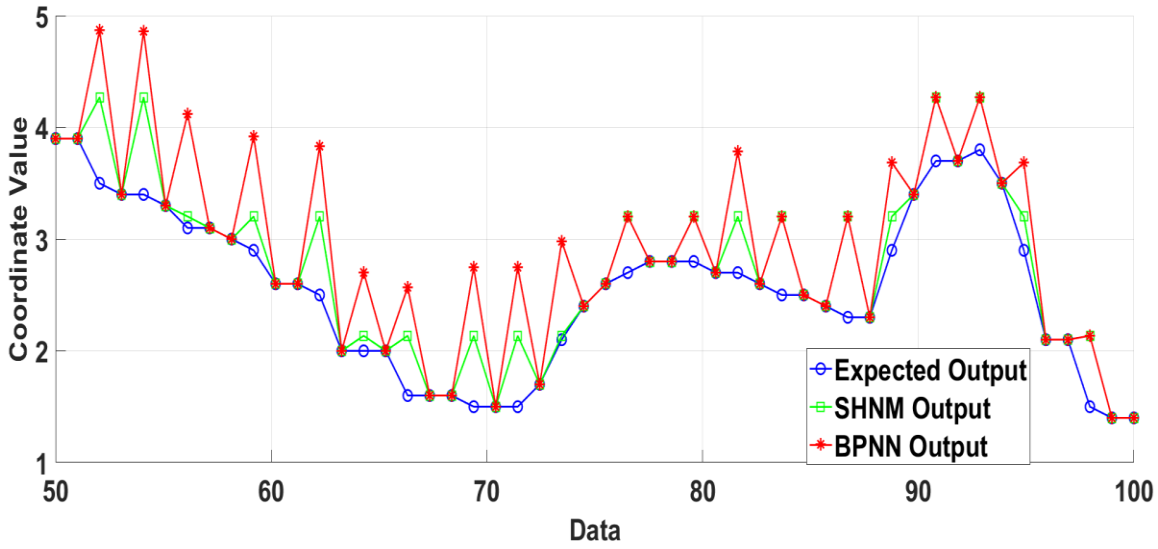

Figure 5.45: Comparison of prediction of Y coordinates with SHNM and BPNN

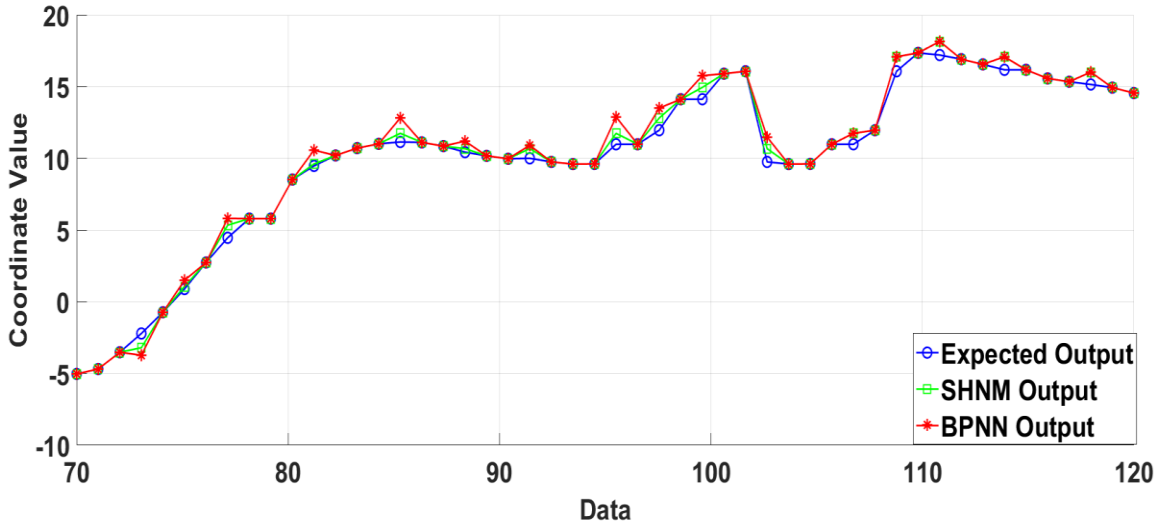

Figure 5.46: Comparison of prediction of Z coordinates with SHNM and BPNN

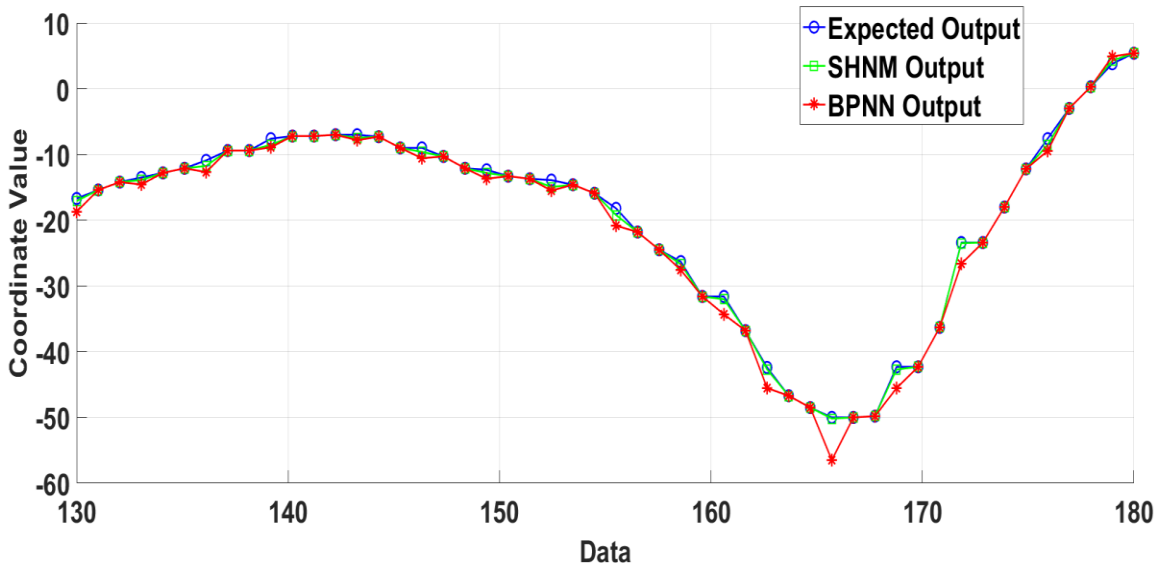

Figure 5.47: Comparison of prediction of Yaw coordinates with SHNM and BPNN

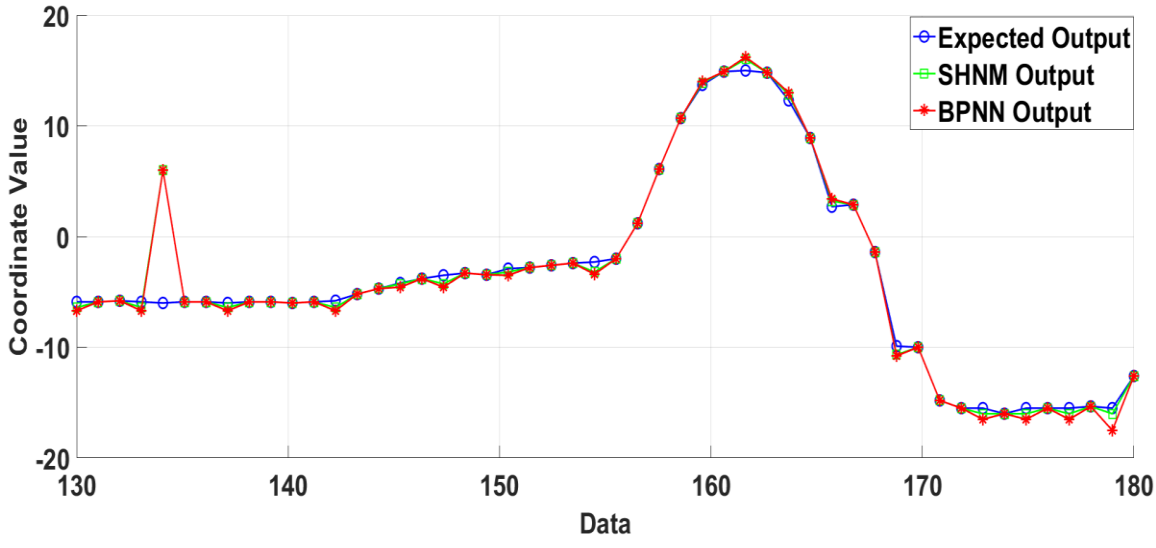

Figure 5.48: Comparison of prediction of Pitch coordinates with SHNM and BPNN

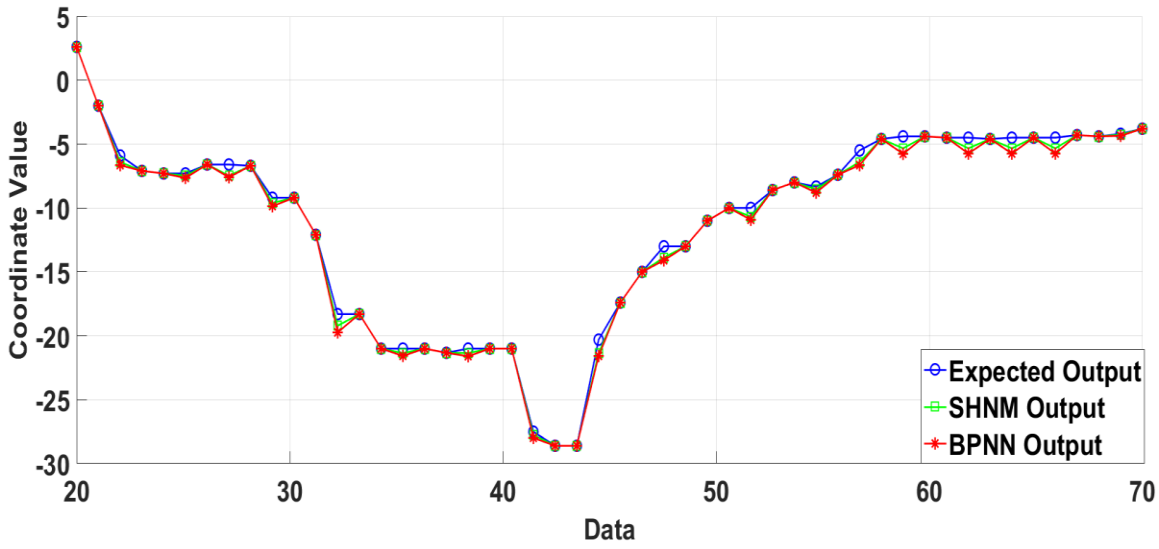

Figure 5.49: Comparison of prediction of Roll coordinates with SHNM and BPNN

5.6.3 COMPARISON OF SELF HEALING NEURAL MODEL AND AUTOREGRESSIVE LINEAR MODEL (ORDER TWO AND THREE) IN THE PREDICTION OF MISSING HEAD MOTION COORDINATES IN OPTICAL TRACKING

In this section, the predicted 6-DoF coordinates are compared with the Autoregressive Linear Model. The accuracy of the prediction depends on the order of the Autoregressive model used for the prediction. In this case, the ARLM of order 1 predicted the missing 6-DoF head coordinates with less accuracy as compared to the ARLM of order 2 and order 3. The ARLM of order more than 3 is not used in this work to avoid the overhead complexity of the prediction system. The prediction is done with the minimum percentage of the missing 6-DoF head coordinates. The threshold of the missing 6-DoF head coordinates is kept 1% in this experiment. The graphical prediction of ALRM of order 3 is shown in a dataset consisting of 10% missing 6-DoF head coordinates. Graphical interpretation of the prediction of 6-DoF head coordinates using ARLM is represented in from Figure 5.50 to Figure 5.61. In graphs, the accuracy obtained

through ARLM (Order 3) is compared with SHNM. The enlarged view of each graph is also provided with each corresponding coordinate parameter. The graphical interpretation of prediction of 1% and 2% missing 6-DoF head coordinates using ARLM (Order 3) is not shown in this section, as due to the large data set the predicted values against the missing values are not clearly observable. The percentage of prediction accuracy of missing 6-DoF head coordinates is computed against the ground truth 6-DoF data acquired in the absence of any kind of interference. Table 5.6 describes the comparison of the predicted results of the ARLM (order 3), SHNM, and BPNN with 1%, 2%, 10%, 25%, and 35% of missing head motion coordinates in a data set using the optical tracker.

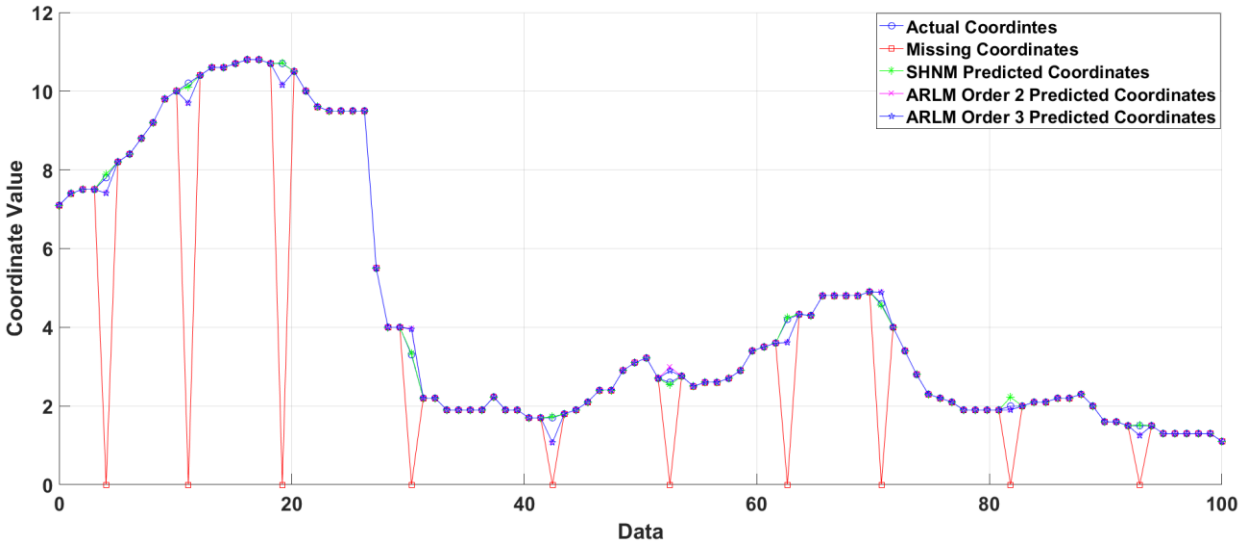

Figure 5.50: Comparison of prediction of X coordinates with SHNM and ARLM

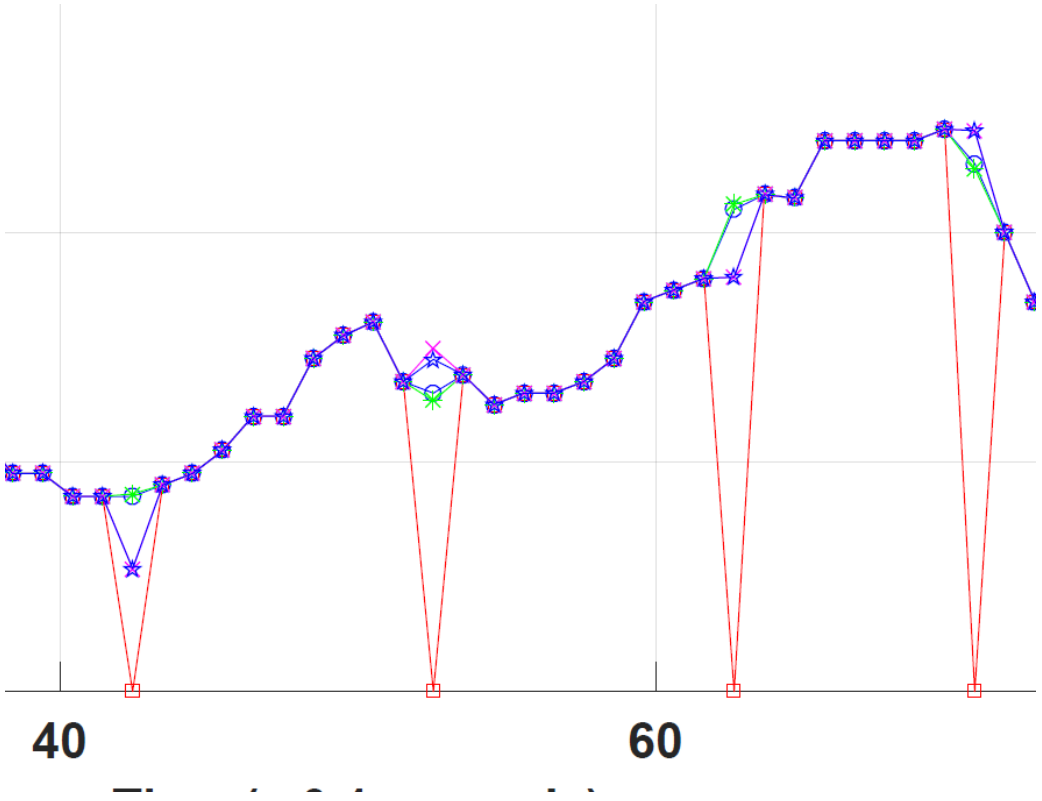

Figure 5.51: Enlarged view of the prediction of X coordinates with SHNM and ARLM

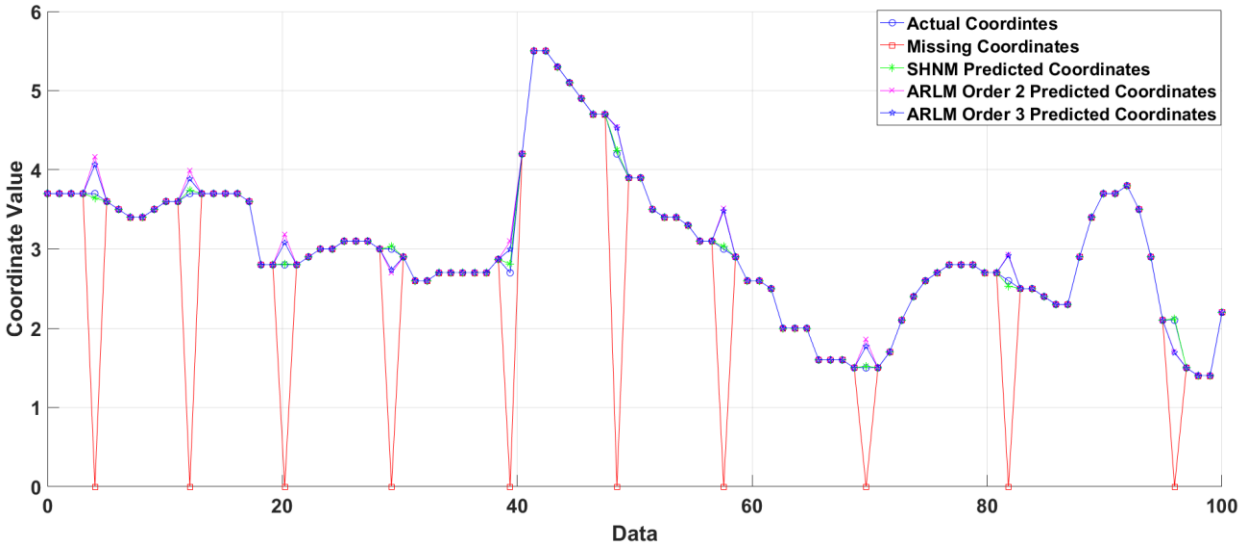

Figure 5.52: Comparison of prediction of Y coordinates with SHNM and ARLM

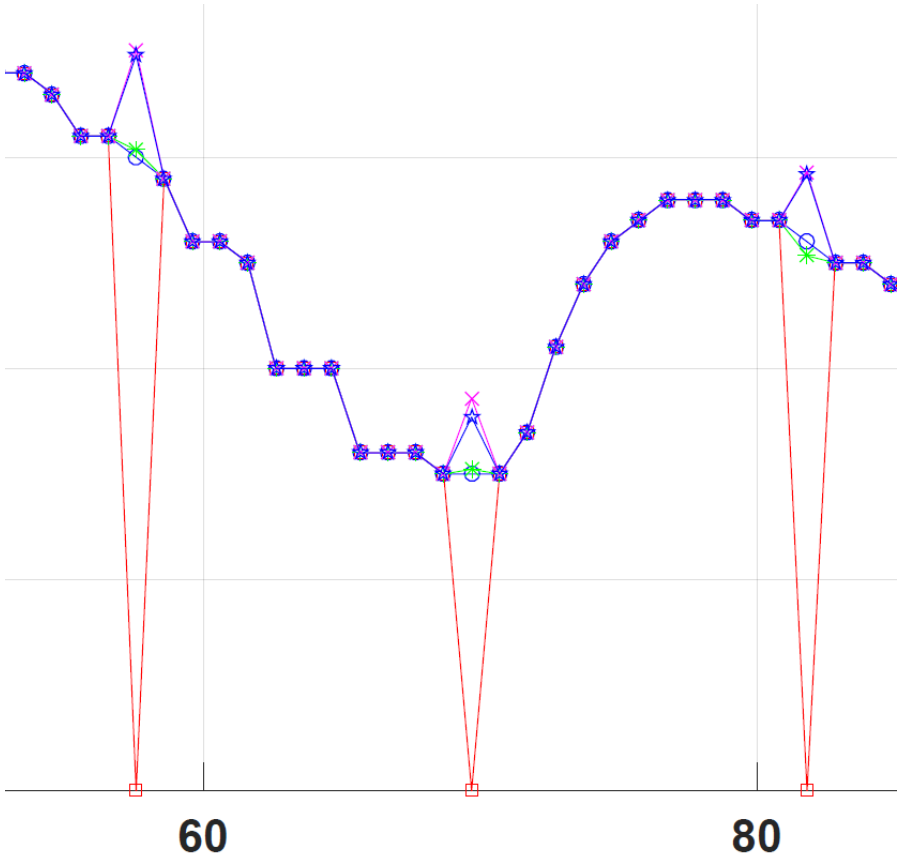

Figure 5.53: Enlarged view of the prediction of Y coordinates with SHNM and ARLM

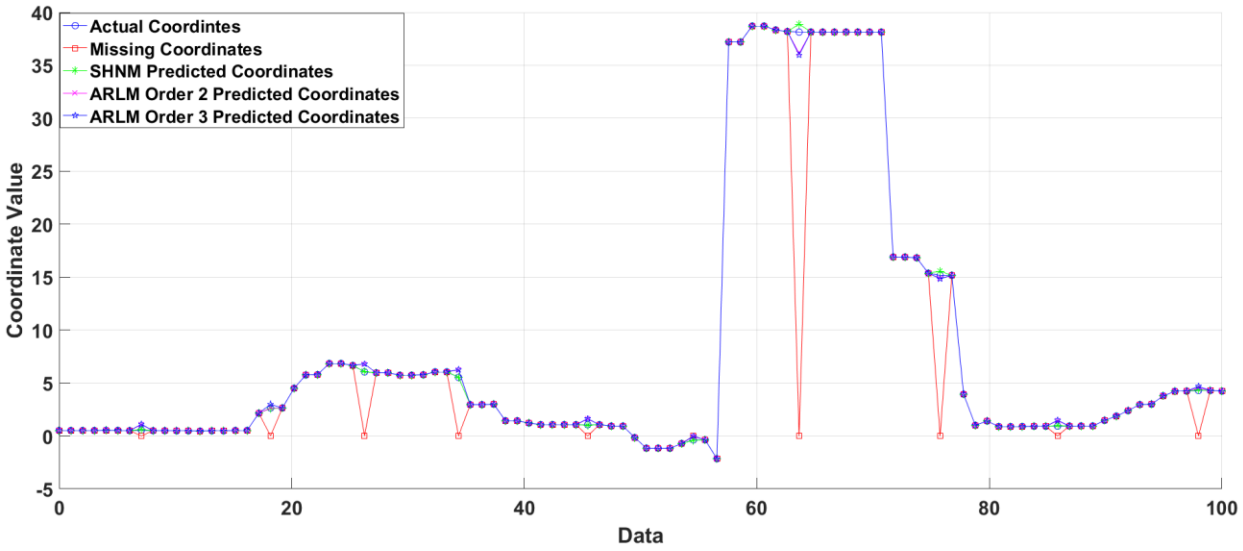

Figure 5.54: Comparison of prediction of Z coordinates with SHNM and ARLM

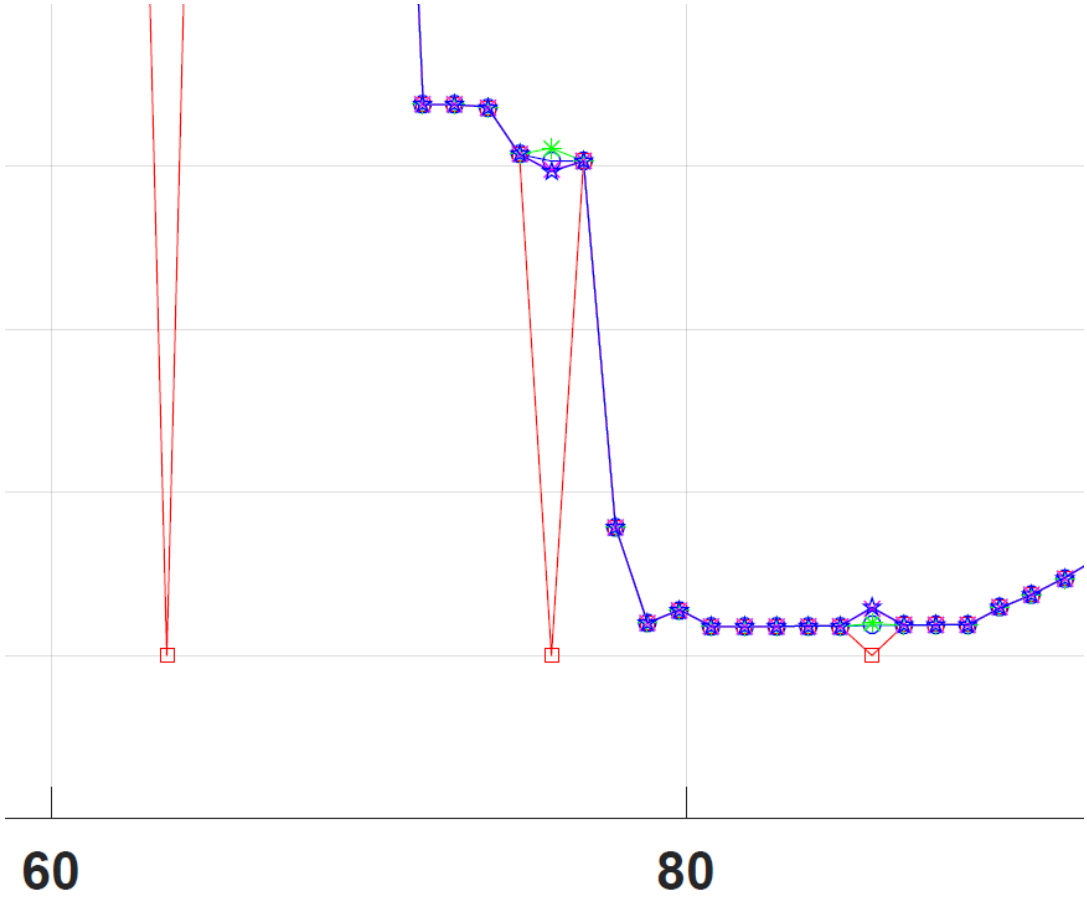

Figure 5.55: Enlarged view of the prediction of Z coordinates with SHNM and ARLM

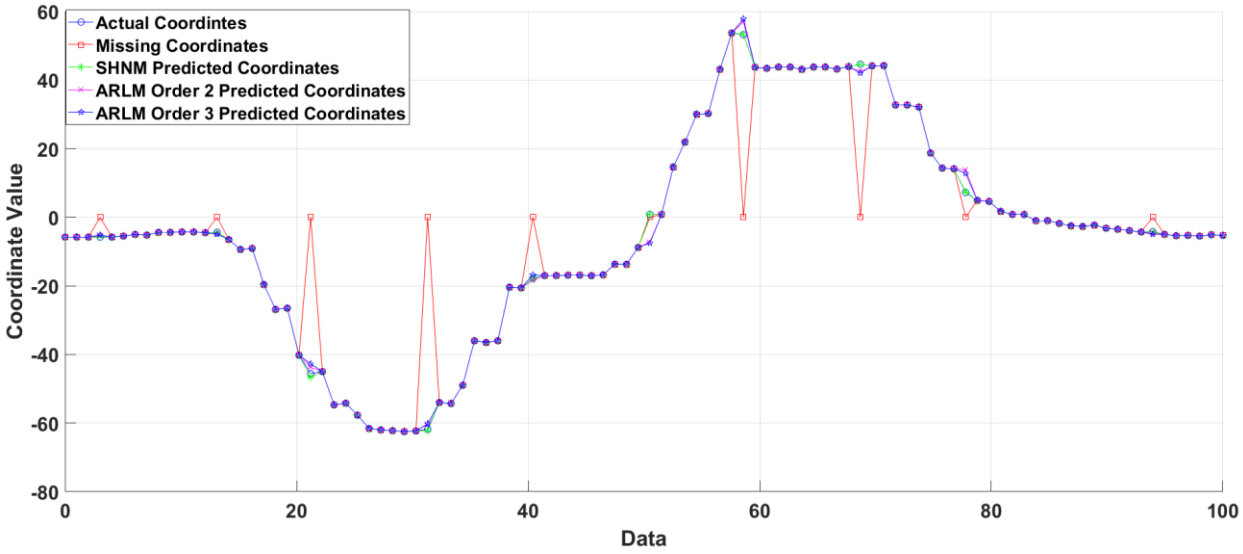

Figure 5.56: Comparison of prediction of Yaw coordinates with SHNM and ARLM

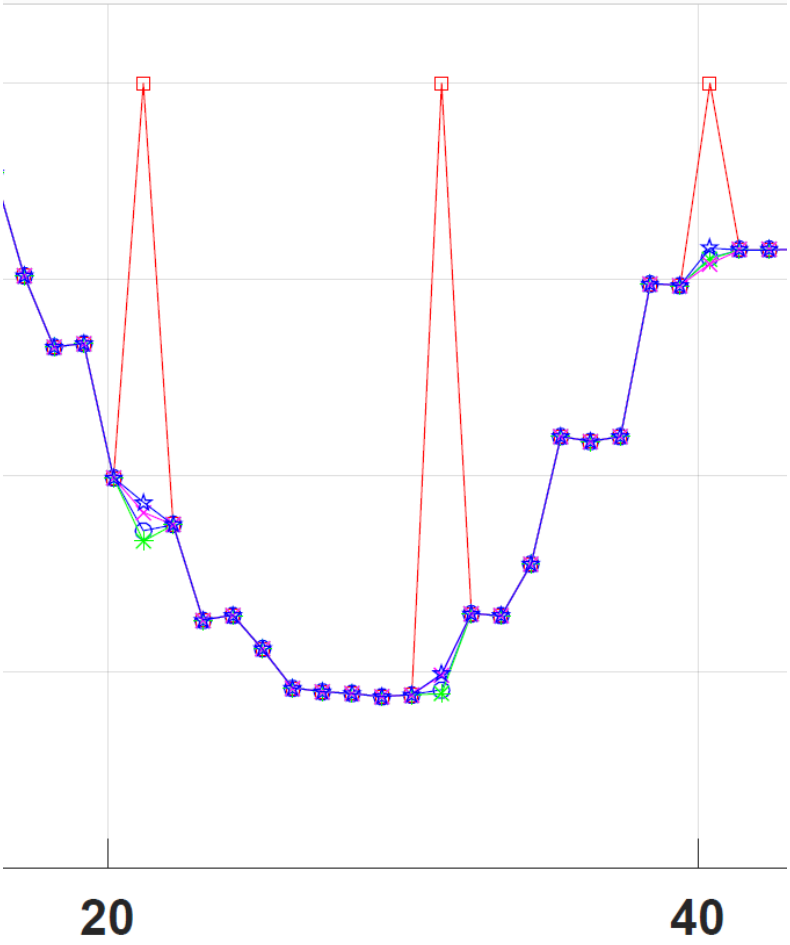

Figure 5.57: Enlarged view of the prediction of Yaw coordinates with SHNM and ARLM

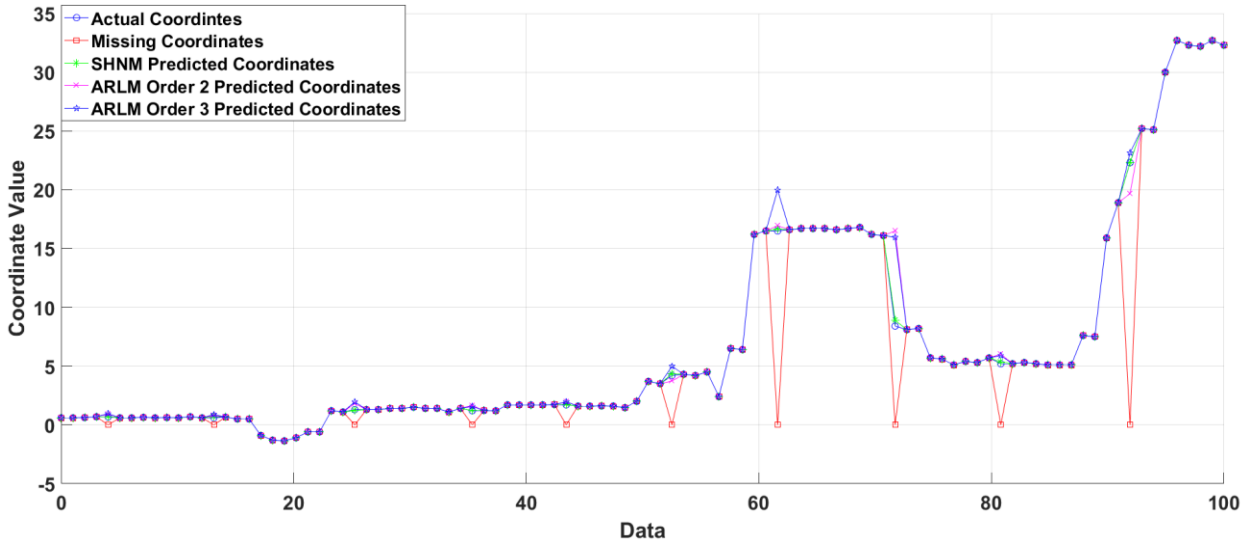

Figure 5.58: Comparison of prediction of Pitch coordinates with SHNM and ARLM

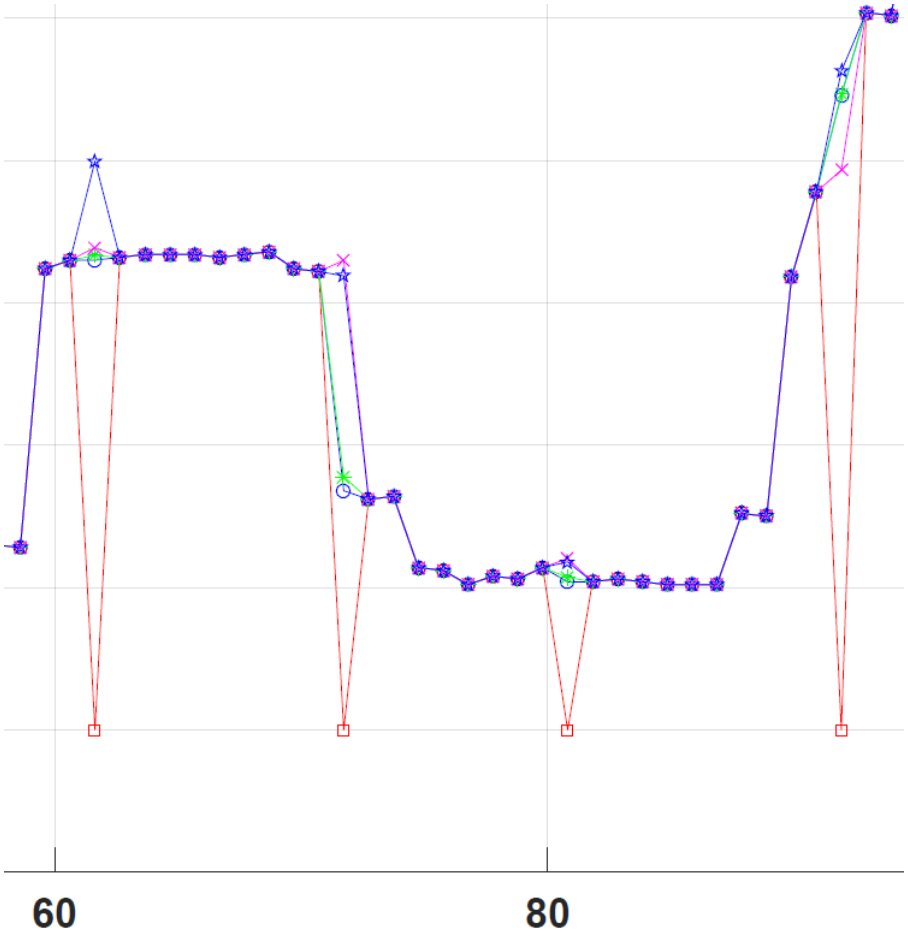

Figure 5.59: Enlarged view of the prediction of Pitch coordinates with SHNM and ARLM

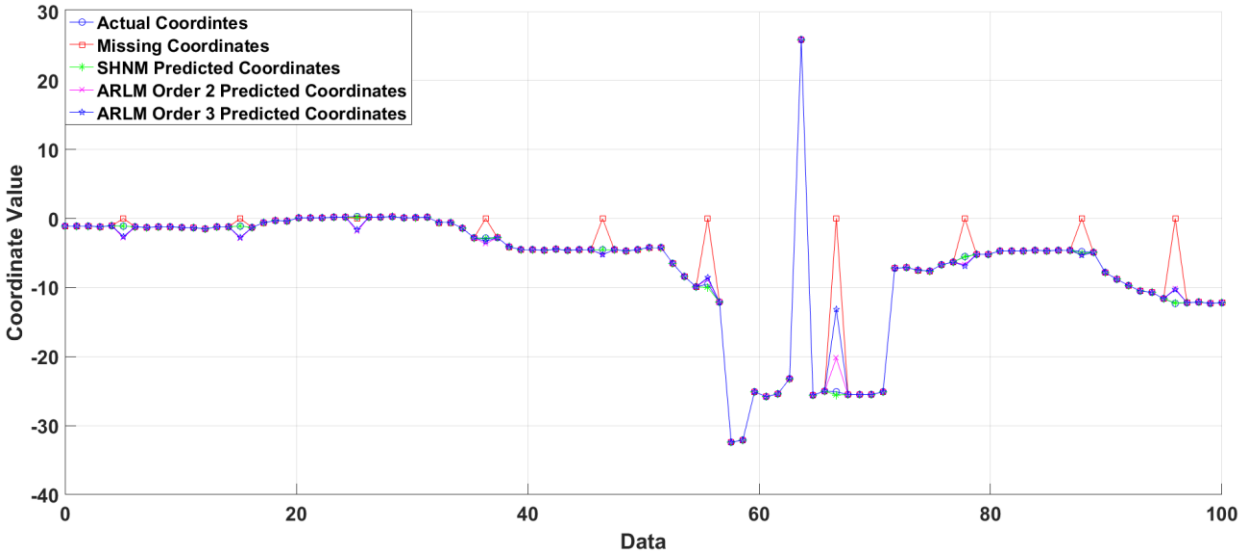

Figure 5.60: Comparison of prediction of Roll coordinates with SHNM and ARLM

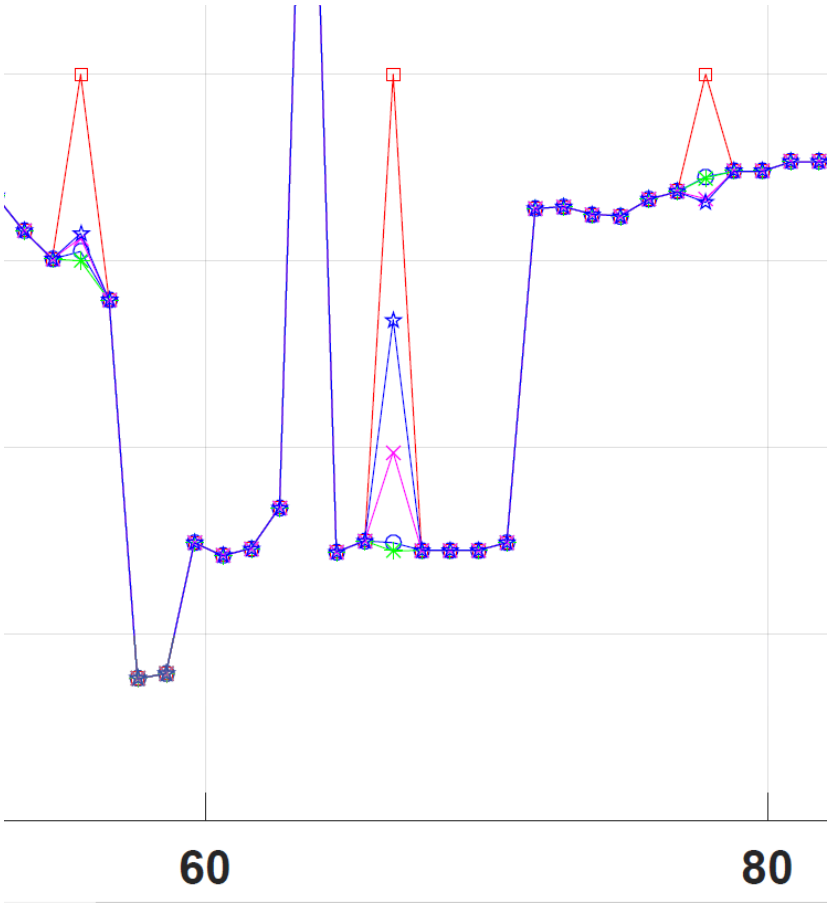

Figure 5.61: Enlarged view of the prediction of Roll coordinates with SHNM and ARLM

Table 5.6 represents the accuracy comparison of SHNM with BPNN and ARLM with different percentages of missing data using the optical tracker.

Table 5.6: Accuracy of comparison of the different techniques used in the prediction of the 6-DoF missing head coordinates with different sets of missing data using the optical tracker.

Parameters	**Accuracy of data against the missing percentage**														
Missing Percentage Of 6-DoF→ Head Coordinates	1%			2%			10%			25%			35%		
Model used→	**SHNM**	BPNN	ARLM	**SHNM**	BPNN	ARLM	**SHNM**	BPNN	ARLM	**SHNM**	BPNN	ARLM	**SHNM**	BPNN	ARLM
X	**98.6%**	89.2%	91.1%	**97.9%**	89.8%	91.3%	**96.14%**	91.05%	90.1%	**95.12%**	90.20%	87.3%	**94.68%**	89.69%	87.6%
Y	**97.2%**	88.1%	90.6%	**96.7%**	88.7%	90.8%	**92.50%**	87.70%	86.3%	**91.34%**	86.57%	84.2%	**89.75%**	84.72%	82.5%
Z	**98.7%**	89.2%	91.4%	**98.1%**	92.1%	93.6%	**92.80%**	87.30%	87.1%	**91.30%**	86.10%	83.9%	**90.91%**	85.63%	83.6%
Yaw	**96.6%**	86.5%	89.6%	**96%**	89.9%	91.8%	**97.10%**	92.44%	90.9%	**96.21%**	91.70%	88.1%	**95.90%**	90.53%	87.6%
Pitch	**97.1%**	87.7%	90.1%	**96.9%**	88.4%	90.1%	**97%**	91.90%	91.2%	**95.87%**	89.9%	86.8%	**95.30%**	89.20%	87.1%
Roll	**94.3 %**	85.3%	88.7%	**93.8%**	85.7%	88.4%	**93.50%**	84.60%	88.5%	**92.45%**	83%	80.1%	**91.11%**	82.81%	88.5%

5.6.4 SUMMARY OF RESULTS OF ACCURACY IN OPTICAL TRACKER

This section discusses the summary of prediction accuracy achieved using different prediction techniques for the optical tracker. The prediction of missing 6-DoF head motion coordinates was done using Self Healing Neural Model (SHNM), Back Propagation Neural Network (BPNN), Adaptive Neuro-Fuzzy Inference System (ANFIS), and Autoregressive Linear Model (ARLM). The results of SHNM, BPNN, and ARLM are compared in Table 5.6. The comparison of SHNM, BPNN, and ANFIS is discussed in section 5.8. It was found that the performance of SHNM was superior to BNNN and ARLM. In the 35%, missing 6-DoF head motion coordinates data set the SHNM yielded the highest accuracy varying from 89.75% to 95.9% (all 6-DoF coordinates), whereas the variation in BPNN and ARLM was 82.81% to 90.53% and 82.5% to 88.5% respectively.

5.7 PREDICTION OF MISSING 6-DoF HEAD MOTION COORDINATES USING ANFIS

The methodology of ANFIS in the prediction of the missed head motion coordinates is discussed in chapter 4 of this thesis. In this section, the data set used for the prediction of missing head coordinates was large. The data set consisted of 5200 instances of the head motion 6-DoF coordinates. The data set was divided randomly as 70% for the training and 30% for the testing. The specifications of the ANFIS model used for the prediction of the missed head coordinates are the same as mentioned in **Table 4.1 of Chapter 4.**

Using ANFIS for prediction, the 6-DoF data was given as input to the training network. The data with missing instances was fed as the input and was compared with the output data of the Fuzzy Inference System. It was noticed that the accuracy of the ANFIS was less than SHNM.

The main shortcoming of ANFIS is that its prediction accuracy decreased in this work involving large data sets as the ANFIS uses heuristic information to develop rules using sample data. However, Neural Network develops the rules which are based entirely on data. Therefore, the accuracy of prediction of missing 6-DoF head coordinates in large data sets of SHNM is more than ANFIS. The training error for 100 epochs is 3.66935, which is higher than the small set data.

Figure 5.62 shows the Fuzzy logic designer for prediction using ANFIS. It can be observed in Figure 5.62 that, the type of input membership function is Gaussian.

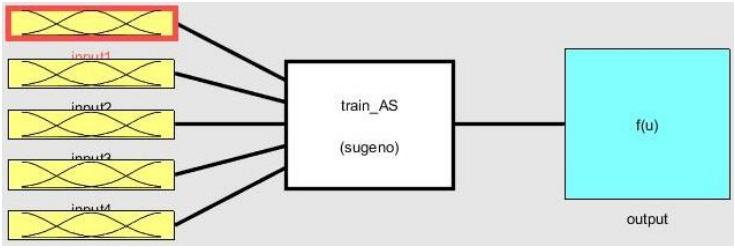

Figure 5.62: Fuzzy logic designer for ANFIS with the large data set

Figure 5.63 shows the plot of 6-DoF head coordinates data used in ANFIS for training. The plot is shown in Figure 5.63 which consists of 3640 instances (70%) of 6-DoF head motion coordinates used for the training.

Figure 5.63: Training data in ANFIS

Figure 5.64 shows the plot of 6-DoF head coordinates data used in ANFIS for training. The plot is shown in Figure 5.64 which consists of 1560 instances (30%) of 6-DoF head motion coordinates used for the testing.

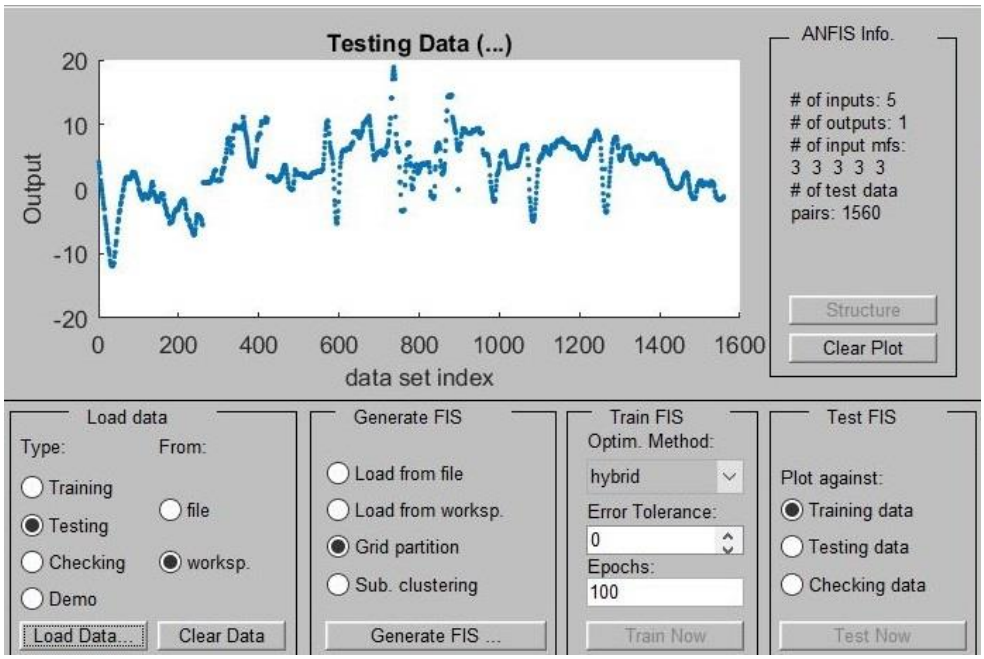

Figure 5.64: Testing data in ANFIS

Figure 5.65 shows the testing of the FIS with the training data set with 3640 instances.

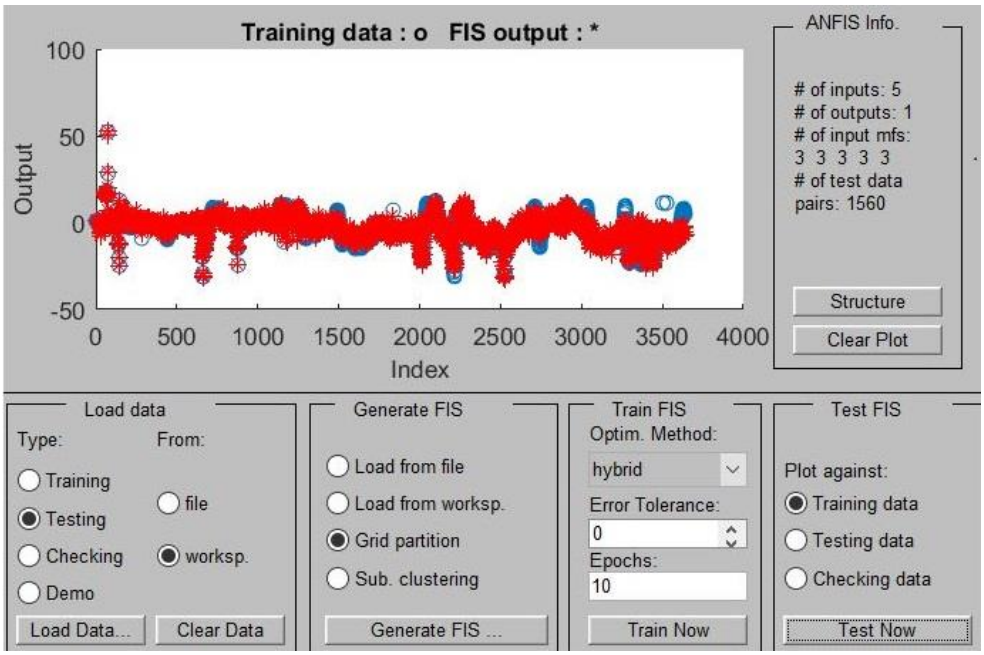

Figure 5.65: Plot of training data against FIS output

Figure 5.66 shows the testing of the FIS with the testing data set with 1540 instances.

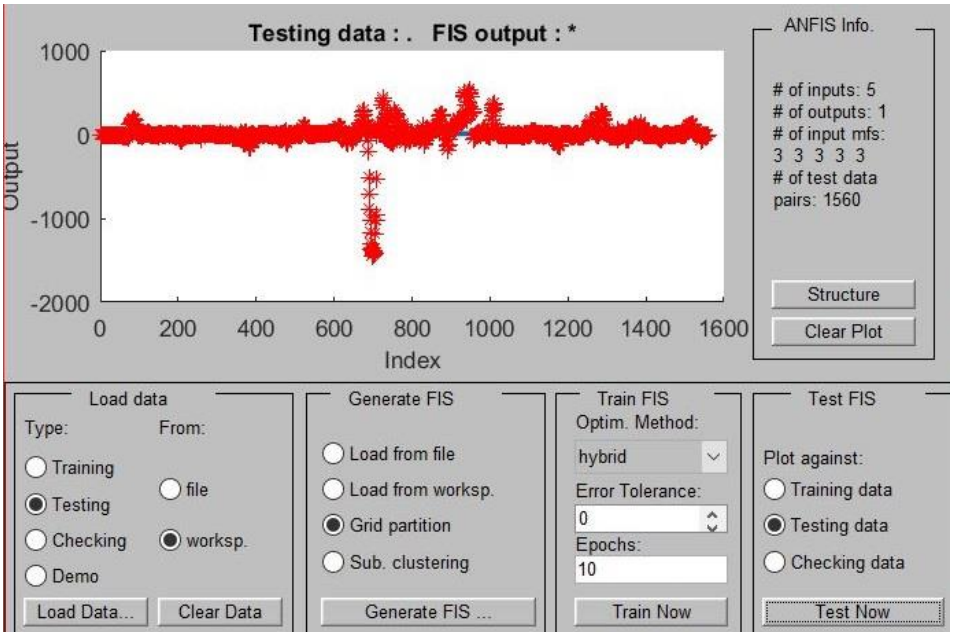

Figure 5.66: Plot of testing data against FIS output

Figure 5.67 describes the ANFIS model used for the prediction of the missing head motion coordinates

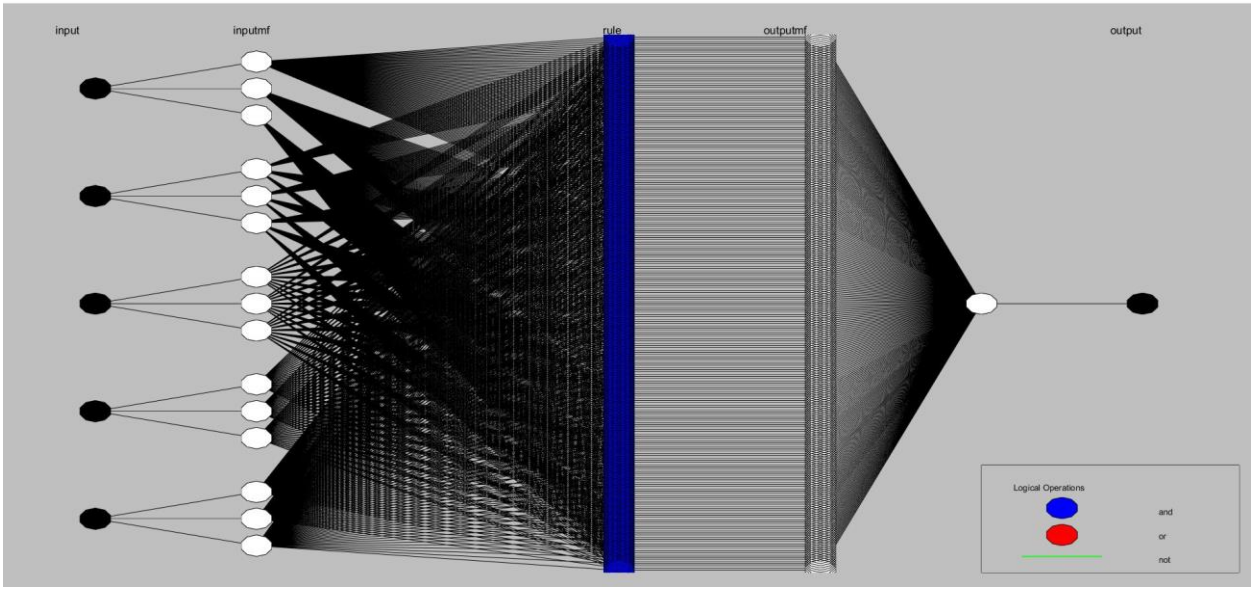

Figure 5.67: Structure of the ANFIS model

Figure 5.68 shows the surface model of input and output of the ANFIS model used for predicting missed head coordinates in the large data set.

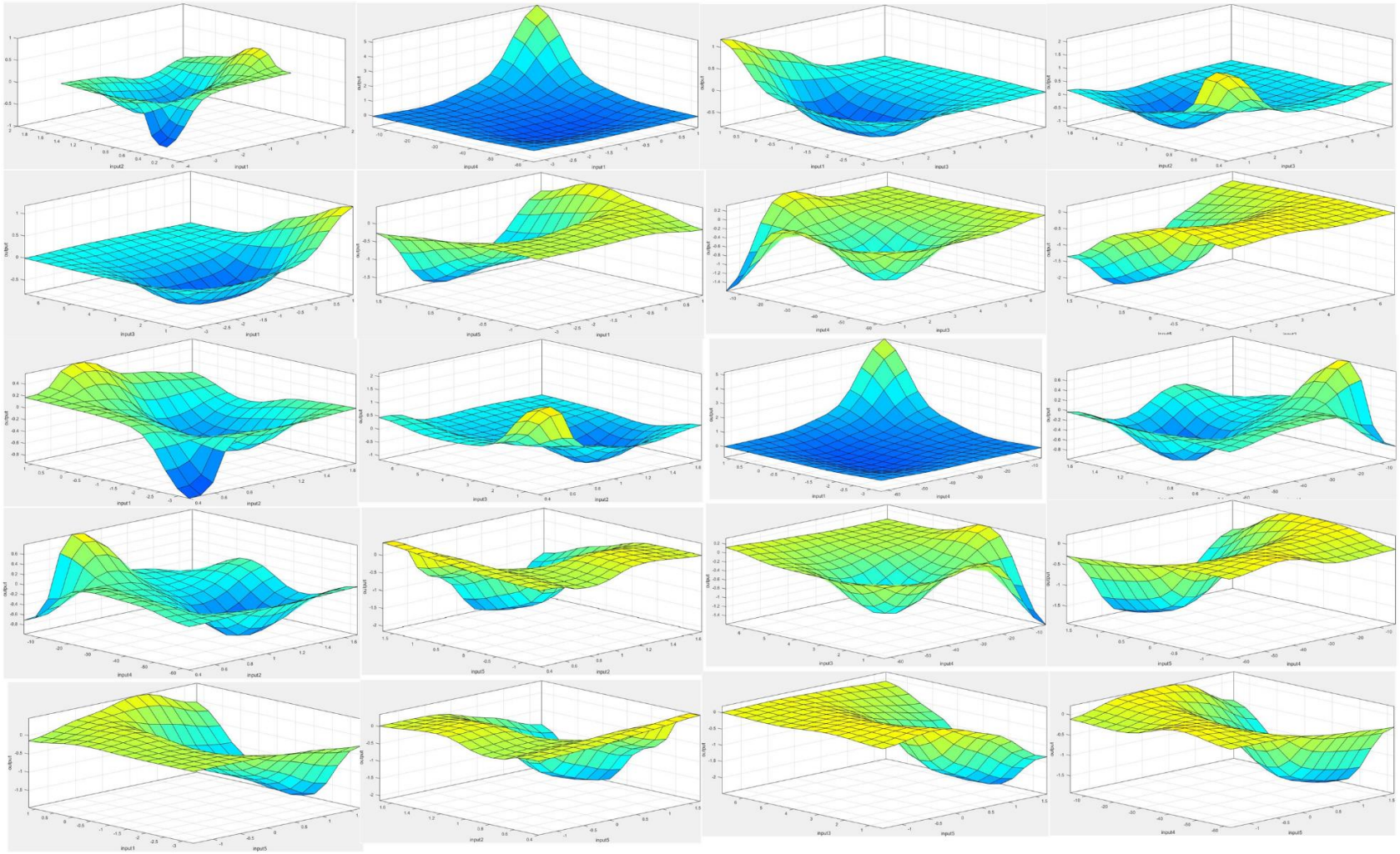

Figure 5.68: Surface model of input and output of the ANFIS model

The prediction accuracy of missed head coordinates using the Adaptive Neuro-Fuzzy Inference System (ANFIS) depends on the dataset. In the prediction of the missed head coordinates, the accuracy of the ANFIS is more in the dataset with a lesser number of head motion coordinates.

The prediction of missing 6-DoF data using ANFIS is performed using two different sets of data. One set of data consists of a large number of instances, in which the performance of ANFIS in the prediction of the missed head coordinates is not up to the mark. The number of instances in the large data set is 5200. The accuracy of the prediction of 6-DoF missed head coordinates achieved in large data set using ANFIS is less than 60% using both optical and electromagnetic trackers individually. The maximum accuracy for the prediction of missing 6-DoF head coordinates is achieved using the Self Healing Neural Model. The other data set having a smaller number of instances of 6-DoF coordinates is also applied to the ANFIS for the prediction of missing 6-DoF head coordinates. The accuracy achieved using ANFIS in a small dataset is more than 80%, which is much more as compared to the large dataset. The graphs shown in Figure 5.64 to Figure 5.69 represents the prediction accuracy of the SHNM, ANFIS, and BPNN for the large data set. The graphs in Figure 5.69 to Figure 5.74 are the magnified version of the graphs consisting of 5200 instances (head coordinates) and Figure 5.64 to Figure 5.74 in this section, shows the prediction accuracy of 60 head motion coordinates. Comparison with ARLM is not shown in Figure 5.69 to Figure 5.74, as a comparison of ARLM, SHNM, and BPNN are discussed separately.

The instances (number of 6-DoF head posture coordinates) used in the small data set is 400. However, in the small dataset also the Self Healing Neural Model has more accuracy as

compared to ANFIS. Performance of the Self-healing Neural Model, ANFIS, and Backpropagation neural network in the prediction of missed head coordinates in the small dataset (400 instances) is shown in **Appendix C** of this thesis.

Figure 5.69 presents the prediction accuracy of all three models (SHNM, ANFIS, and BPNN) for the prediction of the missing translational head coordinate X, and it is found from Figure 5.69 that, the accuracy of the Self-healing neural model outperforms the ANFIS and Backpropagation neural network. The accuracy of SHNM is ≈ 85% and ANFIS is ≈ 45% using Electromagnetic tracker. The accuracy of SHNM and ANFIS of missed head coordinates using Optical tracker is ≈ 95% and ≈ 50% respectively.

Figure 5.69 presents the prediction accuracy of all three models (SHNM, ANFIS, and BPNN) for the prediction of the missing translational head coordinate X, and it is found from Figure 5.69 that, the accuracy of the Self-healing neural model outperforms the ANFIS and Backpropagation neural network. The accuracy of SHNM is ≈ 85% and ANFIS is ≈ 46% using Electromagnetic tracker. The accuracy of SHNM and ANFIS of missed head coordinates using Optical tracker is ≈ 95% and ≈ 50% respectively.

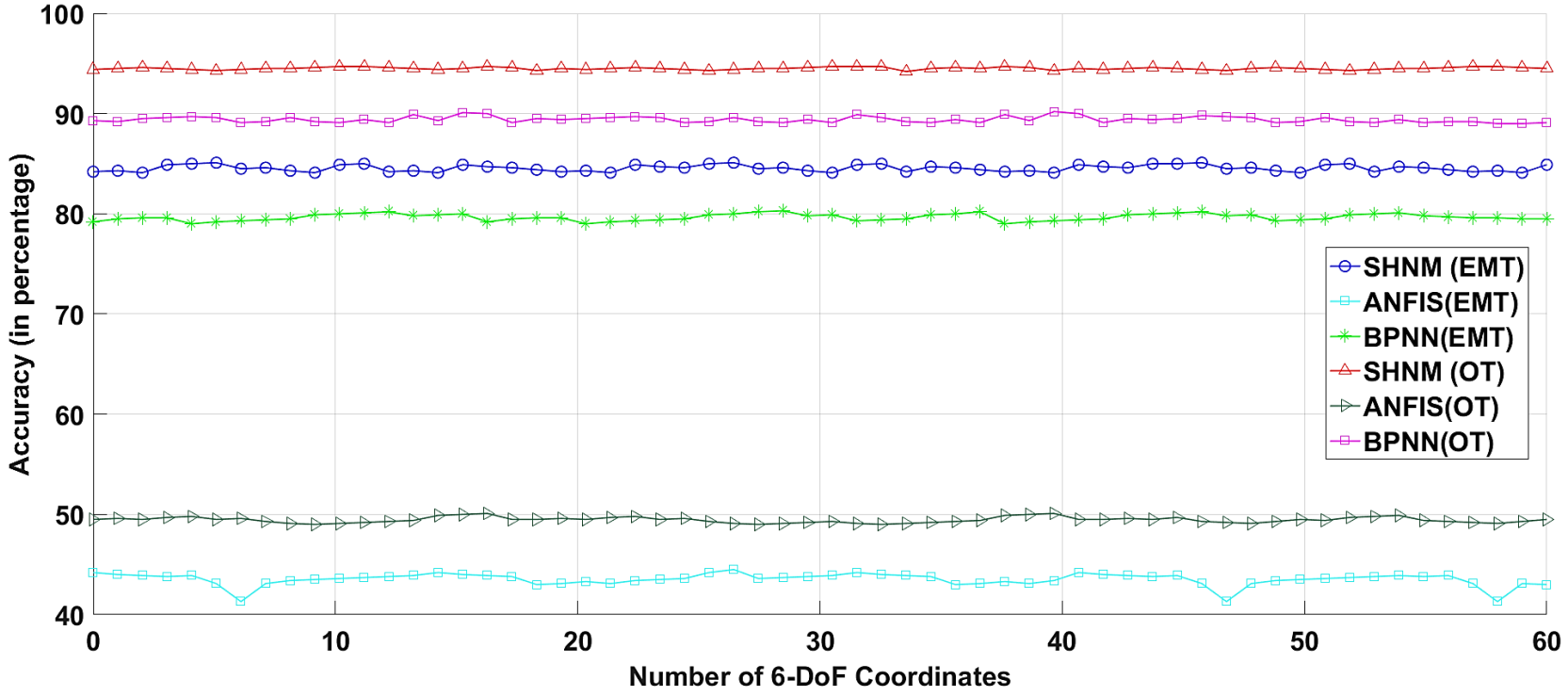

Figure 5.69: Performance evaluation of SHNM, ANFIS, and BPNN in the prediction of missing X (translational) head coordinates in large data set using both optical and electromagnetic tracker

Figure 5.70 presents the prediction accuracy of all three models (SHNM, ANFIS, and BPNN) for the prediction of the missing translational head coordinate Y, and it is found from Figure 5.70 that, the accuracy of the Self-healing neural model outperforms the ANFIS and Backpropagation neural network. The accuracy of SHNM is ≈ 90% and ANFIS is ≈ 53% using Electromagnetic tracker. The accuracy of SHNM and ANFIS of missed head coordinates using Optical tracker is ≈ 90% and ≈ 47% respectively.

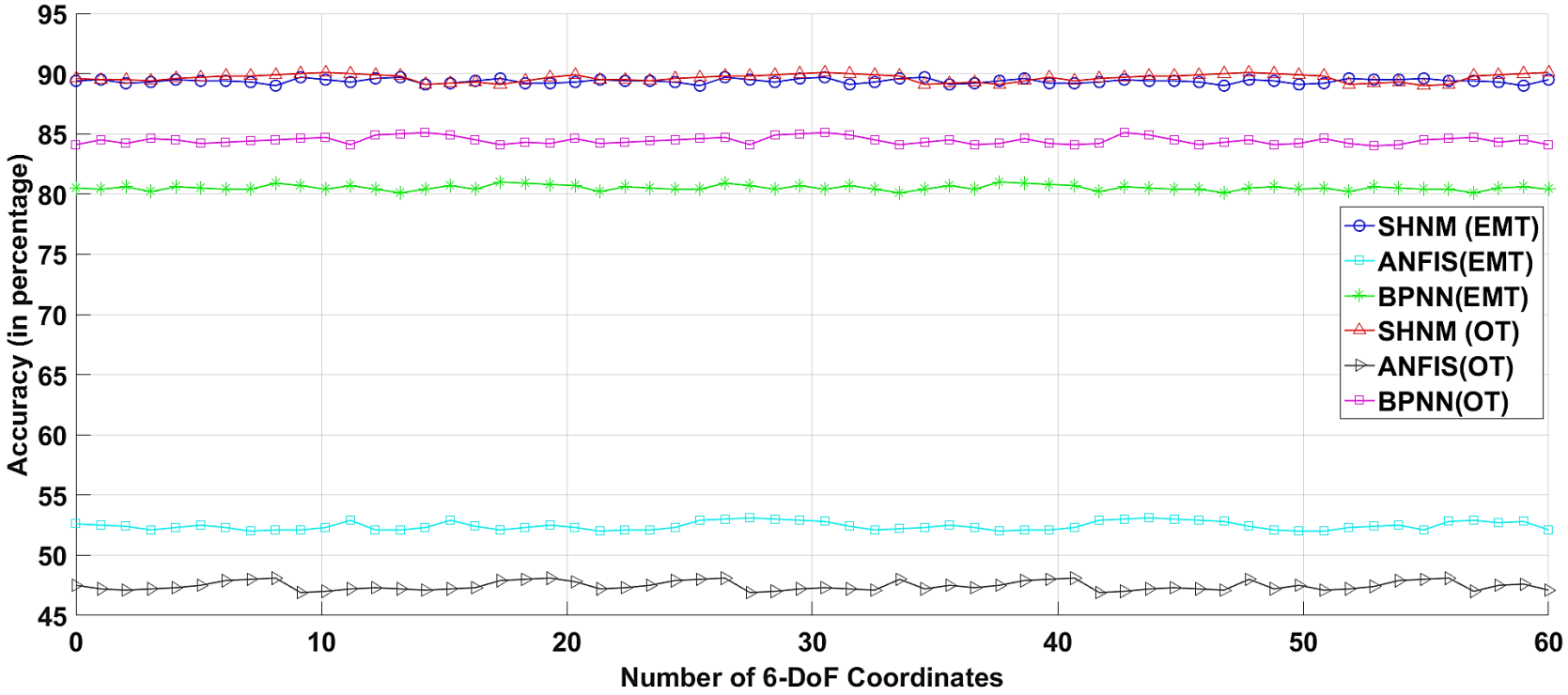

Figure 5.70: Performance evaluation of SHNM, ANFIS, and BPNN in the prediction of Y (translational) head coordinates in large data set using both optical and electromagnetic tracker

Figure 5.71 presents the prediction accuracy of all three models (SHNM, ANFIS, and BPNN) for the prediction of the missing translational head coordinate Z, and it is found from Figure 5.71 that, the accuracy of the Self-healing neural model outperforms the ANFIS and Backpropagation neural network. The accuracy of SHNM is ≈ 87% and ANFIS is ≈ 46% using Electromagnetic tracker. The accuracy of SHNM and ANFIS of missed head coordinates using Optical tracker is ≈ 91% and ≈ 54% respectively.

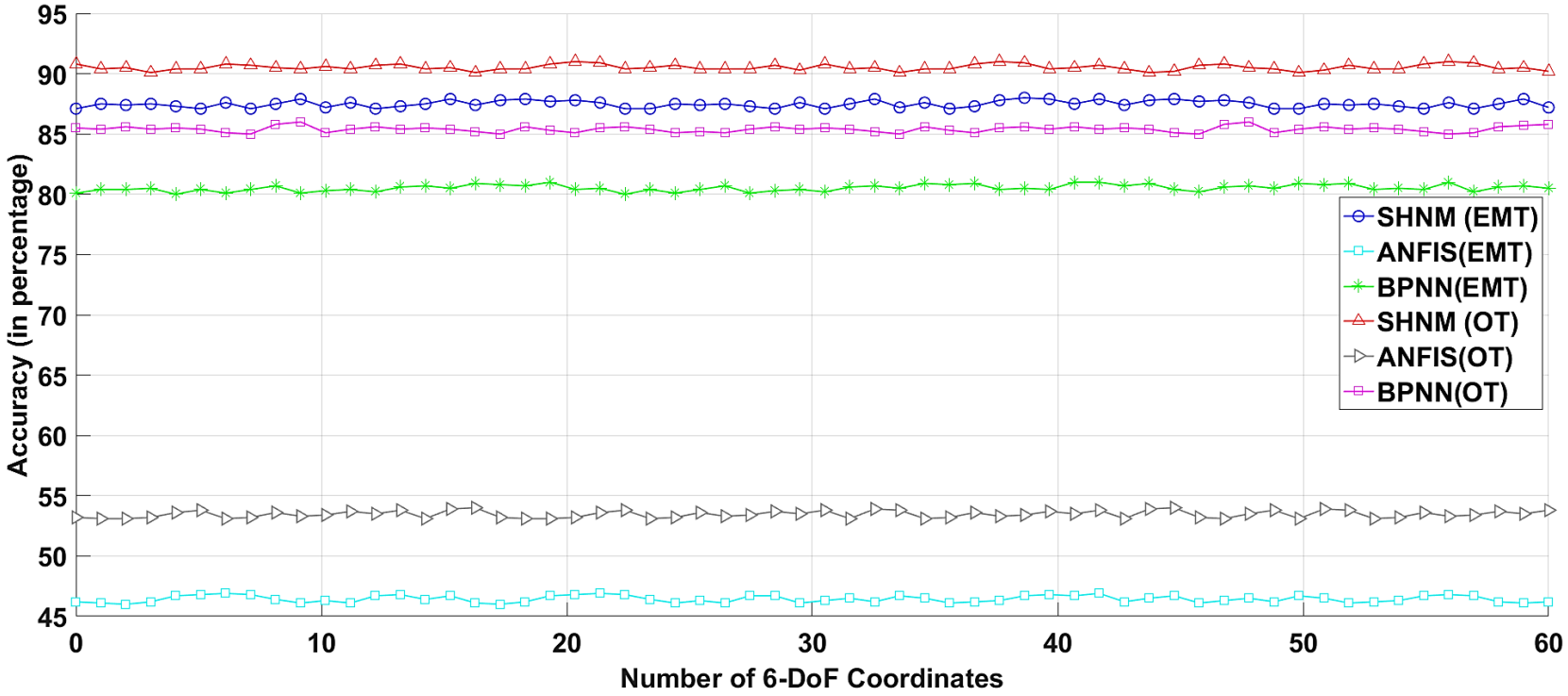

Figure 5.71: Performance evaluation of SHNM, ANFIS, and BPNN in the prediction of Z (translational) head coordinates in large data set using both optical and electromagnetic tracker

Figure 5.72 presents the prediction accuracy of all three models (SHNM, ANFIS, and BPNN) for the prediction of the missing rotational head coordinate Yaw, and it is found from Figure 5.72 that, the accuracy of the Self-healing neural model outperforms the ANFIS and Backpropagation neural network. The accuracy of SHNM is ≈ 89% and ANFIS is ≈ 48% using Electromagnetic tracker. The accuracy of SHNM and ANFIS of missed head coordinates using Optical tracker is ≈ 95% and ≈ 53% respectively.

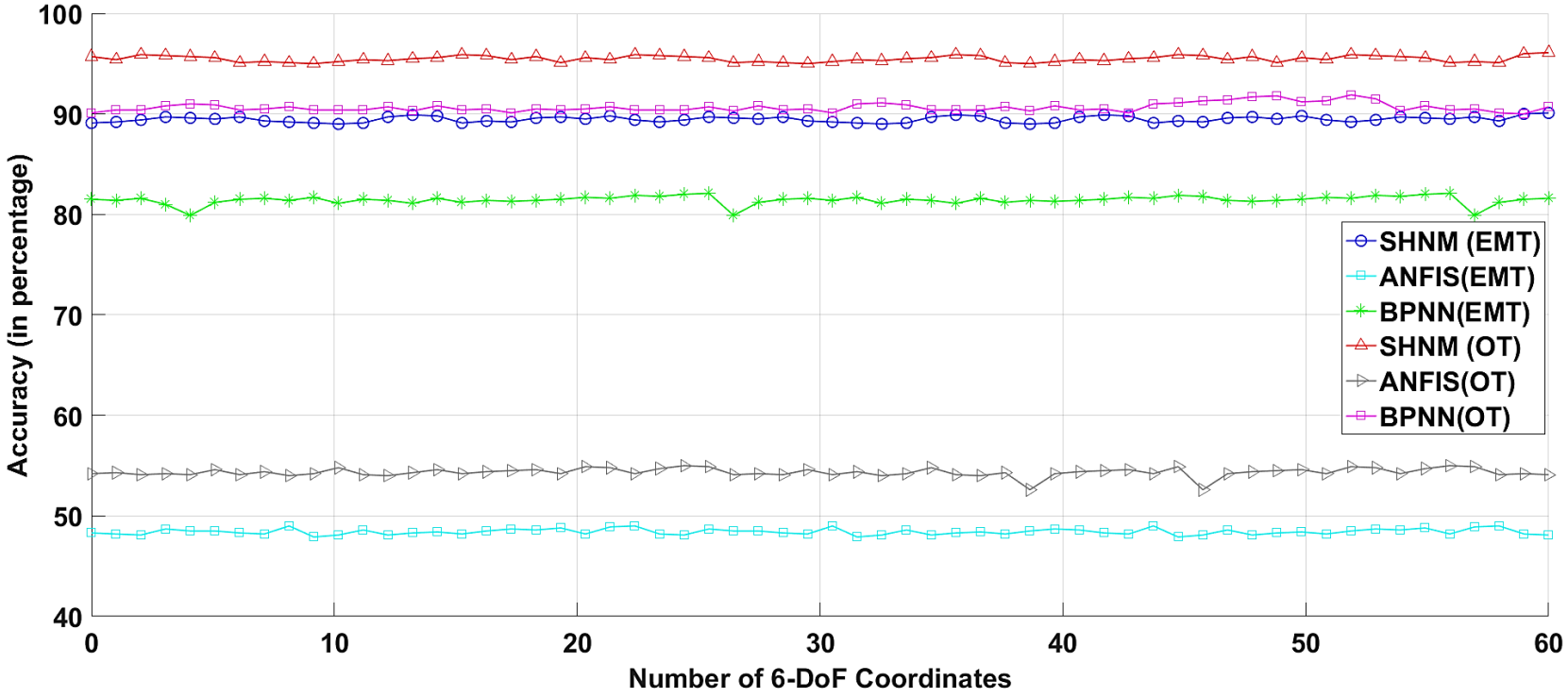

Figure 5.72: Performance evaluation of SHNM, ANFIS, and BPNN in the prediction of Yaw (rotational) head coordinates in large data set using both optical and electromagnetic tracker

Figure 5.73 presents the prediction accuracy of all three models (SHNM, ANFIS, and BPNN) for the prediction of the missing rotational head coordinate Pitch, and it is found from Figure 5.73 that, the accuracy of the Self-healing neural model outperforms the ANFIS and Backpropagation neural network. The accuracy of SHNM is ≈ 90% and ANFIS is ≈ 46% using Electromagnetic tracker. The accuracy of SHNM and ANFIS of missed head coordinates using Optical tracker is ≈ 95% and ≈ 59% respectively.

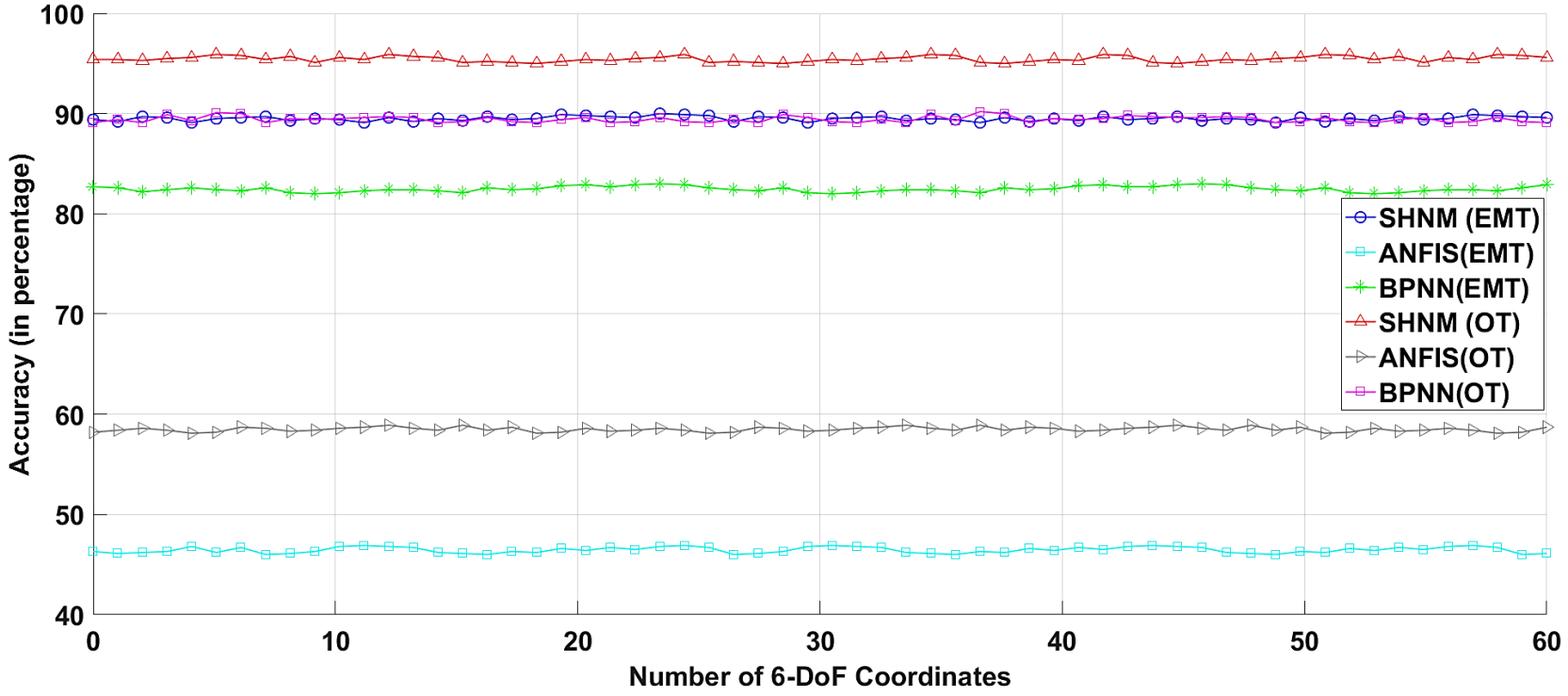

Figure 5.73: Performance evaluation of SHNM, ANFIS, and BPNN in the prediction of Pitch (rotational) head coordinates in large data set using both optical and electromagnetic tracker

Figure 5.74 presents the prediction accuracy of all three models (SHNM, ANFIS, and BPNN) for the prediction of the missing rotational head coordinate Roll, and it is found from Figure 5.74 that, the accuracy of the Self-healing neural model outperforms the ANFIS and Backpropagation neural network. The accuracy of SHNM is ≈ 85% and ANFIS is ≈ 52% using Electromagnetic tracker. The accuracy of SHNM and ANFIS of missed head coordinates using Optical tracker is ≈ 92% and ≈ 60% respectively.

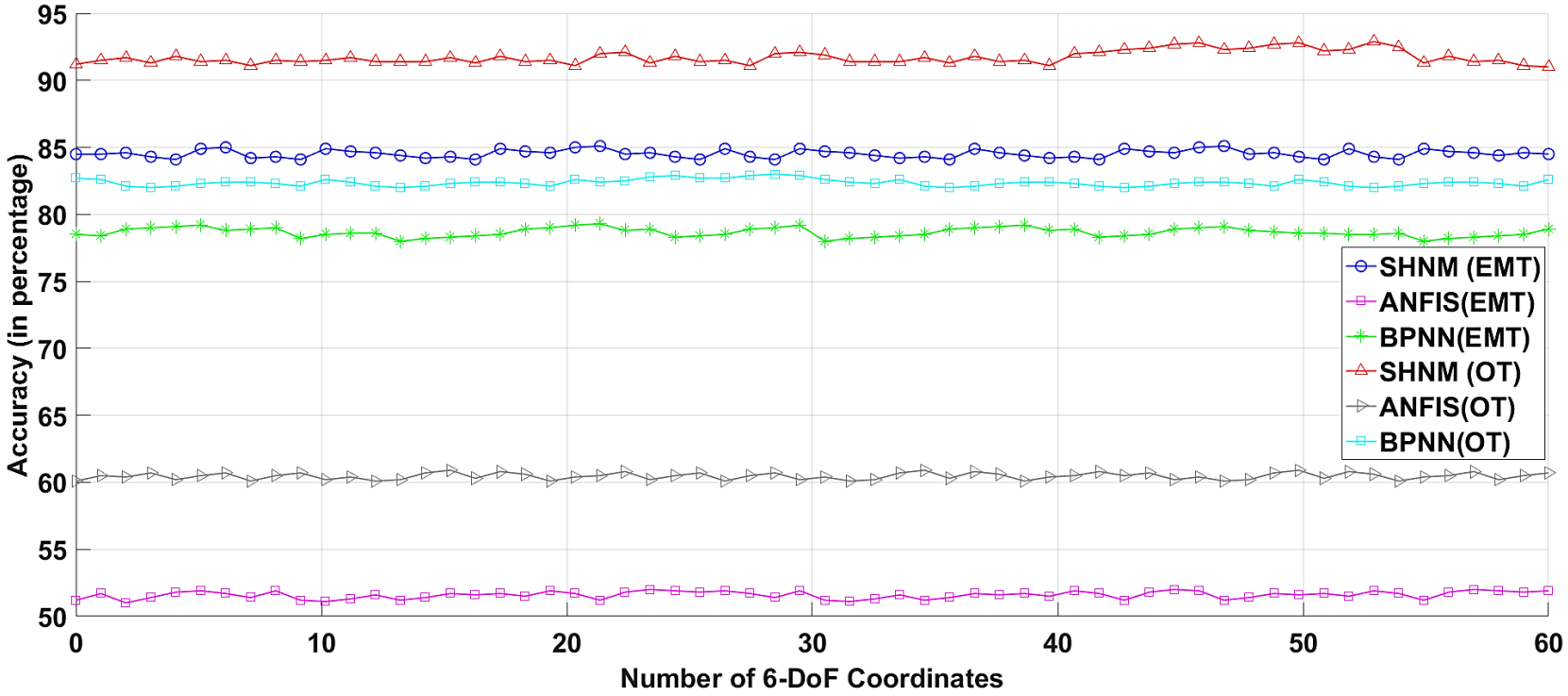

Figure 5.74: Performance evaluation of SHNM, ANFIS, and BPNN in the prediction of Roll (rotational) head coordinates in large data set using both optical and electromagnetic tracker

5.8 ESTIMATION OF LATENCY AND ERRORS IN HEAD TRACKING

The 6-DoF head coordinates can be missed due to stray light interference and by exceeding the range of motion of the head in the cockpit from the stipulated amount of range of head motion box. The horizontal limit of the head motion box is 120 mm and the vertical limit is 70mm in the cockpit.

The data acquisition of 6-DoF coordinates of the head depends on different factors.

In optical tracking, the factors affecting the acquisition of 6-DoF data are light intensity, the distance between transmitter and receiver, number of sensors used, and latency of the hardware as well as prediction algorithm.

In electromagnetic tracking, the 6-DoF data acquisition is affected by interference due to ferromagnetism leading to corruption or missing data, the number of transmitting sensors used, and the latency of hardware. Figure 5.75 shows the different movements of the head during tracking the coordinates of the head.

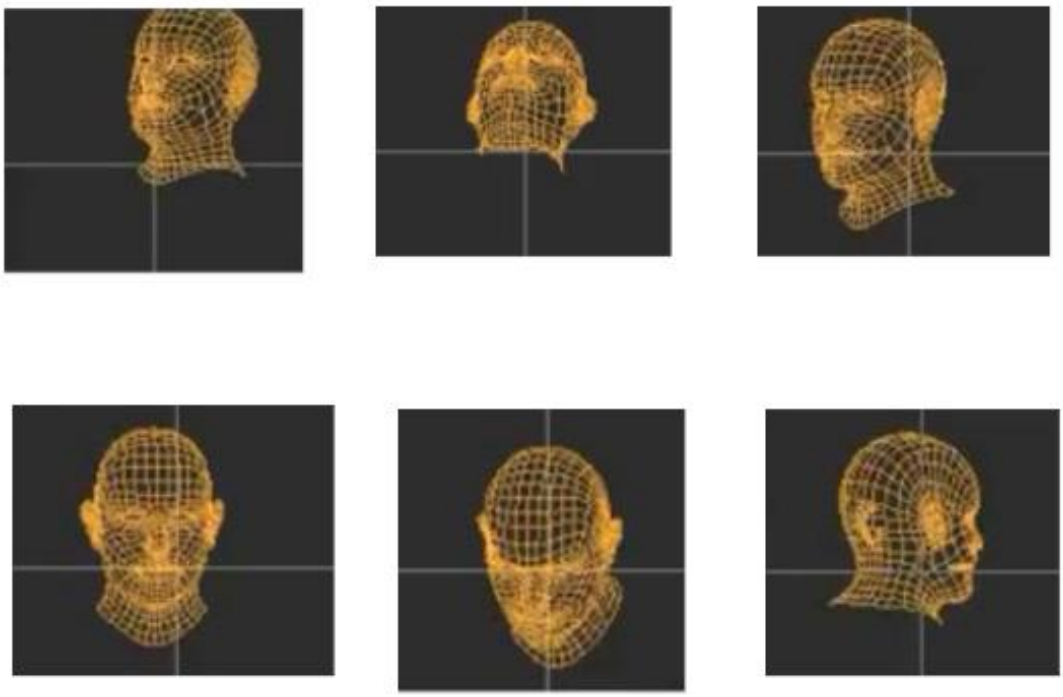

Figure 5.75: Different head movements used to find the latency of the Optical Tracker

In this chapter, the third objective is covered as the basis of error patterns in terms of latency, and positioning accuracy is discussed.

5.9 LATENCY OF OPTICAL TRACKER

The time delay between head movement and acquisition of coordinates of the head through a tracker is known as Latency. The time elapsed between the change in position or orientation of the head and the time the tracker detects the change has several negative effects on the simulation. It should be as minimum as possible. The distance between transmitter and receiver along with placement and orientation of the receiver on the cockpit also affects the time of acquisition of coordinates leading to latency. The latency of different optical trackers is discussed in this section.

Figure 5.76 shows the general hardware latencies of five different trackers, which leads to the choice of optical tracker used in this experiment. The optical tracker with the lowest latency keeping the cost as a dominating factor is TrackIR^{TM} 5 having a latency of 10 milliseconds. Latency in three different sets of missing data has been calculated using the optical and electromagnetic tracker in Table 5.7 and Table 5.8 respectively. Missing data refers to the number of head coordinates, which were not acquired due to external interferences or due to factors like the movement of head tracker beyond HMB range.

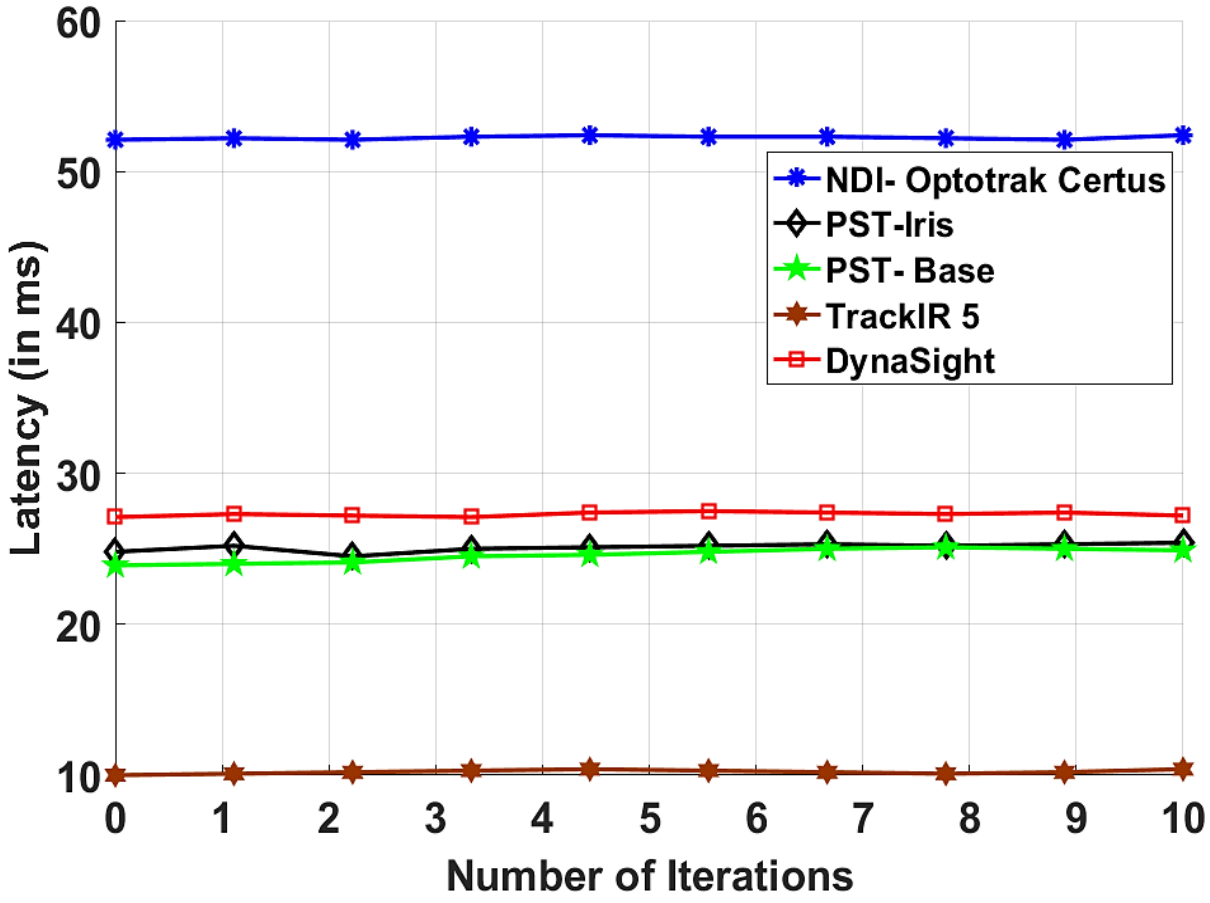

Figure 5.76: Latency of data acquisition of head coordinates using different optical trackers

Table 5.7: Latency of the system of data acquisition and prediction of missing data using the optical tracker

No. of Trackers	One Optical Tracker		**Total Latency (Hardware + System)**
Hardware Latency	10 ms		
Recovery time of X coordinates in missing data set of 4400 instances using SHNM	1% Missing Data	125 ms	135 ms
	2% Missing Data	128 ms	138 ms
	10% Missing Data	200 ms	210 ms
	25% Missing Data	315 ms	325 ms
	35% Missing Data	410 ms	420 ms
Recovery time of Y coordinates in missing data set of 4400 instances using SHNM	1% Missing Data	123 ms	133 ms
	2% Missing Data	125 ms	135 ms
	10% Missing Data	205 ms	215 ms
	25% Missing Data	318 ms	328 ms
	35% Missing Data	413 ms	423 ms
Recovery time of Z coordinates in missing data set of 4400 instances using SHNM	1% Missing Data	198 ms	208 ms
	2% Missing Data	200 ms	210 ms
	10% Missing Data	207 ms	217 ms
	25% Missing Data	319 ms	329 ms
	35% Missing Data	414 ms	424 ms
Recovery time of Yaw coordinates in missing data set of 4400 instances using SHNM	1% Missing Data	200 ms	210 ms
	2% Missing Data	203 ms	213 ms
	10% Missing Data	210 ms	220 ms
	25% Missing Data	325 ms	335 ms
	35% Missing Data	415 ms	425 ms
Recovery time of Pitch coordinates in missing data set of	1% Missing Data	202 ms	212 ms
	2% Missing Data	205 ms	215 ms
	10% Missing Data	213 ms	223 ms

4400 instances using SHNM	25% Missing Data	328 ms	338 ms
	35% Missing Data	419 ms	429 ms
Recovery time of Roll coordinates in missing data set of 4400 instances using SHNM	1% Missing Data	201 ms	211 ms
	2% Missing Data	204 ms	214 ms
	10% Missing Data	213 ms	223 ms
	25% Missing Data	328 ms	338 ms
	35% Missing Data	420 ms	430 ms

5.10 LATENCY OF ELECTROMAGNETIC TRACKER

The tracker used for the tracking of the head is calibrated according to the head motion box of the cockpit. The horizontal limit of the head motion box is 120 mm and the vertical limit is 70mm in the cockpit. If the motion of the head of the pilot exceeds the predefined limit of the head motion box, the 6-doF head coordinates will not be acquired, therefore leading to the missing head motion coordinates.

In electromagnetic tracking, when the head motion of the pilot exceeds the limit of the head motion box, the receiver end of the tracking system will be more prone to external interferences like ferromagnetism. In addition, the acquisition of the data depends upon the hardware latency of the tracker. There is no line of sight problem in an electromagnetic tracker. Hence, the effect of placement of the transmitter and the receiver is very less as compared to an optical tracker. But its tracking area is calibrated according to the Latency of different electromagnetic trackers is discussed in this section. The data prediction using Self Healing Neural Model (SHNM) was done in **MATLAB 2016a**. The prediction time of SHNM was different for each set of missing data. In addition, the prediction time is different for each coordinate. The tracking latency of the hardware used (Electromagnetic tracker Polhemus Patriot^{TM}) is 18.5 milliseconds (ms). The total latency of

the whole system is the addition of the hardware latency and prediction time of SHNM in MATLAB 2016a. The electromagnetic tracker with the lowest latency keeping the cost as a dominating factor is Polhemus Patriot^{TM} having a latency of 18.5 milliseconds. Table 5.8 represents the total latency of the system with 1%, 2%, 10%, 25%, and 35% of missing data.

Table 5.8: Latency of the system of data acquisition and prediction of missing data using Electromagnetic Tracker

No. of Trackers	One Electromagnetic Tracker		**Total Latency (Hardware + System)**
Hardware Latency	≈19 ms		
Recovery time of X coordinates in missing data set of 5200 instances using SHNM	1% Missing Data	205 ms	224 ms
	2% Missing Data	208 ms	227 ms
	10% Missing Data	215 ms	234 ms
	25% Missing Data	320 ms	339 ms
	35% Missing Data	420 ms	439 ms
Recovery time of Y coordinates in missing data set of 5200 instances using SHNM	1% Missing Data	209 ms	228 ms
	2% Missing Data	212 ms	231 ms
	10% Missing Data	217s ms	236 ms
	25% Missing Data	323 ms	342 ms
	35% Missing Data	422 ms	441 ms
Recovery time of Z coordinates in missing data set of 5200 instances using SHNM	1% Missing Data	210 ms	229 ms
	2% Missing Data	213 ms	232 ms
	10% Missing Data	218 ms	237 ms
	25% Missing Data	323 ms	342 ms
	35% Missing Data	424 ms	443 ms
Recovery time of Yaw coordinates in missing data set of 5200 instances using SHNM	1% Missing Data	214 ms	233 ms
	2% Missing Data	216 ms	235 ms
	10% Missing Data	220 ms	239 ms
	25% Missing Data	325 ms	344 ms
	35% Missing Data	426 ms	445 ms
Recovery time of Pitch coordinates in missing data set of 5200 instances using SHNM	1% Missing Data	213 ms	232 ms
	2% Missing Data	217 ms	236 ms
	10% Missing Data	223 ms	242 ms
	25% Missing Data	326 ms	345 ms
	35% Missing Data	428 ms	447 ms
Recovery time of Roll coordinates in missing data set of 5200 instances using SHNM	1% Missing Data	215 ms	234 ms
	2% Missing Data	218 ms	237 ms
	10% Missing Data	223 ms	242 ms
	25% Missing Data	327 ms	346 ms
	35% Missing Data	429 ms	448 ms

5.11 ERRORS IN ELECTROMAGNETIC TRACKER

Positional error is the prime factor, which hinders the accuracy of both electromagnetic and optical head tracker. This chapter deals with the errors that occurred during the acquisition of 6-DoF data both in the electromagnetic and optical tracker. In the case of the electromagnetic tracker, the error in the acquisition of 6-DoF data depends very less on the distance between the transmitter and receiver due to less workspace volume in the cockpit of the simulator. The error generation is mainly due to ferromagnetic interference due to different metals. Table 5.9 describes the interference arising due to different metals. The metals are placed in different positions. In this case, three combinations of placement of the metals are made to study the effect of interference leading to the error generation. The three positions are:

a) Near transmitter
b) Centre of transmitter and receiver
c) Near receiver

The metals used to study the effect are:

a) Stainless Steel
b) Aluminum
c) Mild Steel
d) Cobalt Chrome

In the case of mild steel, the interference was highest near the receiver coils and lowest at the center of transmitter and receiver. The stainless steel generated the minimum interference near the transmitter. Cobalt chrome generated the lowest interference near the receiver and at the center of the transmitter and receiver. Figure 5.77 shows the accuracy plot of the electromagnetic tracker due to the interference of different metals placed at different positions.

Table 5.9: Performance evaluation of electromagnetic tracker due to the interference of different metals placed at different positions

Metal/Alloy induced for interference	Placement of metal/Alloy for interference	Accuracy of acquisition of coordinates (compared with benchmarked data)	Error	Latency of the tracker
Stainless Steel (Least)	Near transmitter	94%	6%	16.6 ms
	At the center of transmitter and receiver	90%	10%	16.7 ms
	Near receiver	85%	15%	16.8 ms
Aluminum	Near transmitter	89%	11%	16.7 ms
	At the center of transmitter and receiver	95%	5%	16.6 ms
	Near Receiver	83%	17%	16.8 ms
Mild Steel (Highest)	Near transmitter	51%	49%	16.3 ms
	At the center of transmitter and receiver	65%	35%	16.1 ms
	Near receiver	25%	75%	16.4 ms
Cobalt Chrome	Near transmitter	85%	15%	16.6 ms
	At the center of transmitter and receiver	96%	4%	16.4 ms
	Near receiver	87%	13%	16.6 ms

Table 5.9 represents the acquisition of the 6-DoF data in the presence of different metals and alloys. The purpose of this experiment is to predict the behavior of the electromagnetic tracker in the presence of ferromagnetism that occurred in the cockpit of the real plane. The placements of the alloys/metals are varied. The metal/alloy are placed near the transmitter, receiver and in the center of transmitter and receiver to study the effect of ferromagnetism. Accuracy in the acquisition of 6-DoF data is different for each metal/alloy. The accuracy of the acquired data is calculated with the benchmark data, which is acquired in the absence of any ferromagnetism. It is observed that mild steel generated the maximum amount of interference and stainless steel generated minimum interference. It is also observed that due to ferromagnetism, there is a slight latency in the acquisition of 6-DoF head coordinates.

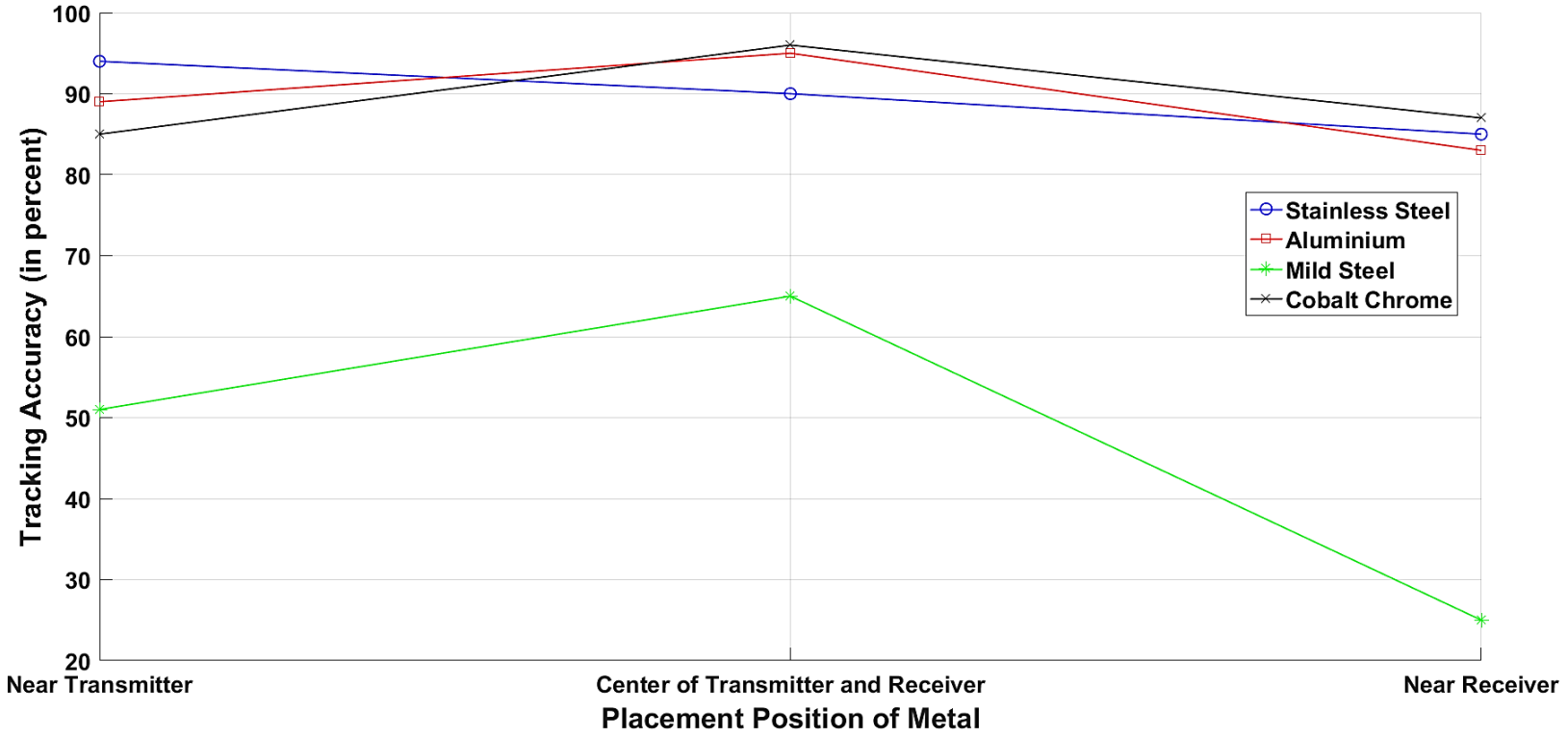

Figure 5.77: Accuracy plot of tracking using the electromagnetic tracker in the presence of the interference due to different metals placed at different positions

5.12 ERRORS IN OPTICAL TRACKER

In the case of the optical tracker, the positional error in the acquisition of 6-DoF data, which is further dependent on the range of head motion box (HMB), light intensity, the latency of the optical tracker, and distance between the transmitter and the receiver. The acquired data using an optical tracker is compared with the data acquired using **Polhemus Fasttrak** electromagnetic tracker treated as the ground truth data, which is more accurate and has less latency than the optical tracker used in this experiment. In the case of missing instances of coordinates of the head, the positional error was nearly 100% as the missing instances were denoted as '0s'. Table 5.10 represents the performance evaluation of optical tracker under different light intensities and different placements of transmitter and receiver.

Table 5.10: Performance evaluation of optical tracker under different light intensities and different placements of transmitter and receiver

Distance	Light intensity	Accuracy of acquisition of coordinates (compared with benchmarked data)	Error	Latency of the tracker
25 cm	3 Lux	86%	14%	9.1 ms
	75 Lux	91.7%	8.3%	9.2 ms
	111 Lux	93%	7%	9.3 ms
	165 Lux	96%	4%	9.3 ms
50 cm	3 Lux	83.3%	16.7%	9.3 ms
	75 Lux	90.6%	9.4%	9.2 ms
	111 Lux	91.7%	8.3%	9.2 ms
	165 Lux	93%	7%	9.1 ms
75 cm	3 Lux	80%	20%	9.5 ms
	75 Lux	88%	12%	9.4 ms
	111 Lux	89.3%	10.7%	9.4 ms
	165 Lux	90.9%	9.1%	9.2 ms
100 cm	3 Lux	78%	22%	9.8 ms
	75 Lux	86.1%	13.9%	9.7 ms
	111 Lux	87.2%	12.8%	9.7 ms
	165 Lux	89%	11%	9.5 ms

Figure 5.78 shows the accuracy plot of optical tracker under different light intensities and different placements of transmitter and receiver.

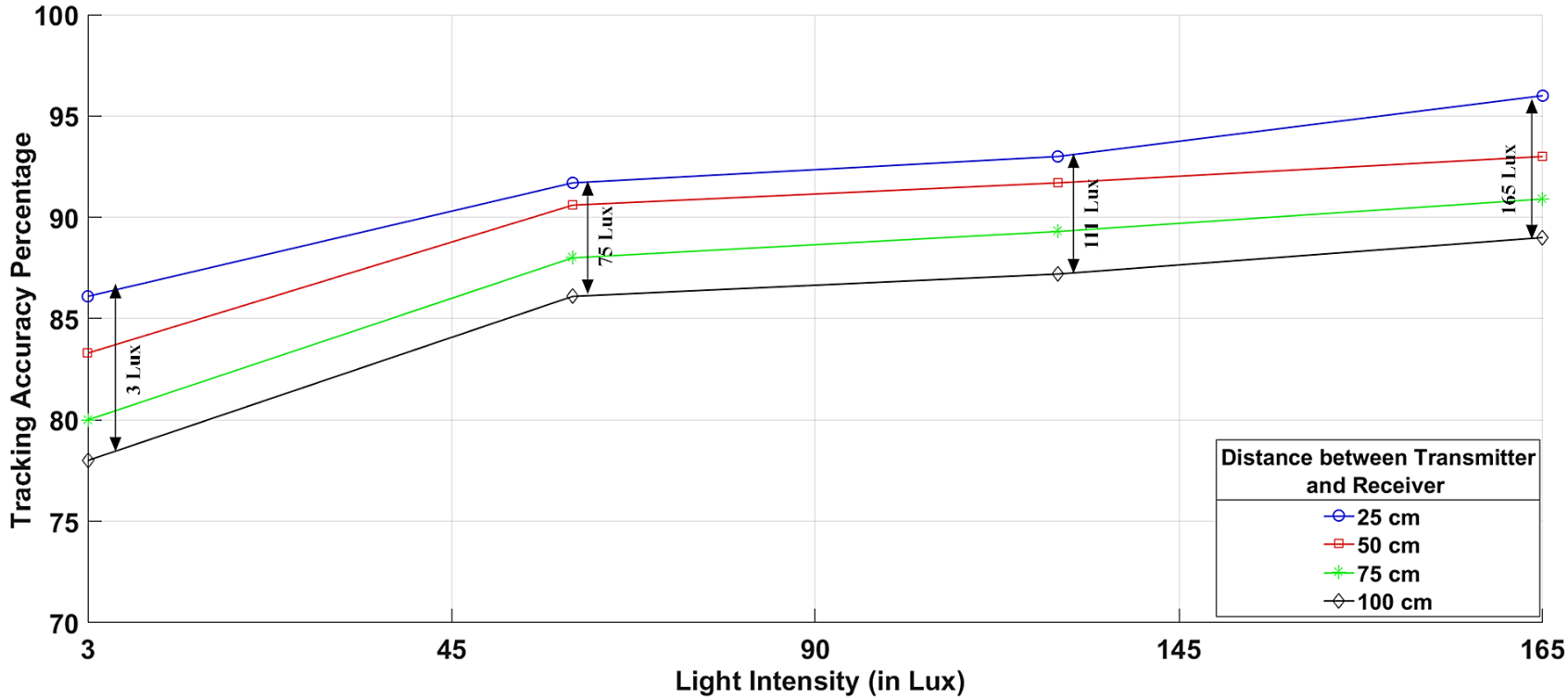

Figure 5.78: Accuracy plot of tracking using optical tracker under different Light Intensities and different placements of transmitter and receiver

5.13 CONCLUSION

This chapter deals with the experimental setup required for the acquisition of 6-DoF coordinates of the head using the electromagnetic and optical tracker. The experiment was conducted on the Cockpit Simulator available at CSIR-CSIO, Chandigarh, India, and the 6-DoF head coordinates were acquired using both electromagnetic and optical trackers under different simulated environmental conditions. The acquired 6-DoF coordinates of the head were missed due to interferences leading to the 6-DoF missing data set. It was also observed during the experiment that, while using both the trackers whenever the head of the pilot exceeds the limit of Head Motion Box (HMB), it leads to the missing of 6-DoF coordinates of the head. Also, the trackers become more prone to external interferences (ferromagnetism in the case of electromagnetic tracker and stray light in the optical tracker). Therefore, to avoid the recalibration of the position of the trackers in the cockpit, it is necessary to calibrate the head trackers with respect to the range of Head Motion Box (HMB). A Self- Healing Neural Model was applied to predict the data with 1%, 2%, 10%, 25%, and 35% missed 6-DoF coordinates of the head. Accuracy of the predicted instances of 6-DoF data of both electromagnetic and optical tracker have been discussed in this chapter. This chapter also discusses the soft computing techniques used in this work to predict the missing data in both electromagnetic and optical trackers. The missing instances of the head coordinates in the 6-DoF head motion data caused by the different kinds of interferences have been predicted using the Self Healing Neural Model, Back Propagation Neural Network, Autoregressive Linear Model, and Adaptive Neuro-Fuzzy Inference System. It has been found that the accuracy of prediction is achieved highest using Self Healing Neural Model for both large and small data sets. Accuracy using the Adaptive Neuro-Fuzzy Inference System is higher in small data sets as compared to the large data set. This chapter also dealt with the latency occurring in head tracking using both optical

and electromagnetic tracker. The factors leading to latency in head tracking are discussed in this chapter. The latency has been estimated for 1%, 2%, 10%, 25% and 35% missing data. The latency of both hardware and software has been discussed in this chapter. Also, the errors in the acquisition of 6-DoF coordinates of the head using both electromagnetic and optical trackers are discussed in this chapter. The errors were calculated with reference to the benchmarked data of the Polhemus Fasttrak electromagnetic tracker. The error in the electromagnetic tracker was calculated with interferences caused by different metals and alloys. Similarly, error in optical tracker was calculated with interferences caused by different light intensities. Accuracy of the data acquisition is plotted for both electromagnetic and optical trackers. The comparison of the accuracy of all the techniques used in the prediction of 6-DoF head coordinates is also presented in this chapter.

6 CONCLUSION AND FUTURE SCOPE

This thesis deals with the introduction of head-up displays, head-mounted displays, and the need for head tracking along with its basic working. Different types of trackers are discussed in this thesis. The trackers discussed are mechanical, acoustic, optical, electromagnetic, and inertial head trackers. During the experiments to acquire the 6-DoF coordinates of the head motion, it was found that electromagnetic and optical tracking is the most suitable tracking technologies as compared to the mechanical, acoustic, and inertial head trackers. Electromagnetic and optical trackers are more robust, lightweight, accurate, and cost-effective trackers as compared to the other three trackers. This thesis also presents the literature survey of the work done in the field of tracking using optical, electromagnetic, and inertial techniques. The problems that occurred during the acquisition of 6-DoF coordinates of the head are also mentioned in the literature survey. The factors and causes of the interferences in electromagnetic and optical trackers are also discussed. The effect of interference leading to inaccurate tracking of head coordinates has also been mentioned in this thesis. It was found that exceeding the motion of head from the range of head motion box of the cockpit led to missing 6-DoF coordinates of the head motion leading to inaccuracy and latency. Other reasons for inaccurate head tracking were the interferences that occurred in trackers. For the electromagnetic head tracker, the effect of ferromagnetic interference due to different the placement of metals and alloys has been discussed. In optical tracking, the source of interference is the stray light present in the cockpit. The latency occurring in both electromagnetic and optical trackers has been discussed in this thesis. Latency also occurred in the algorithm used to predict 6-DoF coordinates of the head which depended on the different sets of the acquired 6-DoF coordinates. The errors in the acquisition of 6-DoF coordinates of the head

using electromagnetic and optical head tracking have been represented in this thesis. The acquisition of 6-DoF coordinates of the head is done in real-time in the cockpit simulator laboratory at CSIO, Chandigarh, India. The 6-DoF coordinates of the head were acquired using electromagnetic and optical trackers under different environmental conditions. The 6-DoF coordinates of the head were acquired under different light intensities, the distance between transmitter and receiver, and different placement and orientations of the transmitter and receiver. The corrupted or missing 6-DoF coordinates of the head due to interferences in both electromagnetic and optical trackers were tried to mitigate by predicting the missing 6-DoF data using soft computing and regression techniques. The missing 6-DoF coordinates of the head were predicted using the Self Healing Neural Model, Back Propagation Neural Network, ANFIS, and Autoregressive Linear Model. Out of all these techniques, the accuracy in prediction of missing 6-DoF coordinates of the head was achieved by Self Healing Neural Model. The Self Healing Neural Model has some shortcomings like the threshold of the model has to select manually by experimenting with the different threshold values. The Self Healing Neural Model is not a multimodal algorithm i.e. is not capable of predicting the 6-DoF head motion coordinates parallelly. ANFIS predicted the missing 6-DoF coordinates with the least accuracy. The accuracy of ANFIS was very less in the prediction of missing 6-DoF coordinates in the large data set. The accuracy of ANFIS was considerably high in the prediction of missing 6-DoF coordinates in the small data sets. the Autoregressive being the less complex method was used to predict the missing 6-DoF coordinates. Its prediction accuracy increased with an increase in the order of the prediction. The order of ARLM is the number of immediately preceding values in the series that are used to predict the value at the present time. In this thesis, the order of the ARLM to predict the missing 6-DoF coordinates is **three**. As the order of the ARLM increases, the undesirable overhead charges

of the whole tracking system including prediction increases. The comparison of accuracy in the prediction of missing 6-DoF coordinates is also presented in this thesis.

6.1 FUTURE SCOPE

After carrying out the research work, it is realized that there are some factors that can be improved in the field of head tracking.

- The software interface can be designed to acquire the 6-DoF data using two or multiple technologies of tracking simultaneously.
- The prediction of data can also be embedded along with data acquisition in real-time.
- Also, the size of the electromagnetic tracker can be reduced by designing the tracker using miniature components.
- Optical trackers can be improved by increasing their FOV to reduce the problem of line of sight and partial occlusions so that the tracking of the head motion coordinates can be improved.
- The Self Healing Neural Model can also be converted to a more efficient multimodal algorithm that should be capable to predict 6-DoF head motion coordinates parallelly, thus decreasing the processing time to a larger extent.

REFERENCES

[1] V. Sharma, F. Song, I. You, and H.-C. Chao, "Efficient Management and Fast Handovers in Software Defined Wireless Networks Using UAVs," *IEEE Network*, Vol. 31, No. 6, pp. 78-85, 2017.

[2] V. Sharma and R. Kumar, "A cooperative network framework for multi-UAV guided ground ad hoc networks," *Journal of Intelligent & Robotic Systems,* Vol. 77, No. 3-4, pp. 629-652, 2015.

[3] V. Sharma, H.-C. Chen, and R. Kumar, "Driver behaviour detection and vehicle rating using multi-UAV coordinated vehicular networks," *Journal of Computer and System Sciences,* Vol. 86, pp. 3-32, 2017.

[4] R. Sabatini, T. Moore, and C. Hill, "A new avionics-based GNSS integrity augmentation system: part 1–fundamentals," *The Journal of Navigation,* Vol. 66, No. 3, pp. 363-384, 2013.

[5] I. E. Sutherland, "A head-mounted three dimensional display," in *Proceedings of the December 9-11, 1968, fall joint computer conference, part I*, 1968, pp. 757-764.

[6] K. Takemura, J. Ido, Y. Matsumoto, and T. Ogasawara, "Drive monitoring system based on non-contact measurement system of driver's focus of visual attention," in *Intelligent Vehicles Symposium, 2003. Proceedings. IEEE*, 2003, pp. 581-586, Columbus, OH, USA,

[7] B.-Z. Li and Y.-P. Shi, "Image watermarking in the linear canonical transform domain," *Mathematical Problems in Engineering*, Vol. 2014, 2014.

[8] N. Goel and K. Singh, "Modified correlation theorem for the linear canonical transform with representation transformation in quantum mechanics," *Signal, Image and Video Processing*, Vol. 8, No. 3, pp. 595-601, 2014.

[9] G. F. Marshall, "Back from the past: the helmet integrated system of Albert Bacon Pratt (1916)," *Optical Engineering*, Vol. 28, No. 11, p. 281247, 1989.

[10] J. E. Melzer and K. Moffitt, "Head mounted displays–designing for the user, 1997," ed: McGraw-Hill, New York, NY.

[11] C. E. Rash, *Helmet mounted displays: Design issues for rotary-wing aircraft* vol. 93: SPIE Press, 1999.

[12] O. Cakmakci and J. Rolland, "Head-worn displays: a review," *Journal of display technology*, Vol. 2, No. 3, pp. 199-216, 2006.

[13] N. Coates, "13.4: Head Mounted Display for Simulation and Visualisation," in *SID Symposium Digest of Technical Papers*, 2003, pp. 184-187, Oxford, UK: Blackwell Publishing Ltd.

[14] A. Sisodia, A. Riser, M. Bayer, and J. P. McGuire, "Advanced helmet mounted display (AHMD) for simulator applications," in *Helmet-and Head-Mounted Displays XI: Technologies and Applications*, 2006, p. 62240O.

[15] D. Hewlett and A. A. Cameron, "Advances in rotary-wing helmet-mounted displays," in *Helmet-and Head-Mounted Displays V*, 2000, pp. 79-90.

[16] M. Velger, "Helmet-mounted displays and sights," *Norwood, MA: Artech House Publishers, 1998.*, 1998.

[17] R. Bala, R. Singh, A. Marwaha, and S. Marwaha, "Wearable Graphene Based Curved Patch Antenna for Medical Telemetry Applications," *Applied Computational Electromagnetics Society Journal*, Vol. 31, No. 5, 2016.

[18] A. Laddi, N. R. Prakash, S. Sharma, and A. Kumar, "Body Area Network based Health Monitoring of Critical Patients: a Brief Review," *International Journal of Instrumentation and Control Systems (lJICS)*, Vol. 2, No. 3, 2012.

[19] M. M. Pankratov, "New surgical three-dimensional visualization system," in *Lasers in Surgery: Advanced Characterization, Therapeutics, and Systems V*, 1995, pp. 143-150.

[20] C. J. Casey, "Helmet-mounted displays on the modern battlefield," in *Helmet-and Head-Mounted Displays IV*, 1999, pp. 270-278.

[21] B. D. Foote, "Design guidelines for advanced air-to-air helmet-mounted display systems," in *Helmet-and Head-Mounted Displays III*, 1998, pp. 94-103.

[22] M. Thomas and H. Geltmacher, "Combat simulator display development," *Information Display*, Vol. 9, pp. 23-23, 1993.

[23] C. J. Casey and J. E. Melzer, "Part-task training with a helmet-integrated display simulator system," in *Large Screen Projection, Avionic, and Helmet-Mounted Displays*, 1991, pp. 175-179.

[24] M. LaCroix and J. Melzer, "Helmet-mounted displays for flight simulators," in *Proc. IMAGE VII Conf*, 1994.

[25] D. J. Weintraub, R. F. Haines, and R. J. Randle, "Head-up display (HUD) utility, II: Runway to HUD transitions monitoring eye focus and decision times," in *Proceedings of the Human Factors Society Annual Meeting*, 1985, pp. 615-619.

[26] E. Fischer and R. F. Haines, "Cognitive issues in head-up displays," 1980.

[27] R. K. Rebo and P. Amburn, "A helmet-mounted virtual environment display system," in *Helmet-Mounted Displays*, 1989, pp. 80-85.

[28] D. J. Rotier, "Optical approaches to the helmet mounted display," in *Helmet-Mounted Displays*, 1989, pp. 14-19.

[29] M. Stojanovic, "Recent advances in high-speed underwater acoustic communications," *IEEE Journal of Oceanic engineering*, Vol. 21, No. 2, pp. 125-136, 1996.

[30] E. E. Geiselman and R. K. Osgood, "Head versus aircraft oriented air-to-air target location symbology using a helmet-mounted display," in *Helmet-and Head-Mounted Displays and Symbology Design Requirements II*, 1995, pp. 214-226.

[31] T. P. Caudell and D. W. Mizell, "Augmented reality: An application of heads-up display technology to manual manufacturing processes," in *System Sciences, 1992. Proceedings of the Twenty-Fifth Hawaii International Conference on*, 1992, pp. 659-669.

[32] M. Ribo, A. Pinz, and A. L. Fuhrmann, "A new optical tracking system for virtual and augmented reality applications," in *Instrumentation and Measurement Technology Conference, 2001. IMTC 2001. Proceedings of the 18th IEEE*, 2001, pp. 1932-1936.

[33] R. Rae and H. J. Ritter, "Recognition of human head orientation based on artificial neural networks," *IEEE Transactions on neural networks*, Vol. 9, No. 2, pp. 257-265, 1998.

[34] A. Gee and R. Cipolla, "Determining the gaze of faces in images," *Image and Vision Computing*, Vol. 12, No. 10, pp. 639-647, 1994.

[35] P. Ballard and G. C. Stockman, "Controlling a computer via facial aspect," *IEEE Transactions on Systems, Man, and Cybernetics*, Vol. 25, No. 4, pp. 669-677, 1995.

[36] S. Asteriadis, K. Karpouzis, and S. Kollias, "Face tracking and head pose estimation using convolutional neural networks," in *Proceedings of the SSPNET 2nd International Symposium on Facial Analysis and Animation*, 2010, pp. 19-19.

[37] M. Bauer, M. Schlegel, D. Pustka, N. Navab, and G. Klinker, "Predicting and estimating the accuracy of n-occular optical tracking systems," in *Mixed and Augmented Reality, 2006. ISMAR 2006. IEEE/ACM International Symposium on*, 2006, pp. 43-51.

[38] C. He, H. T. Şen, S. Kim, P. Sadda, and P. Kazanzides, "Fusion of inertial sensing to compensate for partial occlusions in optical tracking systems," in *Workshop on Augmented Environments for Computer-Assisted Interventions*, 2014, pp. 60-69.

[39] H. T. Sen and P. Kazanzides, "Bayesian filtering to improve the dynamic accuracy of electromagnetic tracking," in *Robotic and Sensors Environments (ROSE), 2013 IEEE International Symposium on*, 2013, pp. 90-95.

[40] C. Nafis, V. Jensen, L. Beauregard, and P. Anderson, "Method for estimating dynamic EM tracking accuracy of surgical navigation tools," in *Medical Imaging 2006: Visualization, Image-Guided Procedures, and Display*, 2006, p. 61410K.

[41] H. Himberg, Y. Motai, and A. Bradley, "A multiple model approach to track head orientation with delta quaternions," *IEEE transactions on cybernetics*, Vol. 43, No. 1, pp. 90-101, 2013.

[42] D. Roetenberg, H. J. Luinge, C. T. Baten, and P. H. Veltink, "Compensation of magnetic disturbances improves inertial and magnetic sensing of human body segment orientation," *IEEE Transactions on neural systems and rehabilitation engineering*, Vol. 13, No. 3, pp. 395-405, 2005.

[43] T. Harada, T. Mori, and T. Sato, "Development of a tiny orientation estimation device to operate under motion and magnetic disturbance," *The International Journal of Robotics Research,* Vol. 26, No. 6, pp. 547-559, 2007.

[44] R. Khadem, C. C. Yeh, M. Sadeghi- Tehrani, M. R. Bax, J. A. Johnson, J. N. Welch, *et al.,* "Comparative tracking error analysis of five different optical tracking systems," *Computer Aided Surgery,* Vol. 5, No. 2, pp. 98-107, 2000.

[45] A. Al-Rahayfeh and M. Faezipour, "Eye tracking and head movement detection: A state-of-art survey," *IEEE journal of translational engineering in health and medicine,* Vol. 1, pp. 2100212-2100212, 2013.

[46] C. He, P. Kazanzides, H. T. Sen, S. Kim, and Y. Liu, "An inertial and optical sensor fusion approach for six degree-of-freedom pose estimation," *Sensors,* Vol. 15, No. 7, pp. 16448-16465, 2015.

[47] C. Hu, M. Q.-H. Meng, and M. Mandal, "A linear algorithm for tracing magnet position and orientation by using three-axis magnetic sensors," *IEEE Transactions on Magnetics,* Vol. 43, No. 12, pp. 4096-4101, 2007.

[48] M. B. Ooi, S. Krueger, W. J. Thomas, S. V. Swaminathan, and T. R. Brown, "Prospective real- time correction for arbitrary head motion using active markers," *Magnetic resonance in medicine,* Vol. 62, No. 4, pp. 943-954, 2009.

[49] D. Van Krevelen and R. Poelman, "A survey of augmented reality technologies, applications and limitations," *International journal of virtual reality,* Vol. 9, No. 2, p. 1, 2010.

[50] X. Suau, J. Ruiz-Hidalgo, and J. R. Casas, "Real-time head and hand tracking based on 2.5 D data," *IEEE transactions on multimedia,* Vol. 14, No. 3, pp. 575-585, 2012.

[51] S. M. LaValle, A. Yershova, M. Katsev, and M. Antonov, "Head tracking for the Oculus Rift," in *Robotics and Automation (ICRA), 2014 IEEE International Conference on*, 2014, pp. 187-194.

[52] E. D. Ragan, R. Kopper, P. Schuchardt, and D. A. Bowman, "Studying the effects of stereo, head tracking, and field of regard on a small-scale spatial judgment task," *IEEE transactions on visualization and computer graphics*, Vol. 19, No. 5, pp. 886-896, 2013.

[53] Y. Kobayashi, D. Sugimura, Y. Sato, K. Hirasawa, N. Suzuki, H. Kage, *et al.*, "3D Head Tracking using the Particle Filter with Cascaded Classifiers," in *BMVC*, 2006, pp. 37-46.

[54] S. Choi and D. Kim, "Robust head tracking using 3D ellipsoidal head model in particle filter," *Pattern Recognition*, Vol. 41, No. 9, pp. 2901-2915, 2008.

[55] C. Rougier, J. Meunier, A. St-Arnaud, and J. Rousseau, "3D head tracking for fall detection using a single calibrated camera," *Image and Vision Computing*, Vol. 31, No. 3, pp. 246-254, 2013.

[56] E. Parvizi and Q. J. Wu, "Real-time 3d head tracking based on time-of-flight depth sensor," in *Tools with Artificial Intelligence, 2007. ICTAI 2007. 19th IEEE International Conference on*, 2007, pp. 517-521.

[57] H. Yoon, D. Kim, S. Chi, and Y. Cho, "A robust human head detection method for human tracking," in *Intelligent Robots and Systems, 2006 IEEE/RSJ International Conference on*, 2006, pp. 4558-4563.

[58] R. A. Pavlik and J. M. Vance, "A modular implementation of Wii remote head tracking for virtual reality," in *ASME 2010 World Conference on Innovative Virtual Reality*, 2010, pp. 351-359.

[59] M. B. López, J. Hannuksela, O. Silvén, and L. Fan, "Head-tracking virtual 3-D display for mobile devices," in *Computer Vision and Pattern Recognition Workshops (CVPRW), 2012 IEEE Computer Society Conference on*, 2012, pp. 27-34.

[60] G. Papadakis, K. Mania, and E. Koutroulis, "A system to measure, control and minimize end-to-end head tracking latency in immersive simulations," in *Proceedings of the 10th International Conference on Virtual Reality Continuum and Its Applications in Industry*, 2011, pp. 581-584.

[61] X. Zhang, W. Hu, H. Bao, and S. Maybank, "Robust head tracking based on multiple cues fusion in the kernel-bayesian framework," *IEEE Transactions on Circuits and Systems for Video Technology*, Vol. 23, No. 7, pp. 1197-1208, 2013.

[62] M. Ariz, J. J. Bengoechea, A. Villanueva, and R. Cabeza, "A novel 2d/3d database with automatic face annotation for head tracking and pose estimation," *Computer Vision and Image Understanding*, Vol. 148, pp. 201-210, 2016.

[63] H. Wang, F. Davoine, V. Lepetit, C. Chaillou, and C. Pan, "3-d head tracking via invariant keypoint learning," *IEEE Transactions on Circuits and Systems for Video Technology*, Vol. 22, No. 8, pp. 1113-1126, 2012.

[64] E. Murphy-Chutorian and M. M. Trivedi, "Head pose estimation and augmented reality tracking: An integrated system and evaluation for monitoring driver awareness," *IEEE Transactions on intelligent transportation systems*, Vol. 11, No. 2, pp. 300-311, 2010.

[65] N. Mollet and R. Chellali, "Virtual and augmented reality with head-tracking for efficient teleoperation of groups of robots," in *Cyberworlds, 2008 International Conference on*, 2008, pp. 102-108.

[66] M. P. Da Silva, V. Courboulay, A. Prigent, and P. Estraillier, "Fast, low resource, head detection and tracking for interactive applications," *PsychNology Journal,* Vol. 7, No. 3, pp. 243-264, 2009.

[67] T. Sko and H. J. Gardner, "Head tracking in first-person games: Interaction using a web-camera," in *IFIP Conference on Human-Computer Interaction*, 2009, pp. 342-355.

[68] D. Cazzato, M. Leo, and C. Distante, "An investigation on the feasibility of uncalibrated and unconstrained gaze tracking for human assistive applications by using head pose estimation," *Sensors,* Vol. 14, No. 5, pp. 8363-8379, 2014.

[69] M. La Cascia, S. Sclaroff, and V. Athitsos, "Fast, reliable head tracking under varying illumination: An approach based on registration of texture-mapped 3D models," *IEEE Transactions on pattern analysis and machine intelligence,* Vol. 22, No. 4, pp. 322-336, 2000.

[70] M. Nabati and A. Behrad, "Robust facial 2D motion model estimation for 3D head pose extraction and automatic camera mouse implementation," in *Telecommunications (IST), 2010 5th International Symposium on*, 2010, pp. 817-824.

[71] Y. Yan, E. Ricci, R. Subramanian, O. Lanz, and N. Sebe, "No matter where you are: Flexible graph-guided multi-task learning for multi-view head pose classification under target motion," in *Computer Vision (ICCV), 2013 IEEE International Conference on*, 2013, pp. 1177-1184.

[72] Y. Yan, E. Ricci, R. Subramanian, G. Liu, O. Lanz, and N. Sebe, "A multi-task learning framework for head pose estimation under target motion," *IEEE transactions on pattern analysis and machine intelligence,* Vol. 38, No. 6, pp. 1070-1083, 2016.

[73] G. Zhao, L. Chen, J. Song, and G. Chen, "Large head movement tracking using sift-based registration," in *Proceedings of the 15th ACM international conference on Multimedia*, 2007, pp. 807-810.

[74] B. Prasad and R. Aravind, "A robust head pose estimation system for uncalibrated monocular videos," in *Proceedings of the Seventh Indian Conference on Computer Vision, Graphics and Image Processing*, 2010, pp. 162-169.

[75] R. Ruddarraju, A. Haro, and I. Essa, "Fast multiple camera head pose tracking," in *Vision Interface*, 2003.

[76] R. Yang and Z. Zhang, "Model-based head pose tracking with stereovision," in *Automatic Face and Gesture Recognition, 2002. Proceedings. Fifth IEEE International Conference on*, 2002, pp. 255-260.

[77] Z. Liu, Z. Zhang, C. Jacobs, and M. Cohen, "Rapid modeling of animated faces from video," *Computer Animation and Virtual Worlds*, Vol. 12, No. 4, pp. 227-240, 2001.

[78] Q. Cai, A. Sankaranarayanan, Q. Zhang, Z. Zhang, and Z. Liu, "Real time head pose tracking from multiple cameras with a generic model," in *Computer Vision and Pattern Recognition Workshops (CVPRW), 2010 IEEE Computer Society Conference on*, 2010, pp. 25-32.

[79] S. Malassiotis and M. G. Strintzis, "Real-time head tracking and 3d pose estimation from range data," in *Image Processing, 2003. ICIP 2003. Proceedings. 2003 International Conference on*, 2003, pp. II-859.

[80] A. Schodl, A. Haro, and I. A. Essa, "Head tracking using a textured polygonal model," Georgia Institute of Technology, 1998.

[81] F. Madrigal, F. Lerasle, and A. Monin, "3D Head Pose Estimation Enhanced Through SURF-Based Key-Frames," in *Applications of Computer Vision (WACV), 2018 IEEE Winter Conference on*, 2018, pp. 75-83.

[82] V. N. Balasubramanian, J. Ye, and S. Panchanathan, "Biased manifold embedding: A framework for person-independent head pose estimation," in *Computer Vision and Pattern Recognition, 2007. CVPR'07. IEEE Conference on*, 2007, pp. 1-7.

[83] V. Krüger and G. Sommer, "Gabor wavelet networks for efficient head pose estimation," *Image and vision computing*, Vol. 20, No. 9-10, pp. 665-672, 2002.

[84] N. Gourier, J. Maisonnasse, D. Hall, and J. L. Crowley, "Head pose estimation on low resolution images," in *International Evaluation Workshop on Classification of Events, Activities and Relationships*, 2006, pp. 270-280.

[85] H. Singh, V. Karar, N. Kumar, and S. S. Saini, "Performance comparison: optical and magnetic head tracking," *International Journal of IT, Engineering and Applied Sciences Research*, Vol. 2, No. 3, pp. 27-32, 2013.

[86] A. Abramson and I. Efrat, "Reduction of multiple harmonics EM noise in helicopter cockpit," in *Acoustics, Speech and Signal Processing (ICASSP), 2011 IEEE International Conference on*, 2011, pp. 1801-1804.

[87] O. Nevo, "Display and sight helmet system," in *Aerospace and Electronics Conference, 1990. NAECON 1990., Proceedings of the IEEE 1990 National*, 1990, pp. 265-270.

[88] G. Zachmann, "Distortion correction of magnetic fields for position tracking," in *Proceedings computer graphics international*, 1997, pp. 213-220.

[89] G. C. Burdea and P. Coiffet, *Virtual reality technology*. USA: John Wiley & Sons, 2003.

[90] G. Veis, "Optical tracking of artificial satellites," *Space Science Reviews,* Vol. 2, No. 2, pp. 250-296, 1963.

[91] J. Borah, "Technology and application of head based control," *NASA,* No. 19990007892, 1998.

[92] E. Foxlin and N. Durlach, "An inertial head-orientation tracker with automatic drift compensation for use with HMD's," in *Virtual Reality Software And Technology,* 1994, pp. 159-173.

[93] S. Emma and S. Tat-hi, "Compensation of time lag between actual and virtual spaces by multi-sensor integration," Las Vegas, NV, USA, 1994.

[94] E. M. Foxlin, M. Harrington, and Y. Altshuler, "Miniature six-DOF inertial system for tracking HMDs," in *Helmet-and Head-Mounted Displays III*, 1998, pp. 214-229.

[95] A. Saidi and M. Mirzaei, "Prediction of AHAS inhibition by sulfonylurea herbicides using genetic algorithm and artificial neural network," *IJCT*, Vol. 23, pp. 121-130, 2016.

[96] V. Sharma, R. Kumar, and P. S. Rana, "Self-healing neural model for stabilization against failures over networked UAVs," *IEEE Communications Letters,* Vol. 19, No. 11, pp. 2013-2016, 2015.

[97] W. Birkfellner, J. Hummel, E. Wilson, and K. Cleary, "Tracking devices," in *Image-Guided Interventions*, ed: Springer, 2008, pp. 23-44.

[98] M. A. Livingston, "Magnetic tracker calibration for improved augmented reality registration. Presence: Teleoperators and Virtual Environments," 1997.

[99] M. A. Nixon, B. C. McCallum, W. R. Fright, and N. B. Price, "The effects of metals and interfering fields on electromagnetic trackers," *Presence*, Vol. 7, No. 2, pp. 204-218, 1998.

[100] T. Molet, A. Aubel, T. Çapin, S. Carion, E. Lee, N. Magnenat-Thalmann, *et al.*, "Anyone for tennis?," *Presence: Teleoperators & Virtual Environments,* Vol. 8, No. 2, pp. 140-156, 1999.

[101] F. H. Raab, E. B. Blood, T. O. Steiner, and H. R. Jones, "Magnetic position and orientation tracking system," *IEEE Transactions on Aerospace and Electronic systems,* No. 5, pp. 709-718, 1979.

[102] F. J. Ferrin, "Survey of helmet tracking technologies," in *Large Screen Projection, Avionic, and Helmet-Mounted Displays*, 1991, pp. 86-95.

[103] P. F. Skopowski, "Immersive articulation of the human upper body in a virtual environment," NAVAL POSTGRADUATE SCHOOL MONTEREY CA, 1996.

[104] T. Shibata, "Head mounted display," *Displays,* Vol. 23, No. 1-2, pp. 57-64, 2002.

[105] E. Foxlin, "Inertial head-tracker sensor fusion by a complementary separate-bias Kalman filter," in *Virtual Reality Annual International Symposium, 1996., Proceedings of the IEEE 1996*, 1996, pp. 185-194.

[106] J. Kim, K. W. Nam, I. G. Jang, H. K. Yang, K. G. Kim, and J.-M. Hwang, "Nintendo Wii remote controllers for head posture measurement: accuracy, validity, and reliability of the infrared optical head tracker," *Investigative ophthalmology & visual science,* Vol. 53, No. 3, pp. 1388-1396, 2012.

[107] M. Ibrani, E. Hamiti, L. Ahma, and B. Shala, "Assessment of personal radio frequency electromagnetic field exposure in specific indoor workplaces and possible worst-case scenarios," *AEU-International Journal of Electronics and Communications,* Vol. 70, No. 6, pp. 808-813, 2016.

[108] G. Leone, R. Persico, and R. Solimene, "A quadratic model for electromagnetic subsurface prospecting," *AEU-International Journal of Electronics and Communications,* Vol. 57, No. 1, pp. 33-46, 2003.

[109] D. K. Bhatnagar, "Position trackers for Head Mounted Display systems: A survey," *University of North Carolina, Chapel Hill TR93,* Vol. 10, 1993.

[110] K. Meyer, H. L. Applewhite, and F. A. Biocca, "A survey of position trackers," *Presence: Teleoperators & Virtual Environments,* Vol. 1, No. 2, pp. 173-200, 1992.

[111] J. G. Hagedorn, S. G. Satterfield, J. T. Kelso, W. Austin, J. E. Terrill, and A. P. Peskin, "Correction of location and orientation errors in electromagnetic motion tracking," *Presence,* Vol. 16, No. 4, pp. 352-366, 2007.

[112] S. Song, W. Qiao, B. Li, C. Hu, H. Ren, and M. Q.-H. Meng, "An efficient magnetic tracking method using uniaxial sensing coil," *IEEE Transactions on Magnetics,* Vol. 50, No. 1, pp. 1-7, 2014.

[113] Y.-W. Chow, "Low-cost multiple degrees-of-freedom optical tracking for 3D interaction in head-mounted display virtual reality," *International Journal of Recent Trends in Engineering,* Vol. 1, No. 1, p. 52, 2009.

[114] M. Buscema, "Back propagation neural networks," *Substance use & misuse,* Vol. 33, No. 2, pp. 233-270, 1998.

[115] K. M. Neaupane and S. H. Achet, "Use of backpropagation neural network for landslide monitoring: a case study in the higher Himalaya," *Engineering Geology,* Vol. 74, No. 3-4, pp. 213-226, 2004.

[116] H. Martins and R. Ventura, "Immersive 3-d teleoperation of a search and rescue robot using a head-mounted display," in *Emerging Technologies & Factory Automation, 2009. ETFA 2009. IEEE Conference on*, 2009, pp. 1-8.

[117] X. Righetti, S. Cardin, D. Thalmann, and F. Vexo, "Immersive flight for surveillance applications," in *IEEE Symposium on 3D User Interfaces*, 2007, pp. 139-142.

[118] F. Dornaika and B. Raducanu, "Single snapshot-based 3D head pose initialization for tracking in a HRI scenario," in *Computer Vision and Pattern Recognition Workshops (CVPRW), 2010 IEEE Computer Society Conference on*, 2010, pp. 32-39.

[119] E. Murphy-Chutorian and M. M. Trivedi, "Hyhope: Hybrid head orientation and position estimation for vision-based driver head tracking," in *Intelligent Vehicles Symposium, 2008 IEEE*, 2008, pp. 512-517.

[120] M. Ashdown, K. Oka, and Y. Sato, "Combining head tracking and mouse input for a GUI on multiple monitors," in *CHI'05 extended abstracts on Human factors in computing systems*, 2005, pp. 1188-1191.

[121] F. Sauer, A. Khamene, and S. Vogt, "An augmented reality navigation system with a single-camera tracker: System design and needle biopsy phantom trial," in *International Conference on Medical Image Computing and Computer-Assisted Intervention*, 2002, pp. 116-124.

[122] G. Welch, G. Bishop, L. Vicci, S. Brumback, and K. Keller, "The HiBall tracker: High-performance wide-area tracking for virtual and augmented environments," in *Proceedings of the ACM symposium on Virtual reality software and technology*, 1999, pp. 1-ff.

[123] T. Morris and M. Donath, "Using a maximum error statistic to evaluate measurement errors in 3d position and orientation tracking systems," *Presence: Teleoperators & Virtual Environments*, Vol. 2, No. 4, pp. 314-343, 1993.

[124] L. Tessens, R. Kehl, A. Pizurica, L. Van Gool, and W. Philips, "A real-time optical head tracker based on 3D prediction and correction," *Proc. of SPS-DARTS 2006*, pp. 39-42, 2006.

[125] J. D. Mulder, J. Jansen, and A. Van Rhijn, "An affordable optical head tracking system for desktop VR/AR systems," in *Proceedings of the workshop on Virtual environments 2003*, 2003, pp. 215-223.

[126] A. Hogue, M. Jenkin, and R. S. Allison, "An optical-inertial tracking system for fully-enclosed VR displays," in *Computer and Robot Vision, 2004. Proceedings. First Canadian Conference on*, 2004, pp. 22-29.

[127] H. Hua, "Integration of eye tracking capability into optical see-through head-mounted displays," in *Proc. SPIE*, 2001, pp. 496-503.

[128] E. Foxlin, Y. Altshuler, L. Naimark, and M. Harrington, "Flighttracker: A novel optical/inertial tracker for cockpit enhanced vision," in *Proceedings of the 3rd IEEE/ACM International Symposium on Mixed and Augmented Reality*, 2004, pp. 212-221.

[129] J. P. Rolland and H. Fuchs, "Optical versus video see-through head-mounted displays in medical visualization," *Presence: Teleoperators and Virtual Environments*, Vol. 9, No. 3, pp. 287-309, 2000.

[130] K. Satoh, S. Uchiyama, H. Yamamoto, and H. Tamura, "Robot vision-based registration utilizing bird's-eye view with user's view," in *Mixed and Augmented Reality, 2003. Proceedings. The Second IEEE and ACM International Symposium on*, 2003, pp. 46-55.

[131] W. A. Hoff, "Fusion of data from head-mounted and fixed sensors," in *First International Workshop on Augmented Reality*, 1998.

[132] B. HKDH, "Neural networks in materials science," *ISIJ international*, Vol. 39, No. 10, pp. 966-979, 1999.

[133] D. Kriesel, *A brief introduction on neural networks*. Germany, 2007.

[134] C. Cortes and V. Vapnik, "Support-vector networks," *Machine learning*, Vol. 20, No. 3, pp. 273-297, 1995.

[135] W. H. Press, S. A. Teukolsky, W. T. Vetterling, and B. P. Flannery, *Numerical recipes 3rd edition: The art of scientific computing*. United Kingdom: Cambridge university press, 2007.

[136] C. M. Bishop, *Pattern recognition and machine learning*. Germany: springer, 2006.

[137] S. Harnad, "The annotation game: On Turing (1950) on computing, machinery, and intelligence," in *The Turing test sourcebook: philosophical and methodological issues in the quest for the thinking computer*, ed: Kluwer, 2006 Amsterdam.

[138] D. Rumerlhar, "Learning representation by back-propagating errors," *Nature*, Vol. 323, pp. 533-536, 1986.

[139] I. Goodfellow, Y. Bengio, and A. Courville, *Deep learning*. United States: MIT press, 2016.

[140] J.-S. R. Jang, "Fuzzy modeling using generalized neural networks and kalman filter algorithm," in *AAAI*, 1991, pp. 762-767.

[141] P. Tahmasebi and A. Hezarkhani, "A hybrid neural networks-fuzzy logic-genetic algorithm for grade estimation," *Computers & geosciences*, Vol. 42, pp. 18-27, 2012.

[142] T. C. Mills and T. C. Mills, *Time series techniques for economists*. United Kingdom: Cambridge University Press, 1991.

[143] S. M. Pandit and S.-M. Wu, *Time series and system analysis with applications* vol. 3: Wiley New York, 1983.

[144] B. K. Rani, K. Srinivas, and A. Govardhan, "Rainfall Prediction with TLBO Optimized ANN," *JSIR,* Vol. 73, pp. 643-647, 2014.

[145] J.-S. Jang, "ANFIS: adaptive-network-based fuzzy inference system," *IEEE transactions on systems, man, and cybernetics,* Vol. 23, No. 3, pp. 665-685, 1993.

[146] A. M. Abdulshahed, A. P. Longstaff, and S. Fletcher, "The application of ANFIS prediction models for thermal error compensation on CNC machine tools," *Applied Soft Computing,* Vol. 27, pp. 158-168, 2015.

[147] D. Young, D. Hall, M. Torelli, Z. Fisk, J. Sarrao, J. Thompson, *et al.*, "High-temperature weak ferromagnetism in a low-density free-electron gas," *Nature,* Vol. 397, No. 6718, p. 412, 1999.

[148] M. J. Wells and M. Venturino, "Performance and head movements using a helmet-mounted display with different sized fields-of-view," *Optical Engineering,* Vol. 29, No. 8, pp. 870-878, 1990.

[149] J. Wilson and P. Wright, "Design of monocular head-mounted displays, with a case study on fire-fighting," *Proceedings of the Institution of Mechanical Engineers, Part C: Journal of Mechanical Engineering Science,* Vol. 221, No. 12, pp. 1729-1743, 2007.

[150] J. Bajana, D. Francia, A. Liverani, and M. Krajčovič, "Mobile tracking system and optical tracking integration for mobile mixed reality," *International Journal of Computer Applications in Technology,* Vol. 53, No. 1, pp. 13-22, 2016.

[151] R. Muñoz-Salinas, E. Yeguas-Bolivar, A. Saffiotti, and R. Medina-Carnicer, "Multi-camera head pose estimation," *Machine Vision and Applications,* Vol. 23, No. 3, pp. 479-490, 2012.

[152] Y. Deldjoo and R. E. Atani, "A low-cost infrared-optical head tracking solution for virtual 3D audio environment using the Nintendo Wii-remote," *Entertainment Computing,* Vol. 12, pp. 9-27, 2016.

[153] B. Czupryński and A. Strupczewski, "High accuracy head pose tracking survey," in *International Conference on Active Media Technology*, 2014, pp. 407-420.

[154] Ö. Ayer, S. Bingöl, T. Altinbalik, and H. Y. Kiliçgedik, "Fatigue life modeling of gear like products using ANN," *IJEMS,* Vol. 23, pp. 239-246, 2016.

[155] R. Osornio-Rios, "Identification of Positioning System for Industrial Applications using Neural Network," *JSIR,* Vol. 76, pp. 141-144, 2017.

Appendix A

Appendix A represents the plots of the prediction of head coordinates using the electromagnetic tracker. Figures E1, E2, and E3 present the prediction of translational (X, Y, and Z) coordinates of the head motion. The dataset used for prediction consisted of 10% of the missing head coordinates.

Figure E1 shows the prediction of the 10% missing X coordinates of the head motion. The **blue line** shows the actual coordinates, the **red line** shows the missing coordinates and the **green line** shows the prediction of the missing head coordinates.

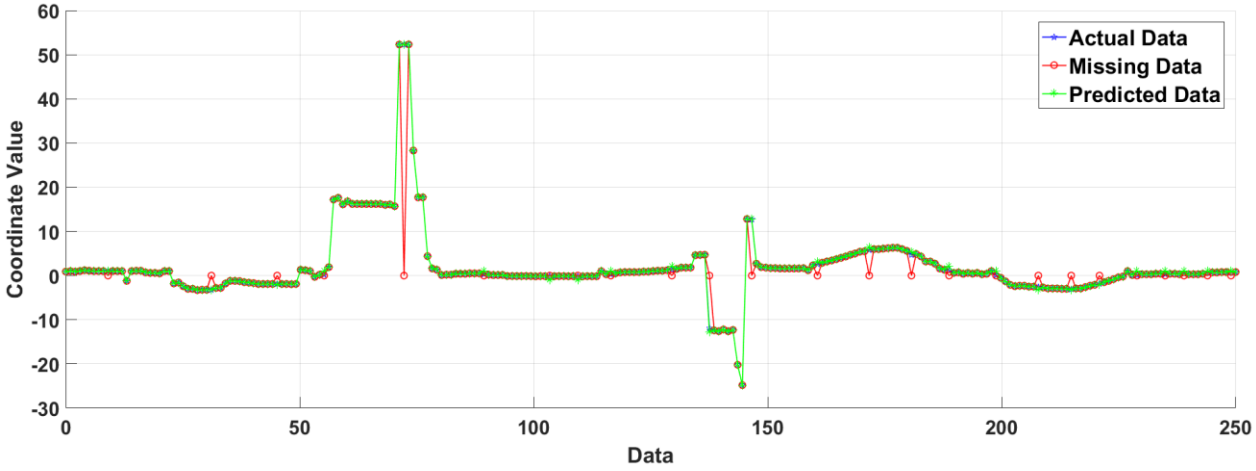

Figure E1: Prediction of X coordinates using SHNM for the data set with 10% missing 6-DoF head coordinates

Figure E2 shows the prediction of the 10% missing Y coordinates of the head motion. The **blue line** shows the actual coordinates, the **red line** shows the missing coordinates and the **green line** shows the prediction of the missing head coordinates.

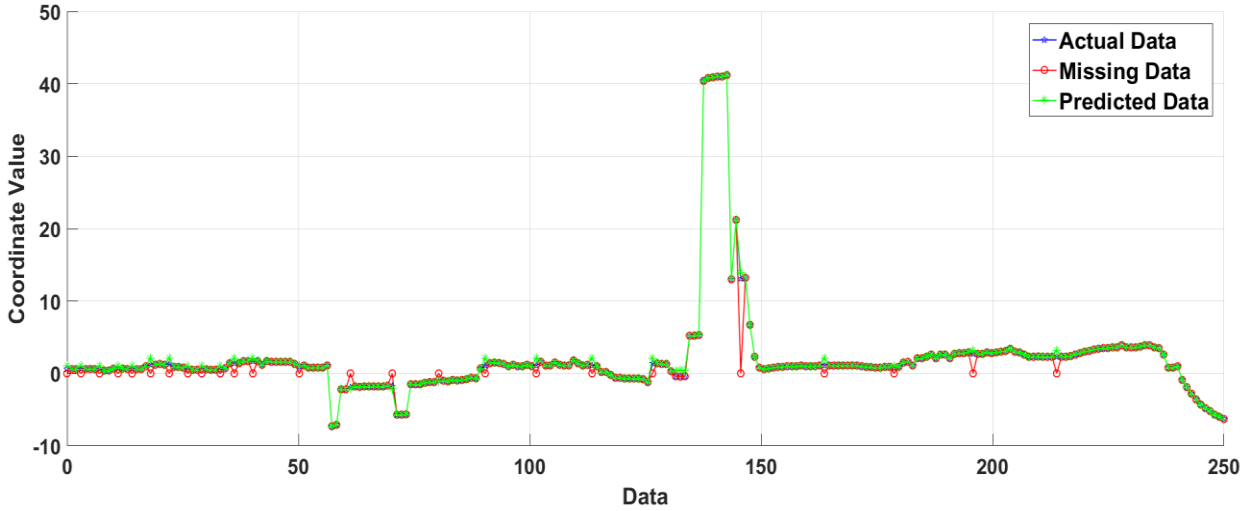

Figure E2: Prediction of Y coordinates using SHNM for the data set with 10% missing 6-DoF head coordinates

Figure E3 shows the prediction of the 10% missing Z coordinates of the head motion. The **blue line** shows the actual coordinates, the **red line** shows the missing coordinates and the **green line** shows the prediction of the missing head coordinates.

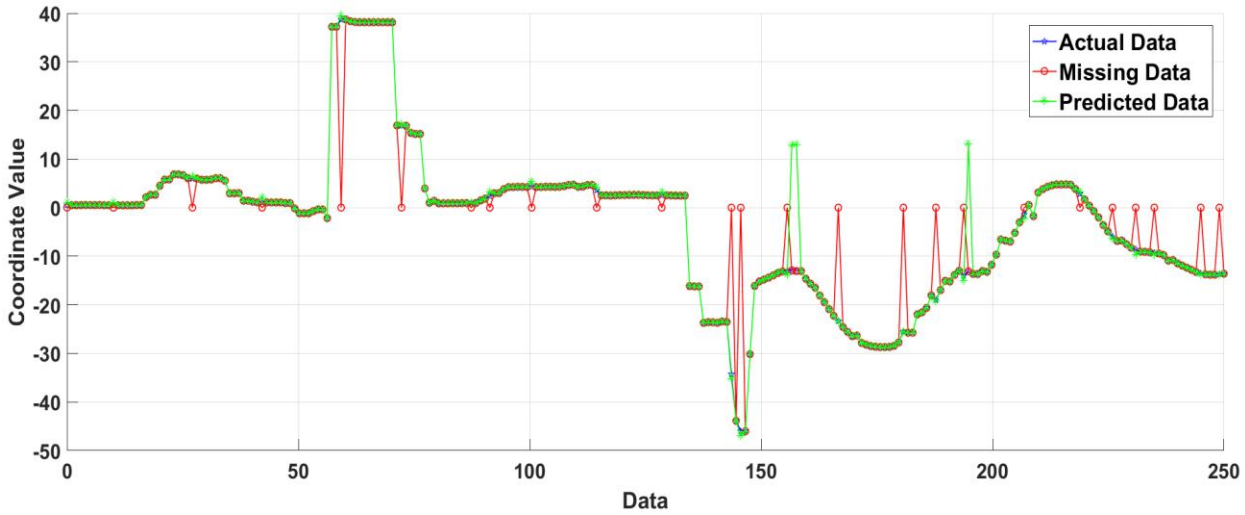

Figure E3: Prediction of Z coordinates using SHNM for the data set with 10% missing 6-DoF head coordinates

Figures E4, E5 and E6 present the prediction of translational (X, Y, and Z) coordinates of the head motion. The dataset used for prediction consisted of 25% of the missing head coordinates. Figure 1 shows the prediction of the 25% missing X coordinates of the head motion. The **blue line** shows the actual coordinates, the **red line** shows the missing coordinates and the **green line** shows the prediction of the missing head coordinates.

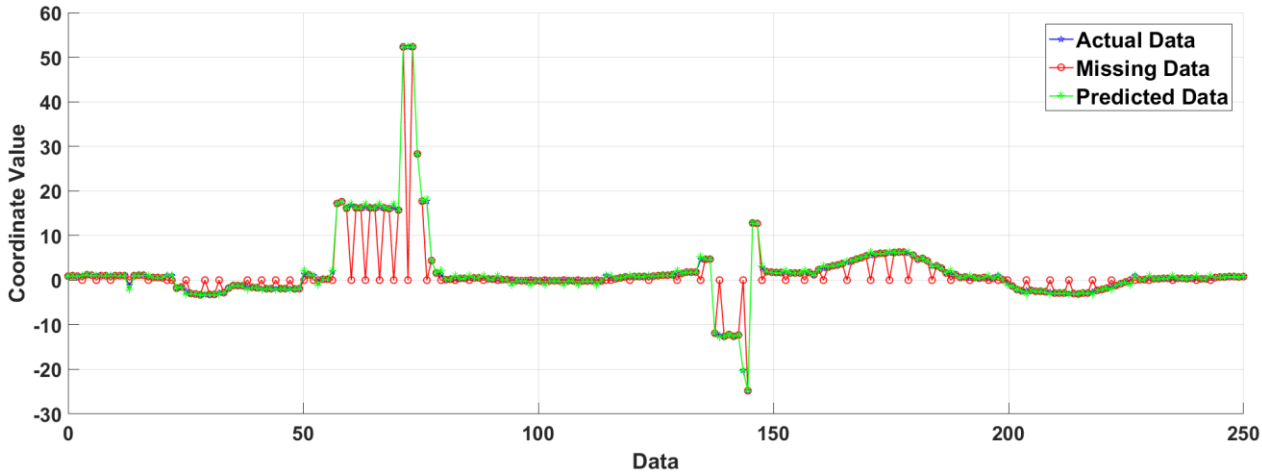

Figure E4: Prediction of X coordinates using SHNM for the data set with 25% missing 6-DoF head coordinates

Figure 5 shows the prediction of the 25% missing Y coordinates of the head motion. The **blue line** shows the actual coordinates, the **red line** shows the missing coordinates and the **green line** shows the prediction of the missing head coordinates.

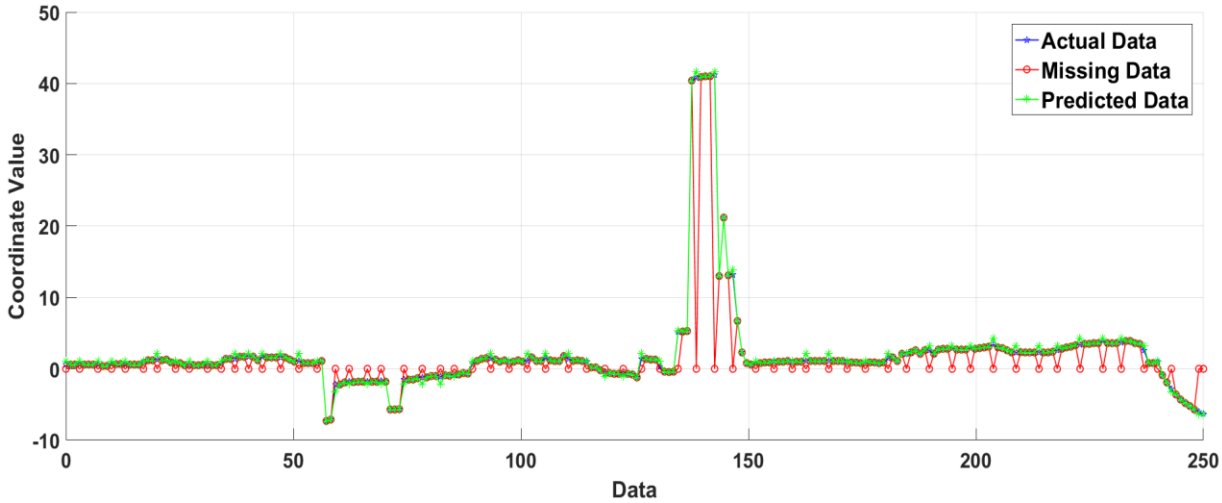

Figure E5: Prediction of Y coordinates using SHNM for the data set with 25% missing 6-DoF head coordinates

Figure E6 shows the prediction of the 25% missing Z coordinates of the head motion. The **blue line** shows the actual coordinates, the **red line** shows the missing coordinates and the **green line** shows the prediction of the missing head coordinates.

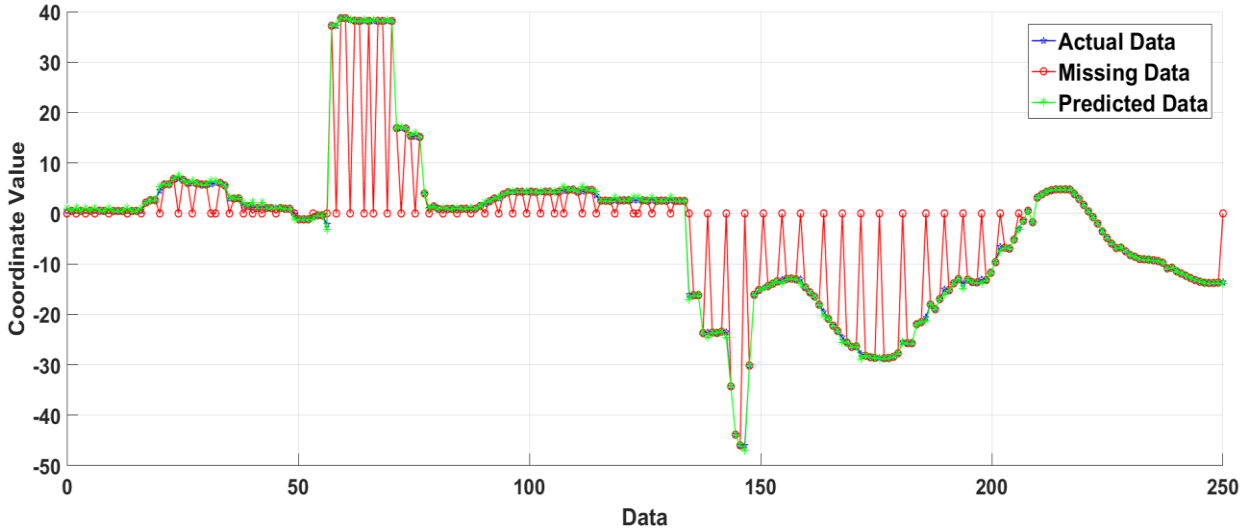

Figure E6: Prediction of Z coordinates using SHNM for the data set with 25% missing 6-DoF head coordinates

Figures E7, E8, and E9 present the prediction of Rotational (Yaw, Pitch, and Roll) coordinates of the head motion. The dataset used for prediction consisted of 10% of the missing head coordinates. Figure E7 shows the prediction of the 10% missing Yaw coordinates of the head motion. The **blue line** shows the actual coordinates, the **red line** shows the missing coordinates and the **green line** shows the prediction of the missing head coordinates.

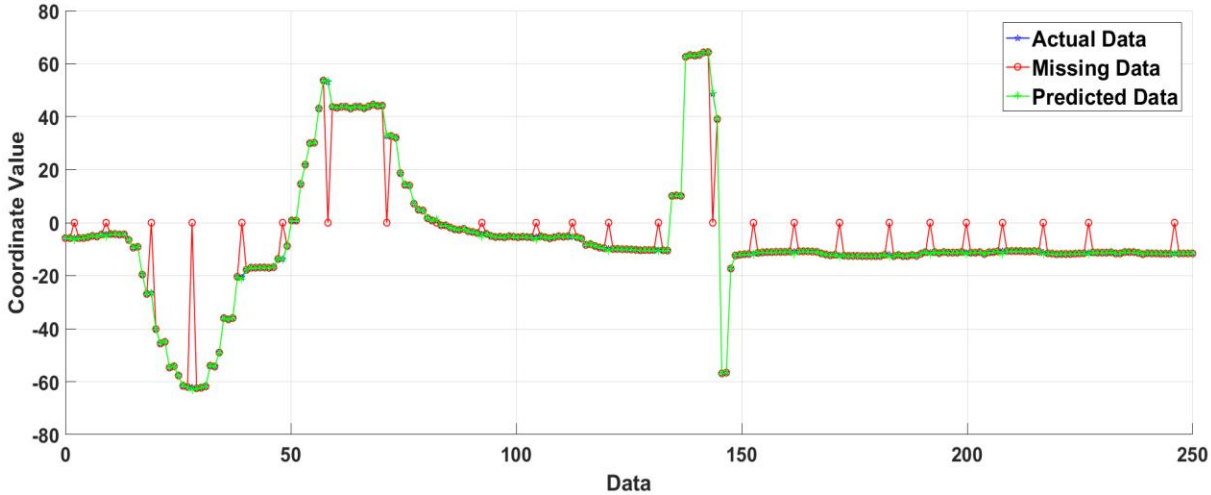

Figure E7: Prediction of Yaw angular coordinates through SHNM for the data set with 10% missing 6-DoF head coordinates

Figure E8 shows the prediction of the 10% missing Pitch coordinates of the head motion. The **blue line** shows the actual coordinates, the **red line** shows the missing coordinates and the **green line** shows the prediction of the missing head coordinates.

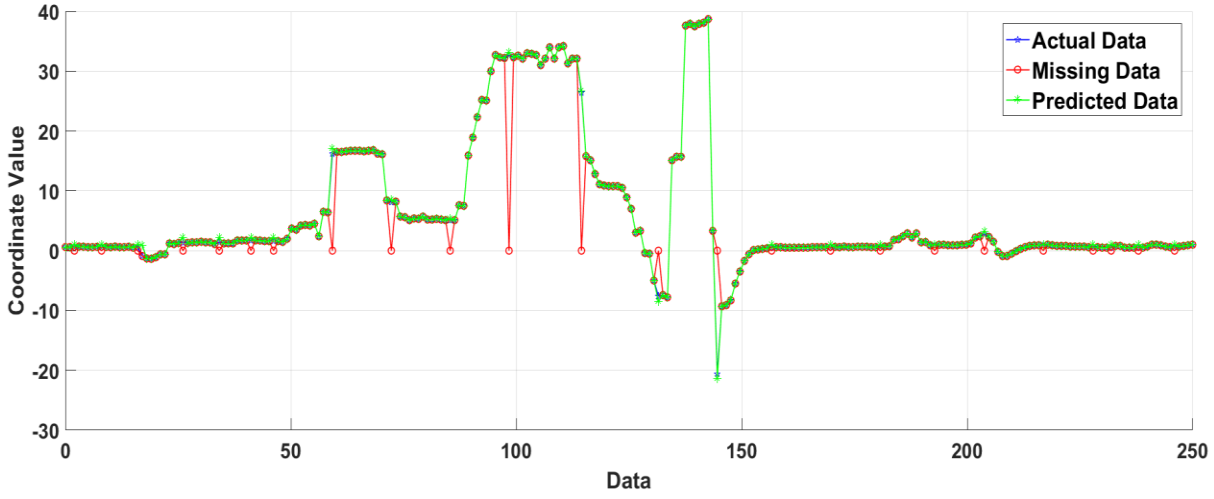

Figure E8: Prediction of Pitch angular coordinates through SHNM for the data set with 10% missing 6-DoF head coordinates

Figure E9 shows the prediction of the 10% missing Roll coordinates of the head motion. The **blue line** shows the actual coordinates, the **red line** shows the missing coordinates and the **green line** shows the prediction of the missing head coordinates.

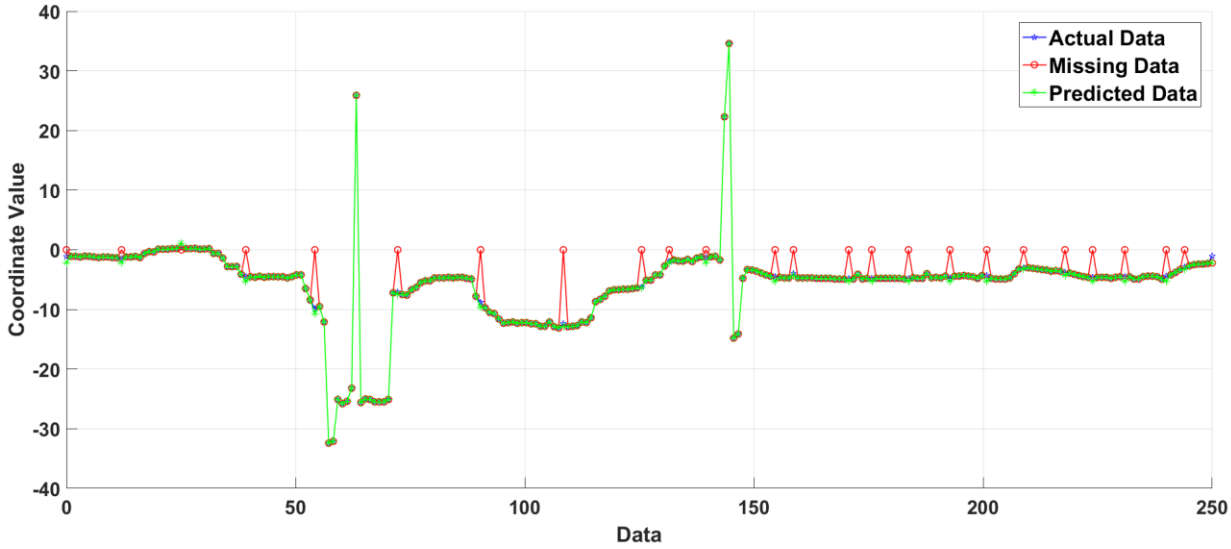

Figure E9: Prediction of Roll angular coordinates through SHNM for the data set with 10% missing 6-DoF head coordinates

Figures E10, E11 and E12 present the prediction of Rotational (Yaw, Pitch, and Roll) coordinates of the head motion. The dataset used for prediction consisted of 25% of the missing head coordinates. Figure E10 shows the prediction of the 25% missing Yaw coordinates of the head motion. The **blue line** shows the actual coordinates, the **red line** shows the missing coordinates and the **green line** shows the prediction of the missing head coordinates.

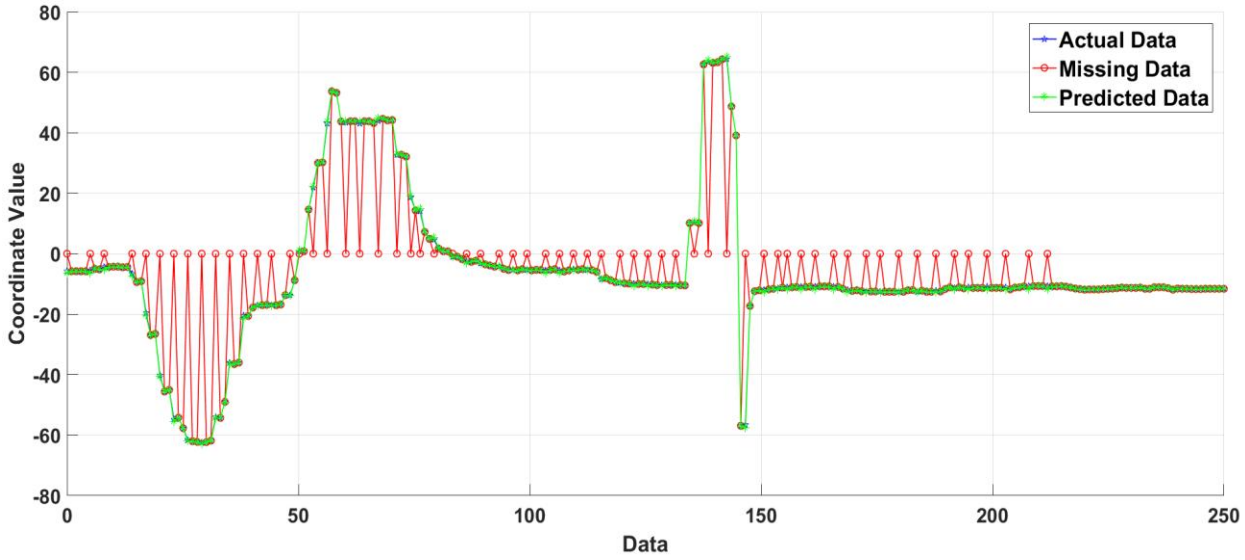

Figure E10: Prediction of Yaw angular coordinates through SHNM for the data set with 25% missing 6-DoF head coordinates

Figure E11 shows the prediction of the 25% missing Pitch coordinates of the head motion. The **blue line** shows the actual coordinates, the **red line** shows the missing coordinates and the **green line** shows the prediction of the missing head coordinates.

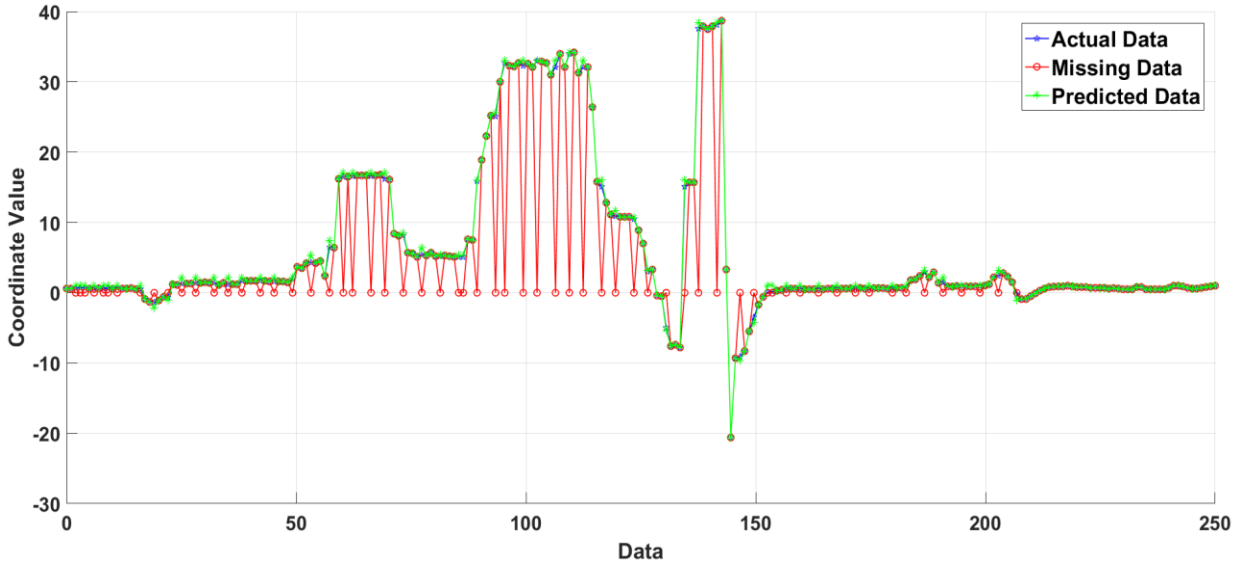

Figure E11: Prediction of Pitch angular coordinates through SHNM for the data set with 25% missing 6-DoF head coordinates

Figure E12 shows the prediction of the 25% missing Roll coordinates of the head motion. The **blue line** shows the actual coordinates, the **red line** shows the missing coordinates and the **green line** shows the prediction of the missing head coordinates.

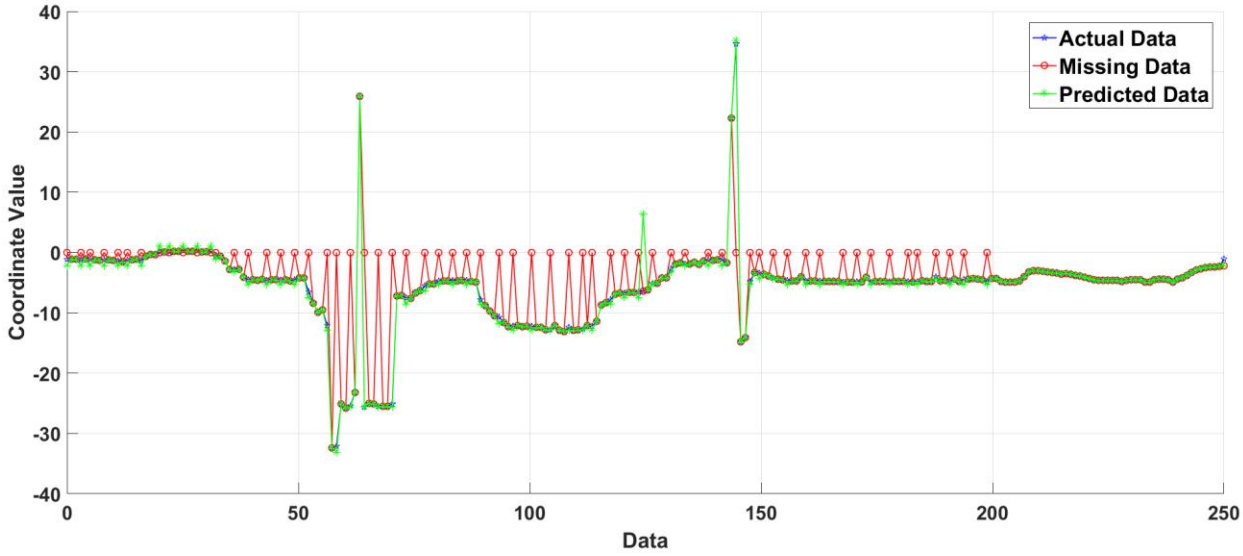

Figure E12: Prediction of Roll angular coordinates through SHNM for the data set with 25% missing 6-DoF head coordinates

Appendix B

Appendix B represents the plots of the prediction of head coordinates using the optical tracker. Figures O1, O2 and O3 present the prediction of translational (X, Y, and Z) coordinates of the head motion. The dataset used for prediction consisted of 10% of the missing head coordinates. Figure O1 shows the prediction of the 10% missing X coordinates of the head motion. The **blue line** shows the actual coordinates, the **red line** shows the missing coordinates and the **green line** shows the prediction of the missing head coordinates.

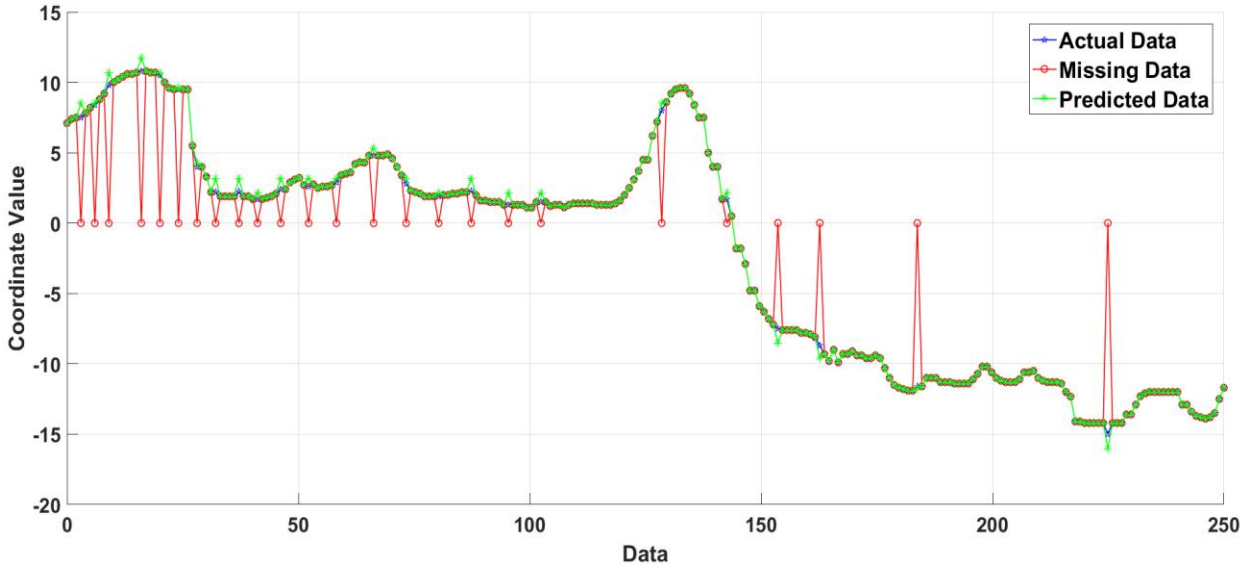

Figure O1: Prediction of X coordinates through SHNM for the data set with 10% missing 6-DoF head coordinates

Figure O2 shows the prediction of the 10% missing Y coordinates of the head motion. The **blue line** shows the actual coordinates, the **red line** shows the missing coordinates and the **green line** shows the prediction of the missing head coordinates.

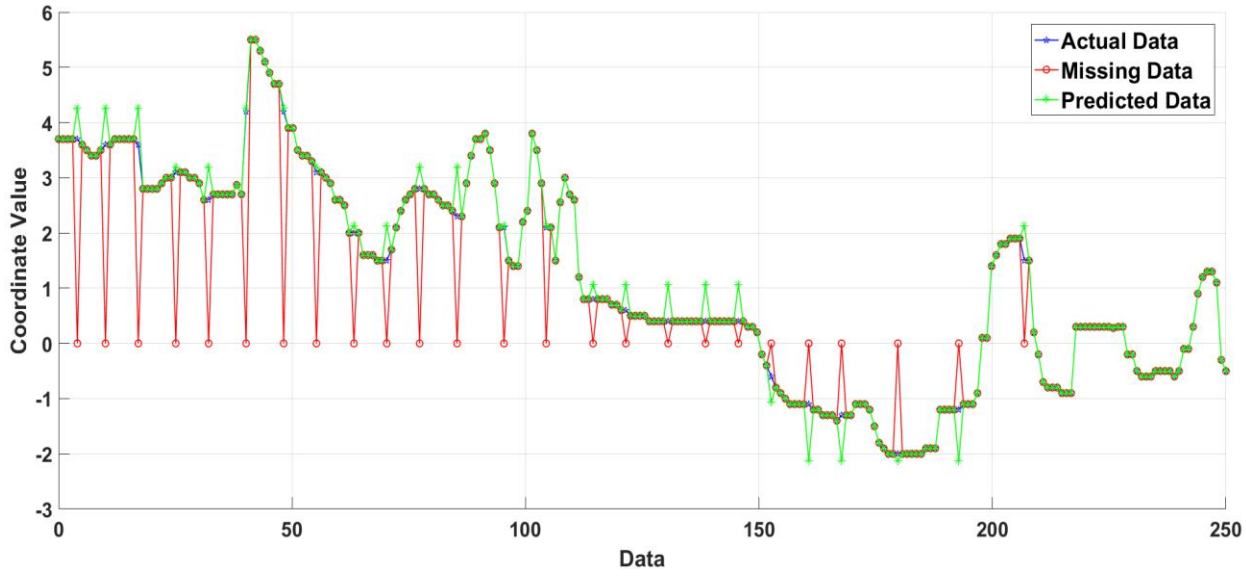

Figure O2: Prediction of Y coordinates through SHNM for the data set with 10% missing 6-DoF head coordinates

Figure O3 shows the prediction of the 10% missing Z coordinates of the head motion. The **blue line** shows the actual coordinates, the **red line** shows the missing coordinates and the **green line** shows the prediction of the missing head coordinates.

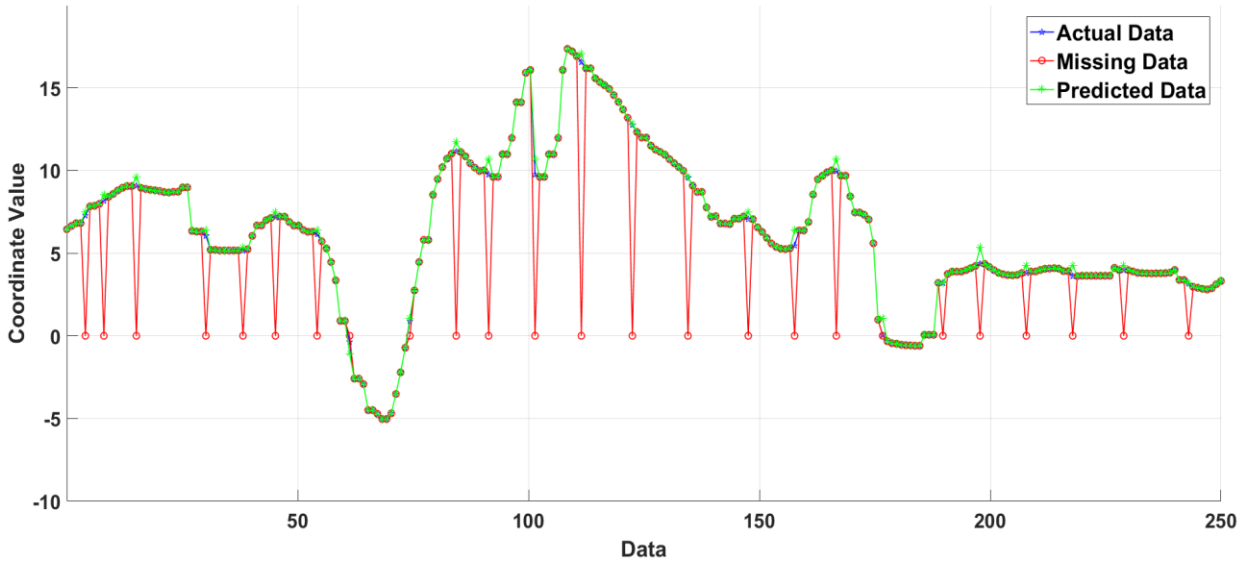

Figure O3: Prediction of Z coordinates through SHNM for the data set with 10% missing 6-DoF head coordinates

Figures O4, O5 and O6 present the prediction of translational (X, Y, and Z) coordinates of the head motion. The dataset used for prediction consisted of 25% of the missing head coordinates. Figure O4 shows the prediction of the 25% missing X coordinates of the head motion. The **blue line** shows the actual coordinates, the **red line** shows the missing coordinates and the **green line** shows the prediction of the missing head coordinates.

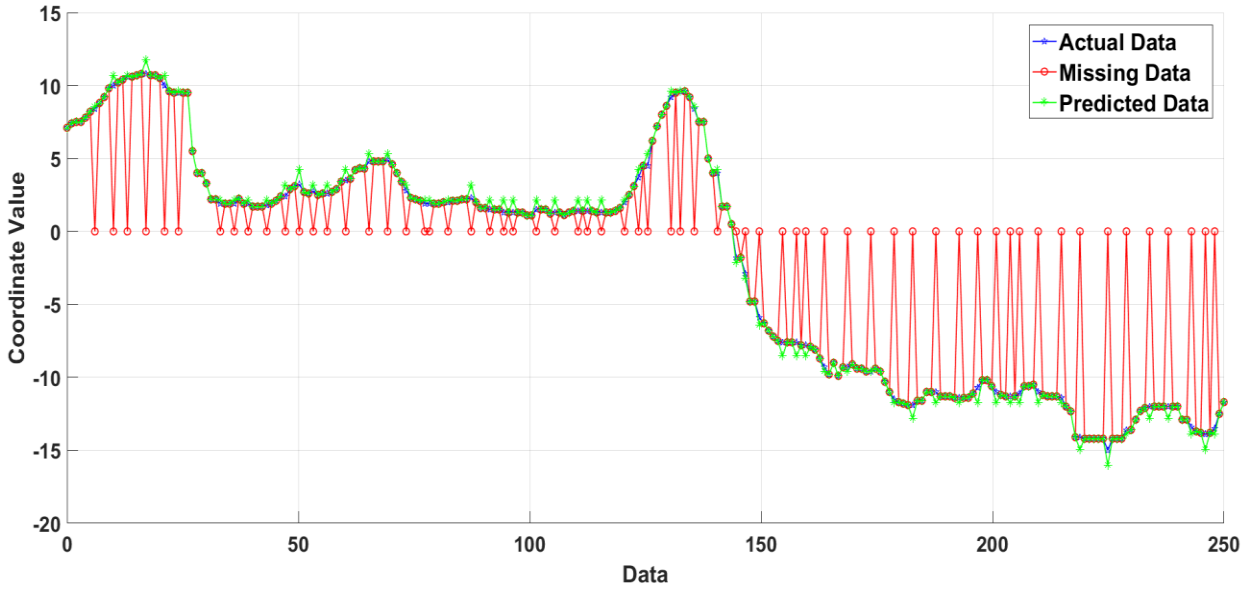

Figure O4: Prediction of X coordinates through SHNM for the data set with 25% missing 6-DoF head coordinates

Figure O5 shows the prediction of the 25% missing Y coordinates of the head motion. The **blue line** shows the actual coordinates, the **red line** shows the missing coordinates and the **green line** shows the prediction of the missing head coordinates.

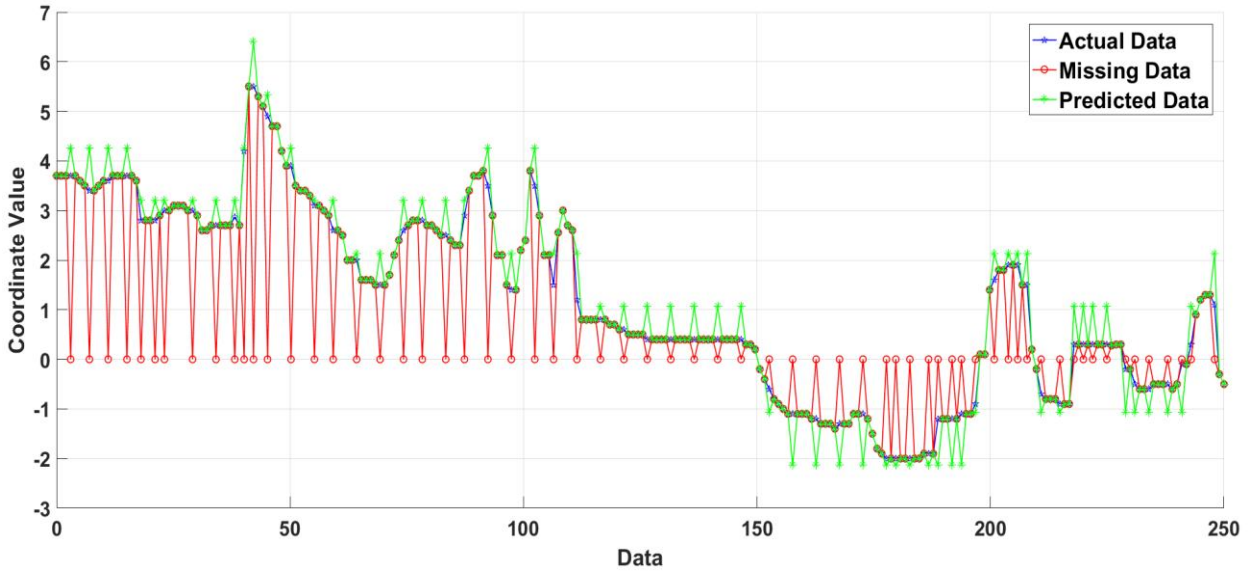

Figure O5: Prediction of Y coordinates through SHNM for the data set with 25% missing 6-DoF head coordinates

Figure O6 shows the prediction of the 25% missing Z coordinates of the head motion. The **blue line** shows the actual coordinates, the **red line** shows the missing coordinates and the **green line** shows the prediction of the missing head coordinates.

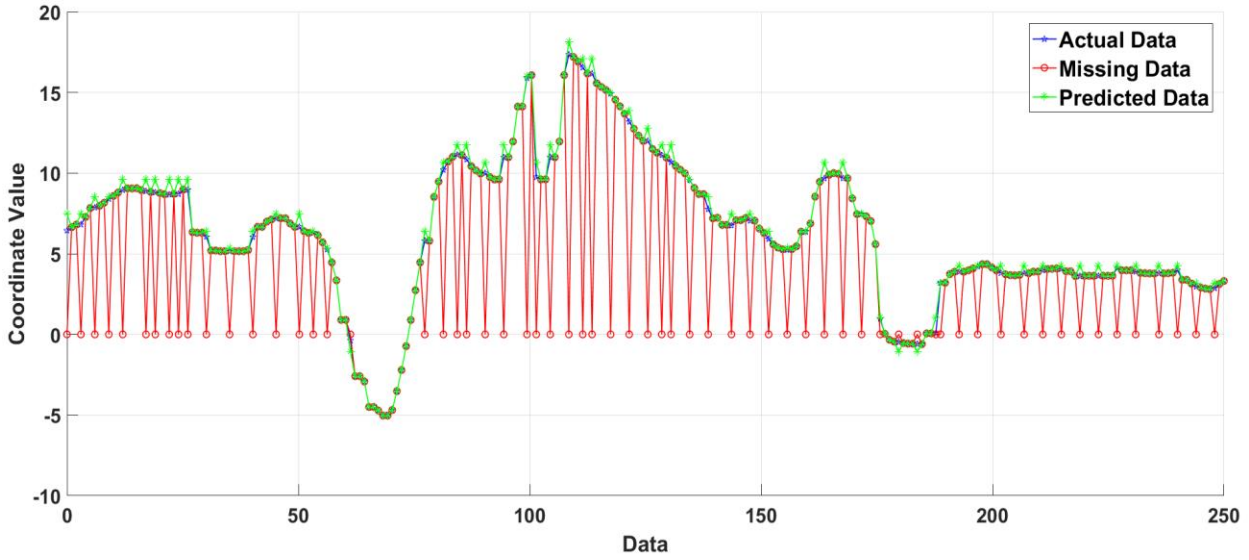

Figure O6: Prediction of Z coordinates through SHNM for the data set with 25% missing 6-DoF head coordinates

Figures O7, O8, and O9 present the prediction of Rotational (Yaw, Pitch, and Roll) coordinates of the head motion. The dataset used for prediction consisted of 10% of the missing head coordinates. Figure O7 shows the prediction of the 10% missing Yaw coordinates of the head motion. The **blue line** shows the actual coordinates, the **red line** shows the missing coordinates and the **green line** shows the prediction of the missing head coordinates.

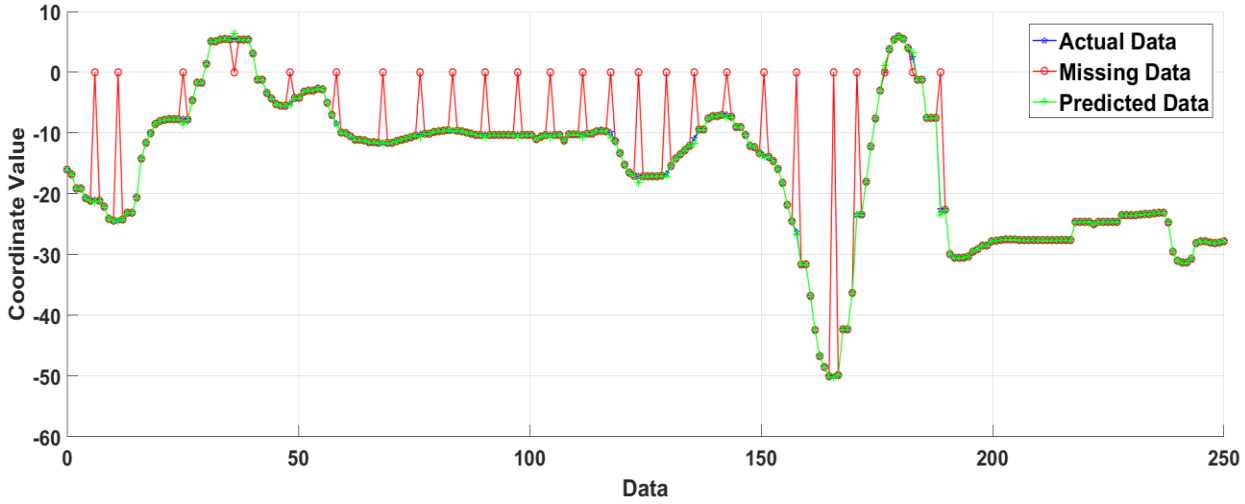

Figure O7: Prediction of Yaw angular coordinates through SHNM for the data set with 10% missing 6-DoF head coordinates

Figure O8 shows the prediction of the 10% missing Pitch coordinates of the head motion. The **blue line** shows the actual coordinates, the **red line** shows the missing coordinates and the **green line** shows the prediction of the missing head coordinates.

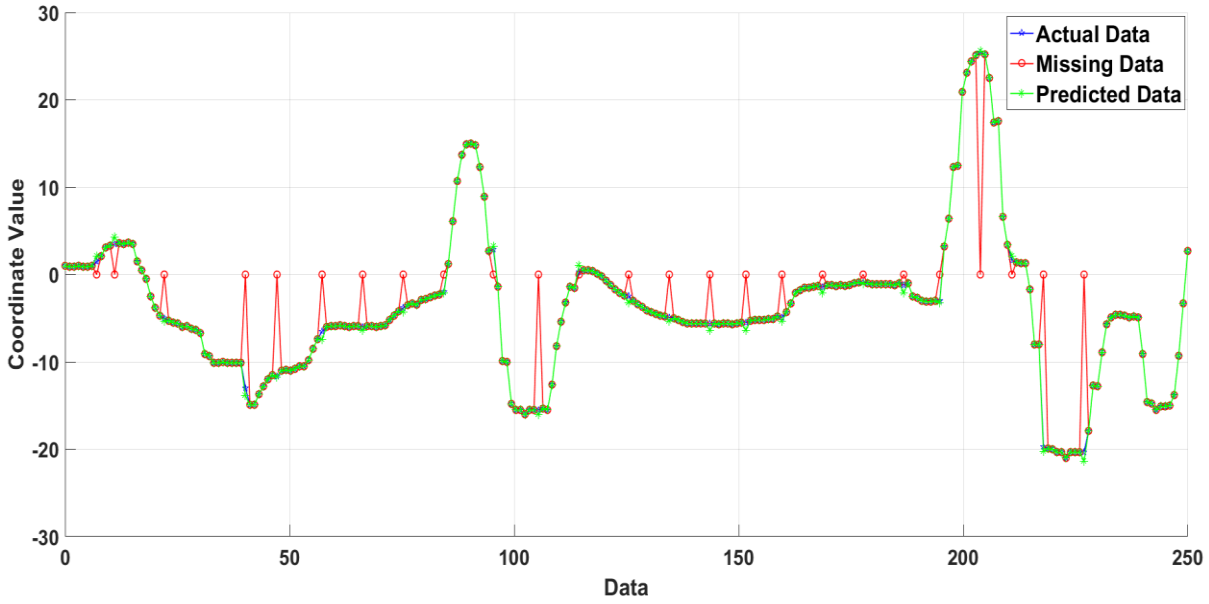

Figure O8: Prediction of Pitch angular coordinates through SHNM for the data set with 10% missing 6-DoF head coordinates

Figure O9 shows the prediction of the 10% missing Roll coordinates of the head motion. The **blue line** shows the actual coordinates, the **red line** shows the missing coordinates and the **green line** shows the prediction of the missing head coordinates.

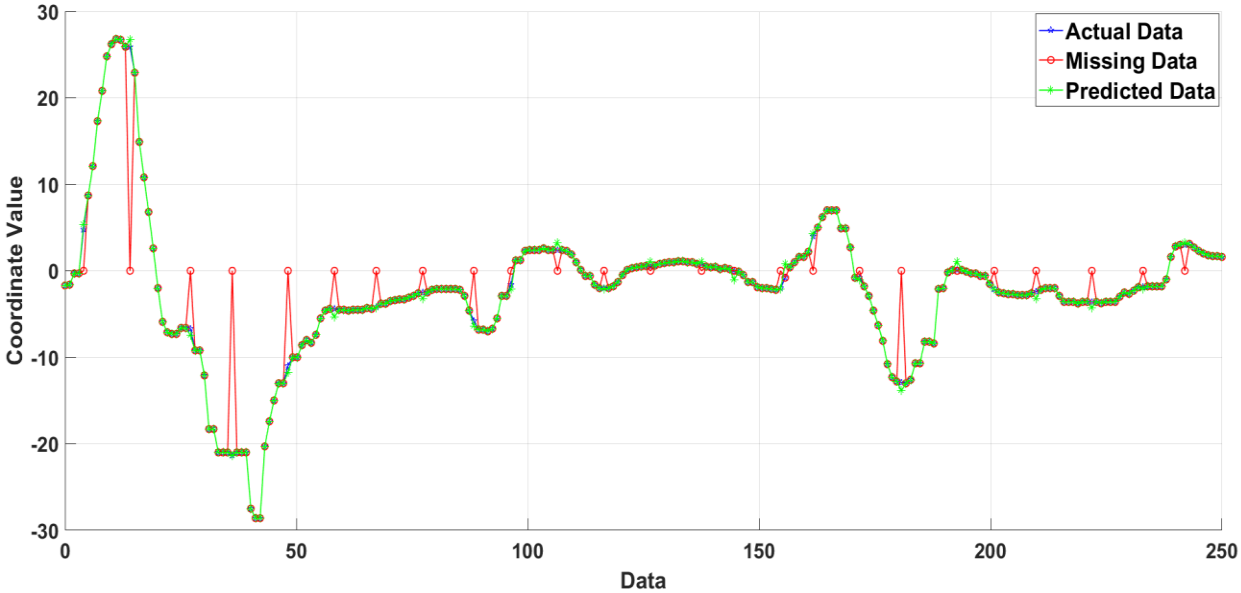

Figure O9: Prediction of Roll angular coordinates through SHNM for the data set with 10% missing 6-DoF head coordinates

Figures O10, O11 and O12 present the prediction of Rotational (Yaw, Pitch, and Roll) coordinates of the head motion. The dataset used for prediction consisted of 25% of the missing head coordinates. Figure O10 shows the prediction of the 25% missing Yaw coordinates of the head motion. The **blue line** shows the actual coordinates, the **red line** shows the missing coordinates and the **green line** shows the prediction of the missing head coordinates.

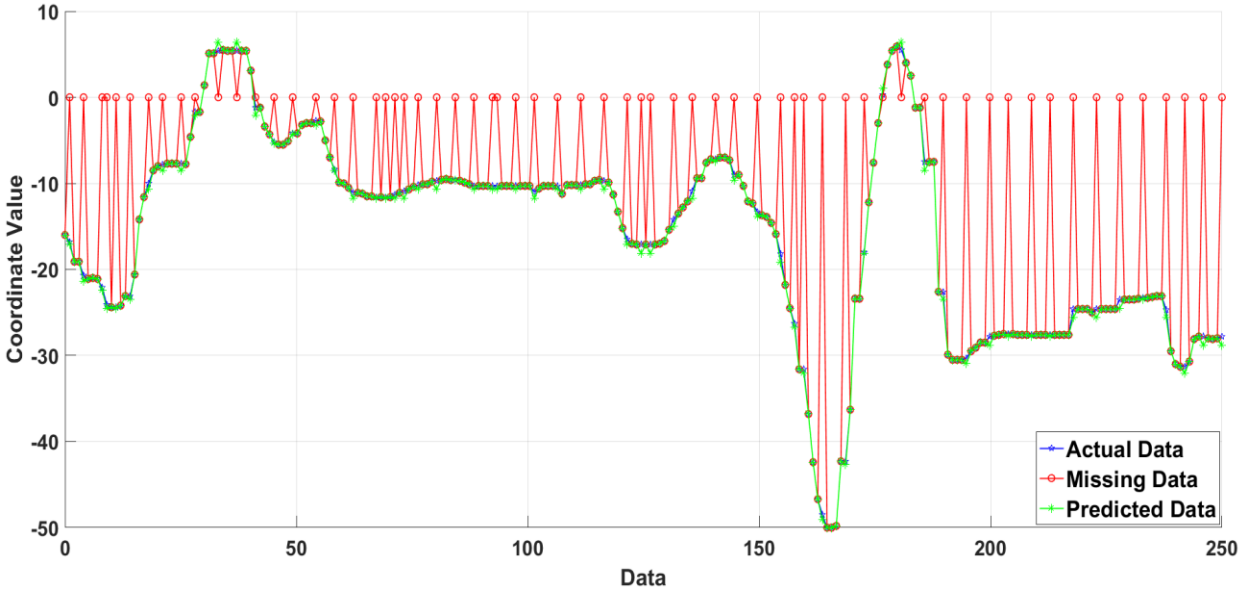

Figure O10: Prediction of Yaw angular coordinates through SHNM for the data set with 25% missing 6-DoF head coordinates

Figure O11 shows the prediction of the 25% missing Pitch coordinates of the head motion. The **blue line** shows the actual coordinates, the **red line** shows the missing coordinates and the **green line** shows the prediction of the missing head coordinates.

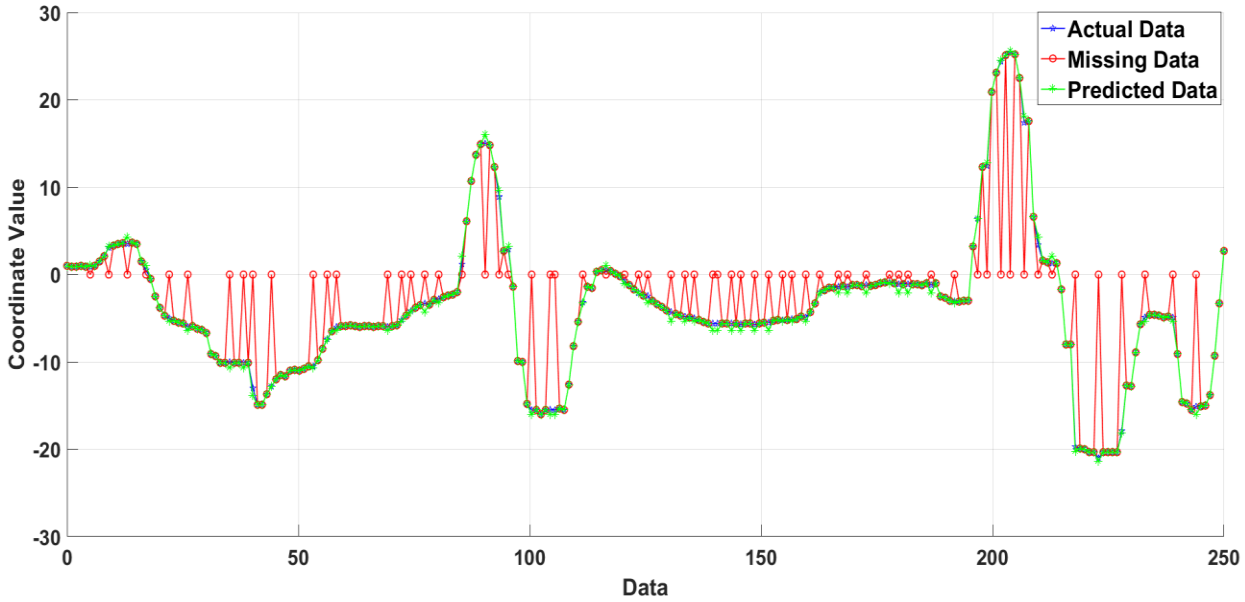

Figure O11: Prediction of Pitch angular coordinates through SHNM for the data set with 25% missing 6-DoF head coordinates

Figure O12 shows the prediction of the 25% missing Roll coordinates of the head motion. The **blue line** shows the actual coordinates, the **red line** shows the missing coordinates and the **green line** shows the prediction of the missing head coordinates.

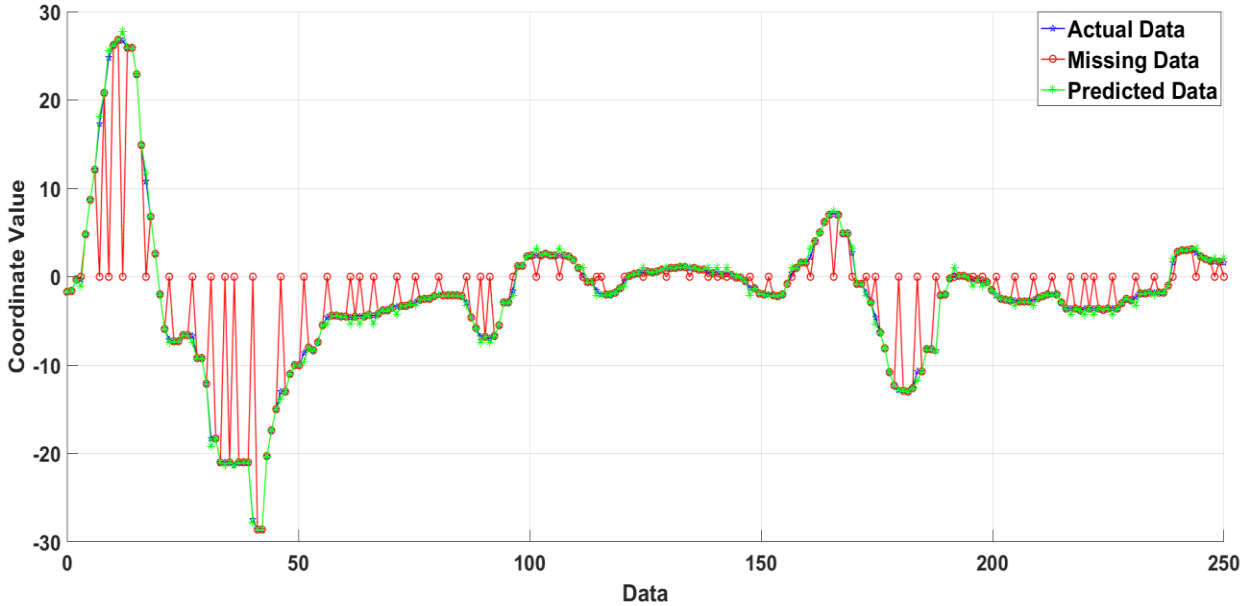

Figure O12: Prediction of Roll angular coordinates through SHNM for the data set with 25% missing 6-DoF head coordinates

Appendix C

Appendix C shows the performance of the Self-healing neural model, ANFIS, and Backpropagation neural network in the prediction of missed head coordinates. The prediction accuracy of the ANFIS depends on the dataset. In the prediction of the missed head coordinates, the accuracy of the ANFIS is more in the dataset with a lesser number of coordinates. In this Appendix, the performance comparison of data prediction of missing coordinates is presented for the data set with 400 instances (small dataset).

The graphs in the figures from A1 to A6 are the magnified version of the graphs consisting of 400 instances (head coordinates) and this the figures in this appendix show the prediction accuracy of 60 coordinates.

Figure A1 presents the prediction accuracy of all three models (SHNM, ANFIS, and BPNN) for the prediction of the missing translational head coordinate X, and it is found from Figure A1 that, the accuracy of the Self-healing neural model outperforms the ANFIS and Backpropagation neural network. The accuracy of SHNM is ≈ 94% and ANFIS is ≈ 89% using Electromagnetic tracker. The accuracy of SHNM and ANFIS of missed head coordinates using Optical tracker is ≈ 92% and ≈ 89% respectively.

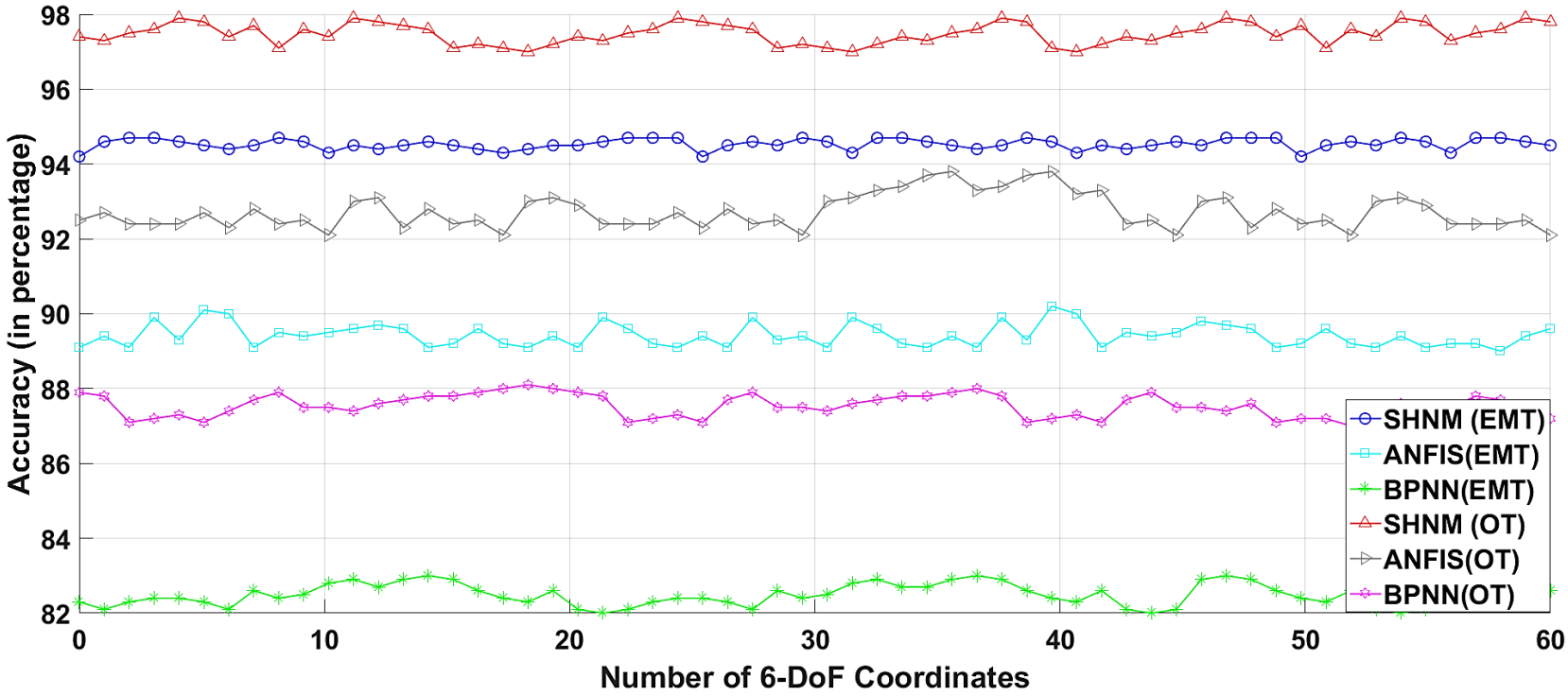

Figure A1: Performance evaluation of SHNM, ANFIS, and BPNN in the prediction of X positional coordinates in small data set using both optical and electromagnetic tracker

Figure A2 presents the prediction accuracy of all three models (SHNM, ANFIS, and BPNN) for the prediction of the missing translational head coordinate Y, and it is found from Figure A2 that, the accuracy of the Self-healing neural model outperforms the ANFIS and Backpropagation neural network. The accuracy of SHNM is ≈ 96% and ANFIS is ≈ 92% using Electromagnetic tracker. The accuracy of SHNM and ANFIS of missed head coordinates using Optical tracker is ≈ 92% and ≈ 89% respectively.

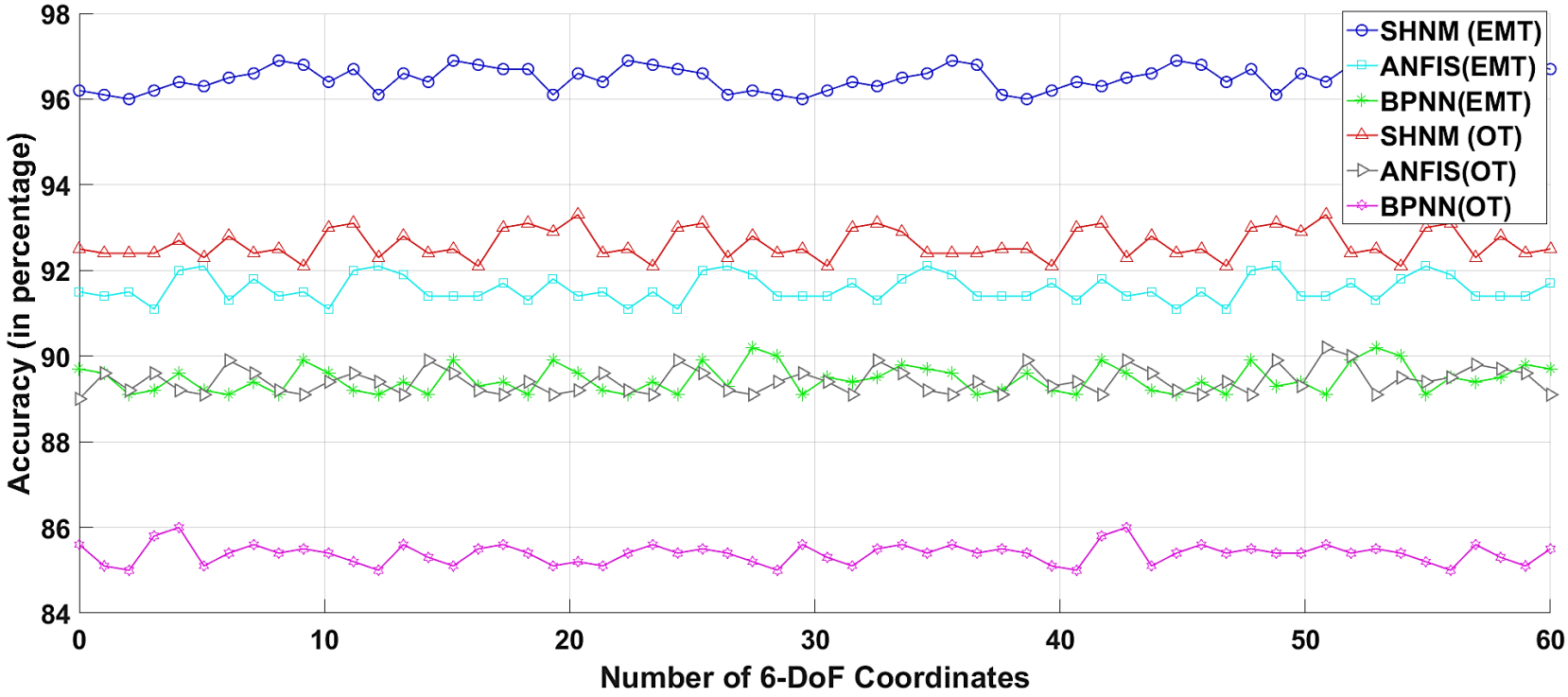

Figure A2: Performance evaluation of SHNM, ANFIS, and BPNN in the prediction of Y positional coordinates in small data set using both optical and electromagnetic tracker

Figure A3 presents the prediction accuracy of all the three models (SHNM, ANFIS, and BPNN) for the prediction of the missing translational head coordinate Z, and it is found from Figure A3 that, the accuracy of the Self-healing neural model is better than the ANFIS and Backpropagation neural network. The accuracy of SHNM is ≈ 94.5% and ANFIS is ≈ 90.5% using the Electromagnetic tracker. The accuracy of SHNM and ANFIS of missed head coordinates using Optical tracker is ≈ 92% to 93% and ≈ 88% to 89% respectively.

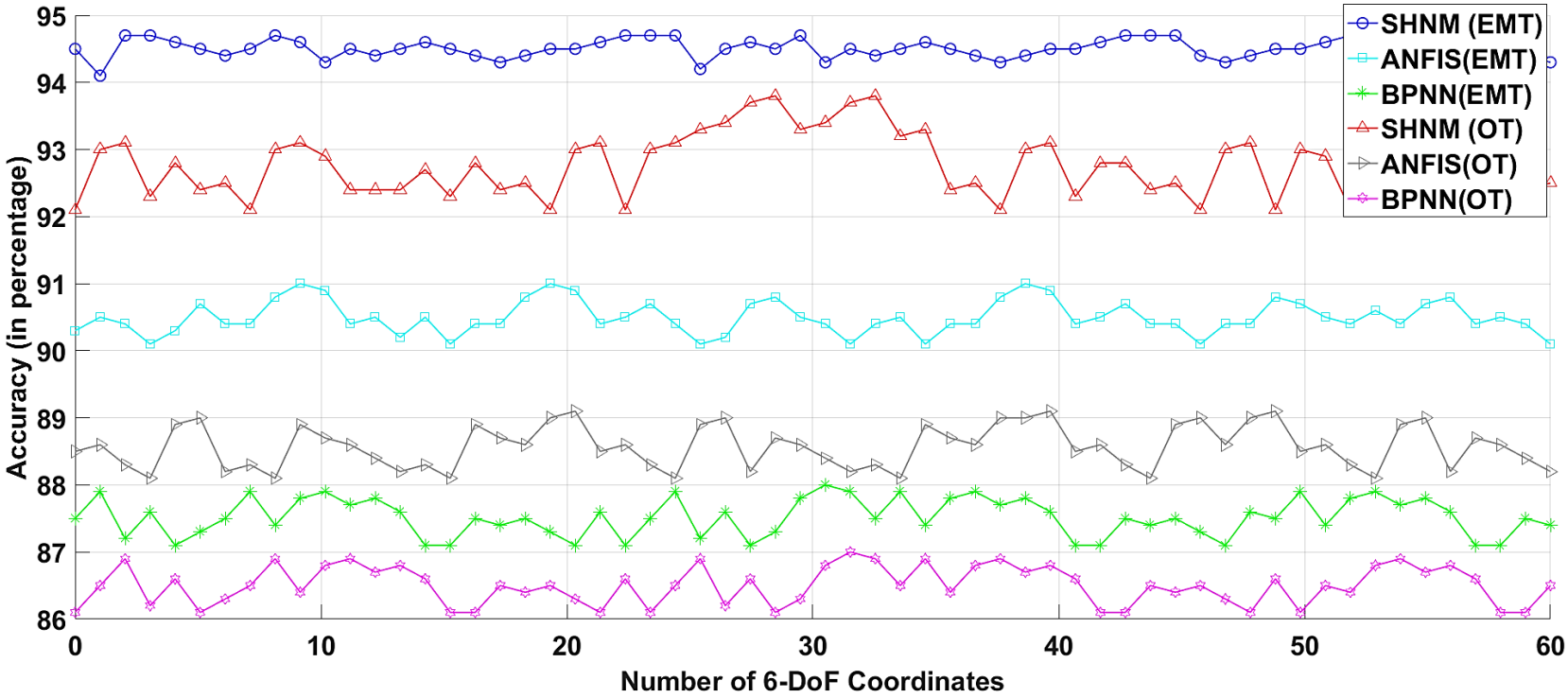

Figure A3: Performance evaluation of SHNM, ANFIS, and BPNN in the prediction of Z positional coordinates in small data set using both optical and electromagnetic tracker

Figure A4 presents the prediction accuracy of all three models (SHNM, ANFIS, and BPNN) for the prediction of the missing rotational head coordinate Yaw, and it is found from Figure A4 that, the accuracy of the Self-healing neural model outperforms the ANFIS and Backpropagation neural network. The accuracy of SHNM is ≈ 94% and ANFIS is ≈ 89% using Electromagnetic tracker. The accuracy of SHNM and ANFIS of missed head coordinates using Optical tracker is ≈ 98% and ≈ 93% respectively.

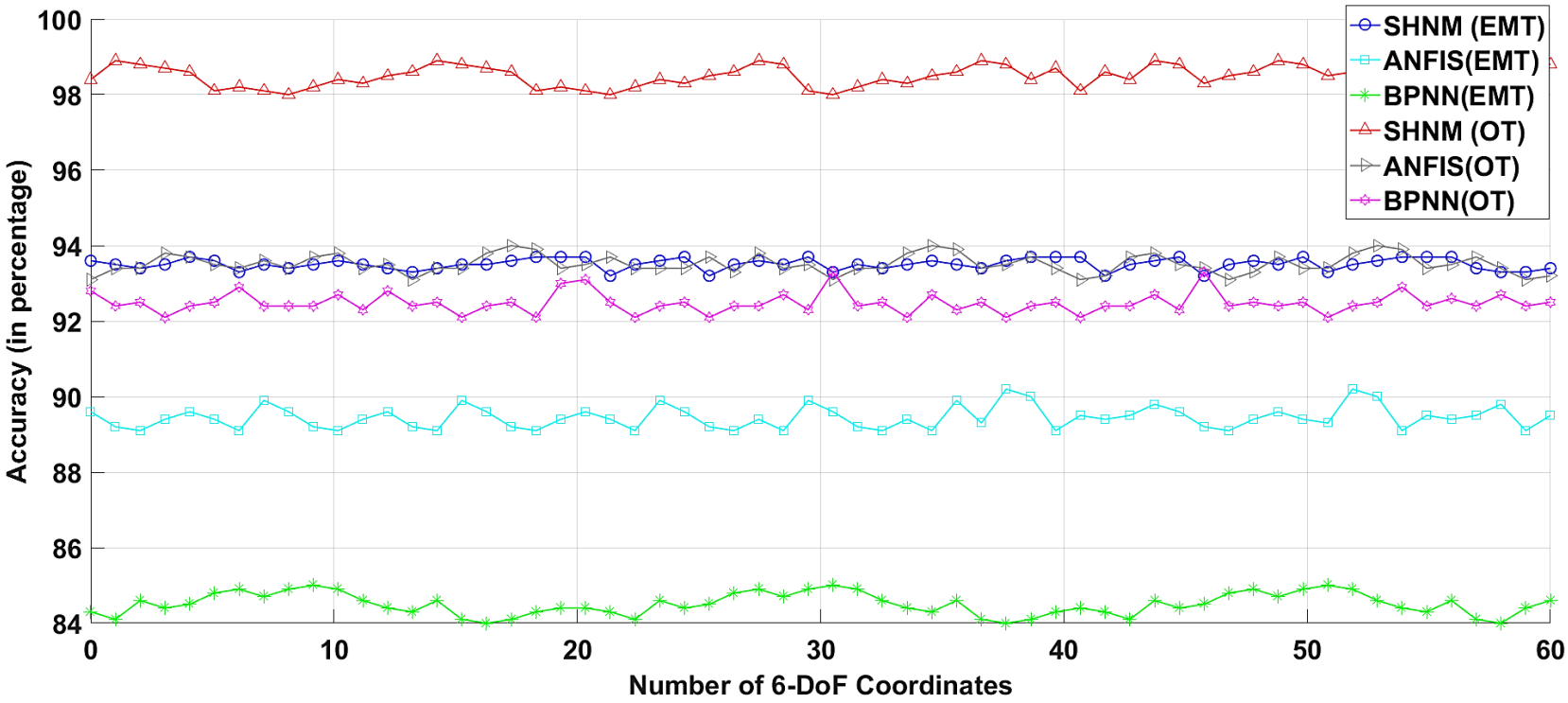

Figure A4: Performance evaluation of SHNM, ANFIS, and BPNN in the prediction of Yaw rotational coordinates in small data set using both optical and electromagnetic tracker

Figure A5 presents the prediction accuracy of all the three models (SHNM, ANFIS, and BPNN) for the prediction of the missing rotational head coordinate Pitch, and it is found from Figure A5 that, the accuracy of the Self-healing neural model is better than the ANFIS and Backpropagation neural network. The accuracy of SHNM is ≈ 96% and ANFIS is ≈ 91% using Electromagnetic tracker. The accuracy of SHNM and ANFIS of missed head coordinates using Optical tracker is ≈ 97% and ≈ 92% respectively.

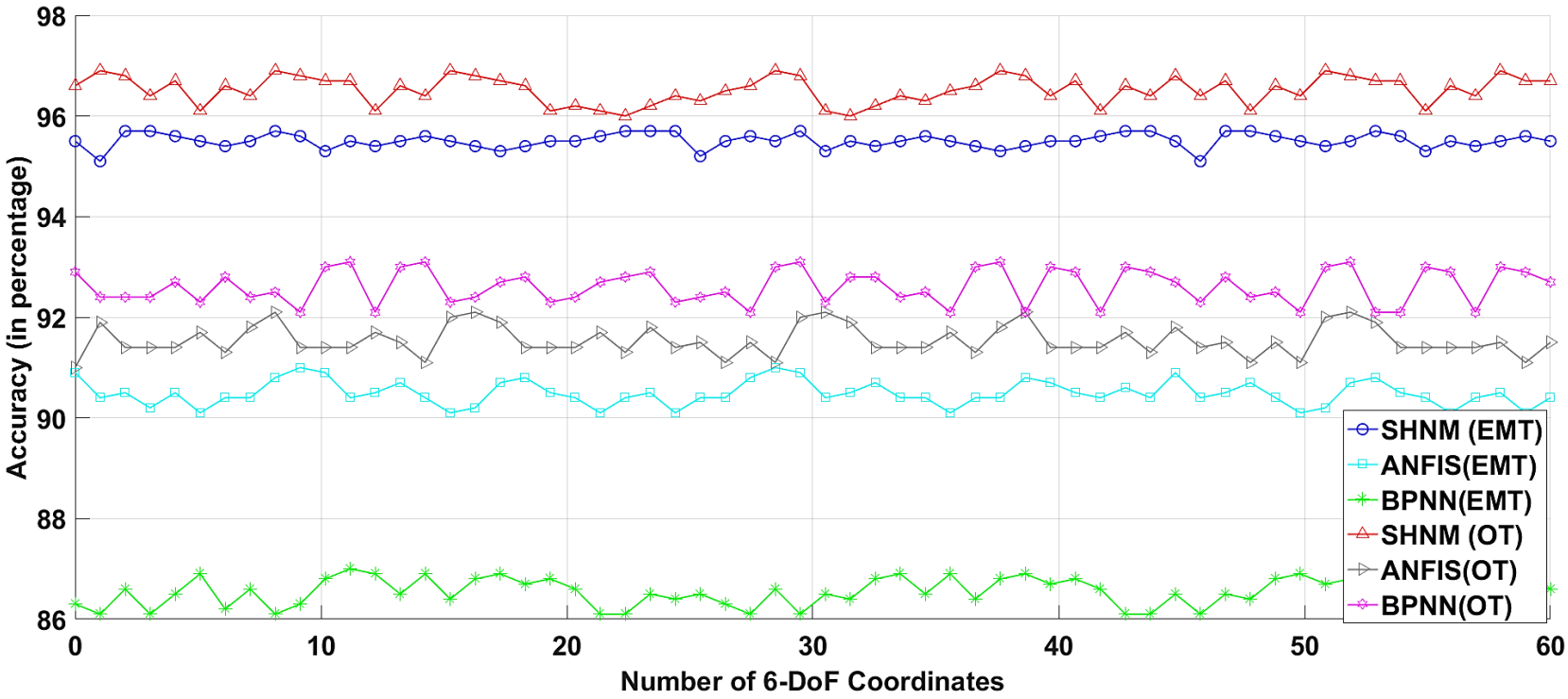

Figure A5: Performance evaluation of SHNM, ANFIS, and BPNN in the prediction of Pitch rotational coordinates in small data set using both optical and electromagnetic tracker

Figure A6 presents the prediction accuracy of all the three models (SHNM, ANFIS, and BPNN) for the prediction of the missing rotational head coordinate Roll, and it is found from Figure A6 that, the accuracy of the Self-healing neural model is better than the ANFIS and Backpropagation neural network. The accuracy of SHNM is ≈ 91% and ANFIS is ≈ 87% using Electromagnetic tracker. The accuracy of SHNM and ANFIS of missed head coordinates using Optical tracker is ≈ 96% and ≈ 93% respectively.

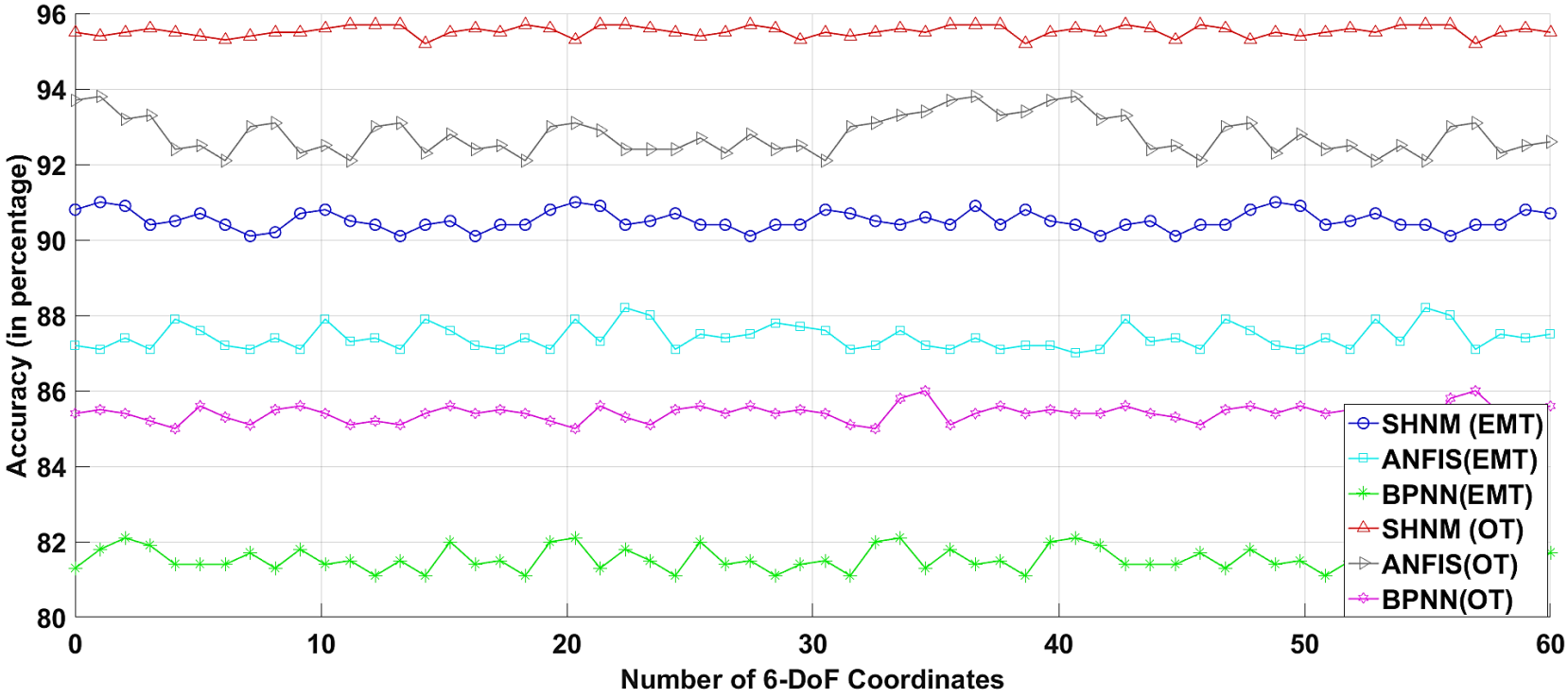

Figure A6: Performance evaluation of SHNM, ANFIS, and BPNN in the prediction of Roll rotational coordinates in small data set using both optical and electromagnetic tracker

LIST OF PUBLICATIONS

1. **Aman Kataria**, Smarajit Ghosh, Vinod Karar "Data Prediction of Electromagnetic Head Tracking using Self Healing Neural Model for Head Mounted Display", Romanian Journal for Information Science and Technology. (**SCIE Indexed-IF 0.422**)- **Accepted for publication (2017)**

2. **Aman Kataria**, Smarajit Ghosh, Vinod Karar "Data Prediction of Optical Head Tracking using Self Healing Neural Model for Head Mounted Display", Vol.77, May 2018, pp. 288-292, Journal of Scientific and Industrial Research. (**SCIE Indexed-IF-0.557)**

3. **Kataria, A**., Ghosh, S., Karar, V., Gupta, T., Srinivasan, K., & Hu, Y. C. (2020). Improved Diver Communication System by Combining Optical and Electromagnetic Trackers. Sensors, 20(18), 5084. (**SCIE Indexed-IF-3.275)**

4. **Aman Kataria**, Smarajit Ghosh, Vinod Karar "Parametric Prediction of Optical Tracker using Machine Learning Techniques for an efficient Head Tracking", Vol.8, Issue 3, Sep 2019, pp. 3045-3050, International Journal of Recent Technology and Engineering. **(Scopus Indexed)**

Posters Presented:

1. **Aman Kataria**, Vinod Karar "Head Tracking Technologies used in Avionics" poster presented at Symposium on Optics and Photonics based Technologies & Instruments for Civil Society (OPTICS 2016) at CSIR-CSIO, Chandigarh.

2. **Aman Kataria**, Smarajit Ghosh, Vinod Karar "Latency in tracking the Head using Head Trackers in Head Mounted Display" Poster presented under the theme " Society Driven

Technological Innovation and Research (STIR-2019)" at CSIR-CSIO, Chandigarh organized by IEEE.

BIOGRAPHY

Aman KATARIA was born in Ambala, India, and received his B.Tech. in Electronics and Communication from Government Engineering College (MIMIT), Malout, India. He pursued his Masters in Engineering in Electronics and Instrumentation control from Thapar Institute of Engineering and Technology, Patiala, India in 2013. His research interest includes Machine Learning, Artificial Intelligence, Image Processing, and Soft Computing. He also served as Lecturer in the National Institute of Technology, Hamirpur in the Electronics & Communication Department. He is working in Central Scientific Instruments Organization (CSIR-CSIO), Chandigarh as Project Associate.

Smarajit GHOSH was born in Midnapur, West Bengal, India. He received his B.Tech. degree in Electrical Engineering and M.Tech degree in Electrical Machines and Power Systems from Calcutta University, Kolkata, India. He did his Ph.D. in 2000 from the Indian Institute of Technology, Kharagpur, India. He served as Lecturer, an Assistant Professor, and Professor in REC (Durgapur, India), BITS (Pilani, India), and SMIT (Sikkim, India), respectively. At present, he is serving as a Professor in the Department of Electrical and Instrumentation Engineering at Thapar University, Patiala, India. He has guided several Ph.D. Scholars and more than 20 Master theses. Along being a recipient of the Bharat Jyoti award, he is credited as the author of several books. He is a **Fellow** of **IE(I), IETE(I)**, and **Life Member of ISTE.** His research interest includes soft computing and distribution systems.

Vinod KARAR was born in Gwalior, India. He received his B.E. degree in electronics engineering from Maulana Azad Regional Engineering College (presently known as Maulana Azad National Institute of Technology), Bhopal, India, M.E. degree in electronics engineering from Punjab Engineering College (presently known as PEC University of Technology), Chandigarh, India, and did his Ph.D. in 2014 from Thapar Institute of Engineering and Technology, Patiala, India. Presently he is serving as Chief Scientist at CSIR-CSIO and as a Professor in AcSIR. He is also serving as Head, Optical Devices and Systems department. He has to his credit more than 80 Technical Reports, 02 Technology Transfers, and has guided several Master's thesis. Dr. Karar is a member of various professional bodies such as IETE, AeSI, ISC, OSI, EMC Society for Engineers, Instrument Society of India, and was recently awarded the Hariramji Toshniwal Gold Medal in 2011 by IETE, India. He is a key member of the team which received the CSIR National Technology Award 2002 and SIATI Award 2011 in his area of research. His research interest includes Artificial intelligence, Aviation, and Soft Computing.